# NANOPARTICLE FLOTATION COLLECTORS

# NANOPARTICLE FLOTATION COLLECTORS

By

SONGTAO YANG, B. Eng., M. Sc.

A Thesis

Submitted to the School of Graduate Studies

in Partial Fulfillment of the Requirements

for the Degree

Doctor of Philosophy

McMaster University

DOCTOR OF PHILOSOPHY (2011) McMaster University
(Chemical Engineering) Hamilton, Ontario

TITLE: Nanoparticle Flotation Collectors
AUTHOR: Songtao Yang
B.Eng. (Jilin University)
M.Sc. (Jilin University)
SUPERVISOR: Professor R. H. Pelton
NUMBER OF PAGES: viii, 159

# Abstract

Flotation is a critical operation in the isolation of valuable minerals from natural ore. Before flotation, chemical collectors are routinely added to ground ore slurries. Collectors selectively bind to mineral-rich particles, increasing their hydrophobicity thus promoting selective flotation. Conventional collectors are small surfactants with a short hydrocarbon tail (2-6 carbons) and a head group, such as xanthate. In this work, much larger hydrophobic polystyrene nanoparticles are evaluated as potential flotation collectors. Experiments involving both clean model mineral suspensions and complex ultramafic nickel ores confirm that conventional water-soluble molecular collectors could be partially or completely replaced by colloidal hydrophobic nanoparticle flotation collectors.

The ability of nanoparticles to induce flotation has been demonstrated by floating hydrophilic, negatively charged glass beads with cationic polystyrene nanoparticle collectors. Mechanisms and key parameters such as nanoparticle hydrophobicity and nanoparticle adsorption density have been identified. Electrostatic attraction promotes the spontaneous deposition of the nanoparticles on the glass surfaces raising the effective contact angle to facilitate the adhesion of beads to air bubbles. The pull-off force required to detach a glass sphere from the air/water interface of a bubble into the water was measured by micromechanics. Coating with nanoparticles allows the beads to attach remarkably firmly on the air bubble. As little as 10% coverage of the bead surfaces with the most effective nanoparticles could promote high flotation efficiencies, whereas conventional molecular collector requires 25% or higher coverage for a good recovery. Contact angle measurements of modified glass surfaces with a series of nanoparticles that covered a range of surface energies were used to correlate the nanoparticle surface properties with their ability to promote flotation of glass beads. Factors influencing nanoparticle deposition on glass, such as nanoparticle dosage, nanoparticle size, conditioning time have been investigated with a quartz crystal microbalance (QCM). Deposition kinetics has been analyzed according to Langmuir kinetics model.

Surface functionalized nanoparticles enhance the ability of nanoparticle collectors to selectively deposit onto surfaces of the desired mineral particles in the presence of gangue materials. Poly (styrene-co-vinylimidazole) based nanoparticle collectors have been developed to selectively deposit onto nickel mineral (pentlandite) in the presence of Mg/Si slime. Flotation tests of ultramafic nickel ores with these nanoparticle collectors have shown improvements in both pentlandite recovery and selectivity. However, cost-effective applications of nanoparticle flotation collectors have yet to be identified.

# Acknowledgements

First, I would like to express my deepest gratitude to my supervisor, Prof. Robert Pelton, for his complete support over the past four years of my studies at McMaster. He was always available and knowledgeable during the compilation of this thesis. His enthusiasm, encouragement, and attitude were uplifting. His thoughts, analysis, and approaches to research were insightful, which led me into the fantastic world of colloid and interface science. He also taught me many skills in paper writing, oral presentations and data modeling. More importantly, he always gave me the freedom to work on what I was mostly interested in with respect to the project. I also appreciate all the opportunities Prof. Pelton gave me to work closely with industry and to attend conferences.

I would also like to thank my supervisory committee members, Prof. Shiping Zhu, and Prof. Michel Brook, for their valuable scientific advice and useful discussions on this research work. I would like to thank Prof. Kari Dalnoki-Veress and Dr. Adam Raegen from the Physics Department for teaching me knowledge of physics related to this project, and for building micromechanical apparatus. Prof. Shiping Zhu and Prof. Emily Cranston are thanked for enhancing my knowledge of polymer science and giving me constant encouragement on my research. Prof. Carlos Filipe is also thanked for his continuous support and encouragement.

I wish to thank Vale Base Metals Technology Development (VBMTD) and Ontario Centres of Excellence (OCE) for funding my research. I acknowledge VBMTD for organizing annual progress review meetings on the ultramafic ore project, which gave exceptional opportunities to share knowledge among researchers from McMaster University, McGill University (Prof. James Finch's group), Columbia University (Prof. Ponisseril Somasundaran's group), Cytec Industries Inc. and VBMTD. I would also like to thank many people from VBMTD for their support, help and valuable discussions. Especially, I am grateful to Drs. Zongfu Dai, Manqiu Xu and Peter Wells for patiently teaching me the basics of mineral processing and giving me the opportunities to perform flotation experiments in VBMTD labs. Ms Julie-Ann Bos is acknowledged for assisting and training me on flotation experiments. Zongfu and Manqiu are acknowledged for help in designing flotation procedures and analyzing flotation results. Moreover, Zongfu and Manqiu have been very generous and helpful friends.

I am indebted to many people from the McMaster Interfacial Technologies Group. I want to thank our laboratory manager Mr. Doug Keller and administrative secretary Ms Sally Watson for their kind support and assistance. In particular, I would like to thank two brilliant summer students, Miles Montgomery and Alexis Ambeault, for their hard work and excellent experimental work. I would also like to thank Dr. Yuguo Cui for sharing his extensive knowledge of physical chemistry, instrument operation and Mathcad modeling, Carla Abarca for her experimental support and discussions, Dan Zhang for his synthesis experience, and Zuohe Wang for many discussions during evenings and weekends. Yaqin Xu, Quan Wen, Behnam Naderizard, Jian Li, Liang Zhang, Pengchao Ren and Vincent Leung are also thanked for their help with my work. All current and previous members from the group are thanked for their encouragement.

I also wish to thank the staff in the Chemical Engineering Department: Ms Kathy Goodram, Ms Lynn Falkiner, Ms Melissa Vasil and Ms Nanci Cole for their administrative assistance, Mr. Dan Wright, Mr. Paul Gatt and Ms Justyna Derkach for their technical support.

Last but definitely not least, I wish to thank my wife, Minghe Wang, for her love, care and support in both my life and my research; and my parents for their love and support. I would also like to thank my fishing friends Fanlong Ning, Wenhe Gong, Leo Hsu, Bo Li, Hanjiang Dong, and other friends for enriching my spare time in Hamilton.

# TABLE OF CONTENTS

# Abbreviation

| | |
|---|---|
| CA | contact angle |
| CCC | critical coagulation concentrations |
| CMC | carboxymethyl cellulose |
| CTAB | cetyltrimethyl ammonium bromide |
| DLS | dynamic light scattering |
| DLVO | Derjaguin-Landau-Verwey-Overbeek |
| DMF | N, N-dimethylformamide |
| EDX | energy-dispersive X-ray diffraction |
| FCS | full circuit simulation |
| FTIR | Fourier transform infrared spectroscopy |
| HEMA | 2-hydroxyethyl methacrylate |
| ICP-OES | inductively coupled plasma-optical emission spectrophotometer |
| MAPTAC | 3-(methacryloylamino) propyl trimethyl ammonium chloride |
| PAX | potassium amyl xanthate |
| Pn | pentlandite |
| QCM-D | quartz crystal microbalance with dissipation |
| SEM | scanning electron microscope |
| St | styrene |
| St-1 | polystyrene |
| St-VI | poly (styrene-co-1-vinylimidazole) |
| TEM | transmission electron microscopy |
| THF | tetrahydrofuran |
| V50 | 2, 2'-azobis (2-methylpropionamidine) dihydrochloride |
| VBTMAC | vinylbenzyltrimethyl ammonium chloride |
| VI | 1-vinyl imidazole |

# Chapter 1 Introduction and Literature Review

## 1.1 Introduction

The Thompson Nickel Belt, located in Manitoba Canada, has approximately 300 million tons of ultramafic low-grade nickel ore deposits containing significant amounts of pentlandite (Pn, $Ni_{4.5}Fe_{4.5}S_8$). [1] These deposits however, have not been exploited or their nickel mining operations have been ceased after a few years of production, because they were considered uneconomical. This situation is now beginning to change as high-grade nickel ores are being depleted. The growing value of nickel in global mineral markets has led to a new ultramafic low-grade nickel ore processing operation in Australia. [2] The general goal of this project is to explore novel approaches for exploiting the Canadian nickel resource.

As publicly announced [3], Thompson Smelter and Refinery, a Vale Canada run nickel mine, will be closing in 2015 in response to the declining ore availability. As well, the Pipe-Kipper (an existing nickel mine in Thompson Manitoba) ultramafic ore project development is on hold. Since 2007, the research and development work for processing the Pipe-Kipper ultramafic ore has been continuingly investigated by VALE Base Metals (Mississauga, Ontario) in collaboration with universities. [1] There appears to be two primary envisioned profits for the Pipe-Kipper project: one is that annually 90 million pounds of nickel will be produced for a twenty-year period, and secondly the re-opening of the old mine will enhance the sustainability of existing assets, extending the lifetime of jobs in the nickel belt region of Manitoba. [4]

Most mineral processing operations include multiple stages of froth flotation to concentrate and isolate the desired product. Before flotation, chemical collectors are routinely added to ground ore slurries. Collectors selectively bind to mineral-rich particles, increasing their hydrophobicity thus promoting selective flotation. [5] Conventional collectors are surfactants with a short hydrocarbon tail and a head group, such as xanthate. A typical conventional collector is potassium amyl xanthate (PAX), which is a small molecule with an extended molecular length of about 1 nm.

In spite of the widespread role of flotation in mineral processing, some ores are difficult to process by flotation. For example, the ultramafic nickel sulfide ore, containing both valuable pentlandite and large quantities of unwanted Mg/Si slime [primarily serpentine, $(MgFe)_3Si_2O_5(OH)_4$] historically responds poorly to flotation. [6] Fibrous, hydrophilic Mg/Si slime can mask the surface of pentlandite (known as "slime coating") due to electrostatic interactions [7] and dramatically depress pentlandite flotation. Consequently, new approaches are required for processing these difficult ores.

In 2006, VALE Base Metals (then CVRD-INCO) approached Dr. Pelton's Interfacial Technologies Group at McMaster University and introduced the challenging ultramafic nickel ore problem. [8] Dr. Pelton proposed a completely new idea based on using colloidally stable nanoparticles, with the diameter ranged from 50 nm to 500 nm, as flotation aids. [9] We hypothesize that the much larger hydrophobic nanoparticles can function as flotation collectors and may provide advantages over the conventional molecular collectors. Relatively large nanoparticles adsorbed on nickel-rich surfaces may be less susceptible to Mg/Si slime coating compared to small patches of conventional surfactant collectors. Later, we coined the term "nanoparticle flotation collectors" [10-11].

The overall objective of this work is to assess the potential of nanoparticle flotation collectors, and correlate nanoparticle properties with their ability to promote flotation of the ultramafic nickel ore. In this chapter, the background information related to this work is reviewed. For clarity, the important fundamental aspects of flotation will be reviewed first, and then major issues in current flotation will be identified. Finally, the potential roles of nanoparticles that may affect the flotation of the ultramafic nickel ore will be discussed.

## 1.2 Flotation

Flotation, or more formally froth flotation, is a complicated physicochemical process. Flotation involves pulverizing ore consisting of the desired mineral and unwanted gangue, into a wet slurry of particles approximately 100 µm in size, then adding a chemical reagent known as the "collector". The collector selectively binds to valuable metal-rich particles, increasing their hydrophobicity and thus promoting bubble/mineral attachment. The treated particle laden bubbles then rise to the surface of the slurry, where they are skimmed off. [5, 12]

### 1.2.1 Elementary Steps in Flotation

To better understand flotation mechanisms, a classical approach is to divide the flotation process into a sequence of substeps for air-bubble/mineral interaction, namely collision, attachment and detachment. [13-14] Bubble/particle collision is the starting event that is determined by the movement of the particles and bubbles along with the hydrodynamic properties of the slurry, which has been extensively studied. [15-18] The bubble/particle attachment and detachment steps unlike collision, are highly dependent upon the surface chemistry of mineral particles and air bubbles. [19-20]

The attachment between mineral particles and air bubbles is considered the most important event for inducing flotation. [21] Ralston and coworkers argued that the attachment step involves three sub-processes (see Figure 1): (1) thinning of the intervening liquid film between the mineral particle and the bubble; (2) rupture of the film to give a three-phase contact (TPC) "nucleus"; and (3) expansion of three-phase contact line (TPCL) from the nucleus to form a stable wetting perimeter. They also gave a detailed modelling of the bubble/particle attachment probability using the product of the probabilities of the three elementary steps. [21-22]

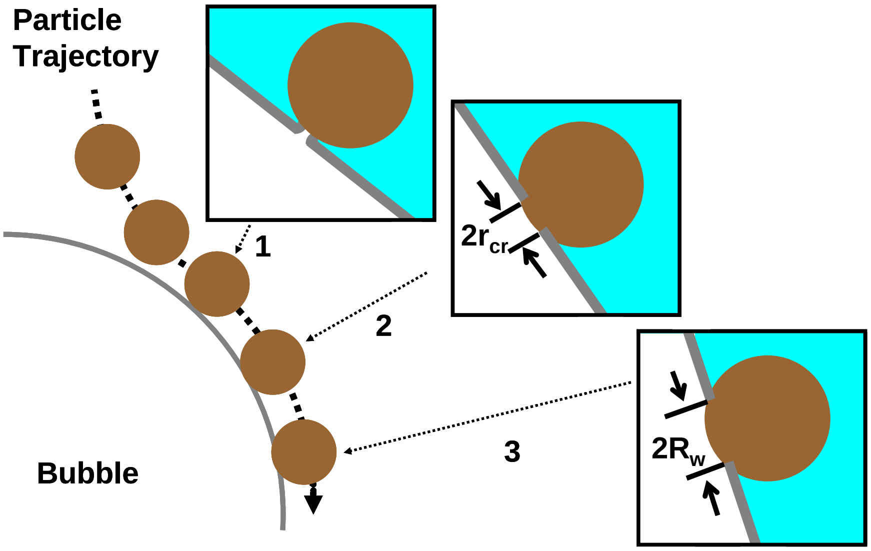

**Figure 1 Illustration of bubble-particle attachment by a mineral particle on its trajectory during flotation, including three elementary steps: 1. thinning liquid film; 2. rupture to give TPC "nucleus" of a critical wetting radius ($r_{cr}$); 3. TPCL expansion to form a stable wetting radius ($R_w$) (Redrawn from Reference [22])**

Gravity and hydrodynamic forces tend to detach mineral particles from bubble surfaces during flotation. [5] It has been recognized that capillary force [23-24] is the major force preventing bubble/particle detachment in flotation. In 1970s, Scheludko et al. [25-26] developed the capillary theory of flotation and emphasized the role of three-phase contact expansion in the kinetics of bubble/particle attachment. In Scheludko's theory, he argued that the formation of the stable dewetting perimeter in flotation may require overcoming some energy barrier, which is called the "line tension". Implementing this line tension approach, he was able to give an expression for predicting the minimum size of floatable mineral particles. [26] Later, Drelich and Miller argued that the uncertainty calculated using line tension was unsatisfactory at predicting experimental results, and gave an alternative expression that appears to be more accurate, but requires contact angle data as a function of air bubble radius. [27] Similarly, extensive work based on Scheludko's theory has been reported to calculate the minimum and maximum size of floatable mineral particles as functions of contact angle, giving flotation domain maps. [28-29]

### 1.2.2 Contact Angle in Flotation

The significance of surface energy of the mineral has been emphasized since the earliest flotation studies. [30-31] Contact angles produced from gas, liquid, and solid phases have historically been used to determine the surface energy of a solid. [32-33] Models such as Young-Dupré, Cassie-Baxter, and Wenzel equations are classically used to predict experimental results. [32]

There appears to be a consensus in the flotation literature that there exists a threshold contact angle required for inducing flotation, and that this minimum depends on system specifics including mineral particle size, hydrodynamic environment, mineral shape, bubble size, etc. [27-29, 34] For example, Anfruns and Kitchener [35] reported a threshold contact angle of 30° for quartz particle flotation. Gardner and Woods reported that a threshold contact angle close to 55° was required for a good flotation recovery of gold spheres. [36] Crawford and Ralston reported a critical threshold value of advancing water contact angle as functions of the particle size for hydrophobized quartz. For example, 40 μm quartz particles required a contact angle of 25°. [28] The early work of Wark et al. reported a critical contact angle of approximately 50° for galena flotation (see Figure 2). [5] From the figure, it is noted that a corresponding 20-25% monolayer coverage of the molecular collector (potassium ethyl xanthate) was required to achieve the 50° contact angle and a good flotation recovery (up to 70%). In summary, the threshold contact angles for flotation in this brief overview ranged from 25 to 55°, which are not superhydrophobic surfaces.

However, a recent review by Chau et al. concludes “So far, there is no rigid quantitative correlation of contact angle on flotation rate recovery”. [20] In addition, contact angle hysteresis and pinning of the three phase contact line complicate modeling. [33, 37-38]

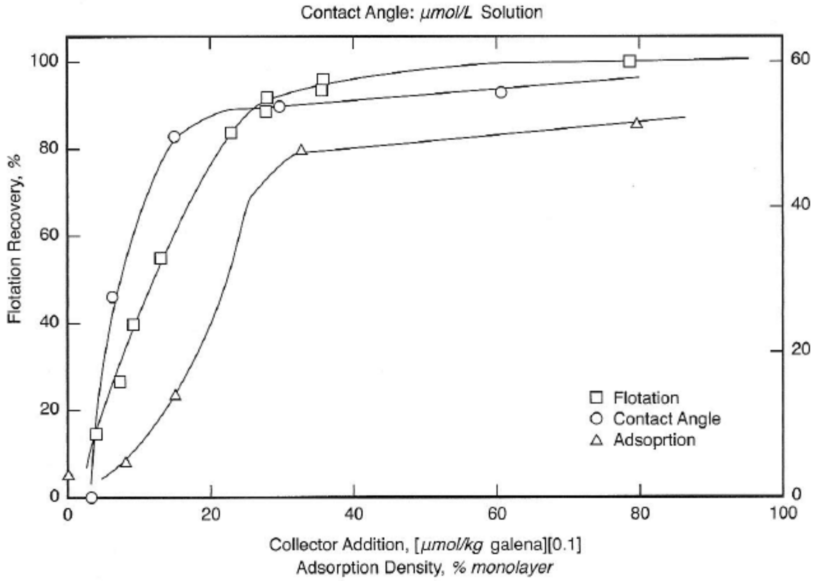

**Figure 2 Contact angle on galena as a function of the concentration of potassium ethyl xanthate expressed in mol/L (data from Wark and Cox 1934), the flotation of galena as a function of the adsorption density of ethyl xanthate expressed in terms of monolayer fraction (data from Bogdanov et al. 1957), and the flotation of galena as a function ethyl xanthate addition expressed in terms of μmol/Kg (data from Gaudin et al. 1928) (Adapted from Figure 4 in Page 16 of Fuerstenau's book [5] )**

## 1.2.3 Flotation Reagents

Flotation reagents are the most essential component of the flotation process. In the early days of developing commercial flotation, the major advances resulted from acquiring more effective flotation reagents. In developing a flotation flowsheet of new ore, a lot of energy, time and attention are given to the selection of reagents for the optimization of flotation results in terms of both recovery and selectivity. [5] On the basis of the function in flotation, flotation reagents are divided into collectors, frothers, modifiers, depressants and flocculants. In this section, I will focus on the role of collectors, and briefly introduce frothers and modifiers. Depressants and flocculants will be given as solution examples in the section of Major Issues.

***1.2.3.1 Collectors*** - The importance of hydrophobicity has been emphasized in both flotation theory and practical operation. Since a majority of natural minerals are hydrophilic, their surfaces must be treated with collectors before flotation. [12] Thus, collectors highlight the most important role of all flotation reagents by regulating the surface properties of mineral particles. The purpose of the collector is to selectively form a hydrophobic layer on a given mineral surface without binding to the gangue materials in flotation slurry; thus allowing the hydrophobized particles to attach to air bubbles, which can be recovered in the froth product. Critical characteristics of a good collector include the ability to selectively adsorb onto desired mineral surfaces and to lower the water/mineral surface energy. The general composition of a conventional molecular collector is a hydrocarbon chain with a reactive or functional head group. The head group reacts with the surface of mineral and the hydrocarbon group chain is oriented away from the surface towards the aqueous environment. [39]

Xanthates for example, are the most common type of collectors used for sulfide minerals. The invention of xanthate as flotation collector in 1925 was a significant development for froth flotation. [40] Xanthates are known as low-cost, easy-to-produce collectors which usually give good flotation efficiency, which has allowed for their application for almost a century. The continued use of xanthate however, has raised ever increasing environmental concern as carbon disulfide is readily emitted from xanthate decomposition, thus engineers and scientists have embarked on looking for the replacement of xanthate collectors. [41]

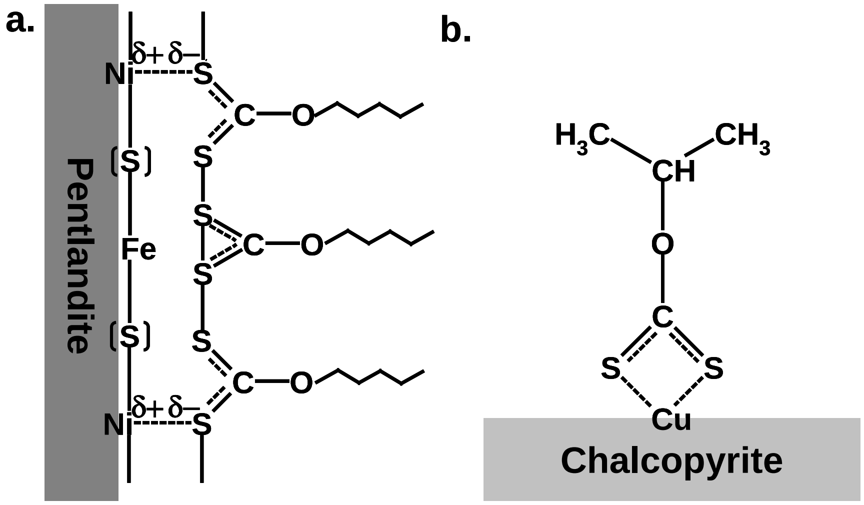

**Figure 3 Schematic drawings showing the chemical formation of Ni-dixanthogen (a. xanthate collector for pentlandite) proposed by Hodgson and Agar, and Cu-diethyldixanthogen (b. isopropyl**

**xanthate collector for chalcopyrite) proposed by Andreev (Redrawn from References [42-43]).**

Binding of collectors to mineral surfaces can be achieved via chemisorption or physical adsorption (e.g., electrostatic interaction). Adsorption of xanthates on a sulphide mineral is an example of chemisorption, whereas adsorption of cationic amine-based collector onto negatively-charged kaolinite is an example of physical adsorption [44]. There have been many studies discussing chemical aspects of the adsorption of xanthate collectors on the mineral surface. [42-43, 45-46] For example, through electrochemical investigations, Hodgson and Agar proposed that xanthate chemisorption at the nickel sites of pentlandite was because of oxidization that took place at the surface of pentlandite to form a dixanthogen. [42] Similarly, Andreev et al.'s studies via Raman spectroscopy of chalcopyrite-xanthate flotation products confirmed the formation of a diethyldixanthogen. [43] The schematic drawings shown in Figure 3 illustrate their proposed dixanthogen formation on mineral surfaces.

Another important category of flotation collectors related to this work is classified as chelating collectors. [47] Investigation of the chelating reagents as flotation collectors has been proposed since early 1930s. [48-49] Some successful attempts of chelating collectors have been reported [50-56], but industrial application of these reagents has not been widely accepted thus far [39]. The chelating collector functions because a ring-like chelation structure is formed with atoms such as O, N, S or P in organic compounds by donating the unshared pair of electrons to metal ion either in solution or at the surface of a mineral. Six- or, five-member rings are common and considered to be the stable structures. Ackerman et al. consider that xanthates also belong to chelating collectors, which form stable four-member rings.[54] In Ackerman et al.'s study, they reported a series of alkyl derivatives of imidazole as chelating flotation collectors for chalcopyrite and pyrite. [54] Note that for imidazole-based organic chemicals interaction with metal ions or metal-rich colloids, some call the interaction as "ligand-metal complexation"[57-58].

***1.2.3.2 Frothers*** - Frothers are used to reduce bubble size in the flotation cell and to enable the formation of a stable froth on the surface of the slurry. A stable froth is necessary in order to maintain bubbles long enough for mineral removal from the cell to maximize flotation performance. [39, 59]

Frothers are usually non-ionic amphiphilic organic compounds that have both polar (e.g., hydroxyl groups) and non-polar (hydrocarbon chains) portions. Frothers adsorb at the bubble surface with a particular orientation: the hydroxyl groups bond with water molecules forming a stabilized water film around the bubble, which resists drainage and retards bubbles coalescence. [39] For example, methyl isobutyl carbinol (MIBC), a simple alcohol-based frother, accumulates at the surface of the bubble with the hydrocarbon chain (isobutyl group) on the air side and the OH group on the water side. Typical frothers currently also include Unifroth and Dowfroth product lines that are based on polypropylene glycol methyl ether. Figure 4 shows the general structure of an alcohol-based frother, its orientation at air/water interface, and structures of MIBC and commercial Dowfroth 250. [59]

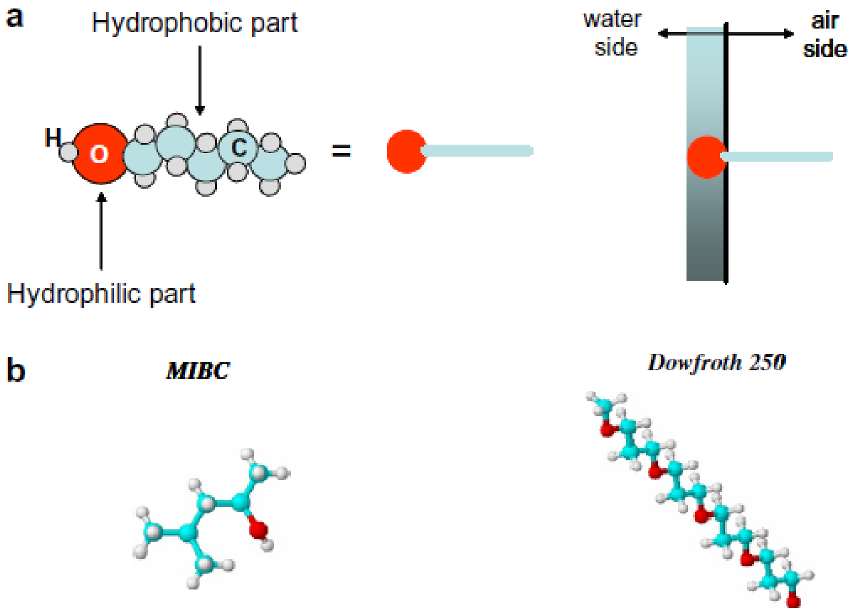

**Figure 4 a. General structure of a frother (alcohol-based) showing amphiphilicity (left) and orientation at the air/water interface (right); b. Examples of two typical frothers, MIBC and Dowfroth 250. (Adapted from Reference [59])**

***1.2.3.3 Modifiers*** - The pH regulators and activators are usually classified as modifiers in flotation. The main function of modifiers is to facilitate the adsorption of collectors onto desired mineral surfaces and thus to govern flotation selectivity. [39] The pH regulators are usually acids and alkalis. Typical industrial pH regulators include sulphuric acid, lime, soda ash, etc. Activators as the name suggests are used to activate flotation. Some sulfide minerals such as sphalerite (ZnS) respond poorly to xanthate collectors due to unstable zinc-xanthate bonding, and hence require the use of "activators" to enhance the adsorption between xanthate and the sphalerite surface. The cupric ion ($Cu^{2+}$), usually in the form of sulfate, is the most common activator. Activator functions via the exchange of $Zn^{2+}$ ions on the surface of sphalerite with the $Cu^{2+}$ ions from the solution to generate extremely low solubility product of copper sulfide (CuS), which is an established activation mechanism. [5, 60] Activation allows sphalerite surfaces to bear some characteristics of copper sulphide which is favorable to xanthate, thus promoting the collector adsorption and flotation.[12, 60]

### 1.2.4 Major Issues

Although froth flotation has been developed and commercially applied for about a century [5], there are still some shortcomings that need to be overcome in order to achieve maximum mineral recovery. The issues have become more and more severe with the high grade ores continuing to diminish and the growth in environmental awareness. Among all issues in current flotation, surface contaminations by hydrophilic features and low flotation efficiency of fine minerals are the two most common ones. In this section, I will focus on the issues in processing sulfide ores, particularly pentlandite.

***1.2.4.1 Surface Contamination of Targeted Particles*** - There is a general consensus in the literature that poor flotation of pentlandite reflects two major factors involving the pentlandite/water interface. Firstly, the oxidation of pentlandite leads to lowered reactivity of alkyl xanthate with the mineral surface, thus interfering with the hydrophobization of pentlandite. Earlier studies [61-62] have shown that sulphide minerals can be floated to some extent without collectors if they are oxidized to an appropriate degree. However, according to the work of Malysiak et al. [63-64] and Legrand et al. [65-66], it has been established that the floatability of pentlandite can be significantly depressed by excessive oxidation. Secondly, the deposition of natural, hydrophilic, Mg/Si slimes onto pentlandite surfaces increases hydrophilicity and interferes with alkyl xanthate adsorption. The problem of the Pipe ultramafic nickel ore described in Introduction section is a typical example. Slime deposition on pentlandite is driven by electrostatic attraction of positively charged slime onto negatively charged pentlandite. Typical positively charged natural slime components include serpentine, chrysotile and lizardite. [7, 67-68]

Approaches have been developed to alleviate each of the above issues. For example, Khan and Kelebek [69] demonstrated that pentlandite oxidation can be inhibited by lowering oxygen exposure. Shackleton et al. [70] and Malysiak et al. [64] reported that the use of ethylenetriamine could deactivate nickel and copper ions by chelation, lowering the deposition of metal oxide species thus inhibiting pentlandite surface contamination. Kirjavainen et al. [71-72] reported surface contamination of pentlandite was attenuated by addition of calcium and thiosulfate ions via activation mechanism.

Depressants have been developed in the last few decades in attempt to eliminate undesirable slime deposition. One of the most common flotation depressants is carboxymethyl cellulose (CMC). [73] Guar, dextrin, and lignin sulfonates have also been used as depressants to enhance the separation of valuable minerals.[74-75] Synthetic polymers were recently tested as depressants in flotation process for various minerals. Beattie and coworkers developed polysaccharides and polyacrylamides as depressants for talc in the flotation of sulphide minerals. [76] INCO Limited (now Vale) developed a combination of a polyamine and a sulphur containing compound as a depressant for arsenide minerals in flotation of mulitisulfide minerals. [77] In their studies, the hydrophilic polymers electro-sterically stabilize the unwanted slimes, reversing their charges and thus alleviating electrostatic driving force that led to slime coating on valuable minerals. In the case of ultramafic nickel ore, CMC adsorption onto Mg/Si slime rendered the surface hydrophilic and negatively charged, which further repelled it from negatively charged pentlandite.

***1.2.4.2 Loss of Fine Particles*** **-** The influence of particle size on the rate of recovery of minerals has been investigated by Gaudin et al. since early 1940s. Fine (e.g., < 20 µm) and ultrafine particles (e.g., < 4 µm) in general have low collision efficiencies with air bubbles and thus have little chance of bubble/mineral attachment, leading to poor flotation recovery of such particles, which is the main reason for the loss of fine mineral particles. [5, 14, 16, 78-79]

Trahar et al. gave a good review on the floatability of very fine particles. [78] In their studies, they found that the minimum sizes for maximum recovery of typical sulfide minerals increased in the order: galena (6 µm), sphalerite (8 µm), pyrrhotite (9 µm), chalcopyrite (15 µm), arsenopyrite (15 µm) and pyrite (20 µm). Note that not all minerals show maximum recovery in exactly the same size range, since the physical properties and induced surface chemistry of minerals are different. Below the minimum size, the flotation recovery falls steadily. [78] For the ultramafic nickel ore, Senior et al. have shown that nickel loss in their process is primarily due to the difficulty of floating and separating pentlandite particles in ultrafine (-10 µm), even in relatively clean systems. [2, 80]

Two major approaches have been developed to alleviate the loss of fine particles, i.e., decreasing bubble size and increasing mineral particle size. [79] Bubble/particle collection efficiency increases with decreasing bubble size. [13, 16, 81] However, the low rising velocity of very small bubbles induces very long flotation time and hence results in a substantial residence time in flotation cell. Small bubbles also cause high water recovery in flotation process which increases the entrainment of gangue minerals, lowering flotation selectivity. [82]

Increasing particle sizes, an alternative for saving fine particles in flotation, is usually achieved by selective flocculation. [79] In selective flocculation approach, the much larger flocs are formed by the bridging interaction of long-chain polymer flocculants with fine particles via electrostatic force, specific chemical interaction, or hydrogen bonding. [83-84] For example, Song et al. [85] has demonstrated that selective flocculation improved flotation of galena and sphalerite fine particles.

## 1.3 Nanoparticles Related Background Review

### 1.3.1 Nanoparticle Applications

Recently, nano/colloidal particles have attracted a lot of interest due to their promising applications in many areas such as drug delivery, biosensor systems, magnetic devices, nanosphere lithography, etc. [86, 87] Among all of nanoparticle applications, there are two remarkable applications related to this work, i.e., defoamers in antifoam technology and stabilizers for Pickering emulsion.

The influence of small hydrophobic particles on the stability of thin liquid films has been extensively reported in the deformer literature. [88-89] Defoamers employ small hydrophobic particles to nucleate and rupture the liquid films (lamella) between air bubbles. Figure 5 shows a sequence of captured video frames showing a bubble coalescence event by using poly (dimethylsiloxane) (PDMS) hydrophobized silica as a defoamer. [89] The relevant reports or developments from defoamer studies are that: hydrophobic particles do nucleate film rupture; rough particles are more effective than smooth ones; and wax crystals and silicone coated silica particles with a few micrometers in diameter are the most effective defoamers.

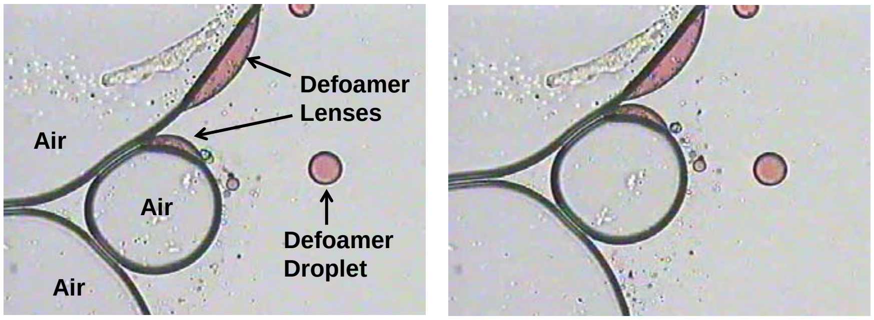

**A) Time = 0s** **B) Time = 5s**

**C) Time = 9s** **D) Time = 10s**

**Figure 5 Sequence of captured video frames showing the migration of a defoamer lens into the film between two air bubbles, causing their coalescence (Reproduced from reference [89])**

Another relevant application for nanoparticles is used for stabilizing Pickering emulsions, where a dense layer of particles at the oil/water interface prevents emulsion droplets aggregation and coalescence. [90-91] By manipulating the surface properties of nanoparticles, it is possible to design colloidal nanoparticles that can function as surfactant molecules, particularly when they adsorb onto a oil/water interface. [92]

## 1.3.2 Nanoparticle Deposition Kinetics

A number of early studies have reported the deposition behaviour of larger particles (e.g. from 0.5 μm to a few micrometers in diameter) onto solid surfaces. [93-96] In these cases, the deposition was reversible under certain conditions; detachment could be easily observed under the influence of high hydrodynamic forces. [97] The particle size is important in the study of particle deposition or aggregation, traditionally 1 μm is a convenient dividing dimension. Colloidal interaction arising from the electric double layer predominates when particle size is less than 1 μm, whereas external forces such as hydrodynamic or gravitational forces become dominant when particles exceed 1 μm in size. [97] The deposition and detachment kinetics for large colloidal particles (i.e. > 1 μm) were usually determined by a combination of both colloidal and hydrodynamic factors. [95]

There have been several papers published recently where a quartz crystal microbalance (QCM) was used to directly track nanoparticle (< 1 μm) deposition. For example, Fatisson and coworkers reported the deposition of $TiO_2$ nanoparticles onto silica over a broad range of solution conditions; in their study, higher deposition rates were observed in the presence of attractive electrostatic interaction in contrast to unfavorable deposition conditions where electrostatic repulsion dominated particle-surface interactions. [98] Similar studies reported the deposition kinetics of various inorganic/organic nanoparticles. The relevant conclusions from these studies include: electrostatic interaction was the major driving force for the deposition; the aqueous chemical environment (i.e. pH, ionic strength) was important; deposition was shown to be typically irreversible at ambient condition; Langmuir kinetics model can be applied to explain the simple case of nanoparticle deposition kinetics; the behavior of deposition and aggregation obeyed Derjaguin-Landau-Verwey-Overbeek (DLVO) theory of colloidal stability. [99-103]

### 1.3.3 Nanoparticle Deposition Influencing Contact Angle

Hydrophobic nanoparticles adsorbing onto hydrophobic mineral surfaces usually gives superhydrophobicity or ultrahydrophobicity. For example, Yan et al. have shown that ordered monolayers of monodisperse tridecafluorooctyltriethoxysilane modified polystyrene particles give very high water contact angles [104] even when the particle surfaces are etched to give large hydrophilic domains between the particles [105]. Similarly, a number of studies have shown that randomly deposited latex on solid surfaces can give high contact angles. [106-108]

Hydrophobic nanoparticles adsorbing onto hydrophilic mineral surfaces should lower the surface energy and increase the contact angle. Surprisingly, we found very few fundamental studies of hydrophilic surfaces decorated with hydrophobic particles. In an early paper, Dettre and Johnson reported the contact angles for hydrophilic glass surfaces decorated with hydrophobic titanium dioxide particles. [109] The water contact angle went from ~ 25 ° for untreated glass to ~ 80 ° when 10% of the glass surface was covered with hydrophobic $TiO_2$ particles. The receding water contact angles, in contrast, were much lower. Takeshita and coworkers described the absorption of cationic latex onto PET; in these experiments both the PET surfaces and the latexes were somewhat hydrophobic, giving relatively small changes in contact angle. [110]

### 1.3.4 Potential Roles of Nanoparticles

In Dr. Pelton's initial proposal of this project, he proposed that by designing and manipulating nanoparticle surface properties, nanoparticles could play three potential roles in processing the ultramafic nickel ore: [9]

1. As collectors that augment current molecular collectors. Cationic hydrophobic nanoparticles deposition onto pentlandite surfaces induces hydrophobicity and nanoscale roughness. Example behavior of this role is illustrated in Figure 6a. Note that pentlandite is negatively charged and Mg/Si slime is positively charged in natural ultramafic nickel ore. [7] In this approach, functional groups such as imidazole, xanthate can be designed onto the hydrophobic nanoparticle surfaces to enhance selectivity and adhesion to pentlandite.

2. As depressants which mop up interfering materials to lessen their adsorption onto pentlandite (see Figure 6b). Nanoparticles can be designed to be hydrophilic and anionic to selectively deposit onto Mg/Si slime.

3. As selective flocculation agents for pentlandite fines.

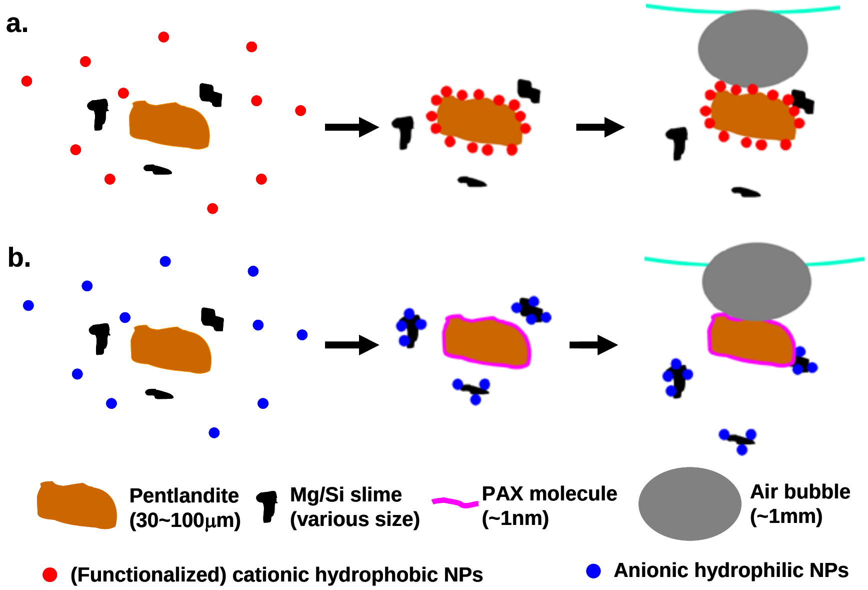

**Figure 6 Potential roles by which nanoparticles might improve flotation: a. (Functionalized) cationic hydrophobic nanoparticles act as collectors; b. Anionic hydrophilic nanoparticles function as depressants which can mop up interfering slimes. (Note: Illustrations are not drawn to scale)**

The first and third roles of nanoparticles require specific interaction with pentlandite whereas the second role requires specific interactions with interfering materials. Throughout the thesis, I adhere to the first role by which nanoparticles may play as flotation collectors (Figure 6a).

## 1.4 Objectives of This Work

The overall objective of my work in this thesis is to assess the potential of nanoparticle flotation collectors. The specific objectives of this research include:

1. To prove that nanoparticles can induce flotation. For that cationic polystyrene nanoparticles and negatively charged glass beads as model mineral particles were used during experimentation.
2. To quantify and model minimum nanoparticle coverage required on glass bead surfaces for inducing a good flotation (high recovery).
3. To correlate nanoparticle hydrophobicity, estimated by contact angle measurements, with the ability of the nanoparticles to promote flotation of the glass beads.
4. To determine factors influencing nanoparticle deposition such as nanoparticle dosage, nanoparticle size, conditioning time and nanoparticle surface charges and to correlate these factors with flotation recovery of the glass beads.
5. To prove that nanoparticles can be designed to specifically bind to and float pentlandite in the presence of unwanted gangue materials.
6. To evaluate nanoparticles as collectors for improved pentlandite flotation in realistic ultramafic nickel ores.

## 1.5 Thesis Outline

*Chapter 1:* This chapter presents the background information of this project, including the fundamental aspects of flotation, major issues in current flotation, nanoparticles related literature review, and the potential roles of nanoparticles in flotation of the ultramafic nickel ore. The specific objectives and an outline of the thesis are also presented herein.

*Chapter 2:* This chapter investigates the mechanisms behind the application of nanoparticles as flotation collectors. Flotation recoveries of hydrophilic glass beads were facilitated with the use of hydrophobic polystyrene nanoparticles. The forces required to pull-off nanoparticle decorated glass beads from air bubbles were measured by micromechanics. A new model for predicting the pull-off forces was proposed. This work has been published in *Langmuir*. [111]

*Chapter 3:* This chapter exploits the role of nanoparticle hydrophobicity in the application of nanoparticle flotation collectors. Contact angle measurements of modified glass surfaces with a series of nanoparticles that covered a range of surface energies were used to correlate the nanoparticle surface properties with their ability to promote flotation of glass beads. This work has been published in *Langmuir*. [112]

*Chapter 4:* This chapter investigates factors influencing nanoparticle deposition onto glass surfaces for the application of nanoparticle flotation collectors, such as nanoparticle dosage, nanoparticle size, conditioning time and nanoparticle surface charges. Deposition kinetics of typical cationic nanoparticles onto silica has been monitored by QCM and analyzed according to Langmuir kinetics model. This work is pending submission to *Colloids and Surfaces A* or *Industrial & Engineering Chemistry Research*.

*Chapter 5:* This chapter develops a new type of nanoparticle flotation collectors based on poly (styrene-co-1-vinylimidazole) for selective isolation of pentlandite from unwanted gangue materials. This work is pending submission to *Mineral Engineering* or *Langmuir*.

*Chapter 6:* This chapter describes flotation results for the ultramafic low-grade nickel sulfide ore in the presence of poly (styrene-co-1-vinylimidazole) based functionalized nanoparticle collectors under industrial conditions. This work is pending submission to *Mineral Engineering* or *American Mineralogist*.

*Chapter 7:* This chapter summarizes the main conclusions and contributions of this project, and proposes future research plans.

## 1.6 References

1. Xu, M.; Scholey, K.; Marcuson, S., Vale-Cytec-University Research Consortium on Processing Low Grade Ultramafic Nickel Ore. *In COM 2011, Conference of Metallurgists, Montreal* **2011**.

2. Senior, G.; Thomas, S., Development and implementation of a new flowsheet for the flotation of a low grade nickel ore. *International journal of mineral processing* **2005,** 78, (1), 49-61.

3. http://www.cbc.ca/news/business/story/2010/11/17/mb-thompson-smelter-refinery-close.html, Thompson refinery shutting down. *CBC news* **2010**.

4. Xu, M., Annual Meeting Minutes on Ultramafic Ore Research. **2011 February**.

5. Fuerstenau, M.; Jameson, G.; Yoon, R., Froth Flotation: A Century of Innovation, Society for Mining, Metallurgy, and Exploration. *Inc.(SME), Littleton, Colorado, USA* **2007**.

6. Mani, H.; Xu, M.; Quinn, P.; Stratton-Crawley, R., The effect of ultramafic mineralogy on pentlandite flotation. *Processing of Complex Ores* **1997,** 1101, 63-76.

7. Edwards, C.; Kipkie, W.; Agar, G., The effect of slime coatings of the serpentine minerals, chrysotile and lizardite, on pentlandite flotation. *International Journal of Mineral Processing* **1980,** 7, (1), 33-42.

8. Pelton, R.; Yang, S.; Xu, M.; Dai, Z., Nanoparticle Flotation Collectors –Innovation from Collaboration. *In COM 2011, Conference of Metallurgists, Montreal* **2011**.

9. Pelton, R., New Approaches to Nickel Processing - a McMaster/ CVRD-INCO Collaboration. *Research Proposal* **2007 January**.

10. Pelton, R.; Yang, S., Nanoparticle Flotation Aids. *United States Provisional Patent Application No. 61/299,173* **2010**.

11. Pelton, R.; Yang, S., Nanoparticle Flotation Collector. In WO/2011/091,522: 2011.

12. Wills, B. A.; Napier-Munn, T., *Wills' mineral processing technology: an introduction to the practical aspects of ore treatment and mineral recovery*. Butterworth-Heinemann London: 2006.

13. Hewitt, D.; Fornasiero, D.; Ralston, J., Bubble–particle attachment. *J. Chem. Soc., Faraday Trans.* **1995,** 91, (13), 1997-2001.

14. Ralston, J.; Fornasiero, D.; Hayes, R., Bubble-particle attachment and detachment in flotation. *Int. J. Miner. Process.* **1999,** 56, (1-4), 133-164.

15. Dobby, G.; Finch, J., Particle size dependence in flotation derived from a fundamental model of the capture process. *Int. J. Miner. Process.* **1987,** 21, (3-4), 241-260.

16. Dai, Z.; Fornasiero, D.; Ralston, J., Particle-bubble collision models--a review. *Adv. Colloid Interface Sci.* **2000,** 85, (2-3), 231-256.

17. Nguyen, A. V., The collision between fine particles and single air bubbles in flotation. *J. Colloid Interface Sci.* **1994,** 162, (1), 123-128.

18. Nguyen, A. V.; Kmet, S., Probability of collision between particles and bubbles in flotation: the theoretical inertialess model involving a swarm of bubbles in pulp phase. *Int. J. Miner. Process.* **1994,** 40, (3-4), 155-169.

19. Ralston, J.; Fornasiero, D.; Mishchuk, N., The hydrophobic force in flotation-a critique. *Colloids Surf. Physicochem. Eng. Aspects* **2001,** 192, (1-3), 39-51.

20. Chau, T.; Bruckard, W.; Koh, P.; Nguyen, A., A review of factors that affect contact angle and implications for flotation practice. *Adv. Colloid Interface Sci.* **2009,** 150, (2), 106-115.

21. Nguyen, A.; Schulze, H.; Ralston, J., Elementary steps in particle--bubble attachment* 1. *Int. J. Miner. Process.* **1997,** 51, (1-4), 183-195.

22. Nguyen, A. V.; Ralston, J.; Schulze, H. J., On modelling of bubble-particle attachment probability in flotation. *Int. J. Miner. Process.* **1998,** 53, (4), 225-249.

23. Fielden, M. L.; Hayes, R. A.; Ralston, J., Surface and capillary forces affecting air bubble-particle interactions in aqueous electrolyte. *Langmuir* **1996,** 12, (15), 3721-3727.

24. Ally, J.; Kappl, M.; Butt, H. J.; Amirfazli, A., Detachment Force of Particles from Air-Liquid Interfaces of Films and Bubbles. *Langmuir* **2010,** 26, (23), 18135-18143.

25. Ivanov, I.; Radoev, B.; Manev, E.; Scheludko, A., Theory of the critical thickness of rupture of thin liquid films. *Trans. Faraday Soc.* **1970,** 66, 1262-1273.

26. Scheludko, A.; Toshev, B.; Bojadjiev, D., Attachment of particles to a liquid surface (capillary theory of flotation). *J. Chem. Soc., Faraday Trans. 1* **1976,** 72, 2815-2828.

27. Drelich, J.; Miller, J. D., The effect of surface heterogeneity on pseudo-line tension and the flotation limit of fine particles. *Colloids Surf.* **1992,** 69, (1), 35-43.

28. Crawford, R.; Ralston, J., The influence of particle size and contact angle in mineral flotation. *Int. J. Miner. Process.* **1988,** 23, (1-2), 1-24.

29. Chipfunhu, D.; Zanin, M.; Grano, S., The dependency of the critical contact angle for flotation on particle size - Modelling the limits of fine particle flotation. *Miner. Eng.* **2011,** 24, (1), 50-57.

30. Corliss, H.; Perkins, C., The Theory of Ore Flotation. *Ind. Eng. Chem.* **1917,** 9, (5), 481-488.

31. Wark, I. W., The Physical Chemistry of Flotation. I. The Significance of Contact Angle in Flotation. *J. Phys. Chem.* **1933,** 37, (5), 623-644.

32. Adamson, A. W.; Gast, A. P.; NetLibrary, I., *Physical chemistry of surfaces*. Wiley New York: 1997.

33. De Gennes, P. G.; Brochard-Wyart, F.; Quéré, D., *Capillarity and wetting phenomena: drops, bubbles, pearls, waves*. Springer Verlag: 2004.

34. Trahar, W., A rational interpretation of the role of particle size in flotation. *Int. J. Miner. Process.* **1981,** 8, (4), 289-327.

35. Anfruns, J. F.; Kitchener, J. A., Rate of capture of small particles in flotation. *Trans. Inst. Min. Metall. Sect. C-Miner. Process. Extr. Metall.* **1978,** 87, (MAR), C81-C82.

36. Gardner, J.; Woods, R., Electrochemical investigation of contact angle and of flotation in the presence of alkylxanthates. I. Platinum and gold surfaces. *Aust. J. Chem.* **1974,** 27, (10), 2139-2148.

37. Pitois, O.; Chateau, X., Small particle at a fluid interface: Effect of contact angle hysteresis on force and work of detachment. *Langmuir* **2002,** 18, (25), 9751-9756.

38. Gillies, G.; Kappl, M.; Butt, H. J., Direct measurements of particle-bubble interactions. *Adv. Colloid Interface Sci.* **2005,** 114, 165-172.

39. Bulatovic, S. M., *Handbook of Flotation Reagents: Chemistry, Theory and Practice: Flotation of Sulfide Ores*. Elsevier Science: 2007; Vol. 1.

40. Keller, C. H., Froth-flotation concentration of ores. In US Patent 1,554,216: 1925.

41. Dong, J.; Xu, M., Evaluation of Environmentally Friendly Collectors for Xanthate Replacement. *Proceedings of the 43rd Annual Canadian Mineral Processors Conference* **2011**.

42. Hodgson, M.; Agar, G., Eilectrochemical Investigations into the Flotation Chemistry of Pentlandite and Pyrrhotite: Process Water and Xanthate Interactions. *Can. Metall. Q.* **1989,** 28, (3), 189-198.

43. Andreev, G.; Barzev, A., Raman spectroscopic study of some chalcopyrite-xanthate flotation products. *J. Mol. Struct.* **2003,** 661, 325-332.

44. Hu, Y. H.; Sun, W.; Jiang, H.; Miller, J. D.; Fa, K. Q., The anomalous behavior of kaolinite flotation with dodecyl amine collector as explained from crystal structure considerations. *Int. J. Miner. Process.* **2005,** 76, (3), 163-172.

45. Grano, S. R.; Prestidge, C. A.; Ralston, J., Solution interaction of ethyl xanthate and sulphite and its effect on galena flotation and xanthate adsorption. *Int. J. Miner. Process.* **1997,** 52, (2-3), 161-186.

46. Vucinic, D. R.; Lazic, P. M.; Rosic, A. A., Ethyl xanthate adsorption and adsorption kinetics on lead-modified galena and sphalerite under flotation conditions. *Colloids Surf. Physicochem. Eng. Aspects* **2006,** 279, (1-3), 96-104.

47. Marabini, A.; Barbaro, M.; Alesse, V., New reagents in sulphide mineral flotation. *Int. J. Miner. Process.* **1991,** 33, (1-4), 291-306.

48. Holman, B. W., Flotation reagents. *Trans. Inst. Mng. and Met.* **1930,** 39, 588-642.

49. Witt, C. C. D.; Batchelder, F., Chelate Compounds as Flotation Reagents. I. *J. Am. Chem. Soc.* **1939,** 61, (5), 1247-1249.

50. Jayne, D., Beneficiation of Acidic Minerals. In US Patent (2380698): 1945.

51. Gutzeit, G., Chelate-forming organic compounds as flotation reagents. *Trans. Am. Inst. Min. Engrs* **1946,** 169, 272-286.

52. Nagaraj, D.; Somasundaran, P., Chelating agents as collectors in flotation: oximes–copper minerals systems. *Mining Eng.* **1981,** 9, 1361.

53. Marabini, A.; Barbaro, M.; Passariello, B., Flotation of cerussite with a synthetic chelating collector. *Int. J. Miner. Process.* **1989,** 25, (1-2), 29-40.

54. Ackerman, P.; Harris, G.; Klimpel, R.; Aplan, F., Use of chelating agents as collectors in the flotation of copper sulfides and pyrite. *Miner. Metall. Process* **1999,** 16, (1), 27-35.

55. Barbaro, M.; Herrera Urbina, R.; Cozza, C.; Fuerstenau, D.; Marabini, A., Flotation of oxidized minerals of copper using a new synthetic chelating reagent as collector. *Int. J. Miner. Process.* **1997,** 50, (4), 275-287.

56. Yekeler, H.; Yekeler, M., Predicting the efficiencies of 2-mercaptobenzothiazole collectors used as chelating agents in flotation processes: a density-functional study. *J. Mol. Model.* **2006,** 12, (6), 763-768.

57. Takafuji, M.; Ide, S.; Ihara, H.; Xu, Z. H., Preparation of poly(1-vinylimidazole)-grafted magnetic nanoparticles and their application for removal of metal ions. *Chem. Mater.* **2004,** 16, (10), 1977-1983.

58. Loo, B. H.; Tse, Y.; Parsons, K.; Adelman, C.; El-Hage, A.; Lee, Y. G., Surface-enhanced Raman spectroscopy of imidazole adsorbed on electrode and colloidal surfaces of Cu, Ag, and Au. *J. Raman Spectrosc.* **2006,** 37, (1-3), 299-304.

59. Finch, J. A.; Nesset, J. E.; Acuña, C., Role of frother on bubble production and behaviour in flotation. *Miner. Eng.* **2008,** 21, (12-14), 949-957.

60. Chandra, A.; Gerson, A., A review of the fundamental studies of the copper activation mechanisms for selective flotation of the sulfide minerals, sphalerite and pyrite. *Adv. Colloid Interface Sci.* **2009,** 145, (1-2), 97-110.

61. Heiskanen, K.; Kirjavainen, V.; Laapas, H., Possibilities of collectorless flotation in the treatment of pentlandite ores. *Int. J. Miner. Process.* **1991,** 33, (1-4), 263-274.

62. Leroux, M.; Rao, S.; Finch, J., Continuous minicell test of collectorless flotation at Mattabi Mines Ltd. *Can. Min. Metall. Bull.* **1994,** 87, (985), 53-57.

63. Malysiak, V.; O'Connor, C.; Ralston, J.; Gerson, A. R.; Coetzer, L.; Bradshaw, D., Pentlandite-feldspar interaction and its effect on separation by flotation. *Int. J. Miner. Process.* **2002,** 66, (1-4), 89-106.

64. Malysiak, V.; Shackleton, N.; O'Connor, C., An investigation into the floatability of a pentlandite-pyroxene system. *Int. J. Miner. Process.* **2004,** 74, (1-4), 251-262.

65. Legrand, D.; Bancroft, G.; Nesbitt, H., Oxidation/alteration of pentlandite and pyrrhotite surfaces at pH 9.3: Part 1. Assignment of XPS spectra and chemical trends. *Am. Mineral.* **2005,** 90, (7), 1042.

66. Legrand, D.; Bancroft, G.; Nesbitt, H., Oxidation of pentlandite and pyrrhotite surfaces at pH 9.3: Part 2. Effect of xanthates and dissolved oxygen. *Am. Mineral.* **2005,** 90, (7), 1055.

67. Bremmell, K. E.; Fornasiero, D.; Ralston, J., Pentlandite-lizardite interactions and implications for their separation by flotation. *Colloids Surf. Physicochem. Eng. Aspects* **2005,** 252, (2-3), 207-212.

68. Pietrobon, M. C.; Grano, S. R.; Sobieraj, S.; Ralston, J., Recovery mechanisms for pentlandite and MgO-bearing gangue minerals in nickel ores from Western Australia. *Miner. Eng.* **1997,** 10, (8), 775-786.

69. Khan, A.; Kelebek, S., Electrochemical aspects of pyrrhotite and pentlandite in relation to their flotation with xanthate. Part-I: Cyclic voltammetry and rest potential measurements. *J. Appl. Electrochem.* **2004,** 34, (8), 849-856.

70. Shackleton, N.; Malysiak, V.; O'Connor, C., The use of amine complexes in managing inadvertent activation of pyroxene in a pentlandite-pyroxene flotation system. *Miner. Eng.* **2003,** 16, (9), 849-856.

71. Kirjavainen, V.; Schreithofer, N.; Heiskanen, K., Effect of some process variables on flotability of sulfide nickel ores. *Int. J. Miner. Process.* **2002,** 65, (2), 59-72.

72. Kirjavainen, V.; Schreithofer, N.; Heiskanen, K., Effect of calcium and thiosulfate ions on flotation selectivity of nickel-copper ores. *Miner. Eng.* **2002,** 15, (1-2), 1-5.

73. Wellham, E.; Elber, L.; Yan, D., The role of carboxy methyl cellulose in the flotation of a nickel sulphide transition ore. *Miner. Eng.* **1992,** 5, (3-5), 381-395.

74. Wang, J.; Somasundaran, P.; Nagaraj, D., Adsorption mechanism of guar gum at solid-liquid

interfaces. *Miner. Eng.* **2005,** 18, (1), 77-81.

75. Beaussart, A.; Mierczynska-Vasilev, A. M.; Harmer, S. L.; Beattie, D. A., The role of mineral surface chemistry in modified dextrin adsorption. *J. Colloid Interface Sci.* **2011,** 357, (2), 510-520.

76. Beattie, D. A.; Huynh, L.; Kaggwa, G. B. N.; Ralston, J., The effect of polysaccharides and polyacrylamides on the depression of talc and the flotation of sulphide minerals. *Miner. Eng.* **2006,** 19, (6-8), 598-608.

77. Dai, Z.; Garritsen, J.; Wells, P.; Xu, M., Aarsenide depression in flotation of mulitisulfide minerals. *US Patent* **2006,** 7,004,326.

78. Trahar, W.; Warren, L., The flotability of very fine particles--A review. *Int. J. Miner. Process.* **1976,** 3, (2), 103-131.

79. Miettinen, T.; Ralston, J.; Fornasiero, D., The limits of fine particle flotation. *Miner. Eng.* **2010,** 23, (5), 420-437.

80. Senior, G.; Shannon, L.; Trahar, W., The flotation of pentlandite from pyrrhotite with particular reference to the effects of particle size. *Int. J. Miner. Process.* **1994,** 42, (3-4), 169-190.

81. Dai, Z.; Dukhin, S.; Fornasiero, D.; Ralston, J., The Inertial Hydrodynamic Interaction of Particles and Rising Bubbles with Mobile Surfaces* 1. *J. Colloid Interface Sci.* **1998,** 197, (2), 275-292.

82. Ahmed, N.; Jameson, G., The effect of bubble size on the rate of flotation of fine particles. *Int. J. Miner. Process.* **1985,** 14, (3), 195-215.

83. Gregory, J.; Charles, R. O. M., Fundamentals of flocculation. *Crit. Rev. Environ. Sci. Technol.* **1989,** 19, (3), 185-230.

84. Somasundaran, P.; Das, K. K.; Yu, X. A., Selective flocculation. *Curr. Opin. Colloid Interface Sci.* **1996,** 1, (4), 530-534.

85. Song, S.; Lopez-Valdivieso, A.; Reyes-Bahena, J.; Lara-Valenzuela, C., Floc flotation of galena and sphalerite fines. *Miner. Eng.* **2001,** 14, (1), 87-98.

86. Gupta, A. K.; Gupta, M., Synthesis and surface engineering of iron oxide nanoparticles for biomedical applications. *Biomaterials* **2005,** 26, (18), 3995-4021.

87. Haynes, C. L.; Van Duyne, R. P., Nanosphere lithography: A versatile nanofabrication tool for studies of size-dependent nanoparticle optics. *J. Phys. Chem. B* **2001,** 105, (24), 5599-5611.

88. Garrett, P., *Defoaming: theory and industrial applications*. CRC Press: FL, 1993.

89. Wang, G.; Pelton, R.; Hrymak, A.; Shawafaty, N.; Heng, Y. M., On the role of hydrophobic particles and surfactants in defoaming. *Langmuir* **1999,** 15, (6), 2202-2208.

90. Aveyard, R.; Clint, J. H.; Nees, D.; Paunov, V. N., Compression and structure of monolayers of charged latex particles at air/water and octane/water interfaces. *Langmuir* **2000,** 16, (4), 1969-1979.

91. Li, J. A.; Stover, H. D. H., Pickering Emulsion Templated Layer-by-Layer Assembly for Making Microcapsules. *Langmuir* **2010,** 26, (19), 15554-15560.

92. Binks, B. P., Particles as surfactants - similarities and differences. *Curr. Opin. Colloid Interface Sci.*

**2002,** 7, (1-2), 21-41.

93. Dabro , T.; Van de Ven, T., A direct method for studying particle deposition onto solid surfaces. *Colloid. Polym. Sci.* **1983,** 261, (8), 694-707.

94. Pelton, R. H.; Allen, L. H., Factors influencing the adhesion of polystyrene spheres attached to Pyrex by polyethyleneimine in aqueous solution. *J. Colloid Interface Sci.* **1984,** 99, (2), 387-398.

95. van de Ven, T. G. M., The capture of colloidal particles on surfaces and in porous material: basic principles. *Colloids Surf. Physicochem. Eng. Aspects* **1998,** 138, (2-3), 207-216.

96. Corak, M.; Van De Wiele, M.; Pelton, R.; Hrymak, A., Polystyrene latex deposition onto polyethylene film consecutively treated with cationic and anionic polymer. *Colloids Surf. Physicochem. Eng. Aspects* **1994,** 90, (2-3), 203-211.

97. Elimelech, M.; Gregory, J.; Jia, X.; Williams, R., *Particle deposition and aggregation: measurement, modelling and simulation*. Butterworth-Heinemann: 1998.

98. Fatisson, J.; Domingos, R. F.; Wilkinson, K. J.; Tufenkji, N., Deposition of TiO2 nanoparticles onto silica measured using a quartz crystal microbalance with dissipation monitoring. *Langmuir* **2009,** 25, (11), 6062-6069.

99. Serizawa, T.; Takeshita, H.; Akashi, M., Electrostatic adsorption of polystyrene nanospheres onto the surface of an ultrathin polymer film prepared by using an alternate adsorption technique. *Langmuir* **1998,** 14, (15), 4088-4094.

100. Fatisson, J.; Ghoshal, S.; Tufenkji, N., Deposition of Carboxymethylcellulose-Coated Zero-Valent Iron Nanoparticles onto Silica: Roles of Solution Chemistry and Organic Molecules. *Langmuir* **2010,** 26, (15), 12832-12840.

101. Gole, A.; Sainkar, S. R.; Sastry, M., Electrostatically controlled organization of carboxylic acid derivatized colloidal silver particles on amine-terminated self-assembled monolayers. *Chem. Mater.* **2000,** 12, (5), 1234-1239.

102. Chen, K. L.; Elimelech, M., Aggregation and deposition kinetics of fullerene (C-60) nanoparticles. *Langmuir* **2006,** 22, (26), 10994-11001.

103. Tretiakov, K. V.; Bishop, K. J. M.; Kowalczyk, B.; Jaiswal, A.; Poggi, M. A.; Grzybowski, B. A., Mechanism of the Cooperative Adsorption of Oppositely Charged Nanoparticles. *J. Phys. Chem. A* **2009,** 113, (16), 3799-3803.

104. Yan, L. L.; Wang, K.; Wu, J. S.; Ye, L., Hydrophobicity of model surfaces with closely packed nano- and micro-spheres. *Colloid Surf. A-Physicochem. Eng. Asp.* **2007,** 296, (1-3), 123-131.

105. Yan, L. L.; Wang, K.; Wu, J. S.; Ye, L., Hydrophobicity of model surfaces with loosely packed polystyrene spheres after plasma etching. *J. Phys. Chem. B* **2006,** 110, (23), 11241-11246.

106. Watanabe, M.; Kawaguchi, S.; Nagai, K., Self-organization of polymer particles on hydrophobic solid substrates in aqueous media. II. Self-organization of cationic polymer particles on polymer films and wettability control with particle monolayers. *Colloid. Polym. Sci.* **2007,** 285, (10), 1139-1147.

107. Sun, C.; Ge, L. Q.; Gu, Z. Z., Fabrication of super-hydrophobic film with dual-size roughness by silica sphere assembly. *Thin Solid Films* **2007,** 515, (11), 4686-4690.

108. Jiang, L.; Zhao, Y.; Zhai, J., A lotus-leaf-like superhydrophobic surface: A porous microsphere/nanofiber composite film prepared by electrohydrodynamics. *Angew. Chem.-Int. Edit.* **2004,** 43, (33), 4338-4341.

109. Dettre, R. H.; Johnson, R. E., Contact Angle Hysteresis. IV. Contact Angle Measurements on Heterogeneous Surfaces1. *J. Phys. Chem.* **1965,** 69, (5), 1507-1515.

110. Takeshita, N.; Paradis, L. A.; Öner, D.; McCarthy, T. J.; Chen, W., Simultaneous Tailoring of Surface Topography and Chemical Structure for Controlled Wettability. *Langmuir* **2004,** 20, (19), 8131-8136.

111. Yang, S.; Pelton, R. H.; Raegen, A.; Montgomery, M.; Dalnoki-Veress, K., Nanoparticle Flotation Collectors: Mechanisms Behind a New Technology. *Langmuir* **2011,** 27, (17), 10438-10446.

112. Yang, S.; Pelton, R. H., Nanoparticle Flotation Collectors II: The Role of Nanoparticle Hydrophobicity. *Langmuir* **2011,** 27, (18), 11409-11415.

# Chapter 2 Nanoparticle Flotation Collectors: Mechanisms Behind a New Technology

In Chapter 2, all of the flotation related experiments were performed by myself with the help of Mile Montgomery who worked with me as a summer student. Micromechanical experiments were also performed by me with the help of Adam Raegen, a postdoc fellow of Dr. Pelton and Dr. Kari Dalnoki-Veress. Adam Raegen built the micromechanical apparatus and trained me how to perform micromechanical experiments. I plotted all experimental data and wrote most part of the first draft. Adam Raegen added the experimental description of micromechanics. Dr. Pelton developed the new “wet-patch” theory to model measured pull-off force and to predict important nanoparticle parameters. Dr. Pelton also helped to analyze data, propose mechanisms, and rewrite my first draft to this final version. Dr. Kari Dalnoki-Veress contributed useful discussions on micromechanical experiments and data analysis.

Langmuir
ARTICLE
pubs.acs.org/Langmuir

# Nanoparticle Flotation Collectors: Mechanisms Behind a New Technology

Songtao Yang, Robert Pelton,* Adam Raegen, Miles Montgomery, and Kari Dalnoki-Veress

McMaster University, 1280 Main Street West, Hamilton, Ontario, Canada L8S 4L7

**ABSTRACT:** This is the first report describing a new technology where hydrophobic nanoparticles adsorb onto much larger, hydrophilic mineral particle surfaces to facilitate attachment to air bubbles in flotation. The adsorption of 46 nm cationic polystyrene nanoparticles onto 43 $\mu$m diameter glass beads, a mineral model, facilitates virtually complete removal of the beads by flotation. As little as 5% coverage of the bead surfaces with nanoparticles promotes high flotation efficiencies. The maximum force required to pull a glass bead from an air bubble interface into the aqueous phase was measured by micromechanics. The pull-off force was 1.9 $\mu$N for glass beads coated with nanoparticles, compared to 0.0086 $\mu$N for clean beads. The pull-off forces were modeled using Scheludko's classical expression. We propose that the bubble/bead contact area may not be dry (completely dewetted). Instead, for hydrophobic nanoparticles sitting on a hydrophilic surface, it is possible that only the nanoparticles penetrate the air/water interface to form a three-phase contact line. We present a new model for pull-off forces for such a wet contact patch between the bead and the air bubble. Contact angle measurements of both nanoparticle coated glass and smooth films from dissolved nanoparticles were performed to support the modeling.

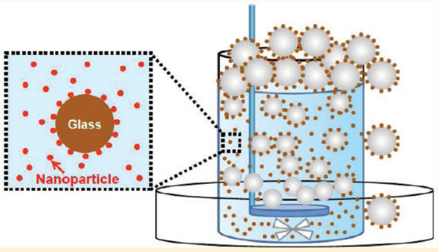

## INTRODUCTION

Annually around 400 million metric tons of mineral is crushed and ground to particles, typically less than 100 $\mu$m in diameter, and then subjected to a process called froth flotation to isolate the valuable components.[1] A critical aspect in flotation is the use of low molecular weight, water-soluble amphiphilic molecules called collectors. Ideally, the collectors selectively bind to those particles rich in the desired mineral, rendering their surfaces more hydrophobic than the undesirable gangue particles. In the flotation process, the more hydrophobic mineral particles attach to air bubbles, rising through the suspension, and the desired mineral particles are carried away with the foam froth. Conventional collectors are low molecular weight surfactants with head groups such as xanthate that promote adsorption on the mineral surfaces. This paper is the first report of a completely new class of collectors based on hydrophobic nanoparticles.

A typical conventional collector is potassium amyl xanthate with an extended molecular length of about 1 nm. By contrast, the work herein involves nanoparticle collectors based on polystyrene with diameters varying between 46 and 120 nm. We report both laboratory scale flotation experiments with glass spheres, a model for mineral particles, and micromechanics[2,3] experiments measuring the force required to detach nanoparticle-coated glass spheres from air bubbles. The goal of our work was to develop an understanding of the mechanisms by which nanoparticles promote flotation with a view to predicting the role of nanoparticle diameter and hydrophobicity on flotation. The following paragraphs briefly summarize the relevant literature, giving some context for our work.

A recent publication edited by Fuerstenau, Jameson, and Yoon[1] gives a good summary of the current understanding of flotation mechanisms. A typical approach to flotation modeling is to divide flotation into a sequence of steps and to develop a probability expression for each step. Nanoparticle flotation collectors are likely to influence two important steps in the sequence of flotation mechanisms: the attachment of the mineral particle to the air bubble surface after collision, and the unwanted detachment of the mineral particles from the bubbles. Ralston et al. argue that the attachment step involves three processes: (1) thinning of the intervening liquid film between the mineral particle and the bubble; (2) rupture of the film to give a three-phase contact "nucleus"; and (3) expansion of the three-phase contact line from the nucleus to form a stable wetting perimeter.[4] The impact of adsorbed nanoparticles on mineral particle/bubble attachment will be addressed in the Discussion section.

The importance of the water contact angle on the mineral surface has been emphasized since the earliest flotation studies.[5] Ralston's group has published detailed flotation kinetic models accounting for hydrodynamic and capillary forces, and model predictions gave good agreement with experimental data.[6,7] A more pessimistic view is given by Chau et al. in their recent review: "So far, there is no rigid quantitative correlation of contact angle on flotation rate recovery."[8] Contact angle hysteresis and pinning of the three-phase contact line complicate modeling.[9−12] Herein we employ polystyrene nanoparticle collectors that we will show increase the contact angle of hydrophilic glass surfaces. Ordered monolayers of monodisperse tridecafluorooctyltriethoxysilane modified polystyrene particles give very high water contact angles[13] even when the particle surfaces are etched to give large distances between the particles.[14] Similarly, a number of studies has

**Received:** May 4, 2011
**Revised:** July 20, 2011
**Published:** July 26, 2011

shown that randomly deposited latex can give high contact angles.[13−16]

Fetzer and Ralston recently reported bubble-surface attachment studies[17] and found that the overall dewetting−attachment step occurs in less than a millisecond. The initial dewetting is very rapid with a low contact angle; they argue that a hydrodynamic model fits this behavior. At longer times, the dewetting rate is lower and the corresponding contact angle is higher. This behavior was explained by pinning on hydrophilic patches. The surfaces used in that study were chemically heterogeneous but topologically smooth. Herein we present contact angle measurements for hydrophilic glass surfaces decorated with hydrophobic polystyrene nanoparticles; the maximum force required to dislodge 43 μm glass spheres from air bubbles; and glass sphere flotation in the presence of nanoparticle flotation collectors.

## ■ EXPERIMENTAL SECTION

**Materials.** Styrene (99%, Sigma-Aldrich) was purified by vacuum distillation. 3-(Methacryloylamino)propyl trimethyl ammonium chloride solution (MAPTAC, 50 wt % in $H_2O$, Sigma-Aldrich) was passed through inhibitor-removing columns. Cetyltrimethylammonium bromide (CTAB, 95%) and 2,2′-azobis(2-methylpropionamidine) dihydrochloride (V50, 97%) were purchased from Sigma-Aldrich and used as supplied. UNIFROTH 250C (99%), a mixture of monomethyl polypropylene glycol, 250 kDa and dipropylene glycol monomethyl ether, was donated by VALE Canada (Mississauga, ON) and was used as supplied. All solutions were made with Type 1 water (Barnstead Nanopure Diamond system).

**Polymerizations.** The polystyrene-*co*-MAPTAC (St-MAPTAC-02-120) latex was prepared by batch emulsion polymerization,[18] whereas St-01-46 was prepared by monomer-starved semibatch emulsion polymerization.[19] The polymerizations were conducted in a three-necked flask equipped with a condenser, two rubber stoppers holding syringe needles (one for nitrogen, the other for monomer addition if the starved-feed charge was employed), and a magnetic stirring bar (controlled by a IKAMAG RCT basic hot plate/stirrer, NC). For St-MAPTAC-02-120, 100 mL of deionized water was charged to the reactor, followed by nitrogen purging for 30 min at 70 °C with 350 rpm stirring. To the reactor were added 5.0 g of styrene and 0.25 g of 50 wt % MAPTAC. After 10 min equilibration, 0.1 g of V50 initiator, dissolved in 10 mL of water, was injected to initiate the polymerization.

For St-01-46, after 15 min polymerization of the initial charge of 0.5 g of styrene, in 100 mL of water with 0.10 g of CTAB and 0.1 g of V50, an additional 4.5 g of styrene was added over 5 h (0.0083 mL/min) from a 10 mL syringe fitted to a syringe pump (NE-1600, New Era Pump System, Inc.). The reaction was stirred at 70 °C for an additional 19 h. The resulting latex was dialyzed for at least 5 days against deionized water, after which the dialysate conductivity was less than 20 μS/cm.

Nanoparticle hydrodynamic diameters were determined by dynamic light scattering (Brookhaven Instruments Corporation, BIC) using a detector angle of 90°. Correlation data were analyzed by BIC dynamic light scattering software (Windows 9KDLSW version 3.34) using the cumulant model, whereas the CONTIN model was used to generate the particle size distributions. The scattering intensity was set between 150 and 250 kcounts/s for each measurement. The duration for each measurement was set to 5 min. Electrophoretic mobility (EM) measurements were performed by using a Zeta PALS instrument (Brookhaven Instruments Corp.) at 25 °C in phase analysis light scattering mode. The reported EM values were the average of 10 runs, with each consisting of 15 scans. Samples for both dynamic light scattering and electrophoretic mobility measurements were prepared in clean vials by dispersing approximately 0.25 g/L of polystyrene nanoparticles in 5 mM NaCl.

**Contact Angle Measurements.** Water contact angle measurements were performed on glass microscope slides (Gold Line Microscope Slides, VWR), which we assumed had similar surface characteristics as the glass beads. In a typical experiment, glass microscope slides were cut to approximated 9.5 mm squares, cleaned (Sparkleen detergent, Fisher Scientific), and immersed in 300 mg/L (for St-01-46) nanoparticle suspension in 5 mM NaCl for times ranging from 10 to 30 min. The treated slides were immersed in ∼1000 mL of water to remove unbound nanoparticles.

The water/air contact angle with treated slides was determined either by using conventional sessile drops placed on dry slides or by observing air bubbles attached to never-dried latex treated glass slides immersed in water. For the latter measurements, air bubbles were formed on thin glass capillary tubes. Standard glass capillaries (1 mm/0.58 mm OD/ID, Word Precision Instruments INC., 1B100-6) were elongated using a pipet puller (Narishige Japan, PN-30). An electrical transformer supplied 2 V to to heat a Pt:Ir (90:10 wt %, diameter 0.5 mm) wire, and the pipet was bent around the wire at a position approximately 5−6 mm from the chokepoint after pulling. The metal wire was then quickly cooled by turning off the transformer, causing the capillary to break cleanly, yielding a capillary with an outer diameter of 20−40 μm.

Air bubbles were formed on the capillary and slowly pushed in contact with treated glass slides, transferring the bubble to the surface. The contact angle measurements were performed using a Krüss contact angle measuring instrument running Drop Shape Analysis (DSA) 1.80.0.2 software. Advancing and receding angles were generated by carefully pushing or pulling the bubble with the glass capillary.

In order to access the hydrophobicity of the nanoparticle surfaces, samples were dried and dissolved in THF (tetrahydrofuran (Certified), Fisher Scientific), 0.65 wt %, and spin coated (SPIN 150 Wafer Spinner running rev: 3.25 software) on glass at 3000 rpm.

**Glass Beads.** Glass beads (30−50 μm) were purchased from Polysciences Inc. The particle size distributions of the glass beads in $5 \times 10^{-3}$ M NaCl were measured with a Malvern Mastersizer 2000 instrument. The particle size distributions were approximately log-normal with an area averaged mean diameter of 43 μm, a standard deviation of 11 μm, and a corresponding specific surface area of 0.057 $m^2/g$. The electrophoretic mobility of the beads in in 5 mM NaCl at ambient pH was $-4.61\ (\pm 0.32) \times 10^{-8}\ m^2\ s^{-1}\ V^{-1}$.

**Flotation.** In a typical flotation experiment, 2 g of glass beads and 1.0 mL of nanoparticles (14.6 g/L for St-MAPTAC-02-120) were added into 120 mL of $5 \times 10^{-3}$ M NaCl in a 150 mL plastic flotation beaker, sitting on a 90 mm diameter plastic Petri dish, which in turn was sitting on a magnetic stirrer (Corning Stirrer, model PC-160). The suspension of glass beads and polystyrene nanoparticles was mixed for 5 min (25 mm × 25 mm cross-shape stirring bar at ∼600 rpm) to facilitate polystyrene nanoparticle deposition onto the glass beads. Next 0.12 mL of 1% UNIFROTH 250C (10 ppm) was added and mixed for an additional 30 s. Flotation was commenced by initiating nitrogen flow (Matheson 604 E700 Flow Controller) at a rate of 2.0 L/min through a Corning Pyrex gas dispersion tube (Fisher Scientific, 11-137E) consisting of a 30 mm coarse glass frit attached by a 90° elbow. During flotation, the stirring rate was increased to ∼900 rpm to avoid bead sedimentation. The foam phase was scraped over the edge of the beaker and collected in the plastic Petri dish. After 1.0−1.5 min, the gas flow was stopped and the plastic collection dish was replaced with a clean dish. The liquid level in the flotation beaker was then topped up with UNIFROTH 250C in 5 mM NaCl at the original concentration. In most of our flotation cases, this sequence was repeated until three to five dishes were collected.

The mass of liquid and beads collected in each dish was measured; the beads were filtered with a Büchner funnel, dried, and weighed. Typically each dish contained 50−60 mL of flotation liquor. The flotation results were expressed as the recovery, the mass fraction of beads which were recovered in the dishes.

**Table 1. Some Properties of the Polystyrene-Based Nanoparticle Collectors**

| nanoparticle designation | diameter, nm (PDI)[a] | electrophoretic mobility × $10^{-8}$ $m^2$ $s^{-1}$ $V^{-1}$ (std error) | contact angle smooth polymer film, $\theta_{np}$[b] | contact angle of bubbles on glass, $\theta$ (std error)[b] |
|---|---|---|---|---|
| St-01-46 | 46 (0.156) | 1.61 (±0.07) | 91 (+0.9) | 40 (±1.6) |
| St-MAPTAC-02-120 | 120 (0.027) | 2.74 (±0.12) | 85 (±1.7) | 23 (±1.2) |

[a] Hydrodynamic diameter from DLS using cumulant model. [b] Static contact angles of submerged bubbles; for examples, see Figure 5.

The extent of nanoparticle deposition on the glass beads was determined by measuring the absorbance of the supernatant nanoparticle dispersion at 500 nm (Beckman Coulter, DU800) before and after deposition (usually 7 min) on the glass beads. The quantity of deposited latex was calculated using a calibration curve of absorbance versus nanoparticle concentration.

Images of recovered glass beads from nanoparticle flotation runs were acquired by using a JEOL JSM-7000F scanning electron microscope.

**Micromechanics.** The adhesion experiment that we employed is similar to that of Colbert et al.,[3] with some alterations. In our experiment, a glass capillary was pulled to a very thin (~20 μm diameter), long, hollow pipet. This pipet was then bent into a "Z"-shape using right angles, with the first bend roughly 2 mm from the end and the second bend roughly 1.5 cm from the first, very near the thick, undeformed capillary. This shape allows for the deflection of the pipet to be directly calibrated and used as a force transducer in experiments.

A chamber containing many micrometer-sized particles was placed on a microscope positioned between two three-axis stages (Newport 462 XYZ) one of which was atop an additional linear stage (Newport VP-25XA). Using optical table mounts and 1″ posts, we mounted the pipet such that the thin, bent parts could move freely within the chamber. Using a syringe and Tygon tubing, suction was used to pick up a bead with the pipet. Using the second (motorized) stage and similar parts, the end of a capillary tube was placed in the chamber while nearly full of liquid, creating a small bubble in the tube. A syringe and tubing were likewise used to move the air until a portion of it was extended beyond the capillary. Pressure could then be exerted on the tubing in order to finely control the size of the free portion of the bubble (its radius of curvature). After aligning the center of the bubble and bead, the motor was moved until contact was made and then used to pull the bubble and bead apart, meanwhile monitoring the bubble shape and pipet deflection.

Pipets were calibrated by holding them vertically and imaging them from the side. As water was slowly pushed out of the end, the drop adhered to the end of the pipet in the unduloidal shape typical of a drop on a fiber, exerting a downward gravitational force. By fitting the shape of the drop and measuring the vertical displacement of the end of the pipet, we were able to find the force constant of each pipet, ranging from 0.005 to 0.1 μN/μm. Graphs of gravitational force versus pipet displacement were remarkably linear over the range in which they were used (up to displacements on the order of tens of micrometers), allowing for simple Hookian spring constants to be obtained. The spring constant multiplied by the bead displacement under load gave the force on the particle and pipet.

## RESULTS

Two polystyrene copolymer nanoparticle dispersions were prepared by emulsion copolymerization. The resulting dispersions were colloidally stabilized by cationic amidine moieties[18] from the initiator and by quaternary ammonium surface groups from the MAPTAC monomer. Particle size distributions of the nanoparticles were measured by dynamic light scattering, and the results are summarized in Table 1 together with the electrophoretic mobilities. Both nanoparticle dispersions were cationic, with St-MAPTAC-02-120 having the greater electrophoretic mobility.

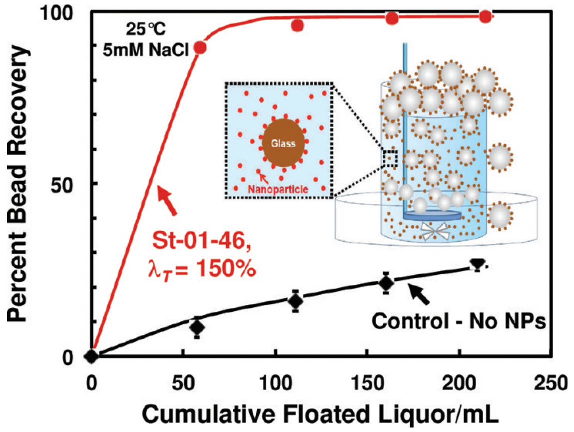

**Figure 1.** Glass bead flotation with and without St-01-46 nanoparticles. The *Y*-axis gives the fraction of added beads collected in the froth. Each point represents the contents of a froth collection dish.

Small scale, batch laboratory flotation experiments were conducted to demonstrate the ability of the nanoparticles to function as flotation collectors. Glass beads with a mean diameter of 43 μm were employed as model mineral particles. A total of 2 g of glass beads was suspended in 0.01 g/L frother, a nonionic surfactant, dissolved in 5 mM NaCl at pH 6.7. Figure 1 compares flotation results with and without the presence of nanoparticle flotation collector St-01-46, a 46 nm cationic polystyrene nanoparticle. The *X*-axis gives the volume of liquid from froth collected in 4 dishes during a flotation experiment. The *Y*-axis gives the cumulative mass fraction of added beads collected in the froth. Without nanoparticle collectors, the fraction of recovered beads increased linearly up to a maximum of about 30%. This was due to hydraulic entrainment, where beads suspended in the water phase were carried over with the water; this is a general effect in flotation.[1] With nanoparticles, virtually all of the beads were removed with the froth after the first couple of dishes (points). Herein we express the nanoparticle concentration in the flotation experiments as a theoretical coverage, $\lambda_T$, defined as the total projected area of the added nanoparticles divided by the total area of the glass beads. Then for the results in Figure 1, $\lambda_T$ was 150%, meaning there were sufficient nanoparticles to form a saturated adsorbed layer on the glass beads. Note that the cationic nanoparticles spontaneously adsorbed onto the negatively charged beads. We will now consider what coverage or extent of nanoparticle adsorption was necessary to promote bead attachment to air bubbles and removal with the froth.

A series of flotation experiments was conducted in which the nanoparticles were first deposited on the beads, then the nondeposited nanoparticles were removed after 5 min, followed by flotation. The results in Figure 2 are expressed as the percentage of beads recovered in the froth as a function of the coverage of nanoparticles actually on the beads (i.e., the total projected area of nanoparticles/total area of bead surface). Note that the maximum coverage of randomly deposited noninteracting but nonoverlapping spheres is ~0.55, whereas electrostatic repulsion, tending to keep the spheres apart, gives an even lower maximum coverage.[20,21] The smaller, pure polystyrene nanoparticles, St-01-46, induced much greater glass bead removal than the larger nanoparticles bearing quaternary ammonium groups. Indeed, good bead recovery was observed with less than 10% of glass surface covered with smaller beads. This is an important observation because it suggests relatively low nanoparticle dosages could give good flotation. Since the early work of Gaudin and others, it has been known that less than 20% of a monolayer coverage of conventional surfactant collectors also can give good flotation (see Figure 4 in Fuerstenau's book[1]) Furthermore, surfactant collectors at low coverage are not uniformly distributed on the mineral surface. Instead, they are present as hemimicelles on the mineral surface.[22]

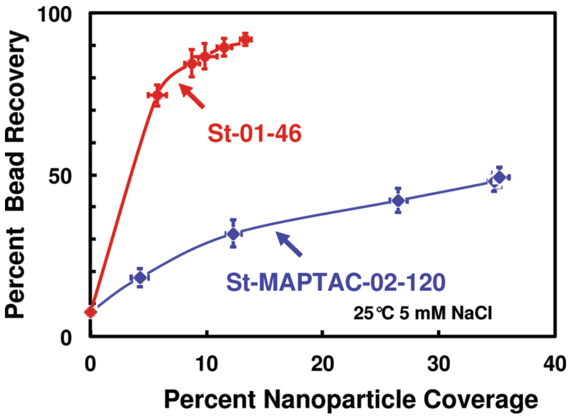

**Figure 2.** Influence of the density of adsorbed nanoparticles on glass bead (43 μm) recovery. Only one dish was collected.

The easy visualization of nanoparticles on mineral surfaces by electron microscopy is one of the advantages of nanoparticle flotation collectors. Figure 3 shows example scanning electron microscopy (SEM) micrographs of glass bead surfaces after flotation with three nanoparticle collectors. All micrographs show high coverages with no large bare patches. Closer examination reveals that the large St-MAPTAC-02-120 particles were mainly present as small aggregates, whereas the smaller St-01-46 was present mainly as individual particles. These observations underscore one of the challenges in the design of nanoparticle collectors. On one hand, a hydrophobic surface such as pristine polystyrene will favor flotation; on the other hand, hydrophilic ionic groups are required for nanoparticle colloidal stability.

Attachment of minerals to air bubbles is a fundamental requirement of flotation. Therefore, a necessary condition for flotation is a finite receding contact angle for the flotation medium on the mineral surface. In order to assess the ability of the nanoparticles to increase the contact angle, we conducted model experiments in which the cationic nanoparticles were

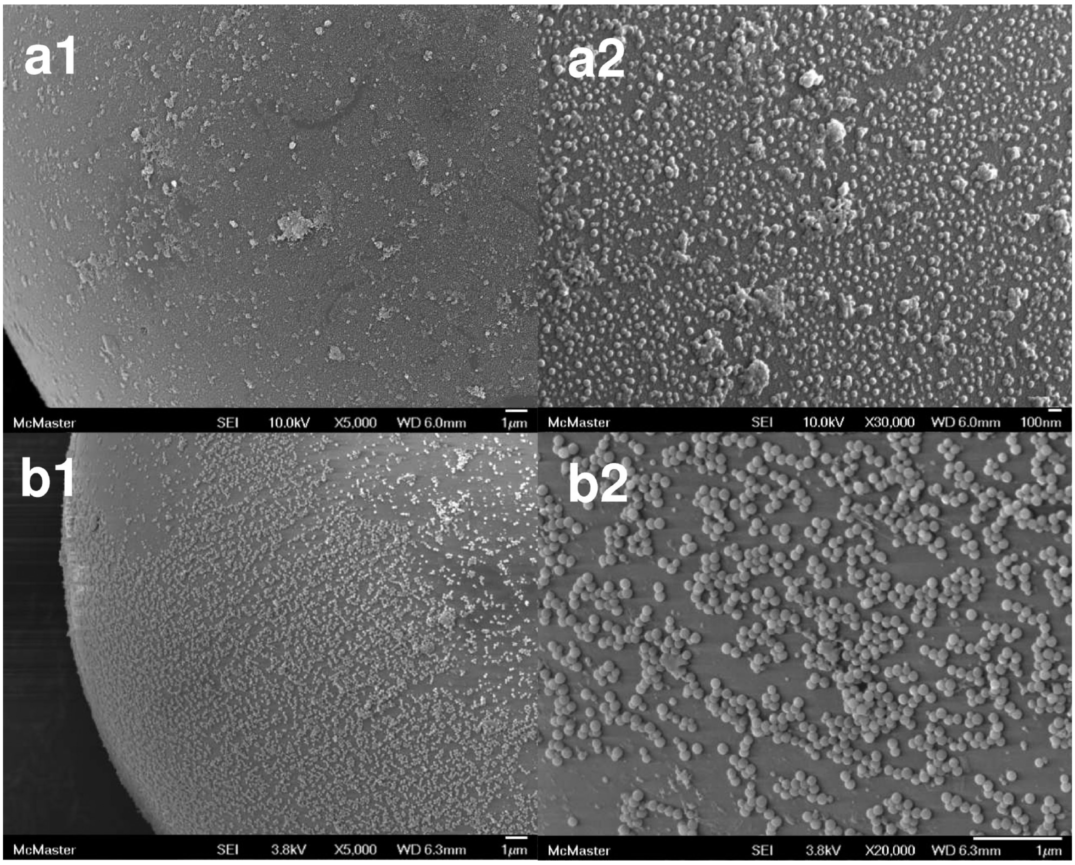

**Figure 3.** SEM images of dried 43 μm glass beads collected after flotation runs using 46 nm St-01-46 (a1,a2) and 120 nm St-MAPTAC-02-120 (b1,b2) nanoparticles.

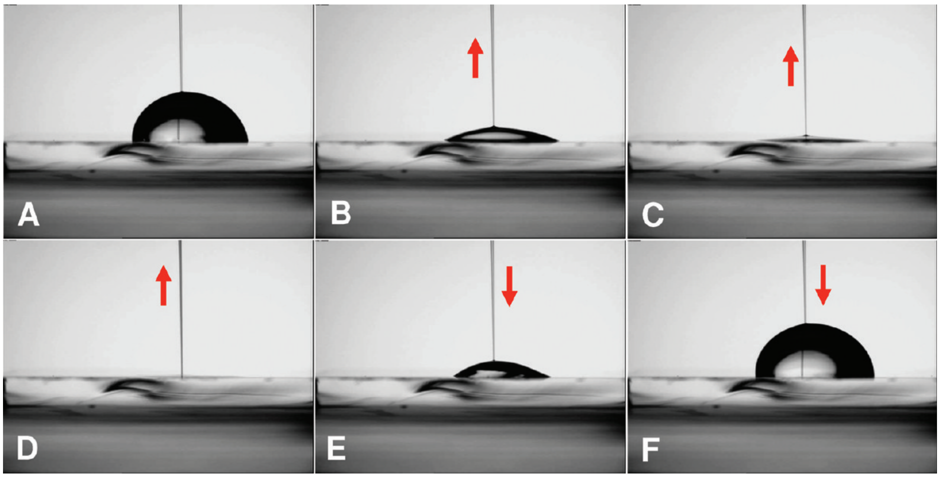

**Figure 4.** Decreasing and then increasing the volume of a sessile drop on glass decorated with deposited St-01-46 nanoparticles. The reappearance of the drop on the original footprint suggests that the receding contact line leaves wet patches on the surface.

allowed to deposit onto clean microscope slides on which we could easily measure water contact angles. In our initial experiments, we dried the glass slides decorated with nanoparticles and measured the advancing and receding water contact angle. Figure 4 shows images of the sessile drop in the sequence in which the drop was evacuated from the surface with a capillary tube and then pumped back onto the slide. The initial advancing angle was about 90°. When the liquid was withdrawn, the three-phase contact line was strongly pinned. Reversing the process, the drop reappeared on its original footprint, suggesting that the receding drop left water on the slide between the nanoparticles (wet patches on the glass).

Initially, we were concerned that the three-phase contact line (TPCL) pushed the glass beads on the glass slide, leaving a hydrophilic circle corresponding to the first drop. To prove that weak nanoparticle adhesion was not a problem, we repeated experiments on the same position on a slide after drying between measurements. The high advancing contact angle on the repeated experiment confirmed that the surface was not swiped clean in the first experiment. Other evidence of strong nanoparticle/glass adhesion includes the following: we took a sample of beads recovered from a flotation experiment and successfully refloated them without adding extra nanoparticles, and none of the electron micrographs of beads showed bare patches corresponding to nanoparticles being dragged on the bead surface.

In our flotation studies, the nanoparticles deposited onto glass bead surfaces submerged in water, with no drying step before bubble attachment. Therefore, we conducted contact angle measurements on immersed, never-dried surfaces, by introducing air bubbles from a micropipet and touching the bubbles to a modified glass surface. Figure 5 shows images of air bubbles on the surfaces of submerged glass slides. For images (a) and (b), glass slides spin coated with a solution formed by dissolving nanoparticle St-01-46 in THF were used. These surfaces were used to obtain an estimate of the equilibrium contact angle for the nanoparticle surfaces. The contact angles formed after bubble attachment were receding angles. Advancing angles were observed by using the micropipet to push the bubble across the surface. The advancing angle on spin coated polystyrene was $\theta_a = 93° \pm 0.8°$, whereas the receding angle of $\theta_r = 87° \pm 1.6°$ was only slightly less.

Images (c) and (d) in Figure 5 show air bubbles on a glass surface decorated with St-01-46 nanoparticles. The advancing contact angle was $\theta_a = 61° \pm 1.1°$, whereas the more relevant receding angle was only $\theta_r = 17° \pm 1.5°$. Table 1 summarizes the key contact angle results for the two nanoparticles. With a cast film contact angle ($\theta_{np}$) of 85°, St-MAPTAC-01-120 was only slightly less hydrophobic than St-01-46 with a contact angle of 91°. However, glass surfaces with a saturated layer of adsorbed particles, St-01-46 gave a contact angle ($\theta$) of 40°, whereas the surface treated with St-MAPTAC-02-120 had an angle of only 23°. Thus, the larger nanoparticles, perhaps because of aggregation, were less effective in increasing contact angle.

All the contact angle measurements were made with pure water, whereas our flotation measurements were made with a frother solution of $5 \times 10^{-3}$ M NaCl and 10 mg/L frother, a nonionic surfactant. The advancing water contact angle of the St-01-46 smooth polymer film decreased from 93° for water to 85° with frother solution, and the attached bubble receding contact angle decreased from 91° in water to 78° in the frother solution. Also, the surface tension of water decreased by about 3 mN/m with frother addition. Frothers are designed to enhance froth stability while having minimum negative impact on the ability of collectors to increase mineral hydrophobicity. This seems to be the case herein.

The attachment and detachment of nanoparticle-coated mineral were further characterized by the micromechanical measurement of adhesion forces holding a glass sphere to an air bubble. Suction was used to attach individual glass spheres to a micropipet that had been bent to give two 90° bends (right-angled Z-shaped) to serve as a cantilever. An air bubble attached to a second, larger pipet was pushed into the glass bead and then retracted. The forces were measured by the displacement of the calibrated cantilever. Details of our method have been published.[2,3] Figure 6 shows images from a measurement for a 55 $\mu$m diameter glass bead with deposited St-01-46 nanoparticles interacting with a 612 $\mu$m diameter air bubble. The plot shows measured force as a function of run time of the stepper motor that drives the capillary supporting the air bubble. For the first 10 s, the bubble was pushed against the glass bead, after which the direction was reversed and the force increased linearly with displacement until the bead detached from the bubble. The corresponding maximum pull-off force was 1.9 $\mu$N. We will show in the Discussion section that this value is consistent with

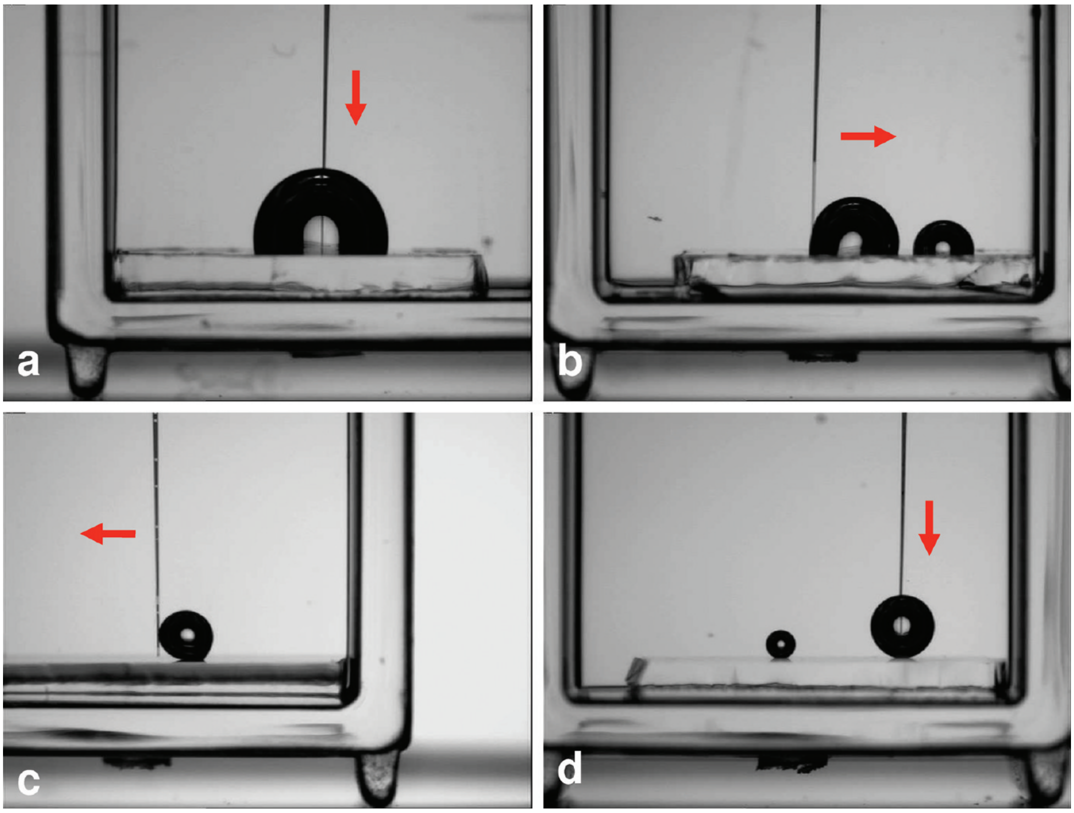

**Figure 5.** Submerged bubble-captive contact angle images. Frames (a) and (b) show smooth films prepared by spin coating with St-01-46 solution in THF. The corresponding contact angles are $\theta_a = 93° \pm 0.8°$, $\theta_r = 87° \pm 1.6°$, $\theta_s = 91° \pm 0.9°$, where subscripts denote a, advancing; b, receding; and s, static, the initial angle upon bubble adhesion. In frame (b), the capillary tubing was the left-hand pushing bubble. Frames (c) and (d) show never-dried glass surfaces with adsorbed St-01-46 nanoparticles giving contact angles of $\theta_a = 61° \pm 1.1°$, $\theta_r = 17° \pm 1.5°$, and $\theta_s = 40° \pm 1.6°$. In frame (c), the bubble was dragged by the capillary tube to generate receding and advancing angles.

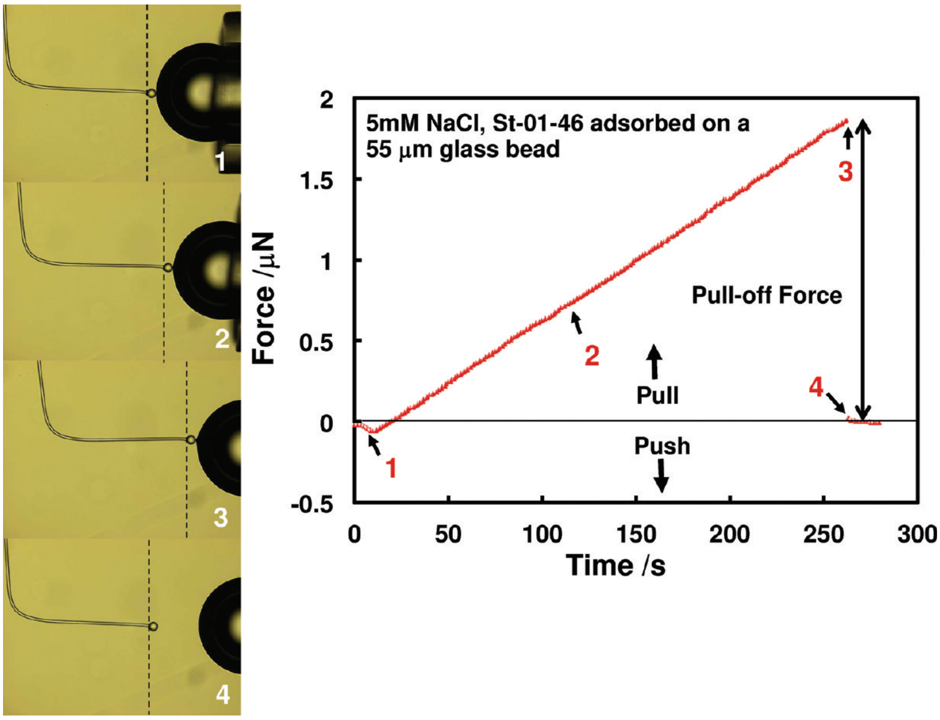

**Figure 6.** Example of a force versus displacement curve for attaching and removing a glass bead from an air bubble. Note that the displacement is expressed as the run time of the stepper motor driving the capillary supporting the air bubble. The bead diameter of 55 $\mu$m was measured from the image.

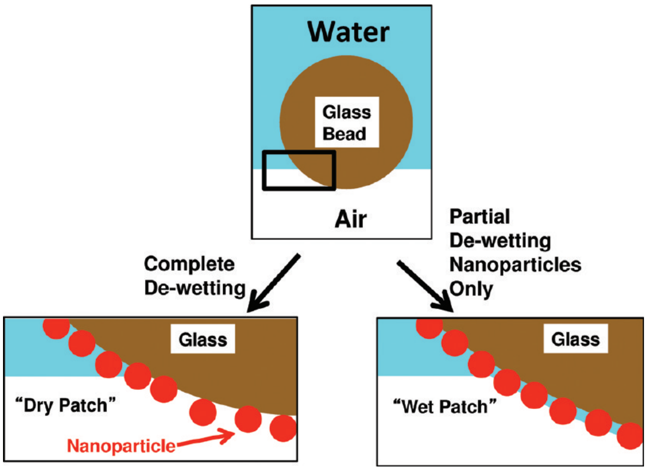

**Figure 7.** Three-phase contact point for two extreme cases of a bubble adhering to a glass sphere with adsorbed nanoparticles. Dry patch is the conventional case, whereas with the wet patch the three-phase contact lines are only on the nanoparticles.

theoretical predictions. Furthermore, there was no evidence of visible air pockets on the spheres after detachment. Measurements performed with clean, untreated beads yielded maximum pull-off forces of only 0.0086 $\mu$N.

## ■ DISCUSSION

There are a few obvious design parameters for nanoparticle flotation collectors, including nanoparticle shape, diameter, surface energy, and coverage on the mineral surface. The obvious role of nanoparticles is to facilitate mineral-bubble attachment and/or to minimize detachment. The goal of the following analysis is to consider the influence of nanoparticle parameters on the various stages of mineral particle flotation with a view to identifying the critical role of nanoparticles and to optimize nanoparticle properties. Specifically, the following analysis will try to explain the key behaviors shown in Figure 2; smaller, more hydrophobic particles are more efficient, and as little as 10% nanoparticle coverage gives high flotation yields.

The micromechanics experiments show a clear contact patch between the sphere and the bubble, approximately 10 $\mu$m in diameter. However, we do not know the detailed structure of this patch. At one extreme, the patch area could be completely dry, as we might expect from a receding three-phase contact line on a smooth hydrophobic surface. At the other extreme, we envision a bonding patch consisting of individual nanoparticles penetrating the air water interface, giving a bubble adhering with many isolated contacts to nanoparticles. The sessile drop experiment in Figure 4 suggests wet patch formation. We will now consider the potential role of nanoparticles in these two extreme cases: the conventional "dry patch" and the "wet patch" with nanoparticle contacts. Figure 7 schematically illustrates a conventional "dry patch" and a "wet patch". Since glass has a finite contact angle, we would expect that the actual situation is between the extremes, islands of water interspersed with the nanoparticles on the contact patch.

**a. "Dry Patch" Adhesion.** The collision of a bubble with a mineral particle causes the deformation of the bubble against the mineral particle surface, giving a thin aqueous film between the particle and the air. This transient structure can undergo two fates. Either the bubble/mineral pair dissociates, or the liquid film thins and ruptures, resulting in mineral/bubble attachment. For mineral particle attachment to a bubble, Ralston et al. argue that the attachment step involves three processes: (1) thinning of the intervening liquid film between the mineral particle and the bubble; (2) rupture of the film to give a three-phase contact "nucleus"; and (3) expansion of the TPCL from the critical radius to form a stable wetting perimeter.[4]

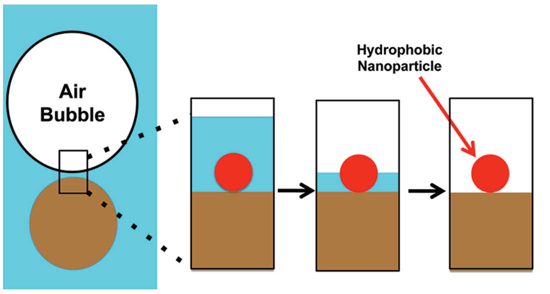

**Figure 8.** Thinning and rupture of the liquid film between a mineral particle with adsorbed nanoparticles and an air bubble.

The influence of small hydrophobic particles on the stability of thin liquid films has been extensively reported in the defoamer literature.[23,24] Defoamers employ small hydrophobic particles to nucleate the rupture of liquid films (lamella) between air bubbles. The relevant conclusions from defoamer studies are that hydrophobic particles do indeed nucleate film rupture; rough particles are more effective than smooth ones; and wax crystals and silicone coated silica particles a few micrometers in diameter are the most effective. By analogy with the defoamer particle mechanisms, we propose that one role for the nanoparticle collectors is to facilitate attachment by increasing the rupture thickness of the water film. In other words, less film drainage is required before rupture, thus increasing the probability of rupture. This mechanism is illustrated in Figure 8 showing that the nanoparticle serves as the dewetting "nucleus". We do not think that thinning and nucleus formation are rate determining because smaller particles are more effective; the minimum nanoparticle coverage is far greater than the very low coverage of particle required for nucleation; and our very limited data suggest that individual spheres are more effective at promoting flotation than are small nanoparticle aggregates.

Ralston's final step in the mineral/bubble attachment process is the expansion of the "contact nucleus" to a macroscopic contact area.[4] This is an expansion of the TPCL on a relatively hydrophilic surface with hydrophobic nanoparticle inclusions. The inverse of this problem (i.e., hydrophilic inclusions on a hydrophobic surface) has been discussed by de Gennes et al.[11] During the dewetting process, the TPCL must jump from hydrophobic patch to patch. The relevant distance scale is the minimum distance between neighboring nanoparticle surfaces. For the case of a square array of spheres on a plane, the minimum surface-to-surface distance between neighboring spheres, $d_{ss}$, is given by the following expression. The interparticle distance is linear with nanoparticle radius at constant coverage where $r$ is the nanoparticle radius and $\lambda$ is the coverage.

$$d_{ss} = r\left(\sqrt{\frac{\pi}{\lambda}} - 2\right) \quad (1)$$

In the absence of a specific model for the probability that the TPCL will expand, it seems reasonable to assume that the smaller the value of $d_{ss}$, the more likely the initial contact nucleus will expand. Therefore eq 1 suggests that TPCL expansion is promoted by increasing the nanoparticle coverage, $\lambda$, and by decreasing the nanoparticle radius. Both of these predictions are in accord with the experimental results in Figure 2.

We now discuss the influence nanoparticle size, hydrophobicity, and coverage on the maximum force required to pull a glass bead from an equilibrium position on the air/water interface into the aqueous phase. Scheludko et al. derived the following expression where $R_m$ is the radius of the glass sphere, $\gamma$ is the surface tension, and $\theta$ is the contact angle.[25,26]

$$\begin{aligned} F_{dry} &= 2\pi R_m \gamma \sin\left(\pi - \frac{\theta}{2}\right) \sin\left(\pi + \frac{\theta}{2}\right) \\ &= 2\pi R_m \gamma \sin^2\left(\frac{\theta}{2}\right) \end{aligned} \tag{2}$$

**b. "Wet Patch" Adhesion.** Our vision of the structure of a wet patch (see Figure 7) is essentially the same as that proposed by Takeshita et al. for the structure of water sitting on a dense layer of latex deposited on a film.[15] The radius of the wet patch, $R_w$, can be expressed as the following function of the apparent contact angle, $\theta$, formed between the bubbles and mineral. In our work, $\theta$ was estimated from contact angles of bubbles adhering to immersed flat surfaces (see Figure 5 and Table 1).

$$R_w = R_m \sin(\theta) \tag{3}$$

We assume that the maximum pull-off force from a wet patch is determined by the nanoparticles on the wet patch periphery. In other words, bead/bubble separation is essentially peeling, and the maximum peel force corresponds to the maximum perimeter of the contact patch. The following expression comes directly where $\zeta$ is the number of nanoparticles per length of line defining the outer edge of the contact patch and $\theta_{np}$ is the contact angle of the nanoparticle surface. Note we measured $\theta_{np}$ by casting the particles into smooth thin films and the values were about 90° (see Figure 5a and b for examples).

$$F_{wet} = 2\pi R_w \zeta 2\pi r \gamma \sin^2\left(\frac{\theta_{np}}{2}\right) \tag{4}$$

If the nanoparticles are randomly distributed, including allowing overlapping particles, $\zeta$ is given by the following expression where $N$ is the number of nanoparticles per unit area.

$$\zeta = N2r = \frac{\lambda}{\pi r^2}2r = \frac{2\lambda}{\pi r} \tag{5}$$

Substituting eqs 3 and 5 into eq 4 gives the following expression for the maximum pull-off force from a wet patch.

$$F_{wet} = 8\pi R_m \sin(\theta)\lambda\gamma \sin^2\left(\frac{\theta_{np}}{2}\right) \tag{6}$$

The wet patch peel analysis, eq 6, predicts no dependence of pull-off force on nanoparticle size, whereas the nanoparticle coverage, $\lambda$, and nanoparticle hydrophobicity, $\theta_{np}$, are important. To compare the dry patch (eq 2) and wet patch models (eq 6) to our experimental pull-off forces (Figure 6), values are required for $\lambda$ and $\theta$; neither was measured during the micromechanics experiment. The Cassie–Baxter contact angle model gives the following relationship between $\theta$ and $\lambda$ where $\theta_m$ is the contact angle on the clean glass, which is about 5°.

$$\cos(\theta) = \lambda\cos(\theta_{np}) + (1 - \lambda)\cos(\theta_m) \tag{7}$$

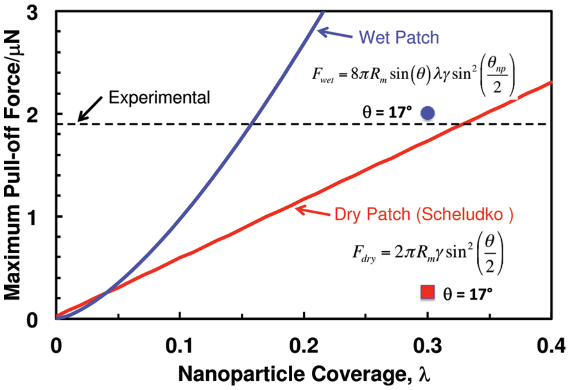

**Figure 9.** Comparing the predictions of the conventional dry patch theory (eq 2) and wet patch theory (eq 6) with the experimental result. The Cassie–Baxter equation (eq 7) was used to estimate the bubble/bead contact angle, $\theta$, as a function of $\lambda$. The parameters used for the calculation were: $R_m = 27.5\ \mu$m, $\theta_m = 5°$, $\theta_{np} = 87°$, and $\gamma = 70$ mN/m. For the two individual points, we used $\theta = 17°$ (from immersed bubble measurements, Figure 5) and $\lambda = 30\%$ (an estimate).

Figure 9 compares the maximum pull-off force as a function of nanoparticle coverage. For coverages above 5%, the wet patch analysis predicts higher pull-off forces than does the conventional dry patch analysis. Both models predict substantial adhesion forces at low coverages, confirming the experimental observation that 5–10% coverage can give high flotation recoveries (see Figure 2). However, we have serious concerns about estimating the contact angle with the Cassie–Baxter equation, which seems to overestimate the angles. For example, the micromechanics experiments were conducted under conditions which should nearly saturate the bead with adsorbed nanoparticles giving $\lambda \sim 30\%$. The corresponding value of $\theta$, from eq 7 is 45°, which is high compared to the 17° we measured in our bubble attachment experiments. Substituting 45 in eq 3 gives a radius of the bead/bubble contact patch of 19 $\mu$m, whereas the micromechanics images suggest a contact radius of ∼5 $\mu$m. Thus, the Cassie–Baxter analysis is overestimating the contact angles. Taking our experimental bubble attachment contact angle, $\theta = 17°$, and estimating $\lambda = 30\%$ gives the two points plotted in Figure 9. The wet patch analysis gives a very good estimate of the experimental result.

Key parameters for both pull-off force models are the nanoparticle coverage and the hydrophobicity of the nanoparticles; neither model predicts that nanoparticle radius is important for pull-off force. Within the uncertainty of the parameters, particularly the radius of the contact patch ($R_w$), we cannot reject either of the models (i.e., eq 2 or 6). Further experiments are required to fully understand the nature of the contact zone between an air bubble and a hydrophilic surface coated with hydrophobic nanoparticles.

In summary, the air bubble attachment experiments, Figure 5, and the micromechanics experiments demonstrate that nanoparticles promote bubble attachment and give large pull-off forces. Our analysis predicts that both attachment and pull-off forces increase with increasing coverage, $\lambda$, and decreasing nanoparticle contact angle ($\theta_{np}$). Furthermore, the initial bubble attachment should be facilitated by larger nanoparticles that will nucleate the rupture of the aqueous film between the bubble and the mineral.

## CONCLUSIONS

This work is the first report of a novel application for nanoparticles as flotation collectors. From a scientific perspective, there are many unanswered questions about the detailed role of the nanoparticles. From a technological perspective, a critical issue is the ability to selectively deposit the nanoparticles onto surfaces of the desired mineral particles in a complex mixture. A future publication will show that nanoparticles can be designed to selectively deposit onto a nickel mineral (pentlandite) in the presence of gangue. The main conclusions from the current work are as follows:

1. Nanoparticles based on polystyrene function as flotation collectors if they adsorb onto mineral surfaces.
2. High flotation efficiencies can be achieved with less than 10% coverage of the glass beads, a mineral model.
3. Smaller and more hydrophobic nanoparticles are the most efficient flotation collectors.
4. The forces required to pull a nanoparticle-coated sphere from the air/water interface of a bubble into the water was determined via micromechanical measurements. The maximum pull-off force ranged from 0.0086 $\mu$N for a clean 55 $\mu$m glass bead to 1.9 $\mu$N for a bead bearing adsorbed 46 nm diameter polystyrene spheres.
5. We propose that the patch where a glass sphere intersects the bubble could be wet, except where nanoparticles protrude through the air/water interface, that is, a wet patch. The pull-off force for a wet patch can be estimated by a peel analysis where the exterior ring of particles on the wet patch accounts for the adhesion. Clearly, more work is required to verify the wet patch hypothesis.

## AUTHOR INFORMATION

### Corresponding Author

*E-mail: peltonrh@mcmaster.ca.

## ACKNOWLEDGMENT

We thank the Centre for Materials and Manufacturing (CMM), a division of the Ontario Centres of Excellence (OCE) in collaboration with VALE Base Metals for funding; VALE, Base Metals Technology Development for funding; and Zongfu Dai and Manqiu Xu from Vale for much help, samples, and advice. Finally, we acknowledge Prof. Ramin Farnood, University of Toronto, and Prof. Lee White, University of South Australia, for mechanistic discussions.

## REFERENCES

(1) *Froth Flotation: A Century of Innovation*; Fuerstenau, M., Jameson, G., Yoon, R., Eds.; Society for Mining, Metallurgy, and Exploration: Littleton, CO, 2007.

(2) Yeung, A. K. C.; Pelton, R.; Micromechanics, A New Approach to Studying the Strength and Breakup of Flocs. *J. Colloid Interface Sci.* **1996**, *184*, 579–585.

(3) Colbert, M. J.; Raegen, A. N.; Fradin, C.; Dalnoki-Veress, K. Adhesion and Membrane Tension of Single Vesicles and Living Cells Using a Micropipette-Based Technique. *Eur. Phys. J. E* **2009**, *30*, 117–121.

(4) Nguyen, A. V.; Schulze, H. J.; Ralston, J. Elementary Steps in Particle--Bubble Attachment. *Int. J. Miner. Process.* **1997**, *51*, 183–195.

(5) Wark, I. W. The Physical Chemistry of Flotation. I. The Significance of Contact Angle in Flotation. *J. Phys. Chem.* **1933**, *37*, 623–644.

(6) Gontijo, C. D.; Fornasiero, D.; Ralston, J. The Limits of Fine and Coarse Particle Flotation. *Can. J. Chem. Eng.* **2007**, *85*, 739–747.

(7) Pyke, B.; Fornasiero, D.; Ralston, J. Bubble Particle Heterocoagulation under Turbulent Conditions. *J. Colloid Interface Sci.* **2003**, *265*, 141–151.

(8) Chau, T. T.; Bruckard, W. J.; Koh, P. T. L.; Nguyen, A. V. A Review of Factors That Affect Contact Angle and Implications for Flotation Practice. *Adv. Colloid Interface Sci.* **2009**, *150*, 106–115.

(9) Pitois, O.; Chateau, X. Small Particle at a Fluid Interface: Effect of Contact Angle Hysteresis on Force and Work of Detachment. *Langmuir* **2002**, *18*, 9751–9756.

(10) Gillies, G.; Kappl, M.; Butt, H. J. Direct Measurements of Particle-Bubble Interactions. *Adv. Colloid Interface Sci.* **2005**, *114*, 165–172.

(11) De Gennes, P. G.; Brochard-Wyart, F.; Quèrè, D. *Capillarity and Wetting Phenomena: Drops, Bubbles, Pearls, Waves*; Springer Verlag: New York, 2004.

(12) Priest, C.; Sedev, R.; Ralston, J. Asymmetric Wetting Hysteresis on Chemical Defects. *Phys. Rev. Lett.* **2007**, *99*, 026103.

(13) Yan, L.; Wang, K.; Wu, J.; Ye, L. Hydrophobicity of Model Surfaces with Closely Packed Nano- and Micro-Spheres. *Colloids Surf., A* **2007**, *296*, 123–131.

(14) Yan, L.; Wang, K.; Wu, J.; Ye, L. Hydrophobicity of Model Surfaces with Loosely Packed Polystyrene Spheres after Plasma Etching. *J. Phys. Chem. B* **2006**, *110*, 11241–11246.

(15) Takeshita, N.; Paradis, L. A.; Öner, D.; Mccarthy, T. J.; Chen, W. Simultaneous Tailoring of Surface Topography and Chemical Structure for Controlled Wettability. *Langmuir* **2004**, *20*, 8131–8136.

(16) Watanabe, M.; Kawaguchi, S.; Nagai, K. Self-Organization of Polymer Particles on Hydrophobic Solid Substrates in Aqueous Media. Ii. Self-Organization of Cationic Polymer Particles on Polymer Films and Wettability Control with Particle Monolayers. *Colloid Polym. Sci.* **2007**, *285*, 1139–1147.

(17) Fetzer, R.; Ralston, J. Dynamic Dewetting Regimes Explored. *J. Phys. Chem. C* **2009**, *113*, 8888–8894.

(18) Goodwin, J. W.; Ottewill, R. H.; Pelton, R. Studies on the Preparation and Characterization of Monodisperse Polystyrene Lattices. 5. Preparation of Cationic Lattices. *Colloid Polym. Sci.* **1979**, *257*, 61–69.

(19) Sajjadi, S. Nanoparticle Formation by Monomer-Starved Semi-batch Emulsion Polymerization. *Langmuir* **2006**, *23*, 1018–1024.

(20) Adamczyk, Z.; Dabros, T.; Czarnecki, J.; Vandeven, T. G. M. Particle Transfer to Solid-Surfaces. *Adv. Colloid Interface Sci.* **1983**, *19*, 183–252.

(21) Adamczyk, Z.; Zembala, M.; Siwek, B.; Warszynski, P. Structure and Ordering in Localized Adsorption of Particles. *J. Colloid Interface Sci.* **1990**, *140*, 123–137.

(22) Atkin, R.; Craig, V. S. J.; Wanless, E. J.; Biggs, S. Mechanism of Cationic Surfactant Adsorption at the Solid-Aqueous Interface. *Adv. Colloid Interface Sci.* **2003**, *103*, 219–304.

(23) Garrett, P. *Defoaming: Theory and Industrial Applications*; CRC Press: Boca Raton, FL, 1993.

(24) Wang, G.; Pelton, R.; Hrymak, A.; Shawafaty, N.; Heng, Y. M. On the Role of Hydrophobic Particles and Surfactants in Defoaming. *Langmuir* **1999**, *15*, 2202–2208.

(25) Scheludko, A.; Toshev, B. V.; Bojadjiev, D. T. Attachment of Particles to a Liquid Surface (Capillary Theory of Flotation). *J. Chem. Soc., Faraday Trans. 1* **1976**, *72*, 2815–2828.

(26) Fielden, M. L.; Hayes, R. A.; Ralston, J. Surface and Capillary Forces Affecting Air Bubble—Particle Interactions in Aqueous Electrolyte. *Langmuir* **1996**, *12*, 3721–3727.

# Appendix: Supporting Materials for Chapter 2

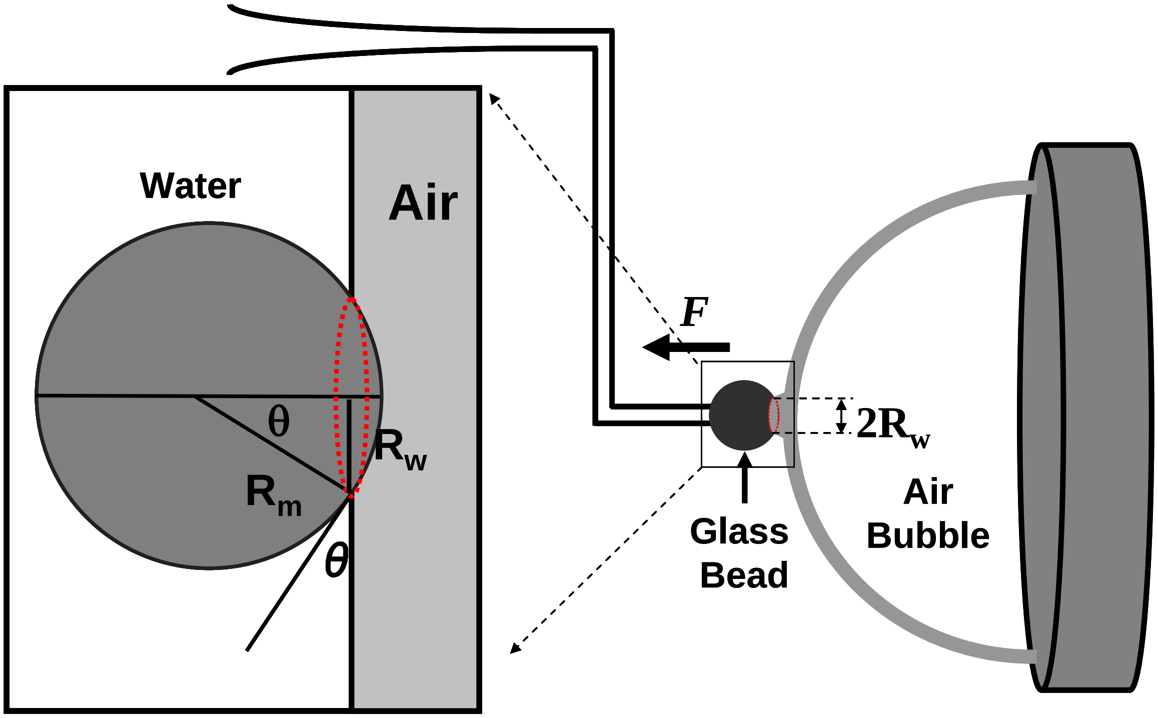

**Figure s1.** A schematic draw showing the setup of our micromechanical experiments, where a nanoparticle-coated glass bead detached from an air bubble. θ is the attached bubble receding contact angle, $R_w$ is radius of the "wet patch", and $R_m$ is the radius of the glass bead.

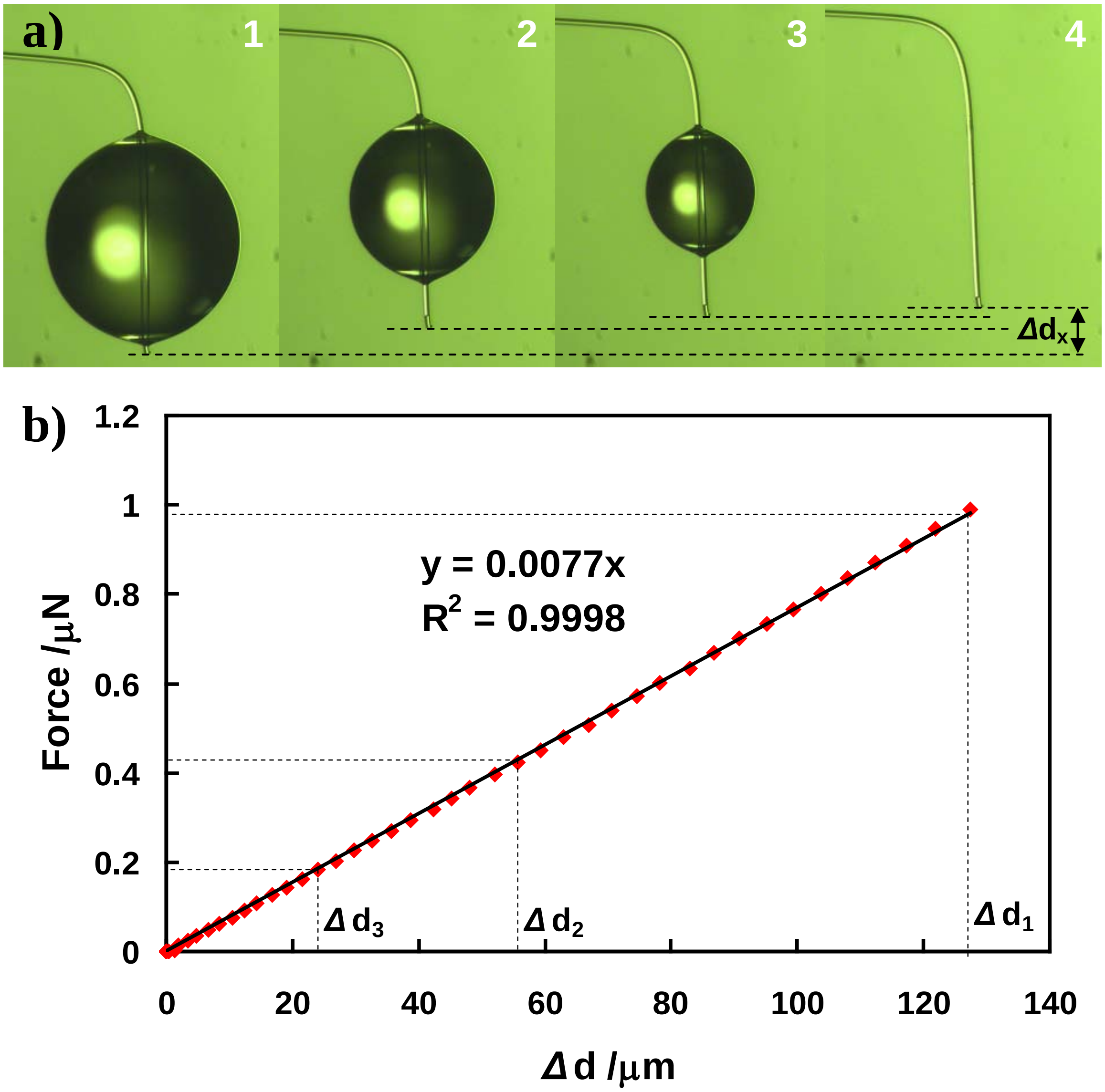

**Figure s2.** Force calibration of the micropipette, expressed as the pipette drag force as a function of pipette displacement. **a)** Photos 1, 2, 3 were taken with the time while water evaporated. Photo 4 was the micropipette reached to the steady-state as water droplet disappeared. **b)** Linear calibration plot of $F_d$ vs. $\Delta$d: the slope equaled 0.0077. This pipette was used to measure the pull-off force for St-01-46 coated glass bead removal from an air bubble.

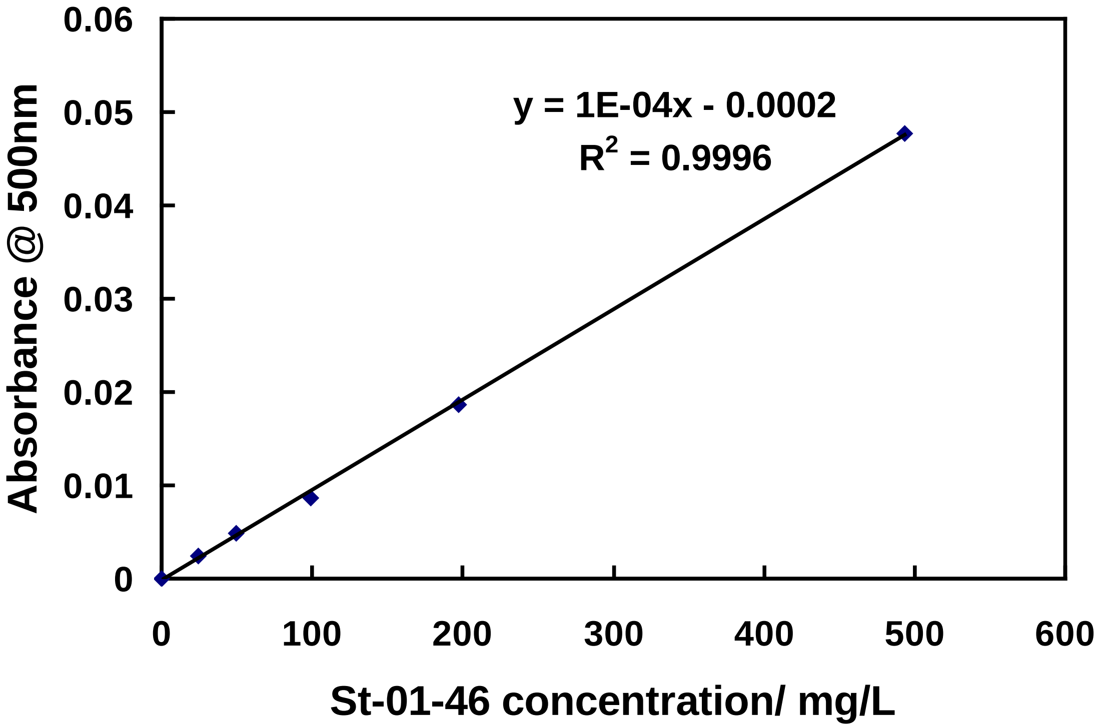

**Figure s3.** The calibration curve used for measuring the extent of St-01-46 covered on glass beads: absorbance at 500 nm versus St-01-46 concentration.

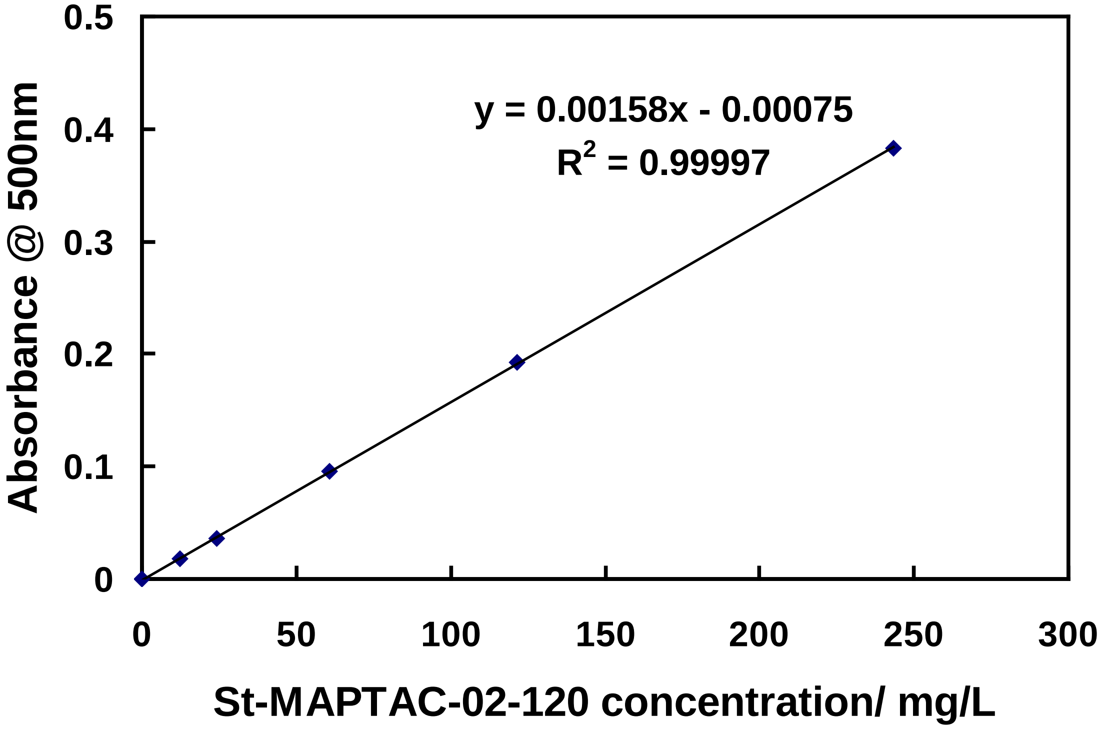

**Figure s4.** The calibration curve used for measuring the extent of St-MAPTAC-02-120 covered on glass beads: absorbance at 500 nm versus St-MAPTAC-02-120 concentration.

# Chapter 3 Nanoparticle Flotation Collectors II: The Role of Nanoparticle Hydrophobicity

In Chapter 3, all of the experiments were performed by myself. I plotted experimental data and wrote the first draft. Dr. Pelton proposed flotation domain showing combinations of mineral particle size and contact angle capable of flotation based on Scheludko's expression. Dr. Pelton helped to analyze data and revise my first draft to this final version.

Langmuir
ARTICLE
pubs.acs.org/Langmuir

# Nanoparticle Flotation Collectors II: The Role of Nanoparticle Hydrophobicity

Songtao Yang and Robert Pelton*

Department of Chemical Engineering, McMaster University, 1280 Main Street West, Hamilton, Ontario, Canada L8S 4L7

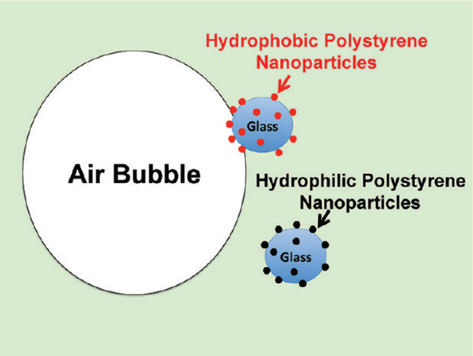

**ABSTRACT:** The ability of polystyrene nanoparticles to facilitate the froth flotation of glass beads was correlated to the hydrophobicity of the nanoparticles. Contact angle measurements were used to probe the hydrophobicity of hydrophilic glass surfaces decorated with hydrophobic nanoparticles. Both sessile water drop advancing angles, $\theta_a$, and attached air bubble receding angle measurements, $\theta_r$, were performed. For glass surfaces saturated with adsorbed nanoparticles, flotation recovery, a measure of flotation efficiency, increased with increasing values of each type of contact angle. As expected, the advancing water contact angle on nanoparticle-decorated, dry glass surfaces increased with surface coverage, the area fraction of glass covered with nanoparticles. However, the nanoparticles were far more effective at raising the contact angle than the Cassie–Baxter prediction, suggesting that with higher nanoparticle coverages the water did not completely wet the glass surfaces between the nanoparticles. A series of polystyrene nanoparticles was prepared to cover a range of surface energies. Water contact angle measurements, $\theta_{np}$, on smooth polymer films formed from organic solutions of dissolved nanoparticles were used to rank the nanoparticles in terms of hydrophobicity. Glass spheres were saturated with adsorbed nanoparticles and were isolated by flotation. The minimum nanoparticle water contact angle to give high flotation recovery was in the range of $51° < \theta_{np_{min}} \leq 85°$.

## INTRODUCTION

Most mineral processing operations include multiple stages of froth flotation to concentrate and isolate the desired product. Typically, ore is ground to give particles that are ~100 $\mu$m in diameter with compositions varying from nearly pure samples of the desired mineral to unwanted gangue. The desired mineral particles are selectively treated with a short-chain, water-soluble surfactant to render the particles sufficiently hydrophobic to attach to air bubbles in the flotation cell.[1] The surfactants, called "collectors", have xanthate or some other headgroup designed to give selective surfactant adsorption and thus hydrophobization of the desired fraction of particles in the ground ore.

Recently, we reported what we believe to be the very first application of nanoparticles as flotation collectors.[2] We replaced the low-molecular-weight, water-soluble surfactant collectors with cationic polystyrene nanoparticles and demonstrated that the nanoparticles induced flotation. We used hydrophilic glass beads as a model for mineral particles. Good flotation recoveries were obtained with as little as 10% surface coverage with the most effective nanoparticles. In addition to flotation results, our first publication reported micromechanical measurements of glass bead/air bubble adhesion. We proposed that nanoparticles increased the contact angle of the mineral particle (or glass bead) surface, facilitating mineral particle attachment to air bubbles.

Nanoparticle design parameters for flotation applications include the particle size, shape, and hydrophobicity. The goal of the work summarized in this article was to determine relationships between nanoparticle hydrophobicity, estimated by contact angle measurements, and the ability of the nanoparticles to promote flotation.

The literature contains many experimental and theoretic studies of contact angle and wetting behaviors of hydrophobic surfaces modified with hydrophobic nanoparticles or nanoscale structures, often giving superhydrophobic behaviors. For example, 2D polystyrene colloidal crystals on hydrophobic substrates display extremely high contact angles.[3−8] With tightly packed hydrophobic spheres on a hydrophobic surface, an advancing sessile drop sits on top of the spheres and does not wet the supporting surface.

In our flotation experiments, hydrophobic nanoparticles adsorb onto hydrophilic mineral surfaces, lowering the surface energy and increasing the contact angle. Surprisingly, we found very few fundamental studies of hydrophilic surfaces decorated with hydrophobic particles. In an early paper, Dettre and Johnson reported the contact angles for hydrophilic glass surfaces decorated with hydrophobic titanium dioxide particles.[9] The water contact angle went from ~25° for untreated glass to ~80° when 10% of the glass surface was covered with hydrophobic $TiO_2$ particles. By contrast, the receding water contact angles were much lower. Takeshita and co-workers described the absorption of cationic latex on PET; in these experiments, both the PET surfaces and the latexes were somewhat hydrophobic, giving relatively small changes in the contact angle.[10]

**Received:** July 18, 2011
**Revised:** August 9, 2011
**Published:** August 10, 2011

Table 1. Recipes for Nanoparticle Preparation and Some Properties of the Resulting Latex, Where the Final Number in the Nanoparticle Designation Is the Average Particle Diameter

| | initial reactor charge (g) | | | | starved-feed charge (g) | | | |
|---|---|---|---|---|---|---|---|---|
| nanoparticle designation | $H_2O$ | St | comonomer or surfactant | V50 | St | comonomer | diameter, nm (PDI)[a] | electrophoretic mobility, $10^{-8}$ $m^2$ $s^{-1}$ $V^{-1}$ (std error)[b] |
| St-01-46 | 100 | 0.5 | 0.10 CTAB | 0.10 | 4.5 | | 46 (0.156) | 1.61 (±0.07) |
| St-01-353 | 100 | 5.0 | | 0.10 | | | 353 (0.097) | 3.42 (±0.27) |
| St-MAPTAC-02-120 | 250 | 5.0 | 0.25 MAPTAC | 0.10 | | | 120 (0.027) | 2.74 (±0.12) |
| St-VBTMAC-03-39 | 100 | 0.5 | 0.30 VBTMAC | 0.06 | 4.5 | 0.90 VBTMAC | 39 (0.177) | 1.79 (±0.10) |
| St-HEMA-04-97 | 100 | 0.5 | 0.10 CTAB | 0.10 | 4.5 | 1.0 HEMA | 97 (0.062) | 1.36 (±0.05) |

[a] Hydrodynamic diameter from DLS using the cumulant model. [b] Measured in 5 mM NaCl at ambient pH.

Herein we report the wetting behaviors of two types of planar surfaces: (1) hydrophilic glass surfaces decorated with more hydrophobic polystyrene nanoparticles (latex) and (2) smooth polymer films formed by spin coating polymer solutions in organic solvents formed by dissolving the nanoparticles. For each type of surface, we performed advancing and receding sessile drop measurements as well as measurements of the receding contact angles formed when bubbles are attached to submerged surfaces. The contact angle measurements were performed as functions of the surface coverage for a series of polystyrene particles with varying hydrophobicity. The wetting results are correlated with the ability of the nanoparticles to induce the flotation of glass beads, thus leading to design criteria for nanoparticle flotation collectors.

## EXPERIMENTAL SECTION

**Materials.** Styrene (99%, Sigma-Aldrich) was purified by vacuum distillation. 3-(Methacryloylamino)propyl trimethyl ammonium chloride solution (MAPTAC, 50 wt % in $H_2O$, Sigma-Aldrich) and 2-hydroxyethyl methacrylate (HEMA, 97%, Sigma-Aldrich) were passed through inhibitor-removing columns. Vinylbenzyltrimethyl ammonium chloride (VBTMAC, 99%), cetyltrimethyl ammonium bromide (CTAB, 95%), and 2,2′-azobis(2-methylpropionamidine) dihydrochloride (V50, 97%) were purchased from Sigma-Aldrich and used as supplied. The frother, UNIFROTH 250C (99%), was donated by Vale Canada (Mississauga, ON). All solutions were made with type 1 water (18.2 MΩ cm, Barnstead Nanopure Diamond system).

**Polymerization.** The recipes used to prepare the nanoparticle suspensions are summarized in Table 1. The polystyrene latex (St-01-353) and the polystyrene-*co*-MAPTAC (St-MAPTAC-02-120) latex were prepared by classic surfactant-free polymerization,[11] whereas St-01-46, St-VBTMAC-03-39, and St-HEMA-04-97 nanoparticle suspensions were prepared by monomer-starved semibatch emulsion polymerization.[12] Detailed descriptions of the polymerizations are given in our first publication.[2]

Nanoparticle hydrodynamic diameters were determined by dynamic light scattering (Brookhaven Instruments Corporation, BIC) using a detector angle of 90°. Correlation data were analyzed by BIC dynamic light scattering software (Windows 9KDLSW version 3.34) using the cumulant model, and the scattering intensity was set between 150 and 250 kcounts/s for each measurement. The duration of each measurement was set to 5 min. Electrophoretic mobility measurements were performed using a Zeta PALS instrument (Brookhaven Instruments Corp.) at 25 °C in phase analysis light scattering mode. The reported mobility values were the average of 10 runs with each consisting of 15 scans. Samples for both dynamic light scattering and electrophoretic mobility measurements were prepared in clean vials by dispersing approximately 0.25 g/L of the polystyrene nanoparticle suspensions in 5 mM NaCl.

**Glass Slide Treatment.** Contact angle measurements (for both sessile water drop methods and the attached bubble method) were performed on glass microscope slides (Gold Line Microscope Slides, VWR), which we assumed had similar surface characteristics to those of the glass beads. Typically, glass microscope slides were cut into approximately 9.5 mm squares, cleaned (Sparkleen detergent, Fisher Scientific), and immersed in ~500 mg/L (for St-01-353) nanoparticle suspension in 5 mM NaCl for times ranging from 30 to 60 min. For smaller nanoparticles (St-01-46, St-MAPTAC-02-120, St-VBTMAC-03-39, and St-HEMA-04-97), the slides were immersed in an ~300 mg/L nanoparticle suspension in 5 mM NaCl for times ranging from 10 to 30 min. The treated slides were then immersed in 1 L of water to remove unbound nanoparticles. Water contact angle measurements were recorded after the slides were air dried.

A series of glass slides with a varying coverage of St-01-46 nanoparticles was prepared by immersing slides into nanoparticle suspensions for fixed times: 10 mg/L (5 and 60 s) and 300 mg/L (10, 30, and 300 s). Usually, two glass slides were prepared under each condition. One slide was used to measure contact angles, and the second one was used to obtain SEM images. The coverage was measured with ImageJ software.

To prepare smooth polymer films for contact angle measurements, dried nanoparticles were dissolved in organic solvent and were spin coated on glass with a SPIN 150 wafer spinner running at 3000 rpm. THF (tetrahydrofuran, certified, Fisher Scientific) was used to prepare St-01-46, St-MAPTAC-02-120, and St-HEMA-04-97 0.65 wt % solutions, whereas St-01-353 was dissolved in chloroform and St-VBTMAC-03-39 was dissolved in DMF (*N*,*N*-dimethylformamide, for HPLC, ≥99.9%, Sigma-Aldrich).

**Contact Angle Measurements.** The water/air contact angle with treated slides was made either by using sessile water drops placed on dry slides or by observing air bubbles attached to never-dried latex-treated glass slides immersed in water. The contact angle measurements were performed using a Krüss contact angle measuring instrument running Drop Shape Analysis (DSA) 1.80.0.2 software.

**Advancing Water Contact Angle ($\theta_a$).** A water drop was formed on the end of a fine glass capillary tube (the tip diameter is ~40 $\mu$m, see next paragraph for preparation), and the drop was contacted with either a dry latex-treated glass slide or a smooth polymer film. Advancing angles were stable and reproducible. Attempts to measure receding angles with a sessile drop were not successful because of pinning when the drop volume was decreased.

**Attached Bubble Receding Contact Angle ($\theta_r$).** To measure the receding contact angle, submerged air bubbles were formed on a thin glass capillary tube. Standard glass capillaries (1 mm/0.58 mm o.d./i.d., Word Precision Instruments Inc., 1B100-6) were elongated using a pipet puller (Narishige Japan, PN-30). An electrical transformer was used to heat a Pt/Ir (90:10 wt %, diameter 0.5 mm) wire at a voltage of 2.0−2.1 V,

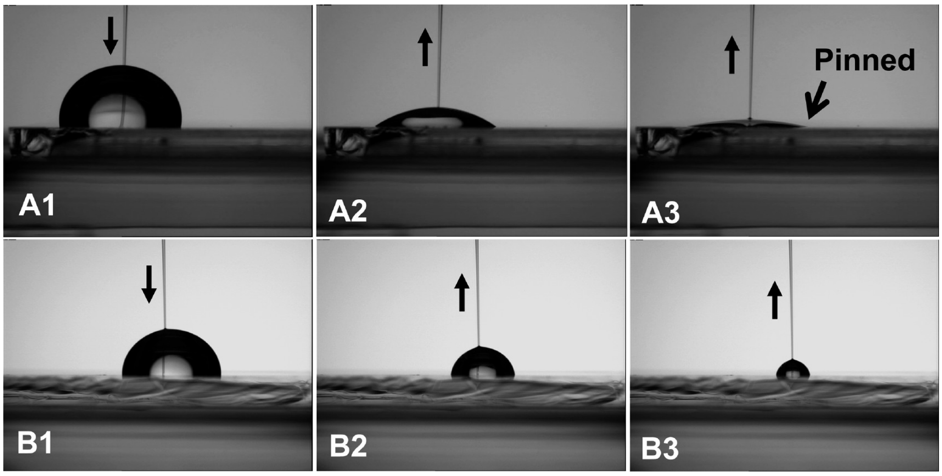

**Figure 1.** Examples of a water drop advancing and then retracting on a glass surface with deposited St-01-46 nanoparticles (frames A1–A3). The three-phase contact line strongly pinned to the surface. Frames B1–B3 show a water drop on a smooth film prepared by spin coating with St-01-46 solution in THF. High contact angles and little pinning are observed.

**Table 2. Contact Angles (CA) of an Attached Bubble Receding and a Water Drop Advancing on a Glass Surface with the Spontaneous Deposition of Various Polystyrene-Based Nanoparticle Collectors and Corresponding Smooth Polystyrene-Based Polymer Films**

| | water contact angle on smooth polymer films | | water contact angle for glass saturated with nanoparticles | |
|---|---|---|---|---|
| nanoparticle designation | sessile drop advancing, $\theta_{npa}$ | bubble attached to immersed film – receding, $\theta_{npr}$ | sessile drop advancing, $\theta_a$ | bubble attached to never-dried surface, $\theta_r$ |
| St-01-46 | 93 ± 2.1 | 91 ± 0.9 | 97 ± 2.9 | 40 ± 1.6 |
| St-01-353 | 88 ± 1.5 | 86 ± 1.6 | 69 ± 3.2 | 29 ± 1.9 |
| St-MAPTAC-02-120 | 86 ± 1.1 | 85 ± 1.7 | 55 ± 0.9 | 23 ± 1.2 |
| St-VBTMAC-03-39 | 71 ± 0.7 | 51 ± 1.5 | 31 ± 2.1 | nonadhering |
| St-HEMA-04-97 | 63 ± 0.9 | 37 ± 2.4 | 22 ± 2.9 | nonadhering |
| glass – no NPs | | | 5.0 ± 2.0 | nonadhering |

and the pipet was bent around the wire at a position approximately 5 to 6 mm from the chokepoint after pulling. The metal wire was then quickly cooled by turning off the transformer and causing the capillary to break cleanly, yielding a capillary with an outer diameter of 20–40 $\mu$m. An air bubble was formed on the capillary and slowly pushed in contact with treated glass slides, transferring the bubble to the surface, yielding a receding contact angle.

**Glass Beads.** Glass beads (30–50 $\mu$m) were purchased from Polysciences Inc. The particle size distributions of the glass beads in $5 \times 10^{-3}$ M NaCl were measured with a Malvern Mastersizer 2000. The particle size distributions were approximately log-normal with an area averaged mean diameter of 43 $\mu$m, a standard deviation of 11 $\mu$m, and a corresponding specific surface area of 0.057 $m^2/g$. The electrophoretic mobility of the beads in 5 mM NaCl at ambient pH was $-4.61$ $(\pm 0.32) \times 10^{-8}$ $m^2$ $s^{-1}$ $V^{-1}$.

**Flotation.** In a typical flotation experiment, 2 g of glass beads and 1.0 mL of nanoparticles (14.6 g/L for St-MAPTAC-02-120) were added to 125 mL of $5 \times 10^{-3}$ M NaCl in a 150 mL plastic flotation beaker, sitting on a 90-mm-diameter plastic Petri dish, which in turn was sitting on a magnetic stirrer (Corning Stirrer, model PC-160). The suspension of glass beads and polystyrene nanoparticles was mixed for 5 min (25 mm × 25 mm cross-shape stirring bar at ~600 rpm) to facilitate polystyrene nanoparticle deposition onto the glass beads. Next, 0.12 mL of 1% UNIFROTH 250C (10 ppm) was added and mixed for 30 additional seconds. Flotation was commenced by initiating nitrogen flow (Matheson 604 E700 flow controller) at a rate of 2.0 L/min through a Corning Pyrex gas dispersion tube (Fisher Scientific, 11-137E) consisting of a 30 mm coarse glass frit attached by a 90° elbow. During flotation, the stirring rate was increased to ~900 rpm to avoid bead sedimentation. The foam phase was scraped over the edge of the beaker and collected in a plastic Petri dish. After 1.0–1.5 min, the gas flow was stopped and the plastic collection dish containing both liquid and beads was weighed; the beads were filtered with a Büchner funnel, dried, and weighed. Typically, each dish contained ~50 mL of the flotation liquor. The flotation results were expressed as the recovery, the mass fraction of beads that was recovered with the froth.

## ■ RESULTS

Five polystyrene-based nanoparticle dispersions were prepared by either surfactant-free emulsion polymerization or starved-feed emulsion copolymerization. Co-monomers were employed to modify the nanoparticle surface properties: MAPTAC or VBTMAC introduced quaternary ammonium cationic groups to supplement cationic amidine groups from the initiator whereas nonionic hydroxyethyl groups from HEMA increased the hydrophilicity of the nanoparticle surfaces. Table 1 summarizes the recipes, particle sizes, and electrophoretic mobilities for the dispersions. The average particle diameters varied from 39

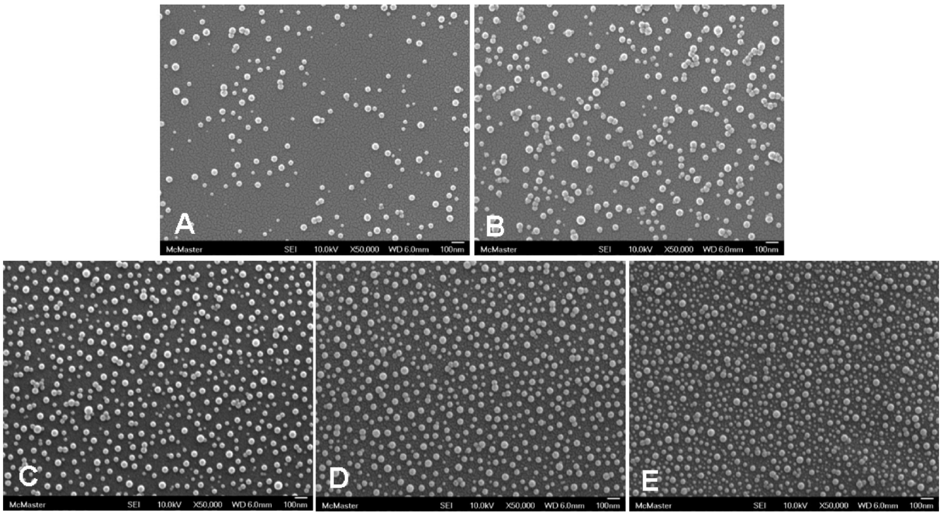

**Figure 2.** SEM images of St-01-46 nanoparticles deposited on glass surfaces with gradually increasing coverage ((A) 5.3%, (B) 13%, (C) 20%, (D) 23%, and (E) 27%) corresponding to the advancing contact angle values shown in Figure 3. Scale bars are 100 nm.

to 353 nm, and all particles had a positive electrophoretic mobility.

Water contact angle measurements were used to rank the hydrophobicities of the five types of nanoparticles. The particles were dissolved in a solvent and spin cast as smooth films on glass. Frames B1−B3 in Figure 1 show examples of a sessile drop on a smooth film made from St-01-46. The advancing contact angles ($\theta_{npa}$) from sessile drop measurements and the receding contact angles from bubbles attached to immersed films ($\theta_{npr}$) are summarized in the left-hand columns of Table 2. For the three most hydrophobic polymer films, the two types of contact angle measurements were in close agreement, whereas the two most hydrophilic films gave a lower receding contact angle when the film was immersed in water. Perhaps the higher content of hydrophilic monomers for the final two polymer films resulted in more surface heterogeneity in the films. We chose the receding contact angle, $\theta_{npr}$, as the most relevant measure of nanoparticle hydrophobicity.

To assess the ability of the nanoparticle collectors to increase the contact angle on mineral surfaces, we performed model experiments in which each nanoparticle collector was deposited onto clean microscope slides on which we could readily measure water contact angles. In these experiments, the anionic surfaces were exposed to excess cationic nanoparticles, ensuring the formation of saturated surfaces. Figure 1A1−A3 shows a sessile water drop placed on a dry glass slide with a saturated monolayer of deposited St-01-46 nanoparticles. The advancing contact angle was high ($\theta_a = 97°$), whereas a receding angle could not be measured because the three-phase contact line was pinned. By contrast, when an air bubble was attached to a submerged, never-dried slide, the receding contact angle was 40° and reproducible. By not allowing the slides to dry after nanoparticle deposition, there was no possibility of trapped air under the tightly packed nanoparticles. The sessile drop advancing angles and the immersed bubble receding angles for all of the nanoparticle-decorated surfaces are summarized in Table 2. For the surfaces treated with the three most hydrophobic nanoparticles, the advancing angles were high and the receding angles were much lower. With the two most hydrophilic particles, we were unable to attach air bubbles to the surfaces to measure a receding angle. Note that the flotation performance with these two more hydrophilic nanoparticle flotation collectors was also very poor.

Clean glass has a low water contact angle whereas glass saturated with the more hydrophobic nanoparticles had a high contact angle. We expected and observed a smooth transition between these states when the contact angle was measured as a function of nanoparticle coverage (i.e., the area fraction of the glass covered with nanoparticles). Figure 2 shows SEM images for a series of glass slides with varying concentrations of St-01-46 nanoparticles. The deposited particles were randomly distributed with little evidence of aggregation. The coverages were measured by image analysis, giving 5.3, 13, 20, 23, and 27%, and the corresponding advancing sessile drop water contact angles were 33, 48, 73, 80, and 97°. Similar measurements were made with St-MAPTAC-02-120, and the results for the two types of nanoparticles are summarized in Figure 3 together with the Cassie−Baxter prediction for St-01-46. Neither of the experimental curves was linear, suggesting that the Cassie−Baxter model was not a good predictor of the contact angle; the failure of this model has been much discussed in the literature.[13] The behavior of St-01-46-decorated glass was particularly deviant. With a surface coverage of less than 30%, the contact angle was approximately equal to the contact angle of a smooth film prepared from St-01-46 (Table 2 and Figure 3). We propose that there are two regimes of behavior for St-01-46. In the first regime, at nanoparticle coverages of up to ∼15%, the interface under the sessile water drop is either a water/nanoparticle interface or a water/glass interface. For the second regime at higher nanoparticle coverages, we propose that there are some areas of glass between closely spaced particles that are not wetted when the sessile drop is placed on the dry surface, giving an air/water interface that is typical of superhydrophobic surfaces.[14,15] The following paragraphs present the influence of nanoparticle coverage and hydrophobicity on the contact angle and flotation efficiency.

The extent of nanoparticle coverage controls the contact angle (Figure 3) and thus the flotation recovery. Figure 4 shows the glass bead recovery as functions of advancing water contact angle St-01-46 and St-MAPTAC-02-120 nanoparticle-treated glass. These curves were constructed by combining experimental flotation recovery versus nanoparticle coverage data with the corresponding

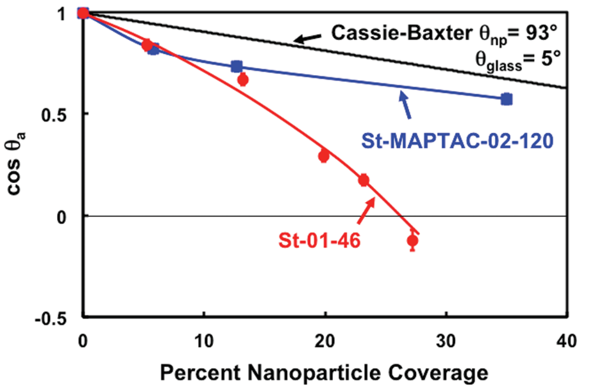

**Figure 3.** Advancing sessile drop water contact angles as functions of the coverage for two types of polystyrene nanoparticles on glass. Neither system shows Cassie−Baxter behavior; we propose that the St-01-46 behavior is explained by trapped air.

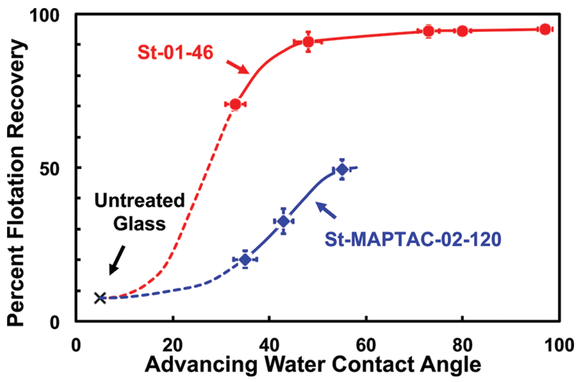

**Figure 4.** Influence of the advancing water contact angle on flotation recovery. The plots were constructed from plots of flotation recovery versus nanoparticle coverage and contact angle versus coverage.

contact angle versus coverage data. The low recovery value for untreated glass corresponded to hydrolytic entrainment where a few beads are carried over with the aqueous phase. Clearly, St-01-46 is a more potent flotation collector than St-MAPTAC-02-120, even when compared at the same contact angle. For both nanoparticles, the maximum recovery occurred when the advancing contact angle was ∼50°.

The hydrophobicity of the nanoparticles, ranked by $\theta_{npr}$, also influences the contact angle and thus the flotation recovery. The five types of nanoparticles in Table 1 were prepared to span the range from hydrophilic to hydrophobic surfaces. Figure 5 shows the percentage of the added glass beads recovered in the froth as a function of three types of contact angles presented earlier and summarized in Table 2. Both the flotation and the contact angle experiments were conducted under conditions where the glass surfaces (spheres for flotation and slides for the contact angle) were saturated with adsorbed nanoparticles. All of the contact angle measurements were made with pure water, whereas our flotation measurements were made with a frother solution of $5 \times 10^{-3}$ M NaCl and 10 mg/L frother, a nonionic surfactant. The advancing water contact angle of the St-01-46 smooth polymer film decreased from 93° for water to 85° with frother solution, and the attached bubble receding contact angle decreased from 91° in water to 78° in the frother solution. Also, the surface tension of water decreased by about 3 mN/m with frother addition. Frothers are designed to enhance the froth stability while having a minimum negative impact on the ability of collectors to increase the mineral hydrophobicity. This seems to be the case herein.

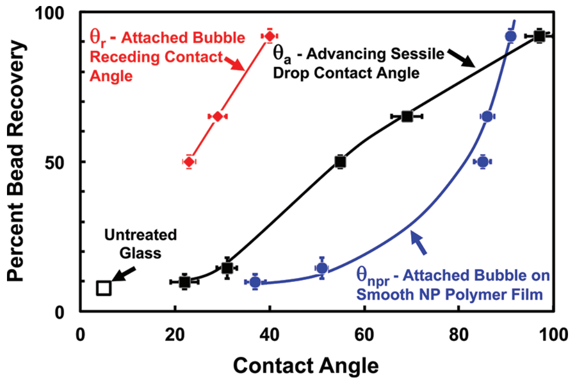

**Figure 5.** Flotation performance of glass beads saturated with adsorbed polystyrene nanoparticles as functions of three types of contact angles measured on glass slides: $\theta_a$ and $\theta_r$ measured with a saturated coating of adsorbed nanoparticles on glass and $\theta_{npr}$ measured by attaching an air bubble to a submerged smooth polymer film. The data points correspond to the five nanoparticles described in Table 1 plus a control experiment with no nanoparticles.

Although each type of contact angle measurement in Figure 5 gave a different value for a given nanoparticle type on glass, the three curves representing the three types of contact angles lead to the same conclusion—the more hydrophobic the nanoparticles, the greater the flotation recovery. With respect to designing nanoparticle flotation collectors, the smooth-cast polymer film receding water contact angle ($\theta_{npr}$) is the most relevant parameter because it should be directly related to the polymer composition. In this approach, we are making the assumption that the surface chemistry of the films cast from polymer solutions is the same as the surfaces of the parent nanoparticles. The results in Figure 5 suggest that the threshold polymer film contact angle for flotation is between 51 and 85°. The three most effective nanoparticles have closely grouped contact angles, whereas the flotation recovery covered a broad range (50 to 92%).

## ■ DISCUSSION

The main objective of our work was to determine the relationship between nanoparticle hydrophobicity and flotation recovery. Optimizing nanoparticle collector properties involves balancing opposing goals. On one hand, the increasing nanoparticle hydrophobicity is likely to improve the flotation recovery. On the other hand, hydrophilic nanoparticles are more colloidally stable than their hydrophobic counterparts. Nanoparticle aggregation needs to be avoided because we expect that heavily aggregated nanoparticles will not be effective collectors. The results in Figure 5 suggest that the contact angle of a nanoparticle surface, $\theta_{npr}$, should be greater than 50°. A surfactant-free polystyrene latex with little or no hydrophilic comonomer satisfies this condition.

The ability of adsorbed nanoparticles to increase their contact angle on mineral surfaces depends on the intrinsic hydrophobicity of the polymer particle surfaces, $\theta_{npr}$, and on the coverage (fraction of the surface covered with particles). The results in Figure 5 were obtained with surfaces saturated with adsorbed nanoparticles. However, it is unlikely that entirely painting mineral surfaces with nanoparticles is economically feasible. Therefore, like conventional molecular collectors, the nanoparticles must function at far below monolayer coverage. The advancing contact angle results for St-01-46 in Figure 3 correspond to a contact angle of 73° at 20% coverage. Dettre and Johnson reported similar results for glass treated with hydrophobic $TiO_2$ nanoparticles.[9]

There appears to be a consensus in the flotation literature that there exists a threshold contact angle required for flotation and that this minimum depends on system specifics including the mineral particle size, hydrodynamic environment, mineral shape, bubble size, and so forth.[16−19] For example, Kitchener[20] reported a threshold contact angle of 30° for quartz particle flotation. Gardner and Woods reported that a threshold contact angle of close to 55° was required for the good flotation recovery of gold spheres.[21] Crawford and Ralston reported a critical threshold value of the advancing water contact angle as a function of the particle size for hydrophobized quartz. For example, 40 $\mu$m quartz particles required a contact angle of 25°.[17] The early work of Gaudin reported a critical contact angle of approximately 50° for galena flotation (Figure 4 in Fuerstenau's book).[1] In summary, the threshold contact angles for flotation in this brief overview ranged from 25 to 55°; these are not superhydrophobic surfaces. Finally, in a recent review Chau et al. conclude "So far, there is no rigid quantitative correlation of contact angle on flotation rate recovery."[22] Nevertheless, our advancing water contact angle results in Figures 4 and 5 suggest that angles in the range of 30−40° are required for flotation. This is consistent with previous studies involving molecular collectors.

It has long been recognized that very small and very large mineral particles cannot be separated by flotation. Very small particles are unable to attach to air bubbles, and very large particles are too heavy to be supported by capillary forces. In their classic analysis of flotation theory, Scheludko et al. gave expressions for the minimum and maximum sizes of floatable particles; both expressions include a term for the contact angle.[23] For example, the following expression gives the maximum diameter, $D_{\max}$, that can be floated where $\gamma$ is the surface tension, $\theta$ is the contact angle, and $\Delta\rho$ is the density difference between water and the mineral particle. Particles larger than $D_{\max}$ are too heavy to be supported by an air bubble.

$$D_{\max} = 2\sqrt{\frac{3\gamma}{2\Delta\rho g}}\sin\left(\frac{\theta}{2}\right) = \alpha \sin\left(\frac{\theta}{2}\right) \qquad (1)$$

Scheludko's expression for the lower particle limit is given by eq 2, where $V$ is the bubble ascent velocity and $K$ is the line tension. According to Drelich and Miller, this expression has been less successful at predicting experimental results because of the uncertainty in $K$;[18] they give an alternative expression that appears to be better but does require contact angle data as a function of the air bubble radius.[19]

$$\begin{aligned} D_{\min} &= 2\left[\frac{3K^2}{V^2\Delta\rho\gamma(1-\cos(\theta))}\right]^{1/3} \\ &= \beta\left(\frac{1}{1-\cos(\theta)}\right)^{1/3} \qquad (2) \end{aligned}$$

Scheludko and subsequently Crawford and Ralston and other authors[19] have used these or similar equations to calculate $D_{\min}$ and $D_{\max}$ as functions of the contact angle, giving flotation domain maps. We used eq 1 to calculate $D_{\max}$ as a function of the contact angle, and the result is shown in Figure 6. Also shown is a $D_{\min}$ curve giving the boundaries for the values of the mineral particle diameter and contact angle, which can be floated. The black squares correspond to experimental points for the advancing contact angle data, $\theta_a$, in Figure 5, and the numbers beside two of the squares give the corresponding flotation recovery for our 43-$\mu$m-diameter glass beads. We did not have values for $K$ or $V$ in our experiments to apply to eq 2, so we arbitrarily chose a value of $\beta$ so that the $D_{\min}$ boundary line separated the low flotation recovery points from the high flotation recovery points.

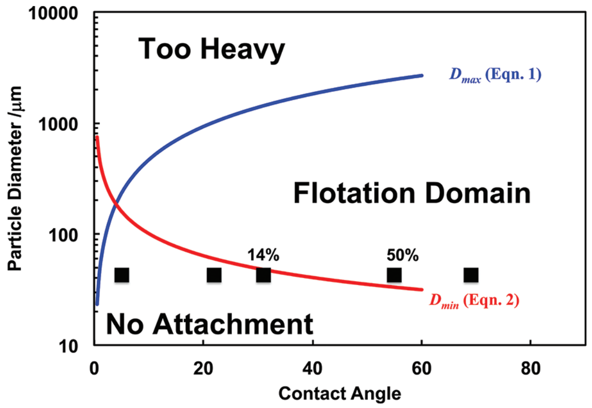

**Figure 6.** Flotation domain showing combinations of the mineral particle size and contact angle capable of flotation based on the analysis of Scheludko[23] using $\alpha = 5343$ $\mu$m for $D_{\max}$, corresponding to our experiments. $\beta = 25$ $\mu$m for $D_{\min}$ was chosen to divide low and high recovery data. The black squares correspond to the advancing water contact angle, $\theta_a$, from Figure 5, and labels indicate the flotation recovery.

The modeling in Figure 6 suggests that for the results in Figure 5 the transition from low to high flotation recovery corresponds to crossing the $D_{\min}$ line. This in turn suggests that for our relatively small 43 $\mu$m glass particles, bubble attachment in the presence of nanoparticles dictates the minimum combination of nanoparticle coverage and nanoparticle hydrophobicity, giving the minimum contact angle required for flotation. By contrast, Figure 6 predicts that for glass particles >∼200 $\mu$m, $D_{\max}$ dictates the minimum required contact angle for flotation. For our results, the comparison of modeling with data cannot be pushed too far because the contact angle measurements in Figures 4 and 5 were performed with pure water whereas the flotation results were performed in the presence of frother. In the Results section, we showed that advancing and receding angles are a little lower in the presence of frother.

In this article, we have focused on the role of nanoparticle hydrophobicity and its impact on the contact angle of nanoparticle-decorated glass. However, the set of nanoparticles in Table 1 spanned particle sizes from 39 to 353 nm. In a future contribution, we will show that although the particle size has a large influence on nanoparticle transport and deposition rates onto mineral surfaces, the influence of nanoparticle size is minor for the flotation recovery of beads saturated with nanoparticles when compared at constant coverage.

The industrial application of nanoparticle flotation collectors requires that the nanoparticles must specifically bind to the desired mineral-rich particles and not to unwanted gangue material. An upcoming conference proceeding in the mineral-processing literature will demonstrate the design of nanoparticle surface chemistry to give specific nanoparticle deposition onto nickel ore (pentlandite) surfaces.[24]

## CONCLUSIONS

Contact angle measurements were used to relate the nanoparticle surface properties to their ability to promote the froth flotation of hydrophilic glass beads. The main conclusions from this work are the following:

(1) The wetting behaviors of nanoparticle-decorated glass depend upon the sample history. Starting with dried surfaces, classic sessile drop measurements, $\theta_a$, gave high advancing angles and indeterminable receding angles because of pinning. By contrast, when the glass surfaces were never dried after hydrophobic nanoparticle deposition, the corresponding receding water contact angles that formed by attached bubbles, $\theta_r$, were reproducible.

(2) Water contact angles on smooth polymer films, formed by spin coating polymer solutions in an organic solvent, were used as a measure of nanoparticle hydrophobicity, and for high flotation recovery, the minimum contact angle for flotation was $51° < \theta_{npr} \leq 85°$ for glass surfaces saturated with adsorbed nanoparticles.

(3) The advancing contact angle on dried glass surfaces increased with nanoparticle coverage. However, the Cassie—Baxter model failed to fit the results, possibly because of some trapped air between the nanoparticles under the sessile drop when the nanoparticle coverage was >15%.

(4) The minimum advancing water contact angle (dried, nanoparticle-decorated glass) for high flotation recovery with nanoparticle collectors is in the range of 30—40°, which is in accord with published results for molecular collectors.

(5) Poor flotation recoveries were observed when the nanoparticles were too hydrophilic or when the coverage was too low. Conventional flotation models suggest that the small 43 $\mu$m glass beads failed to attach to air bubbles in these cases.

## AUTHOR INFORMATION

### Corresponding Author

*E-mail: peltonrh@mcmaster.ca.

## ACKNOWLEDGMENT

We thank the Centre for Materials and Manufacturing (CMM), a division of the Ontario Centres of Excellence (OCE) in collaboration with VALE Base Metals, for funding, VALE Base Metals Technology Development for funding, and Zongfu Dai and Manqiu Xu from Vale for much help, samples, and advice. Finally, we acknowledge Adam Raegen and Kari Dalnoki-Veress from McMaster University for discussions.

## REFERENCES

(1) Fuerstenau, M.; Jameson, G.; Yoon, R. *Froth Flotation: A Century of Innovation*; Society for Mining, Metallurgy, and Exploration: Littleton, CO, 2007.

(2) Yang, S.; Pelton, R.; Raegen, A.; Montgomery, M.; Dalnoki-Veress, K. Nanoparticle Flotation Collectors: Mechanisms Behind a New Technology. *Langmuir* **2011**, *27*, doi: 10.1021/la2016534

(3) Shiu, J.-Y.; Kuo, C.-W.; Chen, P.; Mou, C.-Y. Fabrication of Tunable Superhydrophobic Surfaces by Nanosphere Lithography. *Chem. Mater.* **2004**, *16*, 561–564.

(4) Yan, L.; Wang, K.; Wu, J.; Ye, L. Hydrophobicity of Model Surfaces with Loosely Packed Polystyrene Spheres after Plasma Etching. *J. Phys. Chem. B* **2006**, *110*, 11241–11246.

(5) Watanabe, M.; Kawaguchi, S.; Nagai, K. Self-Organization of Polymer Particles on Hydrophobic Solid Substrates in Aqueous Media. II. Self-Organization of Cationic Polymer Particles on Polymer Films and Wettability Control with Particle Monolayers. *Colloid Polym. Sci.* **2007**, *285*, 1139–1147.

(6) Yan, L.; Wang, K.; Wu, J.; Ye, L. Hydrophobicity of Model Surfaces with Closely Packed Nano- and Micro-Spheres. *Colloids Surf., A* **2007**, *296*, 123–131.

(7) Synytska, A.; Ionov, L.; Dutschk, V.; Stamm, M.; Grundke, K. Wetting on Regularly Structured Surfaces from "Core—Shell" Particles: Theoretical Predictions and Experimental Findings. *Langmuir* **2008**, *24*, 11895–11901.

(8) Synytska, A.; Ionov, L.; Grundke, K.; Stamm, M. Wetting on Fractal Superhydrophobic Surfaces from "Core—Shell" Particles: A Comparison of Theory and Experiment. *Langmuir* **2009**, *25*, 3132–3136.

(9) Dettre, R. H.; Johnson, R. E. Contact Angle Hysteresis. IV. Contact Angle Measurements on Heterogeneous Surfaces$^1$. *J. Phys. Chem.* **1965**, *69*, 1507–1515.

(10) Takeshita, N.; Paradis, L. A.; Öner, D.; McCarthy, T. J.; Chen, W. Simultaneous Tailoring of Surface Topography and Chemical Structure for Controlled Wettability. *Langmuir* **2004**, *20*, 8131–8136.

(11) Goodwin, J. W.; Ottewill, R. H.; Pelton, R. Studies on the Preparation and Characterization of Monodisperse Polystyrene Lattices 0.5. Preparation of Cationic Lattices. *Colloid Polym. Sci.* **1979**, *257*, 61–69.

(12) Sajjadi, S. Nanoparticle Formation by Monomer-Starved Semibatch Emulsion Polymerization. *Langmuir* **2006**, *23*, 1018–1024.

(13) Wang, J.; Bratko, D.; Luzar, A. Probing Surface Tension Additivity on Chemically Heterogeneous Surfaces by a Molecular Approach. *Proc. Natl. Acad. Sci. U.S.A.* **2011**, *108*, 6374–6379.

(14) Li, X.-M.; Reinhoudt, D.; Crego-Calama, M. What Do We Need for a Superhydrophobic Surface? A Review on the Recent Progress in the Preparation of Superhydrophobic Surfaces. *Chem. Soc. Rev.* **2007**, *36*, 1350–1368.

(15) Tuteja, A.; Choi, W.; McKinley, G. H.; Cohen, R. E.; Rubner, M. F. Design Parameters for Superhydrophobicity and Superoleophobicity. *MRS Bull.* **2008**, *33*, 752–758.

(16) Trahar, W. A Rational Interpretation of the Role of Particle Size in Flotation. *Int. J. Miner. Process.* **1981**, *8*, 289–327.

(17) Crawford, R.; Ralston, J. The Influence of Particle Size and Contact Angle in Mineral Flotation. *Int. J. Miner. Process.* **1988**, *23*, 1–24.

(18) Drelich, J.; Miller, J. D. The Effect of Surface Heterogeneity on Pseudoline Tension and the Flotation Limit of Fine Particles. *Colloids Surf.* **1992**, *69*, 35–43.

(19) Chipfunhu, D.; Zanin, M.; Grano, S. The Dependency of the Critical Contact Angle for Flotation on Particle Size - Modelling the Limits of Fine Particle Flotation. *Miner. Eng.* **2011**, *24*, 50–57.

(20) Anfruns, J. F.; Kitchener, J. A. Rate of Capture of Small Particles in Flotation. *Trans. Inst. Min. Metall., Sect. C* **1977**, *87*, C81–C82.

(21) Gardner, J.; Woods, R. Electrochemical Investigation of Contact Angle and of Flotation in the Presence of Alkylxanthates. I. Platinum and Gold Surfaces. *Aust. J. Chem.* **1974**, *27*, 2139–2148.

(22) Chau, T. T.; Bruckard, W. J.; Koh, P. T. L.; Nguyen, A. V. A Review of Factors That Affect Contact Angle and Implications for Flotation Practice. *Adv. Colloid Interface Sci.* **2009**, *150*, 106–115.

(23) Scheludko, A.; Toshev, B. V.; Bojadjiev, D. T. Attachment of Particles to a Liquid Surface (Capillary Theory of Flotation). *J. Chem. Soc., Faraday Trans. 1* **1976**, *72*, 2815–2828.

(24) Pelton, R.; Yang, S.; Xu, M.; Dai, Z. *Nanoparticle Flotation Collectors — Innovation from Collaboration*. COM 2011, Conference of Metallurgists, Montreal, 2011.

# Chapter 4 Nanoparticle Flotation Collectors III: Factors Influencing Nanoparticle Deposition

In Chapter 4, all of the experiments were performed by myself and Mile Montgomery who worked with me as a summer student. I plotted all data and wrote the first draft. Miles helped to edit some parts of the English. Dr. Pelton helped to analyze data, give many suggestions for calculation and edit some parts of the draft to this version. Yuguo Cui contributed many helpful discussions on my experiments and data analysis.

# Nanoparticle Flotation Collectors III – Factors Influencing Nanoparticle Deposition

*Songtao Yang*[†], *Robert Pelton*[†,*], *Miles Montgomery*[†] *and Yuguo Cui*[†]

[†]Department of Chemical Engineering, McMaster University, 1280 Main Street West,
Hamilton, Ontario, Canada L8S 4L7

Corresponding author: peltonrh@mcmaster.ca

**Possibly will be submitted to: *Ind. Eng. Chem. Res. /Colloids and Surfaces A***

## Abstract

This paper investigates the major factors influencing nanoparticle deposition onto target mineral surfaces with respect to using nanoparticles as flotation collectors. Various polystyrene based nanoparticles with diameters ranging from 46 nm to 2.2 μm were evaluated for floating a series of hydrophilic glass beads. Deposition kinetics of nanoparticles onto silica has been measured by quartz crystal microbalance (QCM). Nanoparticle initial dosage, conditioning time, and nanoparticle size have been identified to be important for the extent of nanoparticle deposition onto silica surfaces. The extent of nanoparticle deposition, nanoparticle surface charge and nanoparticle hydrophobicity were important parameters for flotation recoveries. Langmuir kinetics model has been used to predict the deposition kinetics and estimate deposition rate constant of the QCM experiments. Cox-Brenner equation was used to estimate the nanoparticle detachment forces from silica surface in the QCM module. Derjaguin-Landau-Verwey-Overbeek (DLVO) theory was used to explain the driving forces in directing nanoparticle deposition onto silica surfaces.

## Introduction

Froth flotation is an important process for the concentration and isolation of valuable minerals in the mineral processing industry. Typically, ore is crushed and ground to approximately 100 micrometer diameter particles some rich in the desired mineral together with large quantities of unwanted gangue particles. The desired mineral-rich particles are subsequently isolated by froth flotation where the mineral particles in an aqueous suspension adhere onto air bubbles and are isolated with the froth. A critical aspect of froth flotation is the need to specifically treat the desired particle surfaces with a chemical reagent, called a “collector”. The collector functions to selectively render the mineral particles surfaces to be more hydrophobic than the unwanted gangue particles. Conventional collectors are water-soluble surfactants with short hydrophobic tails and specific head groups, such as xanthate, which are designed to give selective adsorption onto the desired fraction of mineral-rich particles from the ground ore. [1-2]

Recently, we have demonstrated that water-soluble collectors can be replaced by hydrophobic polystyrene nanoparticles leading to the first reported use of nanoparticles as flotation collectors. [3-4] Hydrophilic glass beads were used to simulate mineral particles in our study. Our first published paper investigated the mechanisms behind the application of nanoparticle collectors, including flotation results facilitated with the use of nanoparticles and micromechanical measurements of glass bead/air bubble adhesion. [3] We also reported water contact angle measurements on smooth polymer films cast from dissolved parent nanoparticles, which correlated the hydrophobicity of polystyrene based nanoparticles with their ability to facilitate glass bead flotation. We showed that it was required for a polymer film contact angle to be at least in the range from 51° to 85° for a good flotation recovery. [4] However, a number of critical questions for the application of “nanoparticle flotation collectors” remain unanswered. For example, how fast can the nanoparticles adsorb onto the targeted mineral surfaces; are surface charges of the nanoparticles important; do the nanoparticles stick to the air bubbles as well; if so, would nanoparticles on the bubbles interfere with flotation results?

There are several obvious design parameters that influence the efficiency of nanoparticle flotation collectors such as: nanoparticle diameter, nanoparticle shape, nanoparticle softness, nanoparticle surface energy, and the density of nanoparticles adsorbed on the mineral particle surface. Several of these factors are interrelated. The density of nanoparticles adsorbed on a mineral surface should depend upon initial nanoparticle concentration, the nanoparticle deposition rate, conditioning time, and so on. The goal of the current work is to determine the major factors influencing nanoparticle deposition onto glass surfaces and further correlate how these factors affect floating glass beads with the use of nanoparticle collectors.

A number of early studies have reported the deposition behaviour of larger particles (e.g., from 0.5 μm to a few micrometers in diameter) onto solid surfaces. [5-8] In these cases, the deposition was reversible under certain conditions. For example, the detachment was readily observed under high hydrodynamic forces. [9] The particle size is important in the study of particle deposition or aggregation. Usually 1 μm is a traditional and convenient dividing dimension. Colloidal interaction arising from the electric double layer is predominated when particle size is less than 1 μm, whereas external forces such as hydrodynamic or gravitational forces become dominant when particles exceed 1 μm. [9] The deposition and detachment kinetics for large colloidal particles (i.e. > 1 μm) were usually determined by a combination of both colloidal and hydrodynamic factors. [8]

There have been several papers published recently where a quartz crystal microbalance (QCM) was used to directly follow nanoparticle (< 1 μm) deposition. For example, Fatisson and coworkers reported the deposition of $TiO_2$ nanoparticles onto silica over a broad range of solution conditions; in their study, higher deposition rates were observed in the presence of attractive electrostatic interaction in contrast to unfavorable deposition conditions where electrostatic repulsion dominated particle-surface interactions. [10] Similar studies were reported on the deposition kinetics of various inorganic/organic nanoparticles. [11-15] The relevant conclusions in their studies include: electrostatic interaction was the major driving force for the deposition; the aqueous chemical environment (i.e., pH, ionic strength) was important; deposition was shown to be typically irreversible at ambient condition; Langmuir kinetics model can be applied to explain the simple case of nanoparticle deposition kinetics; the behavior of deposition and aggregation obeyed Derjaguin-Landau-Verwey-Overbeek (DLVO) theory of colloidal stability.

In this study, we report our recent investigations on influential factors affecting the application of "nanoparticle flotation collectors" which relates to our previous publications [3-4]. Efforts presented here are to use various polystyrene nanoparticles to promote floating a series of hydrophilic glass beads. Specifically, we evaluated the influence of conditioning time, nanoparticle dosage, nanoparticle coverage, nanoparticle size, and nanoparticle surface charges on the flotation recovery of the glass beads. We also investigated the re-flotation performance of dried recovered glass beads from an original flotation with nanoparticle collectors. Deposition kinetics of a series of typical nanoparticles (ranging from 46 nm to 262 nm in diameter) onto silica has been monitored by QCM. The direct observation of nanoparticles deposition could lead to important insights into the application of nanoparticle flotation collectors.

## Experimental Section

**Materials:** Styrene (St, 99%, Sigma-Aldrich) was purified by vacuum distillation. [3-(methacryloylamino)propyl]trimethylammonium chloride solution (MAPTAC, 50 wt. % in $H_2O$, Sigma-Aldrich) was passed through an inhibitor-removing column. 2, 2'-Azobis (2-methylpropionamidine) dihydrochloride (V50, 97%) and ammonium persulfate (APS, 99%), and cetyltrimethylammonium bromide (CTAB, 95%) were all purchased from Sigma-Aldrich and used as supplied. Surfactant-free amidine white polystyrene latexes (0.76 μm and 2.5 μm, 4% solids) were purchased from Interfacial Dynamics Corporation (IDC, Eugene, OR). Fluorescein dimethacrylate (Fluorescein) was purchased from Polysciences, Inc. and used as supplied. The frother, UNIFROTH 250C (consisting of 60-100% polypropylene glycol methyl ether and 13-30% dipropylene glycol monomethyl ether), was donated by Vale Canada (Mississauga, ON). All solutions were made with Type 1 water (18.2 MΩcm, Barnstead Nanopure Diamond system).

**Polymerization and Characterization:** The recipes used to prepare the nanoparticle dispersions are summarized in Table 1. The surfactant-free polystyrene latex (St-01-353, St-01-262, St-01-F-292, and St-02-280) and the polystyrene-co-MAPTAC (St-MAPTAC-02-120) latex were prepared by classic surfactant free polymerization [16], whereas St-01-46, St-MAPTAC-03-79 and St-MAPTAC-03-F-81 nanoparticle dispersions were prepared by monomer-starved semibatch emulsion polymerization.[17] Details of the polymerizations are the same as described in our previous publication. [3]

Hydrodynamic diameters of prepared polystyrene nanoparticles were measured by dynamic light scattering (DLS, Brookhaven Instruments Corporation) using a detector angle of 90°. Correlation data were analyzed by the DLS software (Windows 9KDLSW Version 3.34) using the cumulant fit method and the scattering intensity was set between 150 and 250 kcounts/s for each measurement. The duration for each measurement was set to 5 min. Transmission electron microscopy (TEM) was used to acquire high resolution images of St-01-46, St-MAPTAC-03-120 and St-01-262 dispersions for the confirmation of their particle size distributions. TEM images were recorded using a JEOL 1200EX TEMSCAN microscope. A drop of the nanoparticle dispersion was dropped on a Formvar-coated copper TEM grid and air dried overnight prior to analysis. Electrophoretic mobility measurements were performed by a Zeta PALS instrument (Brookhaven Instruments Corporation) at 25 °C in phase analysis light scattering mode. The reported mobility values were the average of 10 runs, each consisting of 15 scans. Samples for both dynamic light scattering and electrophoretic mobility measurements were prepared in clean vials by dispersing approximately 0.25 g/L of polystyrene nanoparticles in 5 mM NaCl. Sample pH was adjusted with 0.01 M or 0.1 M HCl and NaOH. Similarly, the purchased surfactant-free amidine polystyrene latex (0.76 μm and 2.5 μm ones, designated as St-01-678 and St-01-2227) were also measured with the DLS and electrophoretic mobility.

To measure the hydrophobicity of the nanoparticle surfaces, dried nanoparticles were dissolved in THF (tetrahydrofuran, certified, Fisher Scientific) or chloroform (for HPLC, ≥99.9%, Sigma-Aldrich), 0.5-1.0 wt%, and spin coated on glass with a SPIN 150 Wafer Spinner (running rev: 3.25 software) at 3000 rpm to form smooth polymer films. Water contact angle measurements were performed on the smooth polymer films using a Krüss contact angle measuring instrument running Drop Shape Analysis (DSA) 1.80.0.2 software. More details of the methodology could be found elsewhere. [4]

**Glass Beads:** Glass beads (30-50 μm) were purchased from Polysciences, Inc. Glass beads, acid-washed (≤106 μm, -140 U.S. sieve); unwashed (≤106 μm, -140 U.S. sieve); and unwashed (150-212 μm, 70-100 U.S. sieve) were all purchased from Sigma-Aldrich. The particle size distributions of the three size-distributed glass beads [30-50 μm, ≤106 μm (both acid-washed and unwashed), and 150-212 μm] in 5 mM NaCl were characterized by a Malvern Mastersizer 2000. The reported size distributions were the average of three repeated measurements for each suspension. The glass beads suspension was prepared by adding the beads into 5 mM NaCl until the obscuration level was within the required apparatus obscuration range.

**Flotation:** In a typical flotation experiment 2 g glass beads and 1.0 mL of polystyrene nanoparticle (27.15 g/L for St-01-353) were added into 125 mL of 5 mM NaCl in a 150 mL plastic flotation beaker, sitting on a 90 mm diameter plastic Petri dish, which in turn was sitting on a magnetic stirrer (Corning Stirrer, Model PC-610). The suspension of glass beads and polystyrene nanoparticles was mixed (conditioned) for 5 minutes (25 mm×25 mm cross-shape stirring bar at ~ 600 RPM) to facilitate polystyrene nanoparticles deposition onto the glass beads. Following conditioning, 0.12 mL of 1% UNIFROTH 250C (10ppm) was added and mixed for an additional 30 seconds. Flotation was commenced by initiating nitrogen flow (Matheson 604 E700 Flow Controller) at a rate of 2.0 L/min through a Corning Pyrex gas dispersion tube (Fisher Scientific, 11-137E) consisting of a 30 mm coarse glass frit attached by a 90 degrees elbow. During flotation the stirring rate was increased to ~ 900 RPM to avoid bead sedimentation. The foam phase was scraped over the edge of the beaker and collected in a plastic Petri dish. After 1.0-1.5 minutes the gas flow was stopped, the plastic collection dish was replaced with a clean dish, and the liquid level in the flotation beaker was topped up with UNIFROTH 250C in 5 mM NaCl at the original concentration. In most of our flotation cases, this sequence was repeated until 3~5 dishes were collected, which is in accordance to commercial incremental flotation runs. The mass of liquid and beads collected in each dish was measured; the beads were filtered with a Büchner funnel, dried and weighed. Typically each dish contained 50-60 mL of flotation liquor. Flotation results were expressed as the recovery which was calculated from the mass fraction of beads collected in the dishes.

Control flotation experiments were conducted with nanoparticles only or glass beads only instead of the mixture of nanoparticles and glass beads.

A UV-vis spectrometer (Beckman Coulter, DU800) was used to measure the concentration of nanoparticle dispersion before and after each of the flotation runs. The extent of nanoparticle deposition on the glass beads was obtained by measuring the absorbance of the supernatant nanoparticle dispersion at 500 nm before and after deposition on the glass beads. The quantity of deposited latex was calculated using a calibration curve of absorbance versus nanoparticle concentration.

Re-flotation experiments of dried recovered glass beads with nanoparticle runs were performed. Dried recovered glass beads were collected from the 3~5 cumulative products of a flotation run using nanoparticles (e.g., St-MAPTAC-03-79). Total weights of collected glass beads were measured before re-dispersing them into the 150 mL plastic flotation beaker with 125 mL of 5 mM NaCl. Next, 0.12 mL of 1% UNIFROTH 250C was added and conditioned for 30 seconds, and the subsequent flotation procedures as aforementioned were repeated.

Images of recovered glass beads from flotation runs with nanoparticle collectors or glass beads from nanoparticle deposition demonstration experiments were acquired by a JEOL JSM-7000F Scanning Electron Microscope.

**Dynamic Adsorption Studies with Fluorescence Images:** St-01-F-292 and St-MAPTAC-03-F-81 dispersions adsorption behaviors onto 30-50 μm glass beads were monitored by an upright Zeiss Axioplan microscope (Germany) connected a Q-Imaging fluorescence and digital camera. The St-01-F-292 and St-MAPTAC-03-F-81 fluorescence nanoparticles, corresponding to St-01-353 or St-01-262 and St-MAPTAC-03-79 used in flotation, were prepared by adding a small amount of fluorescein dimethacrylate. The two fluorescence nanoparticles were excited by a 488 nm laser source and the emission band was set at green range. The 30-50 μm glass beads were placed onto a clean glass slide which was then positioned onto the microscope and the beads were initially pre-focused by a white light. Next, 0.5 mL of either St-01-F-292 or St-MAPTAC-03-F-81 (both 300 mg/L) dispersed in 5mM NaCl was added directly onto the beads. The duration from re-focusing onto the glass beads in the nanoparticle dispersions, turning on the fluorescence laser source and capturing the first image required about 3 minutes. Dynamic adsorption images were subsequently recorded at different intervals.

**Quartz Crystal Microbalance with Dissipation (QCM-D) Measurements:** Deposition of St-01-46, St-MAPTAC-03-120 and St-01-262 onto silica coated sensors, which we assumed possessed similar surface characteristics as to the glass beads used in flotation, was measured using a QCM-D (E4 model from Q-Sense, Sweden). The sensors used were coated with $SiO_2$ (QSX303**,** from Q-Sense). Prior to each deposition experiment, the $SiO_2$ sensors were cleaned by immersing in 2% sodium dodecyl sulfate for at least 5 h followed by copious rinsing with deionized water, drying with $N_2$, and

UV-ozone treatment (15-20 mins). The baselines of the QCM-D were in equilibrium with 5 mM NaCl for ~10 mins before the nanoparticle dispersions in 5mM NaCl were injected into the QCM-D module at 25 °C with a flow speed of 100µL/min. The QCM-D measures change in frequency (*ΔF*) of quartz crystal sensor, and *ΔF* is related to the deposited mass via the Sauerbrey equation [18-20].

$$\Delta m = -\frac{C\Delta F}{n} \qquad \textbf{1}$$

where *Δm* is the deposited mass per unit surface (i.e., mg/m$^2$), *n* is the overtone number used in the measurement, and *C* is mass sensitivity constant for the crystal at 5 MHz (C = 17.7 ngHz$^{-1}$cm$^{-2}$). In our case, *Δm* was calculated from *ΔF* of the 3rd overtone.[10]

## Results

A series of polystyrene nanoparticle dispersions (latexes) were prepared by either surfactant-free emulsion polymerization or starved-feed emulsion copolymerization - the recipes are summarized in Table 1. The properties of both prepared nanoparticles and purchased larger latex are summarized in Table 2. Hydrodynamic diameters (including polydispersity values) of the nanoparticles, measured by dynamic light scattering, are given in the second column of the table. The average particle diameters varied from 46 to 2227 nm. Polydispersity, the intensity-weighted relative variance of the diffusion coefficient, is an important measure of particle size distribution width. When the polydispersity equals zero, the sample is monodisperse; and as the polydispersity increases so does the width of the distribution. TEM images of St-01-46, St-MAPTAC-03-120, and St-01-262 shown in Figure 1 reflect the nanoparticle size distributions measured from DLS. The three nanoparticles were seen as well-distributed nano-size dispersions and St-MAPTAC-03-120 (polydispersity, PD = 0.027) was more highly monodisperse than St-01-46 (PD = 0.156) and St-01-262 (PD = 0.176).

Electrophoretic mobility values of our polystyrene latexes were measured in 5 mM NaCl at ambient pH and the results are given in Table 2. All latexes had a positive electrophoretic mobility apart from St-02-280 which was negatively charged. The co-monomer MAPTAC was employed to modify the nanoparticle surface properties by introducing quaternary ammonium cationic groups to supplement cationic amidine groups from the initiator. We observed that smaller nanoparticles had a lower mobility than larger ones, presumably because the smaller nanoparticles carried nearly equivalent amounts of charged chemical groups which were distributed over a relatively larger surface area, resulting in less surface charge groups per unit area. Figure 2 shows electrophoretic mobilities of four cationic nanoparticle types as a function of pH. At neutral pH, St-01-353 and St-01-46 were positively charged due to the presence of pH-sensitive amidine groups from the initiator V50 [16]. Cationic charges of St-MAPTAC-03-79 and St-MAPTAC-03-120 were attributed to both the amidine and the quaternary ammonium on the MAPTAC moieties. The quaternary ammonium displays a pH independent degree of ionization. Therefore, both St-MAPTAC-03-79 and St-MAPTAC-03-120 remained positively charged at high pH (e.g., pH = 12), whereas the mobilities of St-01-363 or St-01-46 were close to zero or slightly negative.

Water contact angle measurements were used to evaluate the hydrophobicities of the nanoparticles. The latexes were dried and dissolved in a solvent and spin cast as smooth films on glass. The sessile drop water contact angles on the polymer films are summarized in Table 2. The contact angles ranged from 75° for St-MAPTAC-03-79 to 93° for St-01-46, suggesting that all employed latexes were sufficiently hydrophobic to be used as nanoparticle flotation collectors. [4]

The volume-weighted particle size distributions of the four glass beads used in flotation experiments are shown in Figure 3. The particle size distributions of the beads were approximately lognormal. The surface area mean diameters ($D_s$, also known as Sauter mean diameter $D_{32}$) are given in the figure, i.e. 43, 64, 66, and 171 μm. The three smaller glass beads (43μm, acid-washed 64 μm and unwashed 66 μm) were negatively charged with electrophoretic mobilities of -4.61, -3.19, and -2.16 ($\times 10^{-8}$ $m^2s^{-1}V^{-1}$), respectively. As the 171 μm unwashed beads are much larger in size and quickly settle from suspension, electrophoretic mobility measurements were unfeasible.

Percent bead flotation recovery was expressed as $\psi_i$ (where *i* represents how many dishes were used for collection), which was calculated as the mass fraction of the total recovered beads to the original total mass of the beads (2 g). The dosage of nanoparticle collectors was expressed as $\lambda_T$, which we define as the total projected area of the added nanoparticles divided by the total area of the glass beads. For the flotation results involving nanoparticles addition, $\lambda_T$ was greater than 100% implying that the nanoparticles were present in excess.

Flotation performance of each nanoparticle collector was generally determined by calculating the recovery of the collected beads in the first dish. The results of the first-dish flotation recovery ($\psi_1$) for the three smaller glass beads (43 μm, 64 μm acid-washed and 66 μm unwashed) are summarized in Figure 4. Without nanoparticles, only less than 10% of the beads were recovered by hydraulic entrainment whereas much higher recoveries were obtained in the presence of cationic nanoparticles. Negatively charged St-02-280 did not improve recovery on any of the three beads ($\psi_1$ ~ 10%). The most hydrophobic and smallest St-01-46 successfully removed almost all beads ($\psi_1$ ~ 90%) Intermediately sized St-MAPTAC-03 (79 nm and 120 nm) gave acceptable recoveries, ranging from 50% to 77%. The smaller and less hydrophobic 79 nm nanoparticles gave higher recovery than larger 120 nm ones, perhaps due to the higher coverage achieved within the 5 minute conditioning interval. The larger cationic hydrophobic latexes St-01 (262 nm and 353 nm) improved the recoveries up to about 45%, and similarly St-01-262 had a slightly better performance than St-01-353. Through a comparison of all cases using cationic nanoparticles, it is seen that acid-washed beads are more readily floated out than the unwashed beads. Similar tendencies were found to occur, but with less recoveries (not shown in Figure 4), on the flotation of much larger and heavier 171 μm unwashed beads, e.g. St-01-46 resulted in $\psi_1$ = 45% and St-01-262 gave $\psi_1$ = 28%, whereas the control only can recover 4%. The following paragraphs summarize additional detailed results on influential factors found from the use of various nanoparticle collectors.

Figure 5 shows the effect of conditioning time on the flotation of 64 μm acid-washed beads using St-01-353 as collectors. Conditioning time is defined as the time that the beads were exposed to the nanoparticles before the flotation, i.e., nanoparticle deposition time. The cationic nanoparticles required a finite time to deposit on the beads. The cases where excess St-01-353 ($\lambda_T$ = 144%) was conditioned with the beads for 5 mins, 30 mins, and 60 mins gave cumulative recoveries ($\psi_4$) of 65%, 89%, and 94% respectively. Without nanoparticles, after 4 dishes collection less than 35% were recovered. Clearly, latex deposition onto glass beads requires a duration of time to reach a specific coverage or one that is sufficient for a good recovery. Longer times resulted in higher coverages of nanoparticles thus higher flotation efficiencies.

Note the results summarized in Figure 4 are based on the same given conditioning time, i.e., 5 minutes, and the general tendency shows that smaller nanoparticle collectors perform better. A question was raised whether smaller nanoparticle collectors are better if given infinite conditioning time. To answer this question, a series of flotation experiments on the 64 μm acid-washed beads were conducted with St-01-46, St-01-262, and St-01-353 at the same theoretical dosage ($\lambda_T \sim 200\%$) while allowing the conditioning time to extend to ~ 2 hours. The three nanoparticles, having similar surface properties (see Table 2), gave the corresponding first-dish flotation recovery ($\psi_1$) of 83±2.1%, 86±3.4% and 75±1.5%. These recoveries were close recoveries ranged from 75 to 86%. Thus, we believe that if given infinite conditioning time, nanoparticle collectors with similar surface properties over the size range from 46 to 353 nm can give almost the same flotation recovery.

A series of curves similar to Figure 5 are shown in Figure 6a where the conditioning time is constant but the initial concentrations of nanoparticles (St-MAPTAC-03-79) is varied. A higher initial nanoparticle concentration results in a higher flotation recovery, presumably because it leads to a greater amount of the deposition of nanoparticles onto the bead surfaces. The extent of nanoparticle deposition on the glass beads was obtained by measuring the absorbance of the supernatant nanoparticle dispersion at 500 nm before and after deposition on the beads. The quantity of deposited latex was calculated using a calibration curve of absorbance versus nanoparticle concentration. In the cases where 0.05 mL, 0.15 mL, 0.25 mL, and 0.30 mL of 18.55g/L St-MAPTAC-03-79 was added, the corresponding theoretically calculated nanoparticle coverages were 23%, 69%, 115%, and 138% . The actual nanoparticle coverages determined by the latex concentration difference before and after conditioning with the beads were 6.6%, 16%, 25%, and 35%. It is seen that the actual latex coverage ratios are much less than the theoretically calculated ones. The results suggest that not every nanoparticle will deposit onto the beads, even when there are still vacant spots on the bead surfaces and free nanoparticles in the dispersion.

The curve in Figure 6b is constructed from the plot of cumulative flotation recovery ($\psi_4$) versus actual St-MAPTAC-03-79 coverage. The plot shows that in order to achieve a relatively high flotation recovery, very high surface coverage is not required; in fact, a coverage of approximately 25% for St-MAPTAC-02-79 is sufficient to result in a relatively high flotation recovery ($\psi_4 > 85\%$). Nearly all of the beads were recovered when about 35% of the bead surfaces were covered by St-MAPTAC-03-79. The highest actual coverage was further analyzed with ImageJ software. For example, the SEM (see the inset image in Figure 6b) of the surface of a recovered bead from the flotation run with the highest dosage ($\lambda_T = 138\%$) gave an actual coverage of approximately 31%, slightly lower than the 35% coverage measured by UV-vis. However, this particular example was not the most efficient – we have reported similar results where only a coverage of approximately 10% for more hydrophobic St-01-46 (see Table 2, $\theta_{np} = 93°$, whereas $\theta_{np}$ was 75° for St-MAPTAC-03-79) was required for to attain a high recovery. [3] The results indicate that a successful flotation is sensitive to nanoparticle surface chemistry, and more specifically, to the degree of the nanoparticle surface hydrophobicity.

The results of re-flotation (no more nanoparticle addition) on dried glass beads recovered from a flotation run with St-MAPTAC-03-79, compared to the initial flotation results, are shown in Figure 7. Although re-flotation gave a slightly lower recovery ($\psi_4 = 91\%$) than the original flotation run ($\psi_4 = 97\%$), we conclude that most of St-MAPTAC-03-79 nanoparticles still remain adhered to the bead surfaces after re-dispersing them into the flotation liquor. This is an important observation – it suggests that nanoparticle flotation collectors can be effective over a number of stages of a commercial flotation process.

The effect of nanoparticle size on flotation results of 66 μm unwashed beads are shown in Figure 8. Four cationic polystyrene latexes with hydrodynamic diameters of 79 nm, 353 nm, 678 nm and 2227 nm were evaluated as flotation collectors by conditioning each for 5 minutes with the beads. The dosage of each latex was preset to an equivalent theoretical coverage ($\lambda_T \sim 150\%$). Upon the comparison of St-MAPTAC-03-79 and St-01-353, which differ by about a factor of five in diameter, a higher recovery was given by the smaller nanoparticles (92% to 63% respectively) despite the fact that the St-MAPTAC-03 nanoparticles were slightly less hydrophobic according to the contact angle measurements (see Table 2). Also, we observed that St-01-353 performance ($\psi_3 = 63\%$) was better than the larger St-01-678 ($\psi_3 = 49\%$) and St-01-2227 ($\psi_3 = 38\%$) latexes. The smaller nanoparticles are more effective, which possibly reflects the higher number concentration of nanoparticles adsorbed onto the bead surfaces. In addition, we acquired the SEM images (Figure 8b-e) of dried samples collected from each flotation run. The images directly show that more of the small nanoparticles (St-MAPTAC-03-79) were deposited on the bead surfaces compared to St-01-353 and much more than the larger latexes (St-01-678 and St-01-2227). The results indicate that polystyrene latex particle size plays an important role in glass bead flotation. The larger diameter latexes gave lower recoveries than smaller diameter latexes when compared at the same $\lambda_T$ and conditioning time.

Figure 9a shows the difference in flotation efficiencies between two oppositely charged polystyrene latexes on the flotation of negatively charged glass beads. Here we compare two polystyrene latexes of similar size and opposite surface charges, with a conditioning time of 30 minutes with 64 μm acid-washed glass beads. The dosage of each latex was set to approximately the same theoretical coverage ($\lambda_T \sim 210\%$). The incremental flotation results show that cationic St-01-353 could improve glass bead recovery ($\psi_4 = 91\%$), whereas anionic St-02-180 could not ($\psi_4 = 41\%$, approximately the same as the control recovery, $\psi_4 = 35\%$). SEM images of the beads after being conditioned with St-01-353 or St-02-280 dispersions (both ~300 mg/L) for 30 mins and subsequently rinsed a few times with 5mM NaCl are given in Figure 9b and c. A large amount of positively charged St-01-353 were deposited onto the bead surfaces even after rinsing (Figure 9b), whereas very little St-02-280 deposition was found on the bead surfaces (Figure 9c). In all of the flotation experiments presented in this study, electrostatic attraction between oppositely charged glass beads and nanoparticles was used to drive deposition. Thus, the results in Figure 9 are to be expected.

Control flotation experiments of nanoparticles alone were performed in presence of the 10 mg/L frother. Table 3 summarizes the flotation results of three nanoparticle-only flotation runs: two positively charged latexes, St-01-262 and St-MAPTAC-03-120, and the negatively charged St-02-280, and plus a control with the frother only. The quantity of latex recovered was calculated using a calibration curve of absorbance versus nanoparticle concentration in 5 mM NaCl in presence of 10 mg/L frother. The volume of floated liquor ranged from 56 mL to 65 mL, similar to the described flotation runs for glass beads and the froth only (57mL). The recoveries of St-01-262 and St-MAPTAC-03-120 were 54% and 61% respectively, slightly higher than St-02-280 (44%). Corresponding enrichment factors, which we defined as the percent recovered nanoparticles divided by the percent liquid carried over, equaled 1.1, 1.2 and 0.98 for St-01-262, St-03-MAPTAC-120, and St-02-280.

Qualitative dynamic adsorption studies of nanoparticles onto glass beads were monitored by fluorescence images taken at predetermined intervals during conditioning. Figure s1 shows fluorescence images of St-01-F-292 and St-MAPTAC-03-F-81 adsorbed onto 43 μm glass beads. Nanoparticle adsorption behaviors could be analyzed by comparing relative variations in fluorescence intensity. As the operation required approximately 3 minutes to re-focus onto the beads and then capture a picture after adding the fluorescence nanoparticle dispersions, the nanoparticles and glass beads have already interacted for about 3 minutes in the first images acquired, i.e., “a1. start” and “b1. start”. Fluorescence intensity of glass beads adsorbed by St-01-F-292 latex gradually increased over 1 hour, whereas St-MAPTAC-03-F-81 dispersions gave only a slightly increasing intensity from when images were first recorded. The likely cause of this is that the deposition of St-MAPTAC-03-F-81 onto the glass beads has been mostly completed within the first 3 minutes. This observation implies that the adsorption of nanoparticles onto glass beads requires a much longer conditioning time for larger latexes (e.g. St-01-353 or St-01-262) than for smaller ones (e.g. St-MAPTAC-03-79) in flotation. Note that the two cases are compared at equivalent mass concentrations of both latexes.

Detailed deposition kinetics of St-01-46, St-MAPTAC-03-120 and St-01-262 onto $SiO_2$ sensors, followed by the quartz crystal microbalance (QCM), are shown in Figure 10 and Figure 11. Raw data (frequency vs. time) of the deposition are attached in Figure 2s. Figure 10 compares deposition kinetics at the same nanoparticle mass concentration. Figure 11 compares kinetics at the same nanoparticle number concentration. The duration required for each nanoparticle to complete the deposition ranged from 2 mins for St-01-46 to approximately 100 mins for St-01-262 when compared at the same mass concentration (177.5mg/L). The duration only ranged from 15 mins for St-01-262 (1848 mg/L) to 20 mins for St-01-46 (10mg/L) when compared at equivalent numbers of nanoparticles. This observation indicates that larger nanoparticles require a longer time to deposit onto glass surface than smaller nanoparticles at the same mass concentration whereas the deposition rates are similar at the same number concentration. Eq 1 and the fundamental parameters of the polystyrene nanoparticles were related to give further calculations. Figure 10a and Figure 11a show the deposition amount (mass per unit surface, i.e. $mg/m^2$) as functions of time. Figure 10b and Figure 11b show percent nanoparticle coverage as functions of time. Deposition kinetics will be used to explain the flotation results in the discussion section.

## Discussion

The objective of this work was to first, determine the influential factors affecting nanoparticle collectors on the flotation of hydrophilic glass beads; and second, determine the major factors influencing nanoparticle deposition onto the glass surfaces; and, further correlate both dominant factors with the flotation results.

The results of control flotation runs of nanoparticles only summarized in Table 3 show that the volume of floated liquor ranged from 56 mL to 65 mL, which is similar to the flotation runs for glass beads. This observation suggests that these nanoparticles do not act as defoamer particles [21] and had little effect on rupturing the liquid films (lamella) between foam bubbles; otherwise the floated volume would be much lower. The recoveries of St-01-262 and St-MAPTAC-03-120 were 54% and 61% respectively, slightly higher than St-02-280 (44%). Enrichment factors, which show the percent recovered latex carried over the percent liquid volume, equaled 1.1, 1.2 and 0.98 for St-01-262, St-03-MAPTAC-120, and St-02-280. The results suggest that the latexes suspended in water phase were carried over with the water, due to hydraulic entrainment. The polystyrene latexes are easily carried over with the water, probably because polystyrene has a similar density to water (1.05 g/mL to 1.0 g/mL). Slightly higher enrichment factors of cationic latexes than that of anionic latexes (1.1/1.2 versus 0.98) indicate there may be small parts of the cationic latexes adsorbed onto the bubble surfaces via electrostatic force and van de Waals force. Note that air bubble usually has a negative zeta potential [22] at neutral pH in the presence of frother.

Initially, we worried that the excess nanoparticles may adsorb on the air/water interface and interfere with flotation recovery. However, most of our glass bead flotation runs (e.g., with nanoparticles sized less than 353 nm) shown in this study were performed in the presence of an excess nanoparticle dosage and high recoveries were attained. To further investigate this concern, a number of flotation runs with the same initial nanoparticles dosage were conducted. In these experiments, the nanoparticles were first allowed to deposit onto the beads, and the supernatant (containing excess non-deposited nanoparticles) was then removed after conditioning. Fresh flotation liquor was recharged into the suspension before flotation and similar flotation recoveries were achieved. This analogy suggests that the presence of excess nanoparticles in the suspension may have negligible effect on interfering with the flotation results. Thus, we think the critical aspect for the application of “nanoparticle flotation collectors” remains that the nanoparticles must deposit onto the bead surfaces to reach a specific coverage or one that is sufficient for a good recovery.

In this study, we used QCM to measure the deposition of St-01-46, St-MAPTAC-03-120 and St-01-262 onto silica coated sensors, which we assumed possessed similar surface characteristics as to the glass beads used in flotation. To predict nanoparticle deposition kinetics, one could simply apply the Langmuir kinetics model [23-24]:

$$\frac{d\Gamma}{dt} = k_1 N(\Gamma_{\max} - \Gamma) - k_2\Gamma \qquad \mathbf{2}$$

where $k_1$ and $k_2$ are the rate constants for nanoparticle deposition and detachment. $\Gamma_{\max}$ is the maximum amount that can deposit per area (mg/m$^2$), $N$ is the nanoparticle bulk concentration (mg/L), and $t$ is the time. If the deposition of nanoparticles is irreversible, meaning no detachments take place ($k_2 = 0$), the solution of eq 2 gives:

$$\Gamma = \Gamma_{\max}(1 - e^{-k_1 N t}) \qquad \mathbf{3}$$

In our case, $\Gamma_{\max}$ could be determined by the QCM measurements according to eq 1. Thus, eq 3 assuming no detachments take place can be then written as:

$$\Gamma = -\frac{C\Delta F_{\max}}{n}(1 - e^{-k_1 N t}) \qquad \mathbf{4}$$

where $\Delta F_{max}$ is the maximum frequency change of the sensor after nanoparticles deposition measured by the QCM. Upon substituting the fundamental parameters of the nanoparticles into eq 4, the time dependent surface coverage then can be derived as:

$$\lambda = -\frac{3C\Delta F_{\max}}{2nd\rho}(1 - e^{-k_1 N t}) \qquad \mathbf{5}$$

where $\lambda$ is the nanoparticle area-based coverage on the $SiO_2$ sensor, $d$ is the diameter of the nanoparticle, and $\rho$ is the density of polystyrene. For the calculation, we also assume that only a monolayer of nanoparticles was deposited on the surface of the $SiO_2$ sensor.

The equations developed so far are based on the assumption that the deposition is irreversible and there is no detachment once latex deposited. The driving force used in directing nanoparticles deposition is controlled by electrostatic interaction and van der Waals force according to DLVO theory. To analyze whether the latex will detach, one can simply compare the detachment force from either stagnation flow or laminar flow (the estimated type of flow in QCM module) with the colloidal forces from DLVO. Reynolds number is used to correlate the type of flow, given by:

$$\mathrm{Re} = \frac{d_m U \rho_L}{\eta} \qquad \mathbf{6}$$

where $d_m$ is irregular cross-sectional module diameter; $U$ is the average fluid velocity (in m/s), calculated from flow rate (in L/s) divided by the module cross-sectional area; $\rho_L$ is the density of fluid; and $\eta$ is the viscosity of the nanoparticle suspension, which can be estimated from Einstein's equation. The estimated Reynolds number in the QCM module is about 2.5. Thus, only stagnation flow or laminar flow was considered in the QCM experiments.

The detachment forces caused by stagnation flow or laminar flow on a sphere attached to a flat surface could be calculated according to Goldman et al.'s equation [6]:

$$F_d = (1.7)(6\pi\eta r_{np} U) \qquad \mathbf{7}$$

The calculated detachment forces $F_d$ equaled 1.5 pN for St-01-46, 3.9 pN for St-MAPTAC-03-120, and 8.5 pN for St-01-262. This predicted detachment forces are relatively small values [6], suggesting that there was almost no detachment once latex deposited in these QCM measurements.

The maximum nanoparticle deposition coverages with each type of nanoparticle collector measured with QCM (shown in Figure 10 andFigure 11) equaled 28% for St-01-46, 35% for St-MAPTAC-03-120, and 30% for St-01-262. It is noted that the maximum coverage of randomly deposited non-interacting but non-overlapping spheres is ~ 0.55, whereas electrostatic repulsion, tending to keep the spheres apart, gives an even lower maximum coverage. [25] The reason why the maximum coverage of St-MAPTAC-03-120 is larger than other two nanoparticles is probably because of the presence of a small amount of polyMAPTAC on its surface. This may facilitate adsorption and overcome certain self-repulsion between adsorbed nanoparticles. The curves of the deposition are similar to the Langmuir type adsorption.

Revisiting the QCM results, when compared at the same nanoparticle number concentration, Figure 11 shows that the larger St-01-262 deposited slightly faster than the two smaller nanoparticles. This appears contrary to a thermodynamic perspective where larger particles have slower diffusion. However, according to a calculation from DLVO theory, the attractive forces of St-01-262, which had a higher electrophoretic mobility, are much larger than that of the other two latexes. The larger attractive force may somewhat accelerate the deposition. This may explain why the larger St-01-262 deposited slightly faster.

Experimental deposition curves (solid lines in Figure 10 and Figure 11) were compared to those modeled using eq 4 and 5 (dashed lines) by estimating a deposition rate constant which yielded a good fit for each curve. For the two smaller nanoparticles (St-01-46 and St-MAPTAC-03-120), the fitted deposition curves are almost analogous to measured ones. The modeling shows that nanoparticle deposition behavior in these experiments closely obeys Langmuir kinetics model. However, for the largest St-01-262, the model has a poor agreement with the experimental data and the fitting fails to reproduce the kinetics at the high bulk concentration (i.e. 1848 mg/L, especially at the starting times).

In flotation, experiments conducted were primarily compared at the same theoretical area-based coverage ($\lambda_T$), namely, the dosage (in *mg*) divided by nanoparticle unit mass (proportional to nanoparticle unit volume) and multiplied by nanoparticle unit projected area, are equivalent. Thus, the dosage for each nanoparticle collector required to give the same $\lambda_T$ is calculated inversely, i.e., nanoparticle volume divided by nanoparticle area - the cube of the nanoparticle size divided by the square of nanoparticles, so the dosage should be proportional to the first power of nanoparticle size. The results of Figure 10 measured with QCM-D were compared at the same mass concentration, i.e., the masses of latex used are equivalent (177.5 mg/L). Figure 11 compares deposition at the same number concentration, i.e., the amount of nanoparticles is the same, which is proportional to the cube of particle size. The dosage of nanoparticle collectors in flotation is between the two dosages measured with the QCM. For example, if the three nanoparticles are used as examples to get a same theoretical coverage on the glass surface, the required dosage for each will be 64 mg/L for St-01-46, 177.5 mg/L for St-MAPTAC-03-120, and 387.5 mg/L for St-01-262. Therefore, the conditioning time required to complete each deposition is in-between these two cases from the QCM measurements. By analogy we conclude that there are two important parameters which determine the amount of latex deposition and the coverage onto the glass surface – one is the nanoparticle latex bulk concentration ($N$) and the other is conditioning time ($t$), provided that the deposition rate constant is a fixed value for each specific nanoparticle collector. This analysis is in accord with the modeling given by eq 4 and 5.

From kinetic aspects, the smaller the nanoparticles, the faster they diffuse and thus deposit. Smaller nanoparticles give a higher surface coverage in a given time interval for an established latex concentration (see Figure 10b for the first a few minutes). This analysis is in agreement with the estimated deposition rate constant for each nanoparticle to fit the curves in Figure 10 (also Figure 11). For fitting curves in Figure 10, the deposition rate constant $k_1$ is estimated as 0.164 $Lg^{-1}s^{-1}$ for St-01-46, 0.016 $Lg^{-1}s^{-1}$ for St-MAPTAC-03-120 and 0.0023 $Lg^{-1}s^{-1}$ for St-01-262.

In the case of laminar flow or stagnation flow, detachment forces estimated by eq 7 give very small forces and thus have little effect on nanoparticle desorption. However, in flotation when particles exceed 1 μm, external forces such as hydrodynamic forces or gravity should be taken into account for the evaluation of the strength of nanoparticle adhesion. For example, shearing force [26], produced by stirring in flotation, is one of the external forces. In our experiments, while conditioning the glass beads with individual latexes, a lower stirring rate was utilized. While running the flotation, beginning with nitrogen bubbled through until the last dish was collected, a higher stirring rate was applied to ensure that the glass beads are well dispersed and did not settle. The two applied shear forces seem to have no influence on the 79 nm nanoparticle detachment, and possibly have a slight influence on the 353 nm and 678 nm nanoparticle detachments (see cases in Figure 8). However, the shear counter force, dependent on the cross-sectional area of the particles, has a definite negative effect on the deposition of the much larger polystyrene latex (e.g., St-01-2227). [9] In such cases, shear counterforce is possibly dominant over the attractive forces by electrostatic attraction and van der Waals forces. Larger diameter latex produces a higher shear counterforce, possibly resulting in latex more readily detached from bead surfaces. This analysis probably explains the poor collecting power of the larger size (> 1 μm) of latex in flotation. Clearly, future investigations will be required to verify this analysis in greater certainty.

## Conclusions

To summarize, a series of important influential factors in the application of nanoparticle flotation collectors have been investigated, and the dominant factors have been correlated with the nanoparticle deposition behavior. The main conclusions from current work are:

1. Glass beads of widely distributed sizes (i.e., surface area mean diameters of 43 μm, 64 μm, 66 μm and 171 μm) can be floated with hydrophobic polystyrene nanoparticles functioning as collectors.
2. Nanoparticle deposition on to silica surfaces closely obeys Langmuir kinetics model for smaller nanoparticles (e.g., 46 nm and 120 nm ones). The model can be used to predict the extent of nanoparticle covered onto mineral surfaces. Nanoparticle coverage on the bead surfaces increases with either higher latex initial dosage or longer conditioning time, leading to superior flotation recoveries.
3. The deposition rate constant is dependent upon the nanoparticle size. Smaller nanoparticles deposit faster than larger ones, resulting in higher nanoparticle coverage within a given conditioning time and an established dosage, and thus better recoveries.
4. Although nanoparticle size has a large influence on nanoparticle deposition rates onto mineral surfaces, flotation recovery is independent of nanoparticle size when compared at constant high coverage and similar nanoparticle hydrophobicities.
5. Most polystyrene nanoparticles will not detach from glass bead surfaces once deposited.
6. Electrostatic attraction is the major driving force for polystyrene nanoparticles deposition onto glass beads according to analysis from DLVO theory. Negatively charged nanoparticles do not deposit onto glass beads and thus fail to improve recovery.

## Acknowledgement

We thank the Centre for Materials and Manufacturing (CMM), a division of the Ontario Centres of Excellence (OCE) in collaboration with VALE Base Metals for funding. VALE Base Metals Technology Development for funding. Zongfu Dai and Manqiu Xu from Vale for much help, samples and advice. We also acknowledge Ms. Alexis Ambeault for acquiring some electrophoretic mobility data. Finally, we acknowledge Dr. Mark Poggi from Biolin Scientific Inc. for useful discussions.

# Figures

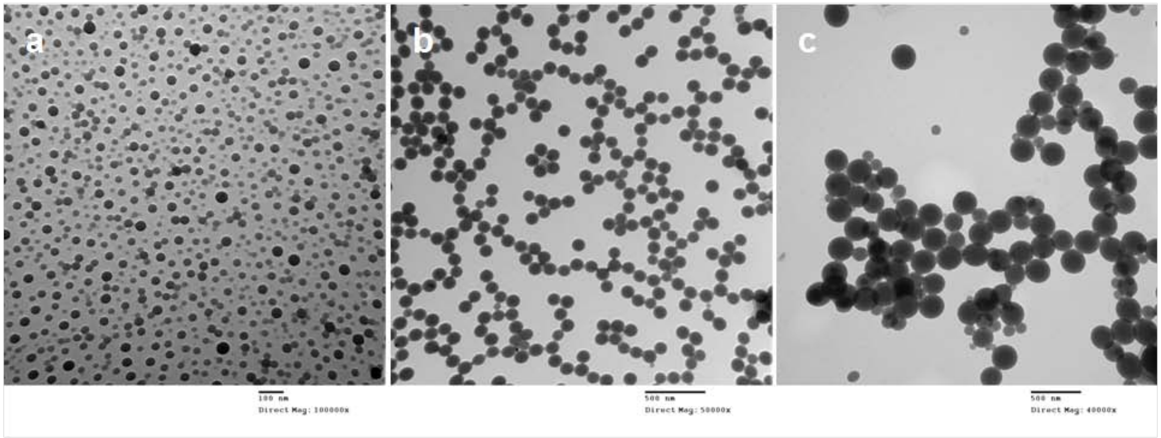

**Figure 1** TEM images of a. St-01-46, b. St-MAPTAC-03-120, and c. St-01-262. Scale bars are 100 nm, 500 nm and 500 nm respectively.

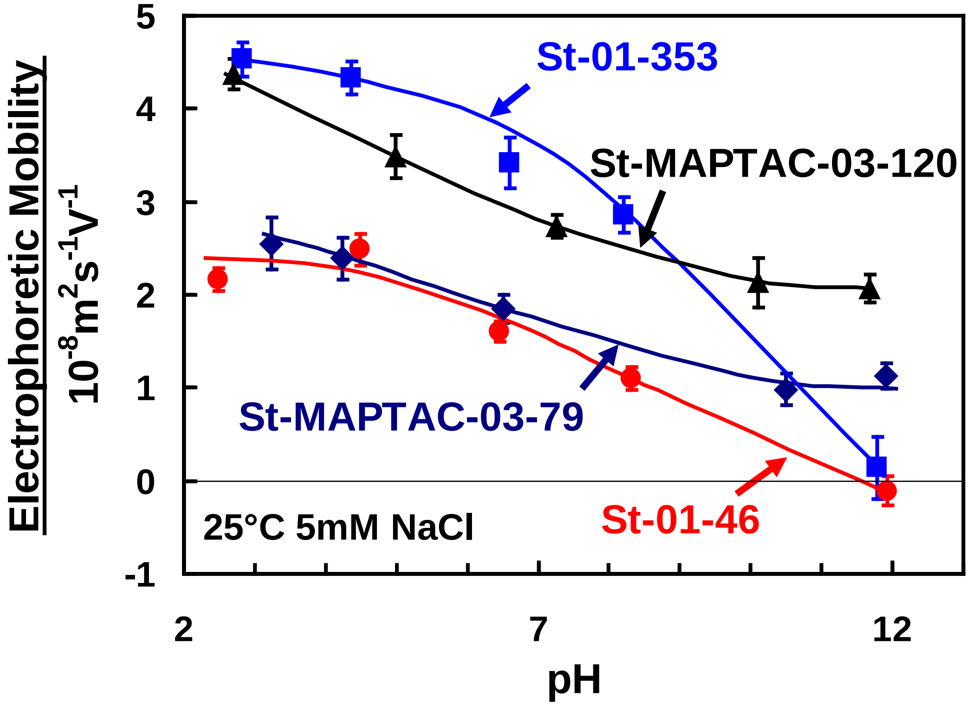

**Figure 2** Electrophoretic mobility values of St-01-353, St-01-46, St-MAPTAC-03-79, and St-MAPTAC-03-120 nanoparticles as a function of pH

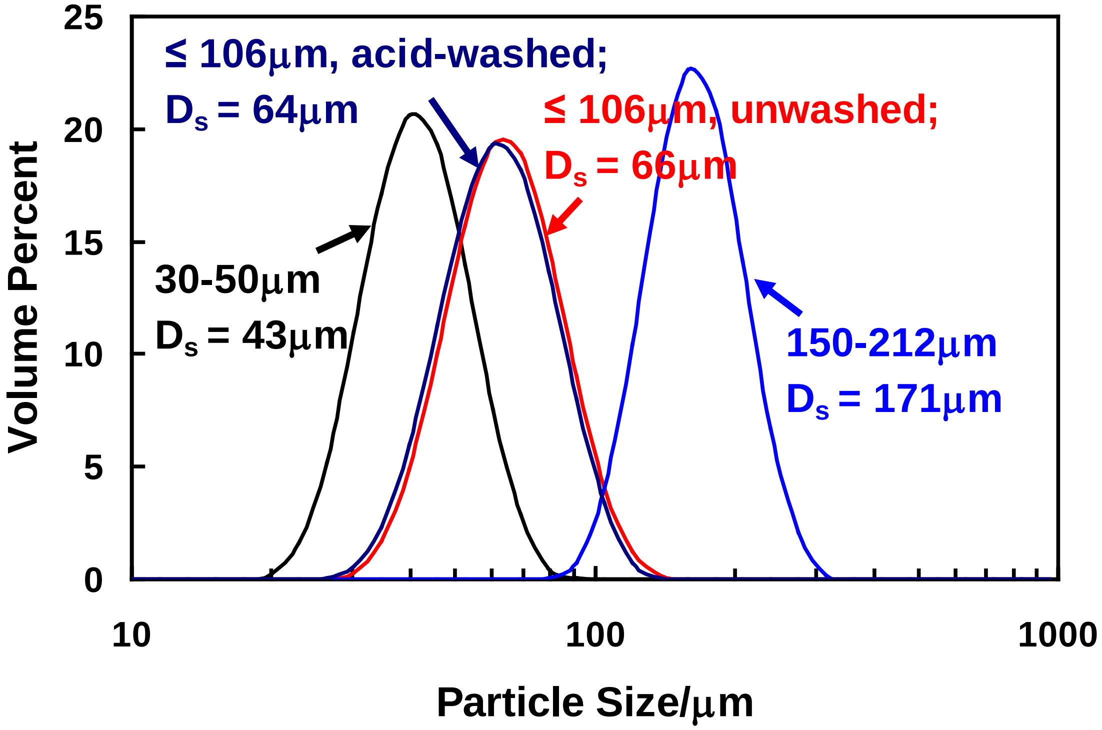

**Figure 3** Mastersizer particle size distributions of four glass beads suspensions. The Sauter mean diameter ($D_s$) values are representative of the diameter of an equivalent sphere with the same volume/surface area ratio as the suspension.

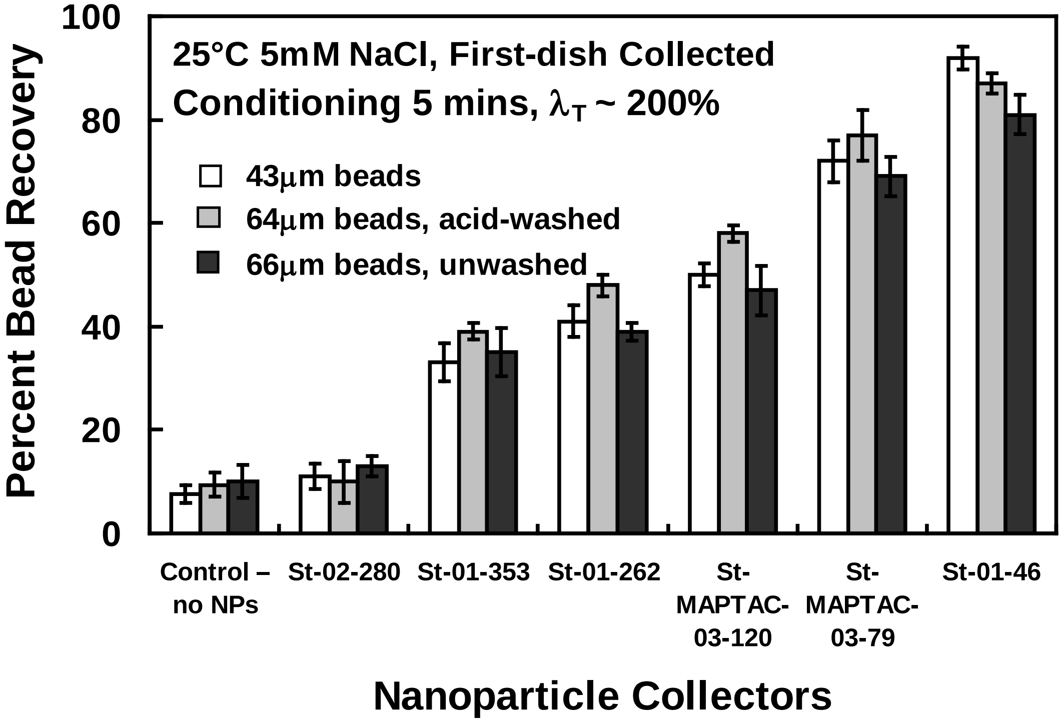

**Figure 4** Summary of the flotation recovery of first-dish collected beads ($\psi_1$) for three different glass beads using various nanoparticles as collectors. Flotation conditions include: nanoparticles dosage $\lambda_T \sim 200\%$, conditioning 5 minutes, 10 mg/L UNIFROTH 250C, in 5 mM NaCl, nitrogen flow rate at 2.0 L/min, and flotation duration 1.0-1.5 minutes. The error bars were estimated as the mass of beads lost from filtration – the weight difference between the total dried beads (recovered by flotation plus remaining in the beaker) and the starting glass bead mass of 2 grams and the results were reproducible.

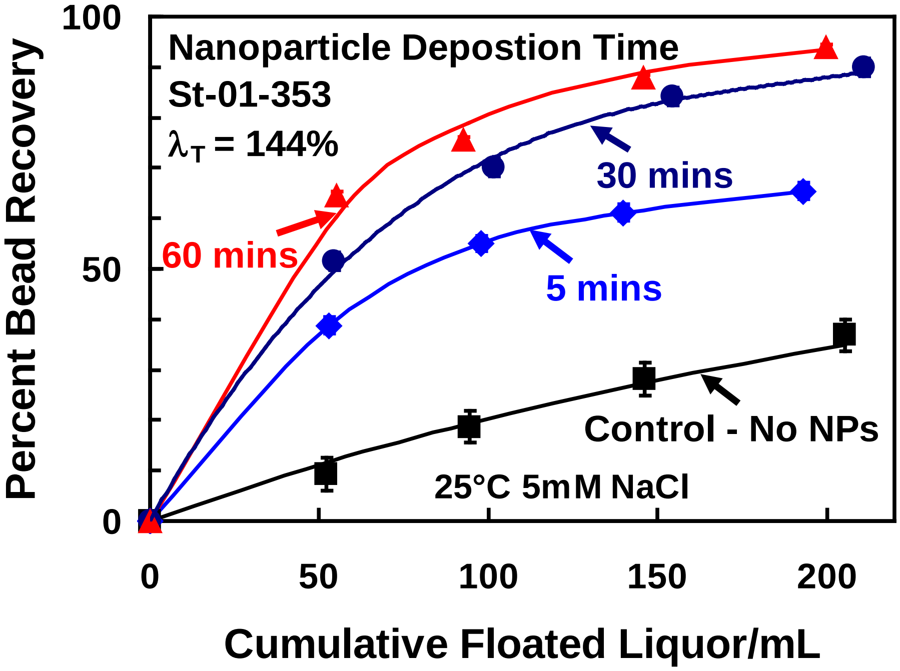

**Figure 5** Influence of the time allowed for nanoparticles to deposit onto 64 μm acid-washed glass beads on the recovery of glass beads. The dosage of St-01-353 nanoparticles was equivalent to 1.44 times the glass bead surface area. The error bars estimated from replicated experiments were smaller than the points for all but the control experiment.

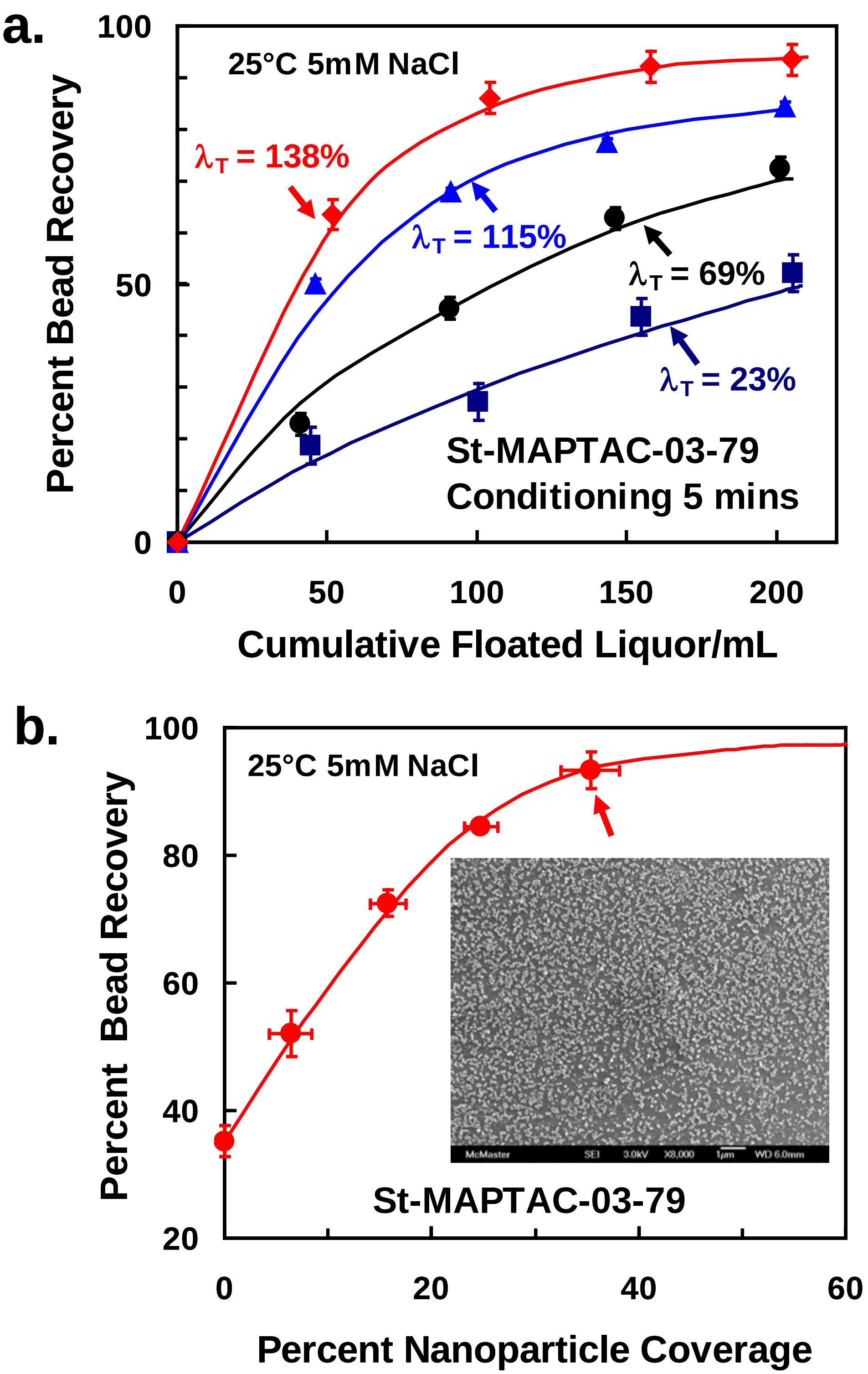
a.
25°C 5mM NaCl
$\lambda_T$ = 138%
$\lambda_T$ = 115%
$\lambda_T$ = 69%
$\lambda_T$ = 23%
St-MAPTAC-03-79
Conditioning 5 mins
Percent Bead Recovery
0
50
100
0
50
100
150
200
Cumulative Floated Liquor/mL
b.
25°C 5mM NaCl
St-MAPTAC-03-79
McMaster SEI 3.0kV X8,000 1μm WD 6.0mm
Percent Bead Recovery
20
40
60
80
100
0
20
40
60
Percent Nanoparticle Coverage

**Figure 6 a.** Flotation recovery of 2 g of 66 μm unwashed glass beads by adding various dosages of 18.6 g/L St-MAPTAC-03-79 (0.05 mL, 0.15 mL, 0.25 mL, and 0.30 mL, equivalent to 0.23, 0.69, 1.15, and 1.38 times the glass bead surface area) for 5 mins conditioning in 5mM NaCl. **b.** Glass bead recovery ($\psi_4$) as a function of St-MAPTAC-03-79 coverage measured by UV-vis. The inset image is the SEM of the surface of a recovered bead from the flotation run with the highest dosage, $\lambda_T = 138\%$.

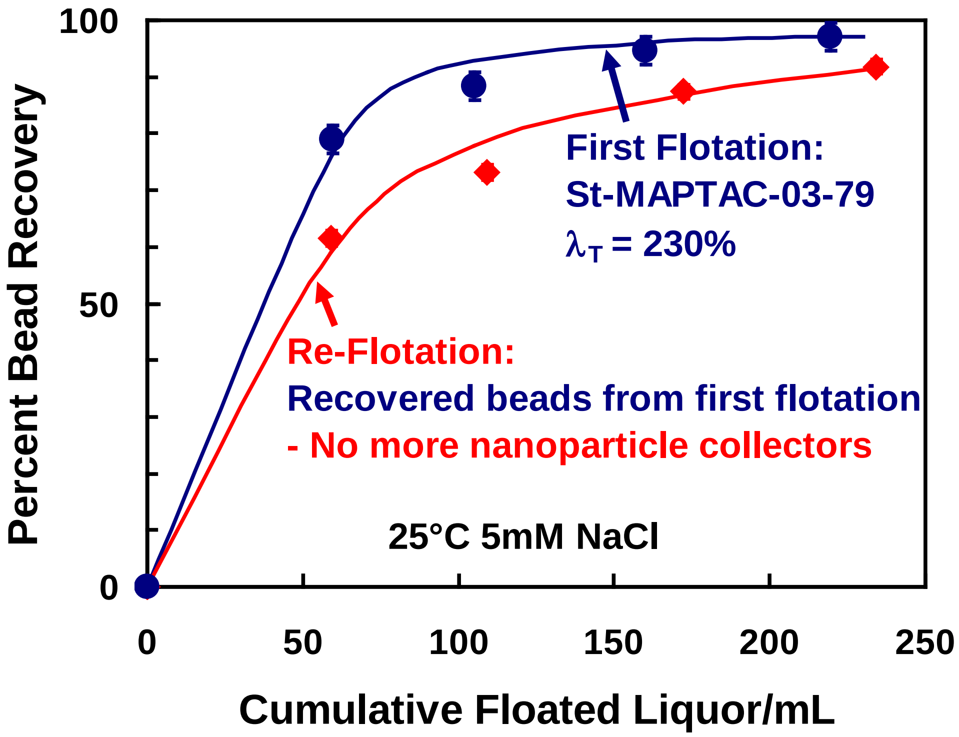

**Figure 7** Comparison of the flotation run of 2 g 66 µm unwashed glass beads by excess addition of 0.5 mL of 18.6 g/L St-MAPTAC-03-79 ($\lambda_T$ = 230%) with the follow-up re-flotation of the 1.95 g dried recovered beads from the initial flotation.

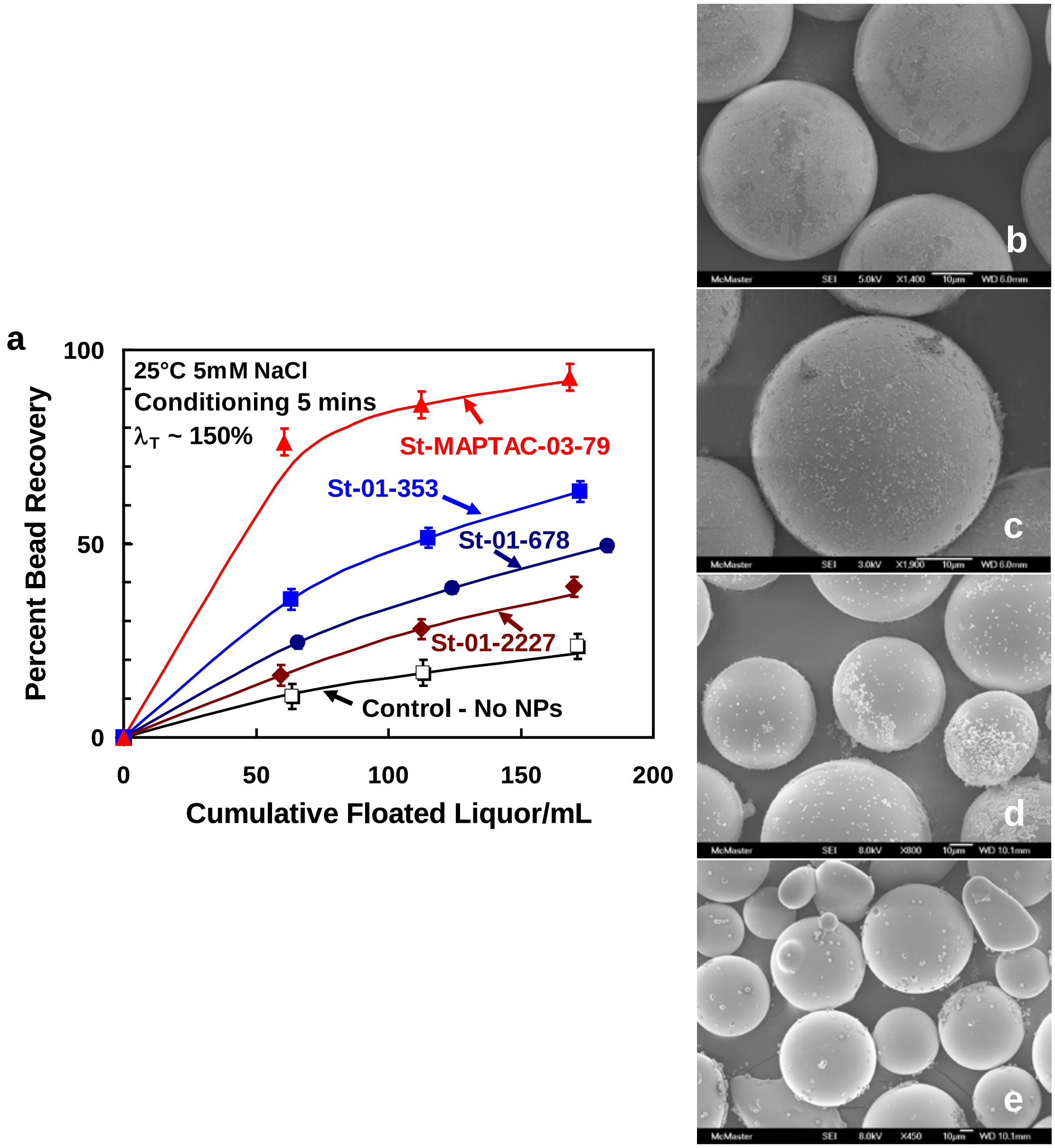

**Figure 8 a.** Flotation recovery of 2 g of 66 μm unwashed glass beads with no polystyrene addition as a control ($\psi_3$=23%, in the case of these parallel runs, three concentrates were collected) and excess addition of various polystyrene nanoparticles (0.33 mL of 18.6 g/L St-MAPTAC-03-79, $\lambda_T$ = 149%; 1.0 mL of 27.2 g/L St-01-353, $\lambda_T$ = 148%; 1.3 mL of 40g/L St-01-678, $\lambda_T$ = 148%; and 4.3 mL of 40 g/L St-01-2227, $\lambda_T$ = 149%) with 5 minutes of conditioning in 5mM NaCl. **b-e.** SEM images of dried glass beads recovered from each corresponding flotation run (b. St-MAPTAC-03-79, c. St-01-353, d. St-01-678, and e. St-01-2227).

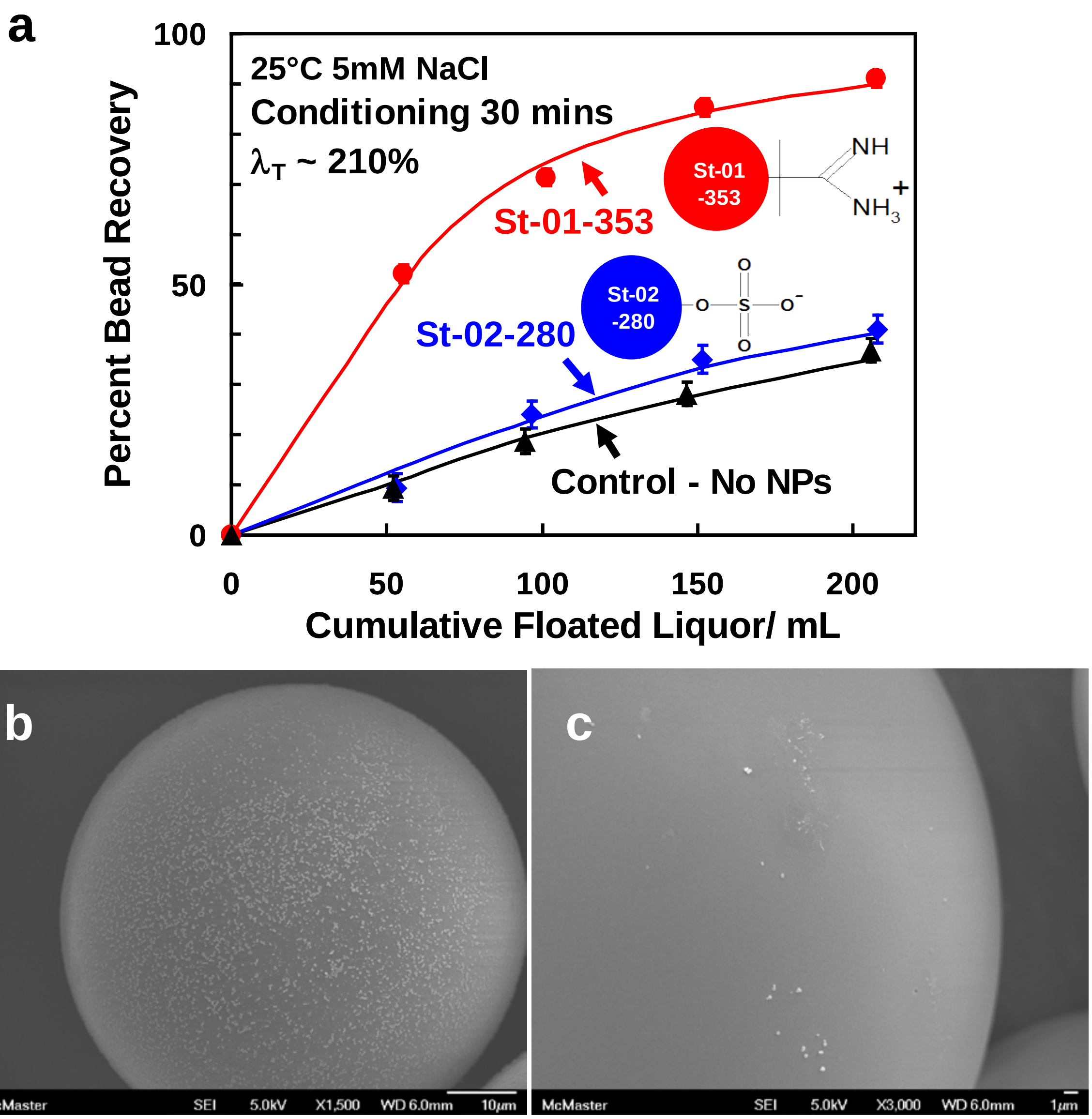

**Figure 9** **a.** Flotation recovery of 2 g of 64 μm acid-washed glass beads by adding an excess dosage of either cationic or anionic polystyrene nanoparticles (1.0 mL of 31.6 g/L St-02-280, $\lambda_T = 211\%$ and 1.5 mL of 27.2 g/L St-01-353, $\lambda_T = 215\%$; black line is the control, $\psi_4 = 35\%$) with 30 minutes conditioning in 5mM NaCl; **b** and **c.** SEM images of the beads after being conditioned with St-01-353 (**b**) or St-02-280 (**c**) dispersions (both ~300 mg/L) for 30 mins and subsequently rinsed with 5mM NaCl.

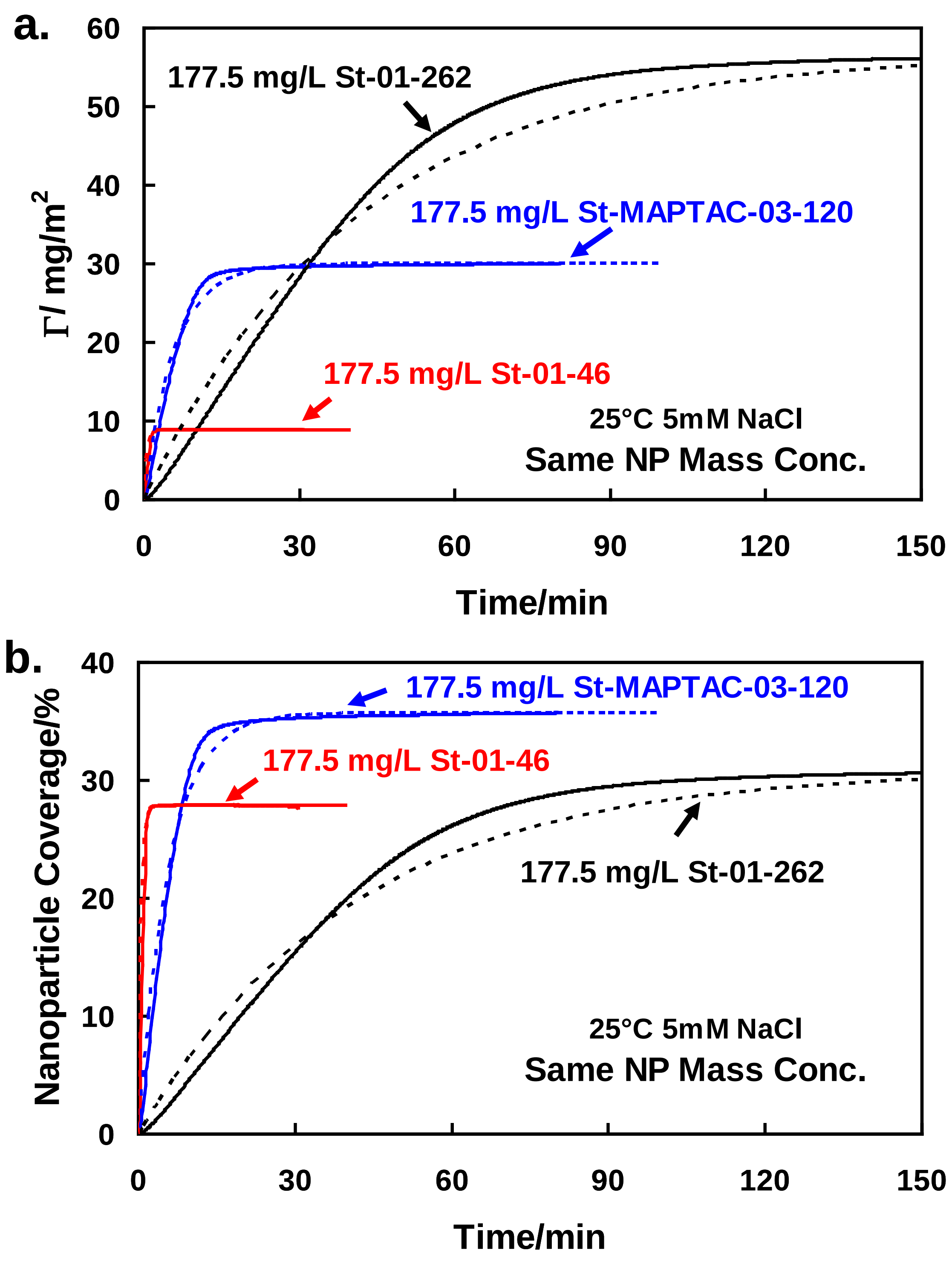
a.
177.5 mg/L St-01-262
177.5 mg/L St-MAPTAC-03-120
177.5 mg/L St-01-46
25°C 5mM NaCl
Same NP Mass Conc.
$\Gamma$/ mg/m$^2$
0
10
20
30
40
50
60
0
30
60
90
120
150
Time/min
b.
177.5 mg/L St-MAPTAC-03-120
177.5 mg/L St-01-46
177.5 mg/L St-01-262
25°C 5mM NaCl
Same NP Mass Conc.
Nanoparticle Coverage/%
0
10
20
30
40
0
30
60
90
120
150
Time/min

**Figure 10** Deposition kinetics (a. deposition amount Γ and b. percent nanoparticle coverage, as functions of time) of St-01-46, St-MAPTAC-03-120 and St-01-262, compared at the same nanoparticle mass concentration (177.5 mg/L), were measured by depositing the nanoparticles onto $SiO_2$ coated sensors monitored with QCM-D (frequency vs. time). Dashed lines were fitted using Langmuir kinetic models (eq 4 and 5) assuming the deposition rate constant, $k_1 = 0.164$ $Lg^{-1}s^{-1}$ for St-01-46, $k_1 = 0.016$ $Lg^{-1}s^{-1}$ for St-MAPTAC-03-120 and $k_1 = 0.0023$ $Lg^{-1}s^{-1}$ for St-01-262.

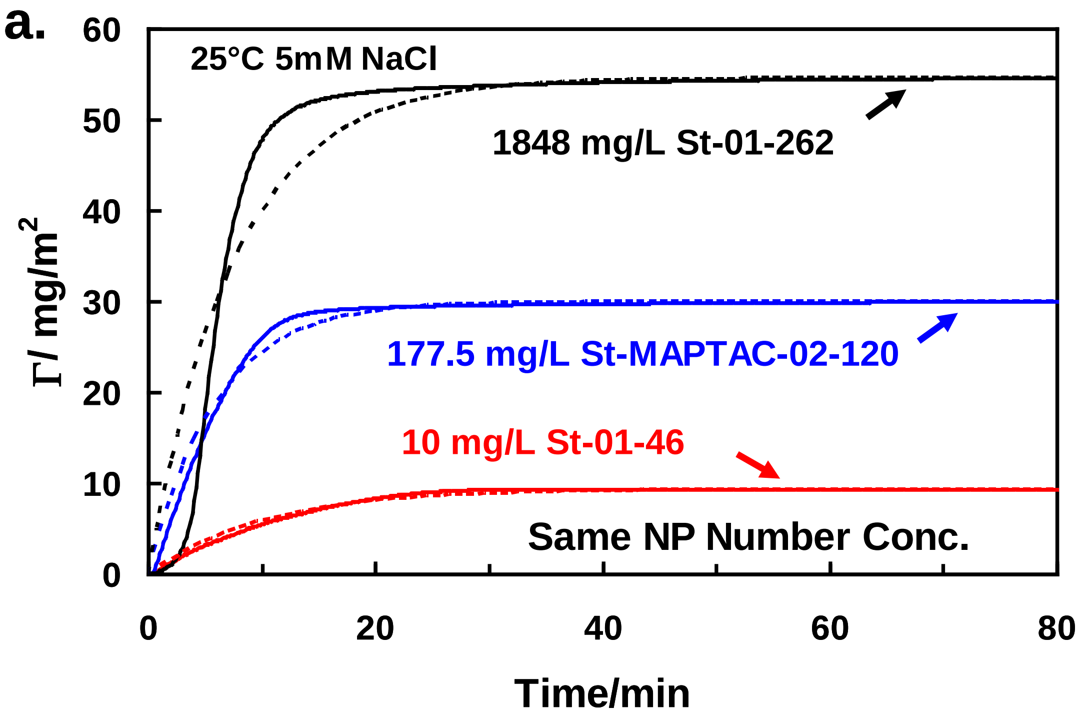
a.
25°C 5mM NaCl
1848 mg/L St-01-262
177.5 mg/L St-MAPTAC-02-120
10 mg/L St-01-46
Same NP Number Conc.
Γ/ mg/m²
0
10
20
30
40
50
60
0
20
40
60
80
Time/min

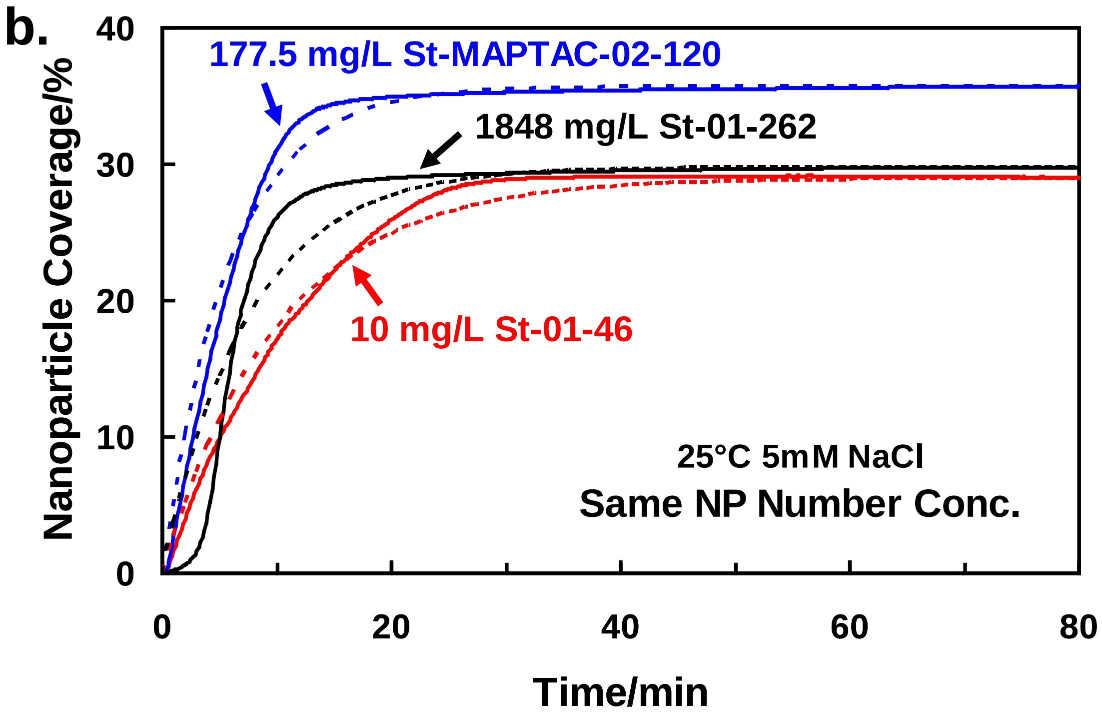
b.
177.5 mg/L St-MAPTAC-02-120
1848 mg/L St-01-262
10 mg/L St-01-46
25°C 5mM NaCl
Same NP Number Conc.
Nanoparticle Coverage/%
0
10
20
30
40
0
20
40
60
80
Time/min

**Figure 11** Deposition kinetics (a. deposition amount Γ and b. percent nanoparticle coverage, as functions of time) of St-01-46, St-MAPTAC-03-120 and St-01-262, compared at the same nanoparticle number concentration ($1.87\times10^{11}$/mL), were measured by depositing the nanoparticles onto $SiO_2$ coated sensors monitored with QCM-D (frequency vs. time). Dashed lines were fitted using Langmuir kinetic models (eq 4 and 5) assuming the deposition rate constant, $k_1 = 0.164$ $Lg^{-1}s^{-1}$ for St-01-46, $k_1 = 0.016$ $Lg^{-1}s^{-1}$ for St-MAPTAC-03-120 and $k_1 = 0.0012$ $Lg^{-1}s^{-1}$ for St-01-262.

## Tables

**Table 1** Recipes for preparation of polystyrene based nanoparticles, where the final number in the nanoparticle designation is the average particle diameter.

| Nanoparticle Designation | Initial Reactor Charge (g) | | | | | Starved-Feed Charge (g) | |
|---|---|---|---|---|---|---|---|
| | Water | St | MAPTAC or CTAB | Fluorescein | V50 (or APS) | St | QACM |
| **St-01-353** | 110 | 5.0 | --- | --- | 0.10 | --- | --- |
| **St-01-262** | 250 | 5.0 | --- | --- | 0.15 | --- | --- |
| **St-01-F-292** | 110 | 5.0 | --- | 0.02 | 0.10 | --- | --- |
| **St-02-280** | 110 | 5.0 | --- | --- | 0.20 APS | --- | --- |
| **St-MAPTAC-03-120** | 250 | 5.0 | 0.25 MAPTAC | --- | 0.10 | --- | --- |
| **St-MAPTAC-03-79** | 250 | 0.5 | 0.125 MAPTAC | --- | 0.06 | 4.5 | 0.125 MAPTAC |
| **St-MAPTAC-03-F-81** | 250 | 0.5 | 0.125 MAPTAC | 0.02 | 0.06 | 4.5 | 0.125 MAPTAC |
| **St-01-46** | 100 | 0.5 | 0.10 CTAB | --- | 0.10 | 4.5 | --- |

**Table 2** Some properties of employed polystyrene based nanoparticles (including the purchased ones)

| **Nanoparticle Designation** | **Hydrodynamic Diameters [a], nm (Polydispersity)** | **Electrophoretic Mobility [a], $10^{-8} m^2 s^{-1} V^{-1}$ (Std. error)** | **Contact Angle [b] on Smooth Polymer Film, $\theta_{np}$** |
|---|---|---|---|
| **St-01-353** | 353 (0.097) | 3.42 ± 0.27 | 88 ± 1.5 |
| **St-01-262** | 262 (0.176) | 4.27 ± 0.21 | 87 ± 1.8 |
| **St-01-F-292** | 292 (0.070) | 3.77 ± 0.16 | --- |
| **St-02-280** | 280 (0.108) | -5.91 ± 0.18 | 92 ± 2.3 |
| **St-MAPTAC-03-120** | 120 (0.027) | 2.74 ± 0.12 | 86 ± 1.1 |
| **St-MAPTAC-03-79** | 79 (0.085) | 1.85 ± 0.15 | 75 ± 2.7 |
| **St-MAPTAC-03-F-81** | 81 (0.149) | 2.34 ± 0.17 | --- |
| **St-01-46** | 46 (0.156) | 1.61 ± 0.07 | 93 ± 2.1 |
| **St-01-678** | 678 (0.126) | 4.43 ± 0.31 | 76 ± 3.5 |
| **St-01-2227** | 2227 (0.205) | 2.08 ± 0.09 | 86 ± 1.9 |

[a] Measured in 5 mM NaCl at ambient pH

[b] Sessile drop water contact angle

**Table 3** Selective control flotation experiments of nanoparticles only in 125 mL 5mM NaCl in the presence of 10 mg/L frother; the standard errors were calculated from three replicated flotation runs

| Targeted Flotation Nanoparticle | Starting Conc., mg/L | Floated Liquor Conc., mg/L | Floated Liquor Volume, mL | Nanoparticle Recovery, wt % | Enrichment Factor [a] |
|---|---|---|---|---|---|
| **St-01-262** | 200 | 207 ± 5.2 | 63 ± 3.1 | 54 ± 2.6 | 1.1 |
| **St-MAPTAC-03-120** | 220 | 261 ± 4.3 | 65 ± 1.5 | 61 ± 1.7 | 1.2 |
| **St-02-280** | 320 | 308 ± 6.3 | 56 ± 4.2 | 44 ± 3.5 | 0.98 |
| **Control – No NPs/ Only Frother** | --- | --- | 57 ± 1.8 | --- | --- |

[a] Enrichment factor represents the percent recovered nanoparticles divided by the percent floated liquid.

# References

1. Fuerstenau, M.; Jameson, G.; Yoon, R., Froth Flotation: A Century of Innovation, Society for Mining, Metallurgy, and Exploration. *Inc.(SME), Littleton, Colorado, USA* **2007**.

2. Wills, B. A.; Napier-Munn, T., *Wills' mineral processing technology: an introduction to the practical aspects of ore treatment and mineral recovery*. Butterworth-Heinemann London: 2006.

3. Yang, S.; Pelton, R. H.; Raegen, A.; Montgomery, M.; Dalnoki-Veress, K., Nanoparticle Flotation Collectors: Mechanisms Behind a New Technology. *Langmuir* **2011,** 27, (17), 10438-10446.

4. Yang, S.; Pelton, R. H., Nanoparticle Flotation Collectors II: The Role of Nanoparticle Hydrophobicity. *Langmuir* **2011,** 27, (18), 11409-11415.

5. Dabro , T.; Van de Ven, T., A direct method for studying particle deposition onto solid surfaces. *Colloid. Polym. Sci.* **1983,** 261, (8), 694-707.

6. Pelton, R. H.; Allen, L. H., Factors influencing the adhesion of polystyrene spheres attached to Pyrex by polyethyleneimine in aqueous solution. *J. Colloid Interface Sci.* **1984,** 99, (2), 387-398.

7. Corak, M.; Van De Wiele, M.; Pelton, R.; Hrymak, A., Polystyrene latex deposition onto polyethylene film consecutively treated with cationic and anionic polymer. *Colloids Surf. Physicochem. Eng. Aspects* **1994,** 90, (2-3), 203-211.

8. Van de Ven, T. G. M., The capture of colloidal particles on surfaces and in porous material: basic principles. *Colloids Surf. Physicochem. Eng. Aspects* **1998,** 138, (2-3), 207-216.

9. Elimelech, M.; Gregory, J.; Jia, X.; Williams, R., *Particle deposition and aggregation: measurement, modelling and simulation*. Butterworth-Heinemann: 1998.

10. Fatisson, J.; Domingos, R. F.; Wilkinson, K. J.; Tufenkji, N., Deposition of TiO2 nanoparticles onto silica measured using a quartz crystal microbalance with dissipation monitoring. *Langmuir* **2009,** 25, (11), 6062-6069.

11. Serizawa, T.; Takeshita, H.; Akashi, M., Electrostatic adsorption of polystyrene nanospheres onto the surface of an ultrathin polymer film prepared by using an alternate adsorption technique. *Langmuir* **1998,** 14, (15), 4088-4094.

12. Gole, A.; Sainkar, S.; Sastry, M., Electrostatically controlled organization of carboxylic acid derivatized colloidal silver particles on amine-terminated self-assembled monolayers. *Chem. Mater.* **2000,** 12, (5), 1234-1239.

13. Chen, K. L.; Elimelech, M., Aggregation and deposition kinetics of fullerene (C60) nanoparticles. *Langmuir* **2006,** 22, (26), 10994-11001.

14. Tretiakov, K. V.; Bishop, K. J. M.; Kowalczyk, B.; Jaiswal, A.; Poggi, M. A.; Grzybowski, B. A., Mechanism of the Cooperative Adsorption of Oppositely Charged Nanoparticles. *J. Phys. Chem. A* **2009,** 113, (16), 3799-3803.

15. Fatisson, J.; Ghoshal, S.; Tufenkji, N., Deposition of Carboxymethylcellulose-Coated Zero-Valent Iron Nanoparticles onto Silica: Roles of Solution Chemistry and Organic Molecules. *Langmuir* **2010,** 26, (15), 12832-12840.

16. Goodwin, J.; Ottewill, R.; Pelton, R., Studies on the preparation and characterization of monodisperse polystyrene latices V.: The preparation of cationic latices. *Colloid. Polym. Sci.* **1979,** 257, (1), 61-69.

17. Sajjadi, S., Nanoparticle Formation by Monomer-Starved Semibatch Emulsion Polymerization. *Langmuir* **2006,** 23, (3), 1018-1024.

18. Sauerbrey, G., Use of quartz crystal vibrator for weighting thin films on a microbalance. *Z Phys* **1959,** 155, 206-222.

19. Höök, F.; Rodahl, M.; Brzezinski, P.; Kasemo, B., Energy dissipation kinetics for protein and antibody-antigen adsorption under shear oscillation on a quartz crystal microbalance. *Langmuir* **1998,** 14, (4), 729-734.

20. Edvardsson, M.; Rodahl, M.; Kasemo, B.; Höök, F., A dual-frequency QCM-D setup operating at elevated oscillation amplitudes. *Anal. Chem.* **2005,** 77, (15), 4918-4926.

21. Wang, G.; Pelton, R.; Hrymak, A.; Shawafaty, N.; Heng, Y. M., On the role of hydrophobic particles and surfactants in defoaming. *Langmuir* **1999,** 15, (6), 2202-2208.

22. Elmahdy, A.; Mirnezami, M.; Finch, J., Zeta potential of air bubbles in presence of frothers. *Int. J. Miner. Process.* **2008,** 89, (1-4), 40-43.

23. Van De Ven, T. G. M., Kinetic aspects of polymer and polyelectrolyte adsorption on surfaces. *Adv. Colloid Interface Sci.* **1994,** 48, 121-140.

24. Ryde, N. P.; Matijevi, E., Deposition and detachment studies of fine particles by the packed column technique. *Colloids Surf. Physicochem. Eng. Aspects* **2000,** 165, (1-3), 59-78.

25. Adamczyk, Z.; Zembala, M.; Siwek, B.; Warszynski, P., Structure and ordering in localized adsorption of particles. *J. Colloid Interface Sci.* **1990,** 140, (1), 123-137.

26. Soltani, M.; Ahmadi, G., Detachment of rough particles with electrostatic attraction from surfaces in turbulent flows. *J. Adhes. Sci. Technol.* **1999,** 13, (3), 325-355.

# Appendix: Supporting Materials for Chapter 4

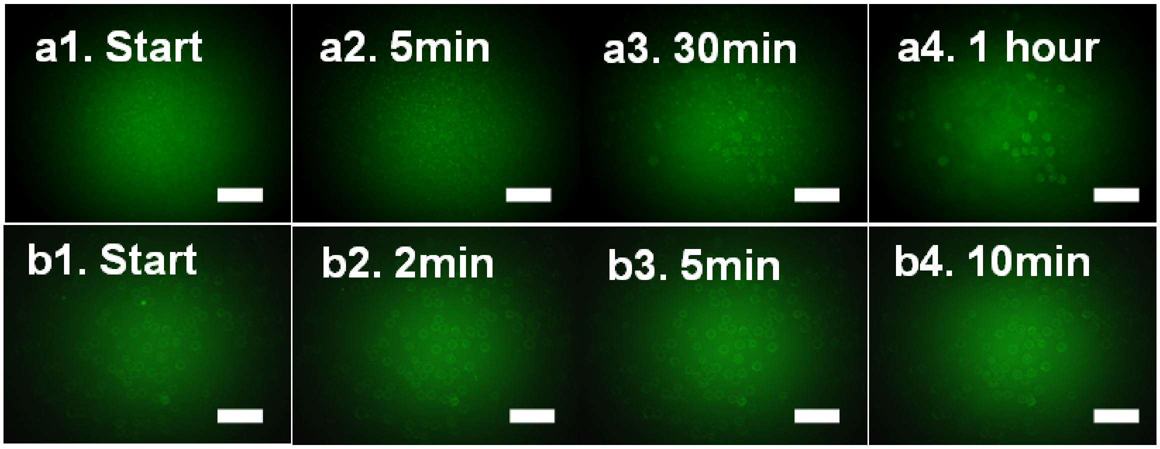

**Figure s1.** Fluorescence images of St-01-F-292 and St-MAPTAC-03-F-81 adsorbed onto 30-50 μm glass beads recorded at various conditioning intervals (a1. start, a2. 5 min, a3. 30 min and a4. 1 hour for St-01-F-292; b1. start, b2. 2 min, b3. 5 min, and b4. 10 min for St-MAPTAC-03-81). All scale bars are 200 μm.

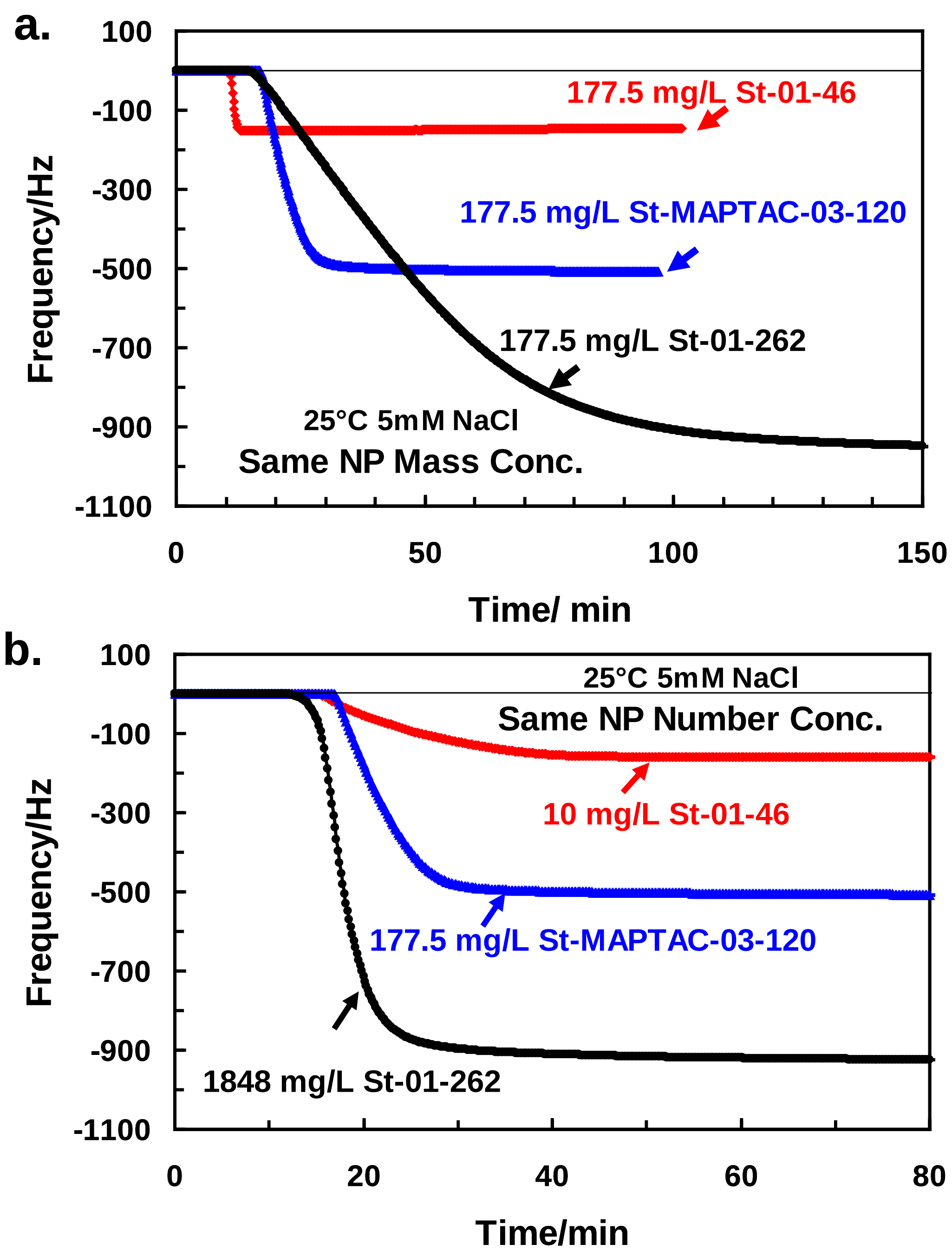

**Figure s2.** Raw deposition data (frequency vs. time) of St-01-46, St-MAPTAC-03-120 and St-01-262 onto $SiO_2$ coated sensor with QCM-D by comparing at a. same nanoparticle mass concentration; b. same nanoparticle number concentration

## Appendix C4: The goal of this model is to calculate Reynolds number and predict nanoparticle detachment forces by Cox-Brenner Equation in the QCM experiemnts

| | |
|---|---|
| $h := 0.5\text{mm}$ | module depth |
| $D_s := 1.4\text{cm}$ | diameter of the sensor |
| $P := 2D_s + 2 \cdot h$ | module cross-sectional wetting perimeter |
| $A_m := D_s \cdot h$ | module cross-sectional area |
| $d := \dfrac{4A_m}{P}$ | irregular module diameter |
| $d = 0.097 \cdot \text{cm}$ | |
| $V_f := \dfrac{100}{60} \cdot 10^{-6} \dfrac{L}{s}$ | flow rate |
| $\rho := 1000 \cdot \text{kg} \cdot \text{m}^{-3}$ | water density |
| $U := \dfrac{V_f}{\pi \cdot \left(\dfrac{d}{2}\right)^2}$ | fluid Velocity |
| $U = 2.276 \times 10^{-3}\,\text{m} \cdot \text{s}^{-1}$ | |
| $\eta_0 := 0.00089\text{Pa} \cdot \text{s}$ | water viscosity |
| $\phi := 0.018\%$ | particle volume fraction |
| $\eta := \eta_0 \cdot (1 + 2.5\phi)$ | Stokes-Einstein equation for hard spherical colloid |
| $\eta = 8.904 \times 10^{-4} \cdot \text{Pa} \cdot \text{s}$ | |
| $Re := \dfrac{d \cdot U \cdot \rho}{\eta}$ | Reynolds number |
| $Re = 2.468$ | Suggesting the type of Laminar flow |

To caculate the detachment forces in Laminar flow:

$$r_{np} := \begin{pmatrix} 23 \\ 60 \\ 131 \end{pmatrix} \text{nm}$$ Nanoparticle radius

$$F_d := (1.7) \cdot \left(6 \cdot \pi \cdot \eta \cdot r_{np} \cdot U\right)$$ Goldman, Cox and Brenner Equation

$$F_d = \begin{pmatrix} 1.494 \\ 3.897 \\ 8.508 \end{pmatrix} \cdot \text{pN}$$ detachment forces

# Chapter 5 Functionalized Nanoparticle Flotation Collectors for Pentlandite Isolation

In Chapter 5, I conducted most of the experiments. Mile Montgomery who worked with me as a summer student performed some of the flotation experiments. I plotted all of the data and wrote the first draft. Dr. Pelton helped to analyze data, give many useful discussions and revise some parts of the draft to this version. Carla Abarca contributed useful discussions and gave some analysis of the FTIR. Zongfu Dai helped to design the experiments, send samples for ICP-OES and give many useful discussions in data plotting. Manqiu Xu gave useful advice and helped with data analysis.

# Functionalized Nanoparticle Flotation Collectors for Pentlandite Isolation

*[†]Songtao Yang, [†]Robert Pelton*, [‡]Zongfu Dai, [†]Miles Montgomery, [†]Carla Abarca and [‡]Manqiu Xu*

[†]Department of Chemical Engineering, McMaster University, 1280 Main Street West,
Hamilton, Ontario, Canada L8S 4L7

[‡]Vale Base Metals Technology Development (VBMTD), 2060 Flavelle Blvd.,
Mississauga, Ontario, Canada L5K 1Z9

Corresponding author: peltonrh@mcmaster.ca

**Possibly will be submitted to: *Mineral Engineering/Langmuir***

## Abstract

This paper describes a series of functionalized nanoparticles based on poly(styrene-co-vinylimidazole) which are used as a new class of flotation collectors for pentlandite flotation. The functional group, 1-vinyl imidazole, of the functionalized nanoparticles was identified by FTIR. The p$K_a$ and the quantity of 1-vinyl imidazole groups on the nanoparticles were measured with conductometric and pH titration. The p$K_a$ of St-VI-MAPTAC-3-158 was estimated to be about 8.0, and the quantity of imidazole groups on St-VI-MAPTAC-3-158 was estimated as 0.55 mmol/g. The binding capacity for the functionalized nanoparticles to nickel ions increases with pH over the pH range of 3.2 to 9.1, suggesting that uncharged imidazole groups have the ability to form imidazole-Ni complexation. Flotation experiments of pentlandite alone and mixtures of pentlandite with either glass beads or Mg/Si slimes in the presence of the functionalized nanoparticles were performed to investigate their collecting power. Cationic polystyrene nanoparticles were effective collectors for pentlandite flotation, and imidazole functionalized nanoparticles performed better than the simple cationic nanoparticles. Possible driving forces in directing the nanoparticles to selectively deposit onto pentlandite are discussed.

## Introduction

Typically mined ore is crushed and ground to particles smaller than approximately 100 micrometer diameter which consist of valuable mineral-rich particles and unwanted gangue materials. Separation of the valuable metal mineral from gangue is achieved by a process known as froth flotation. A critical aspect of froth flotation is the need to specifically treat the desired mineral surfaces with a reagent known as the "collector". The collector functions to selectively render the mineral particles surfaces more hydrophobic than the unwanted gangue particles. By lowering the surface energy, hydrophobic mineral particles selectively adhere onto air bubbles upon particle-bubble collision. The mineral particle laden bubbles then rise to the surface where the froth phase is separated from the unwanted gangue. [1-2]

Despite the extensive role of flotation in mineral processing, some ores are difficult to process by flotation. For example, ultramafic nickel sulfide ore containing both valuable pentlandite (Pn, $Ni_{4.5}Fe_{4.5}S_8$) and large quantities of unwanted Mg/Si slime (predominantly serpentine, $(MgFe)_3Si_2O_5(OH)_4$) responds poorly to flotation. [3] One of the major unsolved issues is how to efficiently separate the pentlandite from the unwanted gangue materials in the presence of slimes. Fibrous Mg/Si slime usually masks the surface of pentlandite and dramatically depresses pentlandite flotation due to charge related effects between oppositely charged pentlandite and slimes. [4] Consequently, new approaches are required for processing these difficult ores.

Conventional molecular collectors are water-soluble surfactants with short hydrophobic tails and specific head groups, such as xanthate. Potassium amyl xanthate (PAX) is a characteristic example of pentlandite collector. The use of xanthate based collectors is an old technology and there are many scientific papers discussing the chemical aspects on the mineral particle surface. [1, 5-6] In addition, the continued use of xanthate has raised ever increasing environmental concern as carbon disulfide is readily emitted from xanthate decomposition. [7]

Recently, we have demonstrated that water-soluble collectors can be replaced by hydrophobic polystyrene nanoparticles leading to the first reported use of nanoparticles as flotation collectors. [8-9] Hydrophilic glass beads were used as a model for mineral particles in our previous studies. Our first published paper investigated the mechanisms behind the application of nanoparticle collectors, including flotation results facilitated with the use of nanoparticles and micromechanical measurements of glass bead/air bubble adhesion. [8] We also reported water contact angle measurements on smooth polymer films cast from dissolved parent nanoparticles, which correlated the hydrophobicity of polystyrene based nanoparticles with their ability to facilitate glass bead flotation. We showed that it was required for a polymer film contact angle to be at least in the range from 51° to 85° for a good flotation recovery. [9] Lately, we observed that nanoparticle deposition onto bead surfaces was a rate controlling event and nanoparticle diameter had a significant influence on nanoparticle transport and deposition rates to mineral surfaces.

Preferable diameters for nanoparticle flotation collectors were found to be in the range of 40 to 300 nm. [10]

This paper is to report on using functionalized nanoparticles as flotation collectors for floating pentlandite from a natural ultramafic ore. One of the primary challenges for the industrial application of nanoparticle flotation collectors is how to enhance the nanoparticles' ability to selectively deposit onto the desired mineral particles instead of unwanted gangue materials. The goal of this study is to develop functionalized nanoparticle collectors for pentlandite flotation and to enhance the selectivity in the separation of pentlandite from unwanted materials. The functional group imidazole, capable of forming the nickel-ligand complex, was designed on the surface of the polystyrene nanoparticles via copolymerization [11-12] of styrene with 1-vinyl imidazole. There has been previous research which provides evidence that the separation of copper sulfides or negatively-charged minerals can be promoted with the use of alkyl derivatives of imidazole as flotation collectors. [13-14] However, in their cases, the derivatives of imidazole were small, water-soluble molecules instead of hydrophobic nanoparticles with imidazole on the surface.

Imidazole-nickel complexation has been used in a number of applications, such as the removal of metal ions in wastewater [15], bioseparation [16], formation of polymer/metal composite [17], etc. Lippert and coworkers [18] reported the detailed structure of poly (1-vinyl imidazole)-Ni complex and found that the stoichiometry of the complex formed in the solution containing excess $Ni^{2+}$ was [1-vinyl imidazole]/[ $Ni^{2+}$] = 6/1 in aqueous solution and 4/1 in aqueous 1 M $KNO_3$, whereas Tamai and coworkers [17] reported that the stoichiometry of [1-vinyl imidazole]/[ $Ni^{2+}$] equaled approximately 2/1.

Herein we describe a new class of flotation collectors based on poly (styrene-co-1-vinylimidazole) nanoparticles for the selective separation of pentlandite from unwanted materials. In this work we report: the functionalized nanoparticles binding capacity with $Ni^{2+}$ ions over a pH range of 3.2-9.1; flotation experiments with nanoparticle collectors on pentlandite only, and mixtures of pentlandite with either glass beads or Mg/Si slimes.

## Experimental Section

**Materials:** Styrene (99%, Sigma-Aldrich) and 1-vinylimidazole (VI, ≥ 99%, Sigma-Aldrich) were purified by vacuum distillation. 3-(methacryloylamino)propyl trimethyl ammonium chloride solution (MAPTAC, 50 wt. % in $H_2O$, Sigma-Aldrich) was passed through an inhibitor-removing column. 2, 2'-azobis (2-methylpropionamidine) dihydrochloride (V50, 97%), cetyltrimethylammonium bromide (CTAB, 95%), sodium sulfide nonahydrate ($Na_2S{\cdot}9H_2O$, ≥ 98%), nickel (II) sulfate hexahydrate ($NiSO_4{\cdot}6H_2O$, 99.99+% metals basis) were purchased from Sigma-Aldrich and used as supplied. The molecular collector, potassium amyl xanthate (PAX), and the frother, UNIFROTH 250C (99%), were donated by VBMTD (Mississauga, ON). All solutions were made with Type 1 water (18.2 MΩcm, Barnstead Nanopure Diamond system).

**Nanoparticle Preparation and Characterization:** The recipes used to prepare functionalized nanoparticle dispersions are summarized in Table 1. The methodology used to prepare the nanoparticles is according to classic surfactant-free polymerization [19] and starved-feed semibatch emulsion polymerization [20]. The experimental design of the polymerizations are similar to that of our previous publication [8], with a few alterations. The polymerizations were conducted in a three-necked flask equipped with a condenser, two rubber stopper holding syringe needles (one for nitrogen, the other for starved-feed monomer addition), and a magnetic stirring bar (controlled by a IKAMAG® RCT basic hot plate/stirrer, NC). Typically, 100 mL of deionized water were charged to the reactor followed by nitrogen purging for 30 minutes at 70°C with 350 rpm stirring. To the reactor were added 0.5 g of styrene and 0.25 g of 50 wt. % MAPTAC (or 0.10 g of CTAB). The mixtures were allowed to equilibrate for 10 minutes before V50 was added to initiate the polymerization. After 15 minutes polymerization of the initial charge, an additional 4.5 g of styrene and 0.25 g of VI dissolved in 4.7 mL water, were added over 5 hours (0.0083 mL/min) from twin 10 mL syringes fitted to a syringe pump (NE-1600, New Era Pump System, Inc., NY). The reaction was stirred at 70°C for an additional 19 hours. The resulting latex was dialyzed for at least one week against deionized water, after which the dialysate conductivity was less than 30μS/cm.

Hydrodynamic diameters of prepared nanoparticles were measured by dynamic light scattering (DLS, Brookhaven Instruments Corporation) using a detector angle of 90°. Correlation data were analyzed by the DLS software (Windows 9KDLSW Version 3.34) using the cumulant fit method and the scattering intensity was set between 150 and 250 kcounts/s for each measurement. The duration for each measurement was set to 5 min. Electrophoretic mobility measurements were performed by a Zeta PALS instrument (Brookhaven Instruments Corporation) at 25 °C in phase analysis light scattering mode. The reported mobilities were the average of 10 runs, each consisting of 15 scans. Sample pH was adjusted with 0.01 M or 0.1 M HCl and NaOH. Samples for both dynamic light scattering and electrophoretic mobility measurements were prepared in clean vials by dispersing approximately 0.25 g/L of the nanoparticles in 5mM NaCl.

Sessile drop water contact angles on smooth polymer films were used as an indication of the hydrophobicity of nanoparticle surfaces. Either the compressed disk method [21] or spin coating of polymer solution from dissolved parent nanoparticles [9] was applied to prepare the smooth films. Suspensions (for the cases of St-MAPTAC-1-79, St-VI-MAPTAC-2-68 and St-VI-MAPTAC-158) were freeze-dried and pressed at 10,000 psi by a Carver® hydraulic press at room temperature with a stainless steel mold which was used to prepare KBr pellets for FTIR. For the latter method, St-4-46 was dissolved in THF (tetrahydrofuran, certified, Fisher Scientific) 0.5-1.0 wt%, and St-VI-5-52 was dissolved in chloroform (for HPLC, ≥99.9%, Sigma-Aldrich). The solutions were spin coated on a glass slide with a SPIN 150 Wafer Spinner (running rev: 3.25 software) at 3000 rpm to form smooth polymer films. The measurements were performed using a Krüss contact angle measuring instrument running DSA 1.80.0.2 software.

FTIR spectra of St-VI-MAPTAC-3-158 and St-4-46 were characterized using a Bio-Rad FTS-40 FT-IR spectrometer. Samples were prepared as KBr pellets. A small amount of freeze-dried nanoparticles was mixed with spectroscopic grade KBr and the mixture was pressed using a Carver® hydraulic press at 10,000 psi to form the pellet. The spectra were scanned over 4000-400 $cm^{-1}$ range with the transmission mode of the instrument.

Conductometric and pH titration were used to establish the amount of 1-vinyl imidazole groups on the surface of functionalized nanoparticles (e.g., St-VI-MAPTAC-3-158). The titration was conducted using a Burivar-I2 automatic buret (ManTech Associates). Nanoparticle dispersion was added into 50mL of 1mM KCl solution to give a ~ 1.0 g/L suspension. The pH was manually lowered to 3.0 and the sample was titrated with 0.1M NaOH under $N_2$ purge. A waiting time of 60 seconds between injections was employed to ensure complete ionic equilibration between the solution and VI groups.

Binding isotherms for $Ni^{2+}$ ions to functionalized nanoparticles (e.g., St-VI-MAPTAC-3-158) was measured as follows. A series of pH buffers (i.e., pH ranged from 3 to 10) were prepared as stock solutions with one-direction addition of 0.1 M/1 M HCl or NaOH. Nickel ion solutions were prepared by dissolving $NiSO_4{\cdot}6H_2O$ in each pH buffer to give a series of concentrations (0.5 mM, 1 mM, 2 mM and 3 mM, corresponding to 29.4, 58.7, 117.4, and 176.1 $mgL^{-1}$ of nickel). Functionalized nanoparticles were dispersed into 40 mL of the prepared $Ni^{2+}$ solutions by ultrasonication for 2 minutes. Next, the mixture was allowed to condition for 30 minutes at 25°C in a shaking water bath (Sheldon Manufacturing Inc., Model: 1217). The nanoparticle phase was then separated using an ultracentrifuge at 20,000 rpm for 30 min. The supernatant was collected and the equilibrium Ni ion concentration in the supernatant was analyzed by atomic absorption spectroscopy (SpectrAA 220, Varian Inc.) equipped with a nickel hollow cathode lamp. The quantity of $Ni^{2+}$ bound to the nanoparticles was determined from the difference of the initial and equilibrium $Ni^{2+}$ concentrations.

**Model Mineral Suspensions:** Glass beads (≤106 μm, -140 U.S. sieve) were purchased from Sigma-Aldrich. Pentlandite (Pn) was purified from a mixture of several high grade rougher concentrates collected from flotation trials at Vale. Ni grade of the purified Pn sample was in the ranged of 25-30%. Note the Ni grade of 100% pure pentlandite, $Ni_{4.5}Fe_{4.5}S_8$, is about 34%. Tails samples were the scavenger flotation tails of the Pipe drill ore sample. Vale's flotation procedures for acquiring Pn and tails included grinding, hydrocyclone desliming followed by rougher and scavenger flotation. The particle size distributions of the glass beads, Pn and tails in 5 mM NaCl were measured with a Malvern Mastersizer 2000.

Both Pn and tails were chemically cleaned, to remove residual xanthate and oxidation products from surfaces. Five grams of Pn and 50 mL of deoxygenated 0.1 M HCl were charged into a three-necked 100 mL flask equipped with a sealable condenser, a rubber stopper with needle for $N_2$ purging, and a magnetic stirring bar. The mixtures were agitated for 1 h followed by settling and decanting the supernatant. The sediment was rinsed with 50~80 mL deoxygenated water a couple of times. The wash water was removed by decantation and 50 mL of deoxygenated 0.5 M $Na_2S \cdot 9H_2O$ solution were added and the suspension was mixed at room temperature for 5 h. After rinsing and decantation with 2×50~80 mL deoxygenated water, the suspensions were diluted with deoxygenated water to give 0.1 g/mL suspensions used for flotation.

**Flotation**: All flotation experiments were performed in a custom lab-scale flotation apparatus. In a typical pentlandite flotation experiment, 10 mL of 0.1 g/mL washed Pn suspension (or mixture of 10 mL 0.1 g/mL Pn and 1.0 g glass beads, or mixture of 10 mL of 0.15 g/mL Pn and 10 mL of 0.15 g/mL tails) and 0.5 mL of functionalized nanoparticles (24.2 g/L for St-VI-MAPTAC-2-68) were added into 115 mL of 5 mM NaCl (or 5mM $Na_2CO_3$) in a 150 mL plastic flotation beaker. The beaker sat on a 90 mm diameter plastic Petri dish, which in turn was sitting on a magnetic stirrer (Corning Stirrer, Model PC-610). The suspension of Pn and nanoparticles was mixed (25 mm×25 mm cross-shape stirring bar at ~ 600 RPM) for 5 minutes (10 minutes for St-VI-MAPTAC-158) to permit the nanoparticles to deposit onto the surface of Pn. Following conditioning, 0.12 mL of 1% UNIFROTH 250C (10ppm) was added and mixed for 30 additional seconds. Flotation was commenced by initiating nitrogen flow (Matheson 604 E700 Flow Controller) at a rate of 2.0 L/min through a Corning Pyrex gas dispersion tube (Fisher Scientific, 11-137E) consisting of a 30 mm coarse glass frit attached by a 90 degrees elbow. During flotation, the stirring rate was increased to ~ 900 RPM to avoid bead sedimentation. The froth phase was scraped over the edge of the beaker and collected in a plastic Petri dish. After 1.0-1.5 minutes the gas flow was stopped, the plastic collection dish was replaced with a clean dish, and the liquid level in the flotation beaker was topped up with UNIFROTH 250C in 5 mM NaCl. This sequence was repeated until 3 or 4 dishes were collected. The mass of “accepts” collected in each dish were weighed and the solids were filtered, dried and weighed.

The dosage of nanoparticles collectors was expressed as $\lambda_T$, which we define as the ratio of the total projected area of the added nanoparticles to the total surface area of pentlandite. For all of flotation results herein involving nanoparticle addition $\lambda_T$ was greater than 100% meaning the nanoparticles were present in excess.

For flotation of the mixed suspensions (Pn + glass beads or Pn + tails), the nickel content of the recovered solids was measured by a Varian Vista inductively coupled plasma - optical emission spectrophotometer (ICP-OES). Approximately 0.25 g of sample was weighed into a zirconium crucible. 3.4 g of sodium peroxide and 2-3 pellets of sodium hydroxide were added to the sample and mixed. The crucible was placed into a muffle furnace at 710°C for 35 minutes. The resulting cake was then leached with water and hydrochloric acid. The solution was bulked to a 250 mL volume and read directly on ICP-OES.

The microstructure of recovered pentlandite or the mixture of Pn/glass beads, Pn/tails from flotation runs with nanoparticle collectors were investigated by using a JEOL JSM-7000F scanning electron microscope (SEM) equipped with energy-dispersive X-ray diffraction (EDX).

## Results

A series of poly (styrene-co-vinylimidazole) based functionalized nanoparticle dispersions were prepared via emulsion copolymerization. Hydrodynamic diameters of the resulting nanoparticles were measured by dynamic light scattering. The average particle diameters of five nanoparticle suspensions varied from 46 to 158 nm. All of the nanoparticle dispersions (latex) had positive electrophoretic mobilities. The results are summarized in Table 2 together with contact angle values. Water contact angle measurements were used to evaluate the hydrophobicities of nanoparticle surfaces. The sessile drop water contact angles on smooth polymer films ranged from 66° for St-VI-MAPTAC-3-158 to 93° for St-4-46, indicating that the hydrophobicity of prepared latexes were in the required range for designing effective nanoparticle flotation collectors. [9]

Figure 1 shows the effect of pH on electrophoretic mobility of the three nanoparticles containing the comonomer MAPTAC. All three nanoparticles are positively charged even at high pH (e.g., pH = 12) due to the quaternary nitrogen on the MAPTAC moieties and the presence of amidine groups from the initiator [19]. In addition, the imidazole groups contribute cationic charge to VI nanoparticles at pH below 5.0. The complex pH-dependent behaviors shown in the figure reflect the pH sensitivity of the amidine ($pK_a$ = 12.4, [19]) and the 1-vinyl imidazole ($pK_a \approx 5.0$, [11, 22]) groups.

FTIR spectra were applied to further investigate whether the 1-vinyl imidazole groups were introduced to the functionalized nanoparticles. Figure 2 shows the spectra comparison of the 500-2000 $cm^{-1}$ region of St-VI-MAPTAC-3-158 to imidazole-free St-4-46, confirming the presence of imidazole on the VI functional nanoparticles. The bands at 1228 $cm^{-1}$ and 665 $cm^{-1}$ from St-VI-MAPTAC-158 are attributed to the stretching vibration of the C-N bond from the imidazole ring, which is in agreement with Lippert et. al.'s early work [18].

Conductometric and pH titration were used to establish the quantity of 1-vinyl imidazole groups on the surface of functionalized nanoparticles. Figure 3 shows the titration results of St-VI-MAPTAC-3-158 dispersions in 1 mM KCl. The measured vinyl imidazole moieties of the functionalized nanoparticles are calculated as 0.55 mmol/g nanoparticles, which is close to the theoretical value. The theoretical functionality equals 0.51 mmol 1-vinyl imidazole per gram of copolymer nanoparticles (see recipes in Table 1) assuming that both comonomers were completely reacted. The measured 1-vinyl imidazole moieties were slightly higher than theoretical ones, suggesting a lower productivity of the polystyrene fraction in the final copolymer product in our experiments.

In addition, the pH titration gave the pKa of St-VI-MAPTAC-3-158 in the range of 7.0-8.0, which is higher than $pK_a$ ~5.0 of poly (1-vinyl imidazole) according to Popping et al.'s work [22]. This indicates the surface groups on St-VI-MAPTAC-3-158 are interacting.

Binding isotherms of $Ni^{2+}$ ions to nanoparticles with (St-VI-MAPTAC-3-158) and without (St-MAPTAC-1-79) 1-vinyl imidazole groups are shown in Figure 4. At the pH of 6.5, St-MAPTAC-1-79 nanoparticles adsorbed very little $Ni^{2+}$ (~ 0.01mmol/g) whereas St-VI-MAPTAC-3-158 adsorbed about 0.14 mmol/g. Clearly, VI functionalized nanoparticles adsorb $Ni^{2+}$ ions. The influence of pH on the binding capacity of functionalized nanoparticles to $Ni^{2+}$ ions is also compared in the figure. Table 3 summarizes the binding capacity at 176.1 $mgL^{-1}$ of [$Ni^{2+}$] for St-VI-MAPTAC-158 to $Ni^{2+}$ ions at solution pHs of 3.2, 5.7, 6.5, 7.8 and 9.1. The stoichiometry of [1-vinyl imidazole]/[$Ni^{2+}$] was estimated as 37/1, 6.9/1, 3.9/1, 3.2/1 and 2.4/1 at each corresponding pH. At the highest measured pH (i.e. 9.1), the stoichiometry equaled approximately 2.4/1, which is close to the reported stoichiometry (about 2/1) of Tamai et al.'s work [17]. When the pH approached 10 or higher in the preparation of the $Ni^{2+}$ ion solution, we observed a light greenish suspension/precipitate in our experiments. Note that $Ni^{2+}$ ion usually hydrolyzes to form nickel hydroxide in aqueous solution when the pH higher than a threshold value (pH of ~9.0) at which hydrolysis starts, and this pH depends upon the concentration of the $Ni^{2+}$ ions as well. [23] For a consistent comparison, we did not make further binding measurements after the aqueous phase changed.

Model mineral suspensions (glass beads, a purified Pn suspension and tails from an ultramafic deposit) for flotation experiments were characterized by both Mastersizer particle size distributions and electrophoretic mobilities. The volume-weighted particle size distributions for the three suspensions are shown in Figure 5. The particle size distributions of the glass beads and the Pn suspensions appeared approximately log normal whereas the distribution of Mg/Si slime tails was asymmetric with a significant lobe at the low end of the distribution. The surface area mean diameters ($D_{32}$, also known as Sauter mean diameter) for each suspension are given in the figure, i.e., 67, 12 and 101 μm for the beads, Pn and tails respectively. The corresponding specific surfaces areas ($\sigma$ in Figure 5, 0.037, 0.1 and 0.022 $m^2/g$) were estimated from the $D_{32}$ diameters assuming non-porous spherical particles.

The electrophoretic mobilities of the glass beads, Pn and tails suspensions are shown as functions of pH in Figure 6. At natural pH, the pentlandite and glass beads were negatively charged with a mobility of about -1.5 and $-2.3\times10^{-8}$ $m^2s^{-1}V^{-1}$ respectively, whereas tails were positively charged with a mobility of roughly $1.8\times10^{-8}$ $m^2s^{-1}V^{-1}$. Under the conditions of the small-scale flotation experiments for mixtures of Pn and tails (in 5mM $Na_2CO_3$, pH = 10.6 ± 0.3), the mobility for negatively charged pentlandite was increased to -3.3, while the positively charged tails decreased to less than 0.5.

Figure 7a shows the flotation recovery of washed pentlandite with the use of St-MAPTAC-1-79 or St-VI-MAPTAC-2-68 nanoparticles. For all experiments, the nanoparticle dosages were sufficient to cover the pentlandite surface. Without nanoparticles, only about 30% Pn was recovered by hydraulic entrainment, whereas higher recoveries were obtained in the presence of the two nanoparticles. In 5mM NaCl, 71% Pn was recovered by St-MAPTAC-1-79 and 90% by St-VI-MAPTAC-2-68. In 5mM $Na_2CO_3$, about 80% Pn was recovered by St-VI-MAPTAC-2-68. Clearly, the addition of either nanoparticle facilitated flotation recovery of Pn in comparison to the control. The functionalized St-VI-MAPTAC-2-68 was more effective than the simple cationic particles St-MAPTAC-1-79, in spite of the fact that the imidazole functionalized particles were less hydrophobic according to the contact angle measurements (see Table 2). One advantage of nanoparticle flotation collectors is that they are easily observed with electron microscopy. Figure 7b and c show SEM micrographs of Pn surfaces after flotation without and with St-VI-MAPTAC-2-68. The micrograph of the Pn with St-VI-MAPTAC-2-68 shows that nanoparticle coverage is relatively high on the Pn surfaces. Figure 7d shows a typical energy-dispersive X-ray diffraction (EDX) spectra example of recovered Pn particle with the use of St-VI-MAPTAC-2-68. The existence of carbon element confirmed the adsorption of nanoparticle collectors onto pentlandite.

Figure 8 summarizes flotation results of the mixed suspensions of washed pentlandite and glass beads with VI functionalized nanoparticles and corresponding imidazole-free ones. The results shown in Figure 8a and d are expressed as cumulative Ni grade versus the cumulative Ni recovery, and the three data points in each graph correspond to three dishes collected during the flotation run. Figure 8a compares the results of St-VI-MAPTAC-2-68 ($\lambda_T$ = 244%) to St-MAPTAC-1-79 ($\lambda_T$ = 316%) in the presence of excess nanoparticle dosage. A slightly higher Ni grade and higher Ni recovery were seen with the imidazole functionalized nanoparticles. Figure 8b and c show SEM micrographs of the sample recovered from the run with St-VI-MAPTAC-2-68. Surfaces of both Pn and glass beads were deposited by nanoparticles, but closer examination (Figure 8c) revealed that a larger quantity of nanoparticles adsorbed onto Pn particle than the bead. This observation indicates that the imidazole functionalized nanoparticles preferred to deposit onto pentlandite surfaces rather than the bead surfaces, and thus yielded a better Ni separation efficiency. Similar and expected results were obtained with the smaller and more hydrophobic nanoparticle collectors. Note that smaller and more hydrophobic nanoparticles are more effective flotation collectors. [8] Figure 8d shows the flotation results comparing St-VI-5-52 to St-4-46 at an equivalent preset nanoparticle dosage ($\lambda_T$ = 100%). A noteworthy higher Ni grade (29% to 24%, the first points) was obtained with St-VI-5-52 than St-4-46, even though the dosages of this comparison are lower than previous ones (Figure 8a). Note the Ni grade of pure pentlandite, $Ni_{4.5}Fe_{4.5}S_8$, is about 34%.

Figure 9a compares the flotation results between the conventional PAX collector and St-VI-MAPTAC-3-158 on a mixture of washed Pn and Mg/Si slime tails in 5mM $Na_2CO_3$. With the use of St-VI-MAPTAC-3-158 a higher cumulative Ni grade (17%, the third point) and a higher cumulative Ni recovery (88%) were acquired, whereas PAX gave a lower cumulative Ni grade (15%, the third point) and a lower cumulative Ni recovery (73%). Both collectors gave similar MgO grade (~12%). Figure 9b and c show SEM micrographs of the recovered Pn surfaces and tails surfaces recovered from the flotation with St-VI-MAPTAC-3-158. A high coverage of nanoparticles is seen on the Pn surfaces whereas there are very few nanoparticles deposited on the slime surfaces.

## Discussion

The main objective of our work was to develop functionalized nanoparticle collectors for selective recovery of pentlandite by froth flotation in the presence of unwanted materials. 1-vinyl imidazole was used as the comonomer via emulsion copolymerization with styrene to prepare the poly (styrene-co-1-vinyl imidazole) nanoparticle collectors. It is noted that poly (1-vinyl imidazole) is considered a weak cationic polyelectrolyte, and its p$K_a$ is approximately 5.0 according to Popping and coworkers [22]. The results of the conductometric and pH titration in Figure 3 suggest that the p$K_a$ of our poly (styrene-co-1-vinyl imidazole) nanoparticles was in the range of 7.0-8.0, which probably because the surface groups on the nanoparticles are interacting.

The correlation of p$K_a$ with pH is classically determined by the following equation:

$$\mathrm{pH} = \mathrm{p}K_a + \log\frac{[\mathrm{VI}]}{[\mathrm{VIH^+}]}$$

where [VI] is the concentration of 1-vinyl imidazole and [$\mathrm{VIH^+}$] is the concentration of corresponding protonated form, 1-vinyl imidazolium ion. The concentration of the two imidazole-based forms can be controlled by varying the pH of the water environment. The lower the pH, the greater the probability that the imidazole groups on the VI functionalized nanoparticles were protonated to the form of imidazolium ion.

For the binding measurements of St-VI-MAPTAC-158 nanoparticles with $Ni^{2+}$ ions shown in Figure 4 and Table 3, we have investigated at the solution pHs of 3.2, 5.7, 6.5, 7.8 and 9.1. At the pH of 3.2, which is lower than the p$K_a$ of 1-vinyl imidazole, the majority of the functionality is present as imidazolium ion form (charged form). By contrast, the functionality is mainly present as imidazole form (uncharged form) at pHs (e.g., 7.8 and 9.1) higher than the p$K_a$. Clearly, the uncharged form of the imidazole on St-VI-MAPTAC-158 binds $Ni^{2+}$ ions up to 0.23 mmol/g (e.g., pH of 9.1), whereas the charged form (imidazolium ion) binds very little $Ni^{2+}$ (~ 0.015 mmol/g, pH of 3.2) . The mechanism for the binding of the VI functionalized nanoparticles to nickel ions is probably via the N-3 atom of 1-vinyl imidazole which donates the unshared pair of electrons to the nickel. A similar mechanism has been proposed by Loo et al.'s study on imidazole binding to colloidal surfaces of Cu, Ag and Au. [24] An illustration of the proposed mechanism is shown in Figure 10 in the case of binding to nickel site of pentlandite. This may explain our experimental observations that the VI functionalized nanoparticles at higher pH can adsorb nickel ions more effectively than the corresponding imidazolium ion form at lower pH. Thus, when the water environmental pH is higher than the p$K_a$ of 1-vinyl imidazole, the VI functionalized nanoparticles should be effective and show good binding affinity to nickel ions. It is noteworthy that, in pentlandite flotation the common oxidation refers that $S^{-2}$ in $Ni_{4.5}Fe_{4.5}S_8$ usually oxidizes to $S^0$, then $SO_3^{-2}$, $SO_4^{-2}$; however, the nickel ion does not oxidize and is mainly present as the form of $Ni^{2+}$. Therefore, we propose that the imidazole-Ni complexation (Figure 10) is possible in pentlandite flotation conditions, e.g., pH~8.0 in 5 mM NaCl, and pH~10 in 5 mM $Na_2CO_3$.

All of the analysis so far we have based on the assumption that the imidazole groups on functionalized nanoparticle surfaces are acting as independent centers. One important question has been raised whether the groups are acting as independent centers or they are acting as a typical polyelectrolyte. To answer this question, we are comparing the average spacing of poly(1-vinyl imidazole) groups extended from nanoparticle surface with the classic Debye length, 1/kappa. Kappa, $\kappa$, is given by the following equation:

$$\kappa = \sqrt{\frac{e_0^2 N_A}{\varepsilon_r \varepsilon_0 kT} \sum_i c_i z_i^2}$$

where $e_0$ is electronic charge, $N_A$ is Avogadro's number, $c_i$ and $z_i$ are the concentration and valence of the counter ions of type $i$, $\varepsilon_r$ is the relative permittivity of water, $\varepsilon_0$ is the permittivity of vacuum. Through calculation, 5 mM NaCl gave the Debye length of 4.3 nm, and 5 mM $Na_2CO_3$ gave the length of 2.5 nm. Our nanoparticles were prepared by starved-feed semibatch polymerization and VI groups were added as secondary starved charge. If the VI groups were all copolymerized on the nanoparticle surfaces and the poly(1-vinyl imidazole) was mostly distributed as homopolymer orienting into water, the extended length of the VI groups (e.g., 0.55 mmol/g VI groups on 158 nm St-VI-MAPTAC-158) may exceed 2.5 nm or 4.3 nm. In such situation, the VI groups may function as independent center, and the imidazole-Ni complexation may accounts for an important driving force for the deposition. Otherwise, the nanoparticles will be act as typical polyelectrolytes, and the electrostatic force and van der Waal force will be dominant.

Hydrophobicity of nanoparticle surfaces is another important parameter when designing nanoparticle collectors. [9] In our study, the contact angle measurements summarized in Table 2 suggest that increasing 1-vinyl imidazole and MAPTAC in nanoparticle composition could lower the contact angles. Our previous study has shown that pristine polystyrene nanoparticles performed better than surface modified counterparts in glass beads flotation.[8-9] Thus, the optimization of poly (1-vinyl imidazole) functionalized nanoparticle collectors should balance the content of VI and MAPTAC when copolymerization with styrene. Relatively small ratios of VI/MAPTAC to St (see recipes in Table 1) satisfy the prerequisites.

We now talk about our flotation results. The flotation results of Pn only, summarized in Figure 7, indicate that the addition of either cationic nanoparticle collector can promote flotation recovery as the Pn is negatively charged in 5mM NaCl. Electrostatics and van der Waals forces can be applied to explain the nanoparticles deposition onto the Pn surfaces. Although we observed that the functionalized St-VI-MAPTAC-2-68 has advantages over the simple cationic particles St-MAPTAC-1-79 for Pn recovery, we cannot definitively conclude that imidazole functionalized particles are superior nanoparticle flotation collectors for the selective separation of Pn in the presence of unwanted materials.

To investigate whether imidazole-Ni complexation directs the functionalized nanoparticles to selectively deposit onto Pn, we designed the flotation experiments with mixed suspensions of washed pentlandite and glass beads. Note that both Pn and glass beads were negatively charged. The flotation results summarized in Figure 8a and d clearly show that St-VI-MAPTAC-2-68 and St-VI-5-52, the imidazole functionalized nanoparticles, gave a better Ni separation in terms of both Ni recovery and Ni grade. The results also indicate that electrostatics alone (the cases of St-MAPTAC-1-79 and St-4-46) provides little selectivity. The SEM images in Figure 8b and c illustrate that nanoparticles (St-VI-MAPTAC-2-68) with 1-vinyl imidazole (VI) surface ligands preferentially bind to Pn even in the presence of glass beads with more negative charges (see Figure 6).

Furthermore, we simulated a more realistic situation by mixing washed Pn with tails sample (Mg/Si slime) isolated from a Pipe drill core sample. The results shown in Figure 9a compare the conventional PAX collector to the imidazole functionalized nanoparticle collector. St-VI-MAPTAC-3-158 gave a better Ni grade-recovery curve than that did by PAX. Both collectors gave similar low MgO grade, suggesting that St-VI-MAPTAC-158 interacted with MgO-containing species in a manner similar to PAX (i.e., the nanoparticles did not deposit onto Mg/Si slime). Note that the nanoparticle concentration was six times greater than the PAX so the comparison was biased. Nevertheless, these results do suggest that it is possible to design nanoparticle collectors that give both high recovery and good selectivity against gangue materials.

In this study, of course imidazole groups on the surface of functionalized nanoparticles are capable of binding nickel ions under the conditions of the flotation experiments (i.e., pH ranging from 6.7 to 10.6). For all demonstrated flotation experiments involving Pn, the Pn suspensions were carefully washed with the use of deionized water for several times at the end of the washing procedure. The nickel ion concentration in the washed pentlandite suspension should be relatively low. Thus, the imidazole nanoparticles can be readily directed onto pentlandite surfaces, which we assumed to have higher local concentration of $Ni^{2+}$ ions than the free $Ni^{2+}$ ions in solution. However, in natural ore flotation tests, the crushed and ground slurry should have much higher concentration of nickel ions dissolved from Pn surface. The imidazole functionalized nanoparticles may interact with the free nickel ions in the aqueous solution while they deposit onto the Pn surfaces. This may affect imidazole functionalized nanoparticles deposition efficiency. Clearly, future work will be required to investigate the influence of $Ni^{2+}$ ion strength in the flotation slurry.

## Conclusions

In summary, we have developed functionalized nanoparticles based on poly(styrene-co-vinylimidazole) which were used as a new class of flotation collectors for pentlandite flotation. Based on the work we have described, the following conclusions are drawn:

1. Cationic polystyrene nanoparticles were effective collectors for pentlandite flotation and the 1-vinyl imidazole functionalized nanoparticles performed better than the simple cationic nanoparticles in terms of both Ni recovery and Ni grade.
2. The functionalized nanoparticles with imidazole surface ligands preferentially bind to pentlandite in the presence of oppositely charged tails or even in the presence of same negatively charged glass beads. The functionalized nanoparticle collectors provide good selectivity for pentlandite over either oppositely charged hydrophilic materials or same charged ones.
3. Aside from electrostatics, we propose that imidazole-Ni complexation accounts for an additional driving force which directs the nanoparticles to selectively deposit onto pentlandite.
4. The functional group, 1-vinyl imidazole, of the functionalized nanoparticles was identified by FTIR. The $pK_a$ and the quantity of 1-vinyl imidazole groups on the nanoparticles were measured using conductometric and pH titration, e.g., the $pK_a$ of St-VI-MAPTAC-3-158 was in the range of 7.0-8.0 and the quantity of imidazole groups on St-VI-MAPTAC-3-158 was estimated as 0.55 mmol/g.
5. The binding capacity for the functionalized nanoparticles to nickel ions increases with pH over the pH range of 3.2 to 9.1. This observation suggests that the nanoparticles may show good binding affinity to nickel-rich surfaces when the medium pH is higher than the $pK_a$ of 1-vinyl imidazole.

## Acknowledgment

We thank the Centre for Materials and Manufacturing (CMM), a division of the Ontario Centres of Excellence (OCE) in collaboration with Vale Base Metals Technology Development (VBMTD) for funding this research. We also acknowledge Analytical Lab at VBMTD for measuring ICP-OES. The McMaster team thank Zongfu Dai, Manqiu Xu and Peter Wells of Vale for patiently teaching us the basics of mineral processing.

## Figures

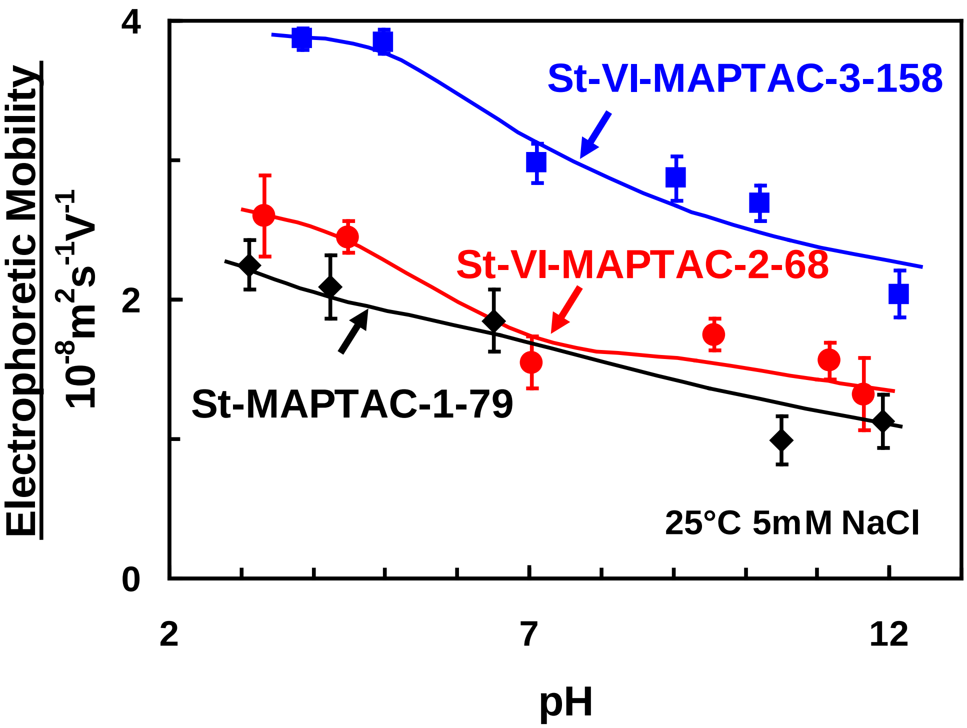

**Figure 1** Electrophoretic mobility of St-MAPTAC-1-79, St-VI-MAPTAC-2-68 and St-VI-MAPTAC-3-158 nanoparticles as a function of pH

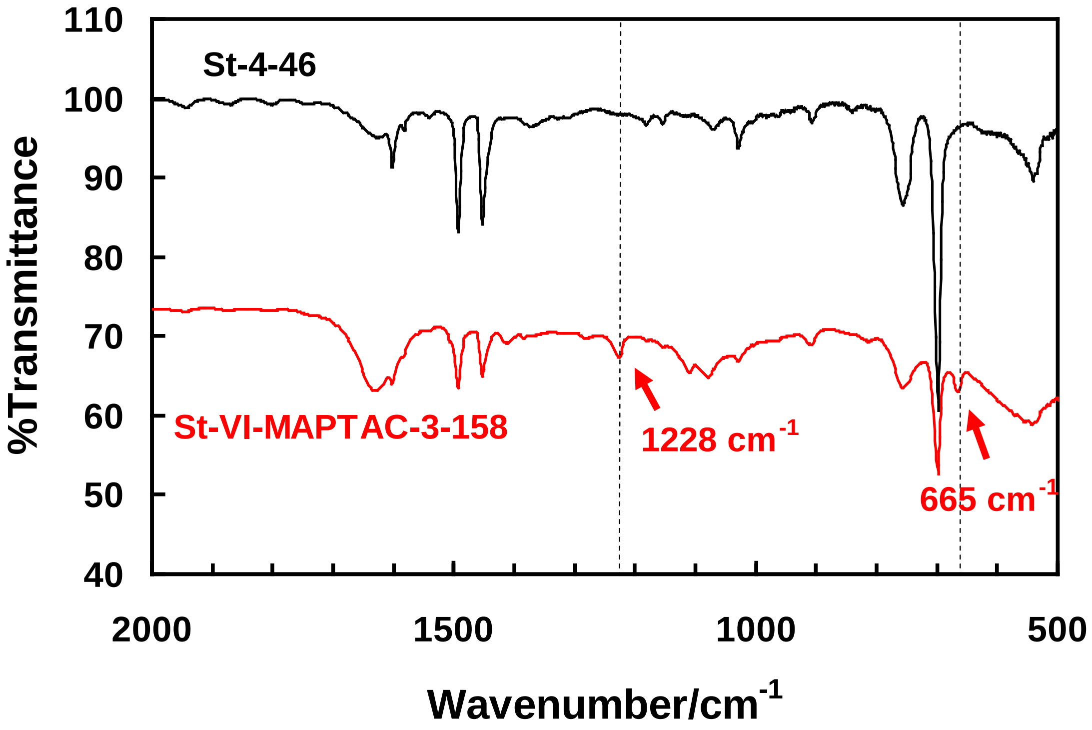

**Figure 2** FTIR spectra of the 500-2000 cm$^{-1}$ region for St-VI-MAPTAC-3-158 and St-4-46, showing the presence of vinyl imidazole on the functional nanoparticles. The bands at 1228 cm$^{-1}$ and 665 cm$^{-1}$ are owing to the stretching vibration of the C-N bond from the imidazole ring.

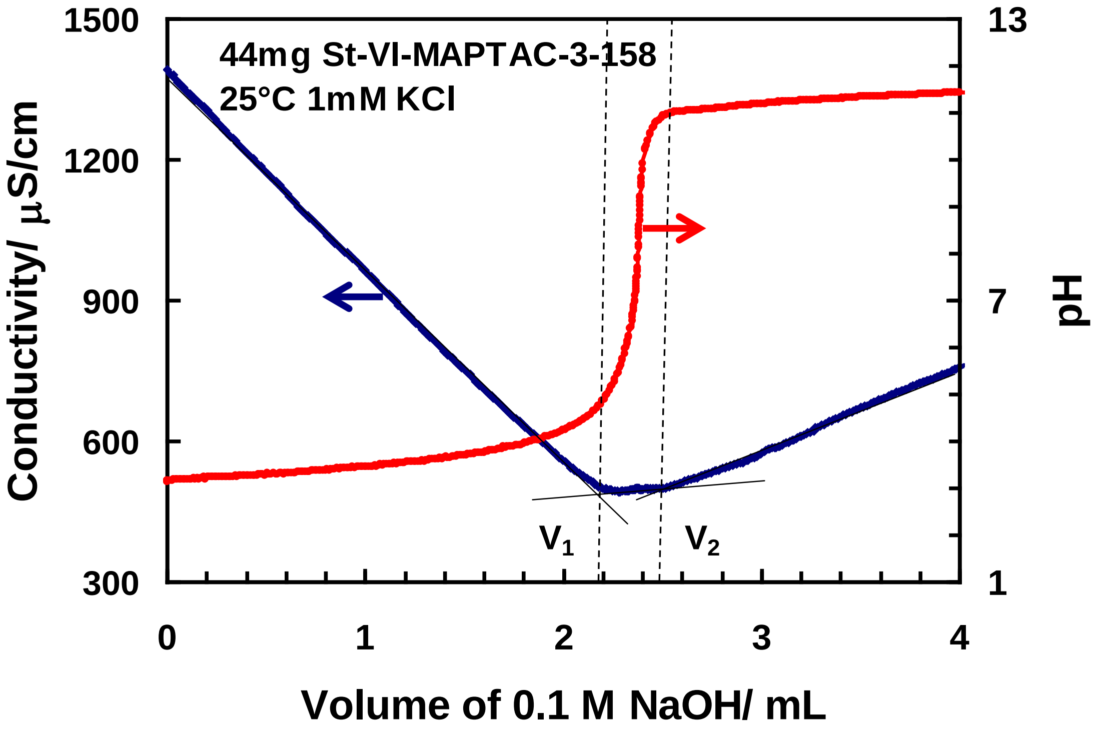

**Figure 3** Conductometric and pH titration of St-VI-MAPTAC-3-158 dispersion in 1mM KCl. The vinyl imidazole moieties of the functionalized nanoparticles are calculated as 0.55 mmol/g NPs. The pH titration gave the p$K_a$ of St-VI-MAPTAC-3-158 in the range of 7.0-8.0.

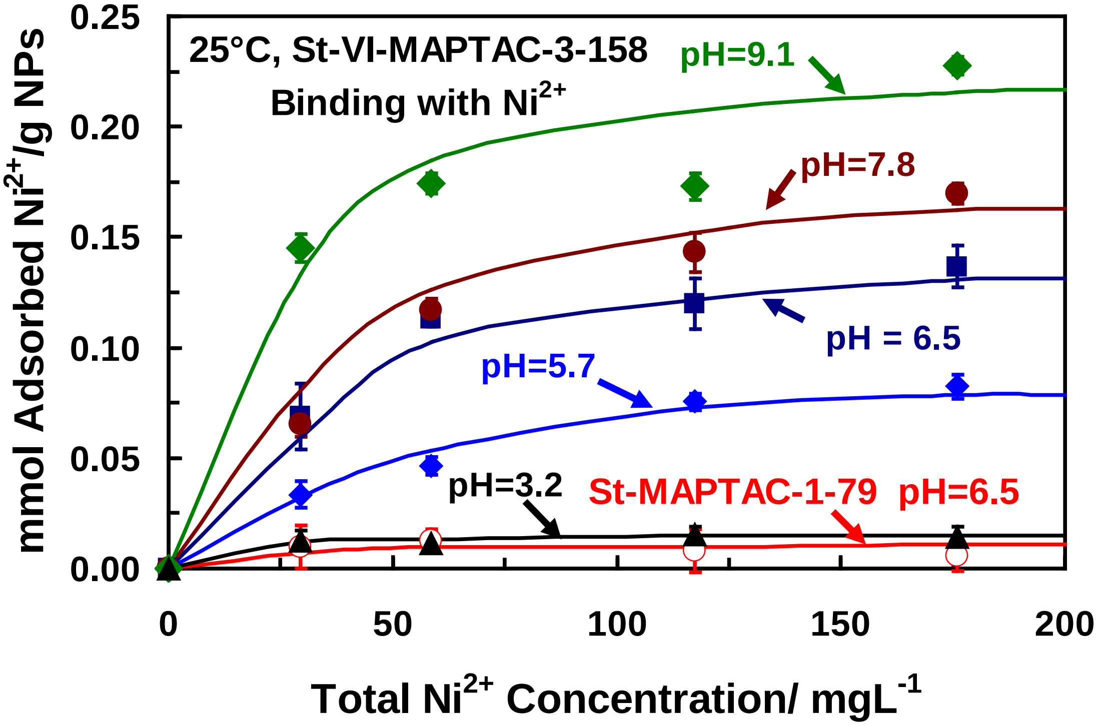

**Figure 4** Binding isotherms of $Ni^{2+}$ ions to St-VI-MAPTAC-3-158 as functions of total $Ni^{2+}$ concentration over a pH range of 3.2-9.1. Initial concentration of $NiSO_4$ are 0.5 mM, 1 mM, 2 mM and 3 mM, corresponding to 29.4, 58.7, 117.4, and 176.1 $mgL^{-1}$ of nickel. Imidazole-free St-MAPTAC-1-79 binding of $Ni^{2+}$ ions is also shown in the figure as the red line of empty circles.

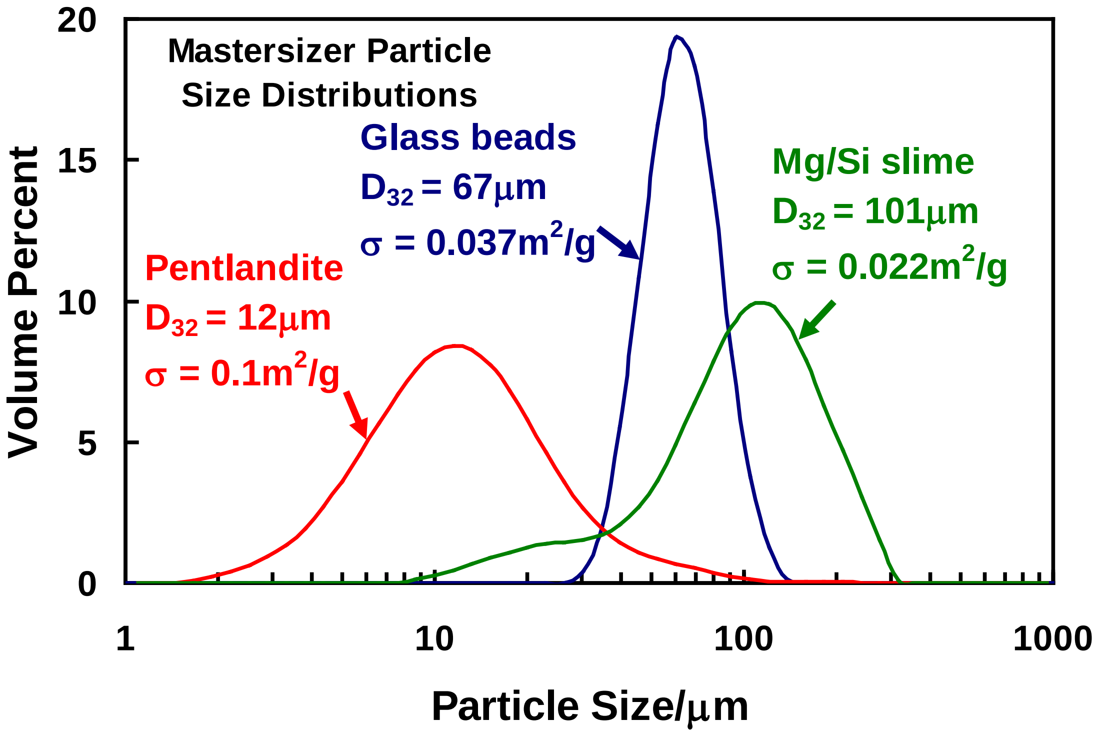

**Figure 5** Particle size distributions for model mineral suspensions measured with a Mastersizer laser diffraction instrument. The surface area mean diameter ($D_{32}$, also known as Sauter mean diameter) is representative of the diameter of an equivalent sphere with the same volume/surface area ratio as the suspended particle, and $\sigma$ is the corresponding specific surface area.

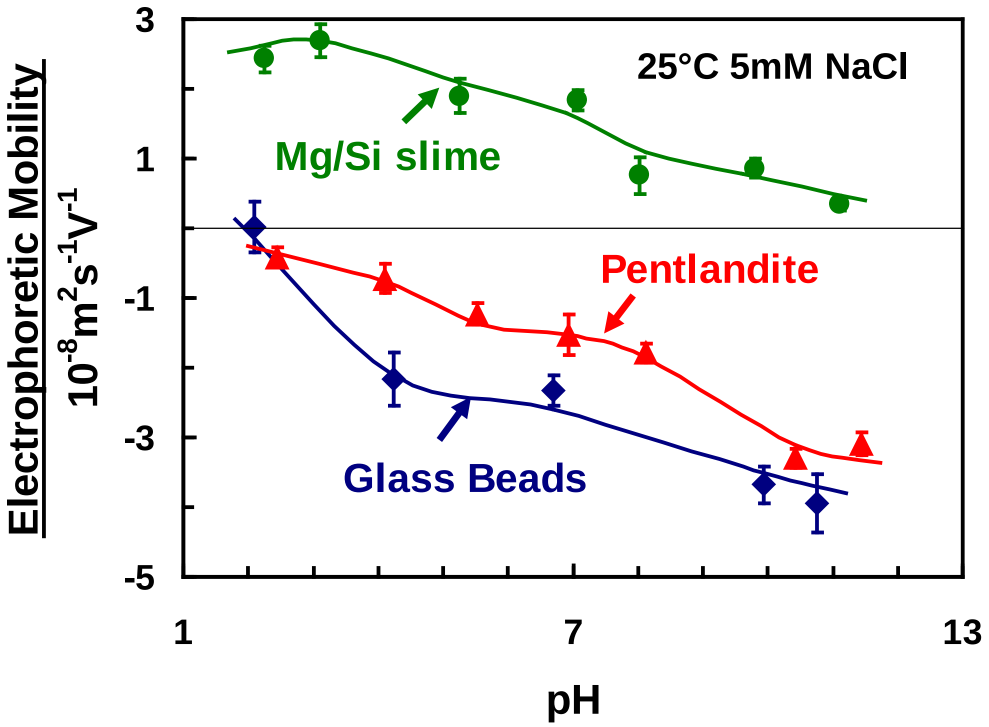

**Figure 6** Electrophoretic mobility values of the Pn, glass beads and tails (labeled as Mg/Si slime) as a function of pH

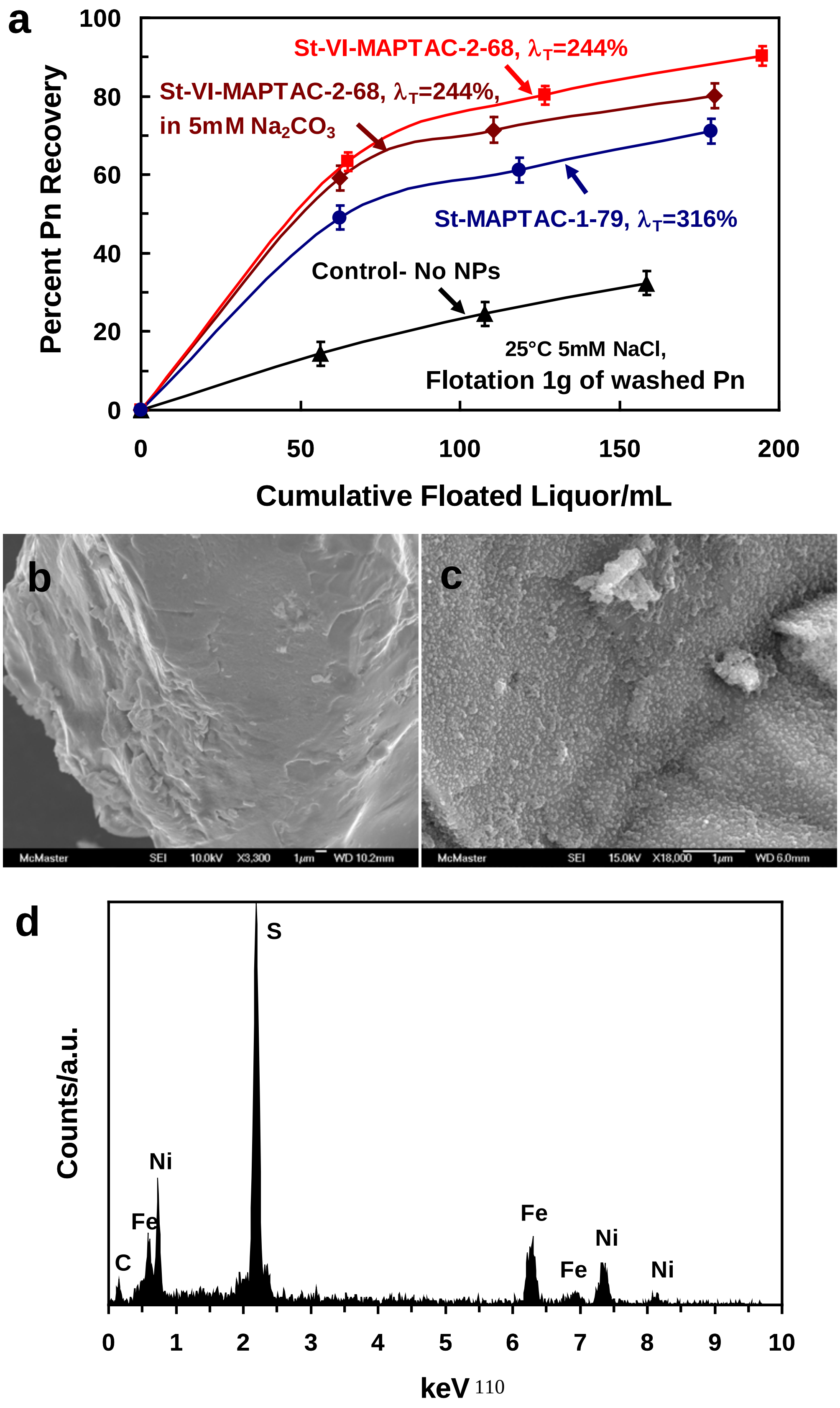
a
Percent Pn Recovery
0
20
40
60
80
100
0
50
100
150
200
Cumulative Floated Liquor/mL
St-VI-MAPTAC-2-68, λ$_T$=244%
St-VI-MAPTAC-2-68, λ$_T$=244%,
in 5mM Na$_2$CO$_3$
St-MAPTAC-1-79, λ$_T$=316%
Control- No NPs
25°C 5mM NaCl,
Flotation 1g of washed Pn
b
McMaster SEI 10.0kV X3,300 1μm WD 10.2mm
c
McMaster SEI 15.0kV X18,000 1μm WD 6.0mm
d
Counts/a.u.
S
Ni
Fe
C
Fe
Ni
Fe
Ni
0
1
2
3
4
5
6
7
8
9
10
keV

**Figure 7 a.** Pentlandite flotation with the two types of nanoparticle collectors and a control (without nanoparticles). Pn flotation runs with St-VI-MAPTAC-2-68 were performed in either 5 mM NaCl or 5 mM $Na_2CO_3$. **b. and c.** SEM images of Pn particles: no nanoparticles (**b**), and sample collected from flotation run with St-VI-MAPTAC-2-68 in 5 mM NaCl (**c**). **d.** Energy-dispersive X-ray diffraction (EDX) spectra of recovered Pn particles with the use of St-VI-MAPTAC-2-68. The existence of carbon element confirmed the adsorption of nanoparticle collectors.

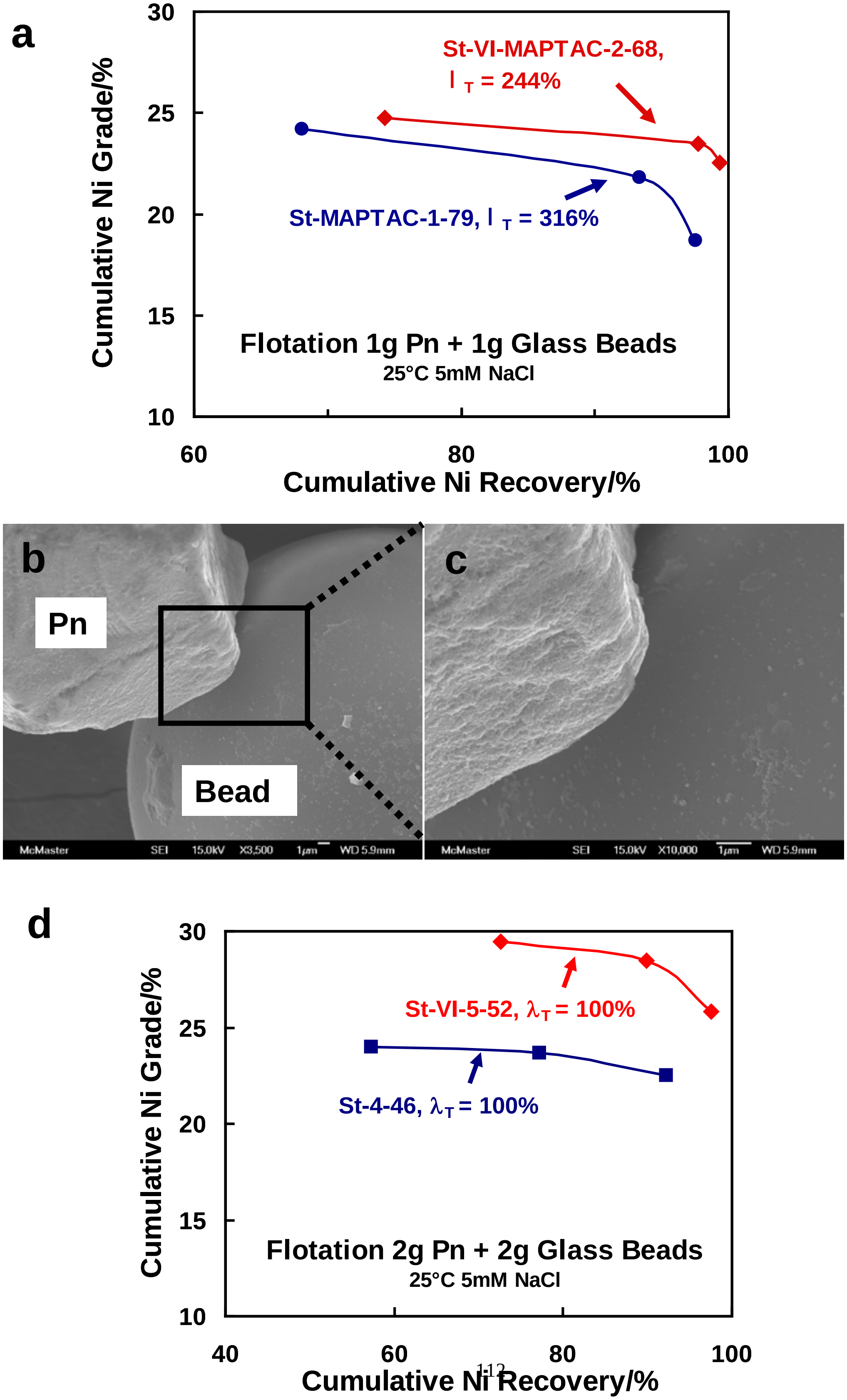
a
Cumulative Ni Grade/%
30
25
20
15
10
60
80
100
Cumulative Ni Recovery/%
St-VI-MAPTAC-2-68,
l T = 244%
St-MAPTAC-1-79, l T = 316%
Flotation 1g Pn + 1g Glass Beads
25°C 5mM NaCl
b
Pn
Bead
McMaster SEI 15.0kV X3,500 1μm WD 5.9mm
c
McMaster SEI 15.0kV X10,000 1μm WD 5.9mm
d
Cumulative Ni Grade/%
30
25
20
15
10
40
60
80
100
Cumulative Ni Recovery/%
St-VI-5-52, λT = 100%
St-4-46, λT = 100%
Flotation 2g Pn + 2g Glass Beads
25°C 5mM NaCl

**Figure 8** The results of flotation a mixture of washed pentlandite and glass beads in 5 mM NaCl. **a.** comparing St-MAPTAC-1-79 ($\lambda_T$ = 316%) to St-VI-MAPTAC-2-68 ($\lambda_T$ = 224%); **b. and c.** SEM images of the sample recovered from the run with St-VI-MAPTAC-2-68; Image **c** is a higher magnification of a part from Image **b**; the fractions of Pn and glass beads were marked inside each image. **d.** comparing St-4-46 ($\lambda_T$ = 100%) to St-VI-5-52 ($\lambda_T$ = 100%). The nanoparticles containing imidazole surface groups were more effective.

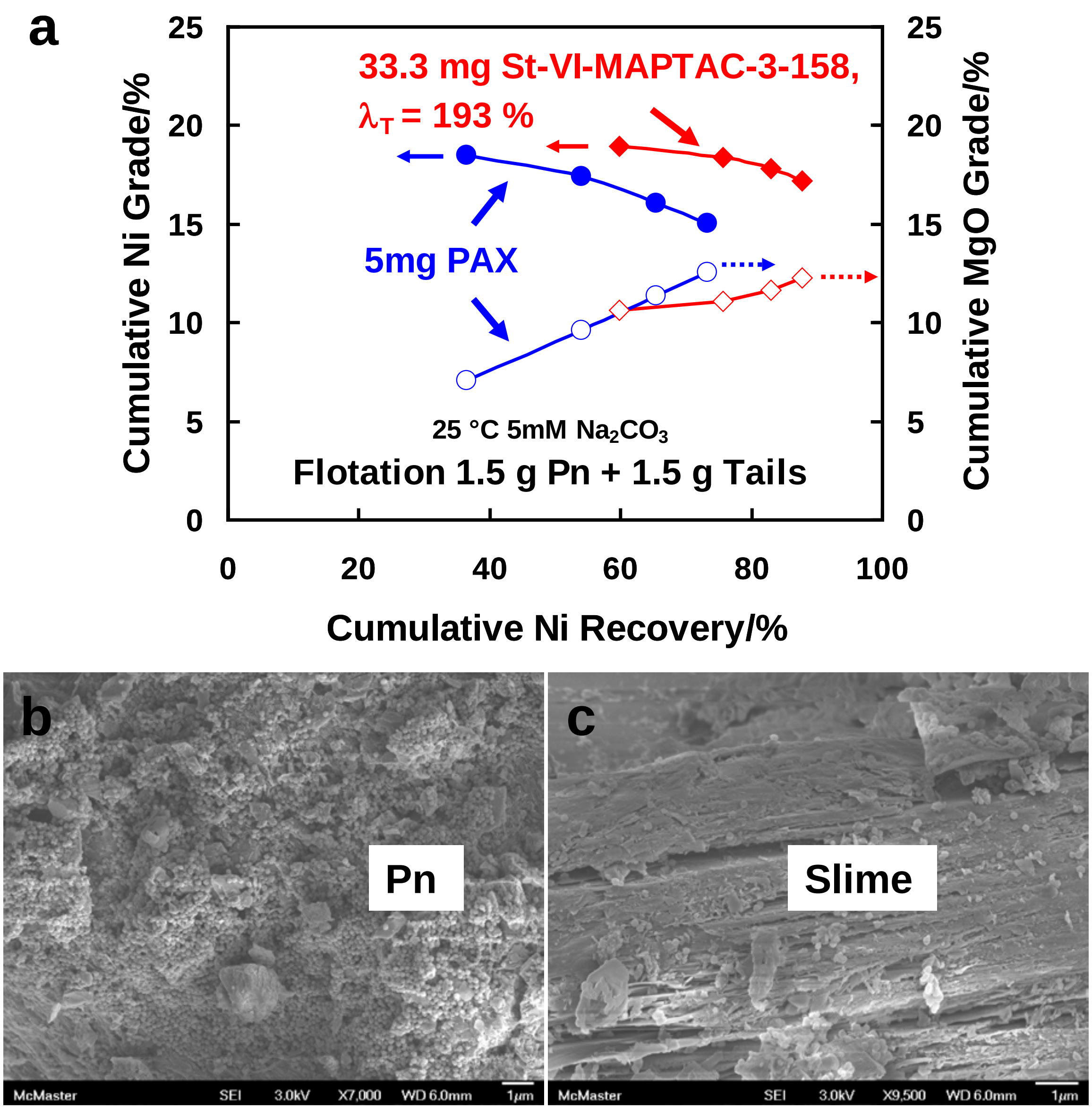

**Figure 9 a.** Comparing conventional PAX to nanoparticle collector (St-VI-MAPTAC-3-158) for flotation of a mixture of washed Pn and ultramafic Mg/Si slime tails in 5mM $Na_2CO_3$; **b. and c.** SEM images of the sample recovered from the run with St-VI-MAPTAC-3-158; Image **b** is a typical surface of pentlandite covered by many nanoparticles; Image **c** is a representative slime surface adsorbed by very few nanoparticles.

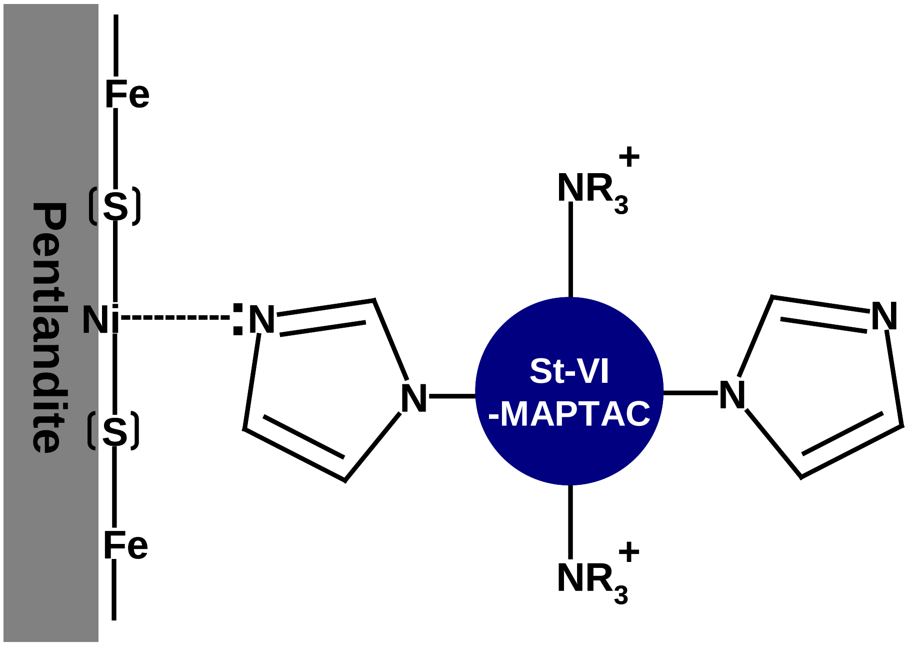

**Figure 10** Proposed mechanism for the binding of the VI functionalized nanoparticles to nickel site on pentlandite surface, probably via the N-3 atom of 1-vinyl imidazole which donates the unshared pair of electrons to the nickel.

# Tables

**Table 1** Recipes for preparation of polymeric functionalized nanoparticles, where the last number in the nanoparticle designation is the average particle diameter.

| **Nanoparticle Designation** | **Initial Reactor Charge (g)** | | | | **Starved-Feed Charge (g)** | | | |
|---|---|---|---|---|---|---|---|---|
| | **Water** | **St** | **MAPTAC or CTAB** | **V50** | **St** | **MAPTAC** | **VI** | **Water** |
| **St-MAPTAC-1-79** | 250 | 0.5 | 0.125 MAPTAC | 0.06 | 4.5 | 0.125 | --- | 4.7 |
| **St-VI-MAPTAC-2-68** | 100 | 0.5 | 0.125 MAPTAC | 0.06 | 4.5 | --- | 0.125 | 4.9 |
| **St-VI-MAPTAC-3-158** | 100 | 0.5 | 0.125 MAPTAC | 0.10 | 4.5 | --- | 0.25 | 4.7 |
| **St-4-46** | 100 | 0.5 | 0.10 CTAB | 0.10 | 4.5 | --- | --- | --- |
| **St-VI-5-52** | 100 | 0.5 | 0.10 CTAB | 0.10 | 4.5 | --- | 0.125 | 4.9 |

**Table 2** Some properties of polymeric functionalized nanoparticle collectors

| Nanoparticle Designation | Hydrodynamic Diameters [a], nm (Polydispersity) | Electrophoretic Mobility [a], $10^{-8} m^2 s^{-1} V^{-1}$ (Std. error) | Contact Angle [b] on Smooth Polymer Film, $\theta_{np}$ |
|---|---|---|---|
| **St-MAPTAC-1-79** | 79 (0.085) | 1.85 ± 0.15 | 78 ± 4.5 |
| **St-VI-MAPTAC-2-68** | 68 (0.159) | 1.75 ± 0.19 | 71 ± 3.8 |
| **St-VI-MAPTAC-3-158** | 158 (0.033) | 2.98 ± 0.14 | 66 ± 2.9 |
| **St-4-46** | 46 (0.156) | 1.61 ± 0.07 | 93 ± 2.1 |
| **St-VI-5-52** | 52 (0.075) | 1.79 ± 0.11 | 87 ± 1.7 |

[a] measured in 5 mM NaCl at ambient pH

[b] sessile drop water contact angle

**Table 3** Binding capacity for St-VI-MAPTAC-158 to $Ni^{2+}$ ions at various solution pHs; the quantity of VI content on St-VI-MAPTAC-158 was estimated as 0.55 mmol/g by conductometric titration.

| **pH of $Ni^{2+}$ Solution** | **mmol Adsorbed $Ni^{2+}$ /g St-VI-MPTAC-158 (Std. error)** | **Stoichiometry of [VI]:[$Ni^{2+}$] (x:1)** |
|---|---|---|
| 3.2 | 0.015 ± 0.003 | 37 ± 6.1 |
| 5.7 | 0.08 ± 0.006 | 6.9 ± 0.5 |
| 6.5 | 0.14 ± 0.01 | 3.9 ± 0.2 |
| 7.8 | 0.17 ± 0.01 | 3.2 ± 0.2 |
| 9.1 | 0.23 ± 0.01 | 2.4 ± 0.2 |

# References

1. Fuerstenau, M.; Jameson, G.; Yoon, R., Froth Flotation: A Century of Innovation, Society for Mining, Metallurgy, and Exploration. *Inc.(SME), Littleton, Colorado, USA* **2007**.

2. Wills, B. A.; Napier-Munn, T., *Wills' mineral processing technology: an introduction to the practical aspects of ore treatment and mineral recovery*. Butterworth-Heinemann London: 2006.

3. Mani, H.; Xu, M.; Quinn, P.; Stratton-Crawley, R., The effect of ultramafic mineralogy on pentlandite flotation. *Processing of Complex Ores* **1997,** 1101, 63-76.

4. Edwards, C.; Kipkie, W.; Agar, G., The effect of slime coatings of the serpentine minerals, chrysotile and lizardite, on pentlandite flotation. *Int. J. Miner. Process.* **1980,** 7, (1), 33-42.

5. Shannon, L.; Trahar, W., The role of collector in sulphide ore flotation. *Advances in Mineral Processing: a Half-Century of Progress in Application of Theory to Practice* **1986**, 408-425.

6. Jameson, G. J., New technology and science in flotation separations. *Curr. Opin. Colloid Interface Sci.* **1998,** 3, (4), 351-359.

7. Dong, J.; Xu, M., Evaluation of Environmentally Friendly Collectors for Xanthate Replacement. *Proceedings of the 43rd Annual Canadian Mineral Processors Conference* **2011**.

8. Yang, S.; Pelton, R. H.; Raegen, A.; Montgomery, M.; Dalnoki-Veress, K., Nanoparticle Flotation Collectors: Mechanisms Behind a New Technology. *Langmuir* **2011,** 27, (17), 10438-10446.

9. Yang, S.; Pelton, R. H., Nanoparticle Flotation Collectors II: The Role of Nanoparticle Hydrophobicity. *Langmuir* **2011,** 27, (18), 11409-11415.

10. Yang, S.; Pelton, R. H.; Montgomery, M.; Cui, Y., Nanoparticle Flotation Collectors III: Factors Influencing Nanoparticle Depositon. **2011,** in preparation.

11. Sutton, R.; Thai, L.; Hewitt, J.; Voycheck, C.; Tan, J., Microdomain characterization of styrene-imidazole copolymers. *Macromolecules* **1988,** 21, (8), 2432-2439.

12. Kim, H.; Daniels, E. S.; Dimonie, V. L.; Klein, A., Preparation and characterization of imidazole functionalized microspheres. *J. Appl. Polym. Sci.* **2006,** 102, (6), 5753-5762.

13. Jayne, D., Beneficiation of Acidic Minerals. In US Patent (2380698): 1945.

14. Ackerman, P.; Harris, G.; Klimpel, R.; Aplan, F., Use of chelating agents as collectors in the flotation of copper sulfides and pyrite. *Miner. Metall. Process* **1999,** 16, (1), 27-35.

15. Takafuji, M.; Ide, S.; Ihara, H.; Xu, Z., Preparation of poly (1-vinylimidazole)-grafted magnetic nanoparticles and their application for removal of metal ions. *Chem. Mater.* **2004,** 16, (10), 1977-1983.

16. Lee, I. S.; Lee, N.; Park, J.; Kim, B. H.; Yi, Y. W.; Kim, T.; Kim, T. K.; Lee, I. H.; Paik, S. R.; Hyeon, T., Ni/NiO core/shell nanoparticles for selective binding and

magnetic separation of histidine-tagged proteins. *J. Am. Chem. Soc.* **2006,** 128, (33), 10658-10659.

17. Tamai, H.; Yasuda, H., Preparation of Copolymer Particles of Styrene with N-Vinylimidazole-Metal Complexes. *J. Colloid Interface Sci.* **1997,** 185, (1), 287-289.

18. Lippert, J.; Robertson, J.; Havens, J.; Tan, J., Structural studies of poly (N-vinylimidazole) complexes by infrared and Raman spectroscopy. *Macromolecules* **1985,** 18, (1), 63-67.

19. Goodwin, J.; Ottewill, R.; Pelton, R., Studies on the preparation and characterization of monodisperse polystyrene latices V.: The preparation of cationic latices. *Colloid & Polymer Science* **1979,** 257, (1), 61-69.

20. Sajjadi, S., Nanoparticle formation by monomer-starved semibatch emulsion polymerization. *Langmuir* **2007,** 23, (3), 1018-1024.

21. Yang, F.; Liu, S.; Xu, J.; Lan, Q.; Wei, F.; Sun, D., Pickering emulsions stabilized solely by layered double hydroxides particles: The effect of salt on emulsion formation and stability. *J. Colloid Interface Sci.* **2006,** 302, (1), 159-169.

22. Popping, B.; Deratani, A.; Sebille, B.; Desbois, N.; Lamarche, J.; Foissy, A., The effects of electrical charge on the adsorption of a weak cationic polyelectrolyte onto silica, silicon carbide and calcium fluoride. *Colloids Surf.* **1992,** 64, (2), 125-133.

23. Palmer, D. A.; Bénézeth, P.; Wesolowski, D. In *Solubility of nickel oxide and hydroxide in water*, 14th International Conference on the Properties of Water and Steam in Kyoto 2004.

24. Loo, B.; Tse, Y.; Parsons, K.; Adelman, C.; El Hage, A.; Lee, Y., Surface enhanced Raman spectroscopy of imidazole adsorbed on electrode and colloidal surfaces of Cu, Ag, and Au. *J. Raman Spectrosc.* **2006,** 37, (1 3), 299-304.

# Chapter 6 Functionalized Nanoparticle Flotation Collectors for Processing a Complex Ultramafic Nickel Sulfide Ore

In Chapter 6, all of the nanoparticles were designed and prepared by myself. Flotation experiments were conducted at VBMTD by me and Julie-Ann Bos who is a flotation technician from VBMTD. All of the SEM experiments were conducted by me at McMaster. Carla Abarca performed the experiments to measure nanoparticle colloidal stability. Zongfu Dai and Manqiu Xu designed flotation procedures, helped to analyze data, and gave many useful discussions. Zongfu Dai plotted most of the flotation results. I plotted other results and wrote the first draft. Zongfu helped to edit some parts of my draft, mostly the flotation part. Dr. Pelton helped to analyze data, calculate theoretical nanoparticle dosage and revise some parts of the draft to this version.

# Functionalized Nanoparticle Flotation Collectors for Processing a Complex Ultramafic Nickel Sulfide Ore

*[†]Songtao Yang, [‡]Zongfu Dai, [†]Carla Abarca, [‡]Manqiu Xu, [‡]Julie-Ann Bos, and [†]Robert Pelton**

[†]Department of Chemical Engineering, McMaster University, 1280 Main Street West,
Hamilton, Ontario, Canada L8S 4L7

[‡]Vale Base Metals Technology Development (VBMTD), 2060 Flavelle Blvd.,
Mississauga, Ontario, Canada L5K 1Z9

Corresponding author: peltonrh@mcmaster.ca

**Possibly will be submitted to: *Mineral Engineering/ International Journal of Mineral Processing/ American Mineralogist***

## Abstract

This paper reports flotation results for an ultramafic low-grade nickel sulfide ore in the presence of poly(styrene-co-1-vinylimidazole) based functionalized nanoparticles with both incremental rougher flotation and full circuit simulation (FCS) procedures. Cationic imidazole functionalized nanoparticles selectively bind to pentlandite and function as flotation collectors. There appears to be advantages in the combined use of PAX and cationic functionalized nanoparticles. Incremental rougher flotation tests with the combined use of the two types of collectors gave both higher recovery and better selectivity (grade). A 7% higher Ni recovery can be achieved compared to the use of PAX alone. The additional nanoparticle collector used in the FCS tests gave a Ni grade almost twice as that of using PAX alone, although the nickel recovery is slightly lower. However, the required dosages of nanoparticles are two to three orders of magnitude greater than that to give ~10% coverage - a minimum required dosage for good recoveries in our previous model studies. The possible reasons for the requirements of very high nanoparticle dosages may include: nanoparticle aggregation induced by PAX and $Na_2CO_3$, low latex deposition efficiency in flotation slurry, and potential contamination

on nanoparticle surfaces. The strength of nanoparticle-mineral adhesion and the positive impacts of nanoparticle aggregates in processing the difficult ultramafic ore are discussed.

## Introduction

The Thompson Nickel Belt, located in Manitoba Canada, has approximately 300 million tons of ultramafic low-grade nickel ore deposits containing significant amounts of pentlandite (Pn, $Ni_{4.5}Fe_{4.5}S_8$). These deposits however, have not been exploited or their nickel mining operations have been ceased after a few years of production, because they were considered uneconomical. [1] This situation is now beginning to change as high-grade nickel ores are being depleted. The growing value of nickel in global mineral markets has led to a new ultramafic ore processing operation in Australia. [2]

Ultramafic nickel sulfide ore consisting of both valuable pentlandite and large quantities of unwanted Mg/Si slime (predominantly serpentine, $(MgFe)_3Si_2O_5(OH)_4$) has historically been difficult to process by flotation. [3-4] Hydrophilic, fibrous Mg/Si slime usually masks the surface of pentlandite due to electrostatic interaction and dramatically depresses pentlandite flotation. [3] Consequently, new approaches are required for processing these difficult ores.

Depressants have been developed in the last few decades in attempt to lessen undesirable slime deposition. Depressants are usually composed of hydrophilic polymers. They electro-sterically stabilize unwanted slimes, reversing their charges and thus alleviating electrostatic interactions that led to slime coating of valuable minerals. One of the most widely used flotation depressants is carboxymethyl cellulose (CMC). [5] Guar, dextrin, and lignin sulfonates have also been used as depressants to enhance the separation of valuable minerals. [6-7] Synthetic polymers were recently tested as depressants in flotation process for various minerals. Beattie and coworkers developed polysaccharides and polyacrylamides as depressants for talc in the flotation of sulphide minerals. [8] INCO Limited (now Vale) developed a combination of a polyamine and a sulphur containing compound as a depressant for arsenide minerals. [9] In the case of ultramafic nickel ore, CMC was used to enhance the hydrophilicity of Mg/Si slime and to modify the slime to be negatively charged, further preventing the deposition from negatively charged pentlandite. [10]

In flotation, a critical aspect is the need for a reagent known as a “collector” to selectively modify the desired mineral surfaces to be more hydrophobic than unwanted gangue materials. Conventional molecular collectors for sulfide mineral flotation are water-soluble surfactants with short hydrophobic tails and specific head groups, such as xanthate. [11] For example, potassium amyl xanthate (PAX) is a characteristic collector for pentlandite flotation. In recent years, the synergetic effects of mixed collectors have been widely investigated. [12-13] The purpose of the combined use of two or more collectors is to increase flotation performance, in terms of recovery, grade, or selectivity of specific minerals.

Recently, we have demonstrated that water-soluble collectors can be partially or completely replaced by hydrophobic polystyrene-based nanoparticles leading to the first reported use of nanoparticles as flotation collectors. [14-15] The ability of nanoparticles to induce flotation was demonstrated by floating hydrophilic, negatively charged glass beads with cationic polystyrene nanoparticle collectors. Electrostatic attraction promoted the spontaneous deposition of the nanoparticles onto the glass surfaces raising the effective contact angle to promote the adhesion of the beads to air bubbles. As little as 10% coverage of the bead surfaces with our most effective nanoparticles could promote high flotation efficiencies [14]. Furthermore, we developed functionalized nanoparticles based on poly (styrene-co-1-vinylimidazole) which were used as a new class of flotation collectors for the isolation of pentlandite. [16-17] In addition to electrostatics, surface ligand (imidazole)-Ni complexation possibly accounts for an additional driving force in directing the nanoparticles to selectively deposit onto Pn. [17] Clean model mineral suspensions and small-scale laboratory flotation runs were applied in our previous studies. Herein we evaluate flotation performances in the presence of functionalized nanoparticle collectors by floating a complex ultramafic nickel sulfide ore obtained from the Pipe deposit of Thompson Nickel Belt, Manitoba Canada, with scale-up (1.0 kg ore in 4.2L, to previous small-scale, a few grams in ~100 mL [17]) batch flotation tests.

In this study, we hypothesize that nanoparticle collectors may provide advantages over conventional molecular collectors for processing complex ultramafic nickel ore. The hydrophobic nanoparticles confer both hydrophobicity and nanoscale roughness, and both properties may be important for flotation. The objective of current work is to enhance the existing flotation efficiency attained by the conventional molecular collector (PAX) by adding functionalized hydrophobic nanoparticle collectors. In this work we report: flotation results for the complex ultramafic nickel sulfide ore by using PAX alone, functionalized nanoparticle collector alone, and synergetic using of both collectors, with both incremental rougher flotation and full circuit simulation (FCS) procedures.

## Experimental Section

**Materials:** Styrene (99%, Sigma-Aldrich) and 1-vinylimidazole (VI, ≥ 99%, Sigma-Aldrich) were purified by vacuum distillation. 3-(methacryloylamino)propyl trimethyl ammonium chloride solution (MAPTAC, 50 wt. % in $H_2O$, Sigma-Aldrich) was passed through an inhibitor-removing column. 2, 2'-azobis (2-methylpropionamidine) dihydrochloride (V50, 97%), cetyltrimethylammonium bromide (CTAB, 95%) were purchased from Sigma-Aldrich and used as supplied. For nanoparticle preparation and characterization, all solutions were made with Type 1 water (18.2 MΩcm, Barnstead Nanopure Diamond system).

The molecular collector, potassium amyl xanthate (PAX); and the frother, Unifroth 250c, were donated by VBMTD (Mississauga, ON). Soda ash ($Na_2CO_3$) was used to adjust the pH of the flotation slurry. A complex ultramafic low-grade nickel sulfide ore obtained from the Pipe deposit of Thompson nickel belt, Manitoba Canada, was used. The ore was crushed to -6 mesh before primary grinding. The major valuable mineral is pentlandite, associated with iron sulfide mineral (pyrrhotite, $Fe_{1-x}S$, and pyrite, $FeS_2$, *etc.*), and large amounts of gangue materials predominantly serpentine. For flotation tests involving the ore, regular tap water in the lab of Vale Base Metals Technology Development (Mississauga, ON) was used to prepare flotation process water.

**Nanoparticle Preparation and Characterization:** The recipes used to prepare functionalized nanoparticle collectors are summarized in Table 1. The methodology used to prepare the nanoparticles is according to classic surfactant-free polymerization [18] and starved-feed semibatch emulsion polymerization [19]. The experimental design of the polymerizations are similar to that of our previous publication [14], with a few alterations. The polymerizations were conducted in a three-necked flask equipped with a condenser, two rubber stoppers holding syringe needles (one for nitrogen, the other for starved-feed monomer addition), and a magnetic stirring bar (controlled by a IKAMAG® RCT basic hot plate/stirrer, NC). Typically, 100 mL of deionized water were charged to the reactor followed by nitrogen purging for 30 minutes at 70°C with 350 rpm stirring. To the reactor were added 0.5 g of styrene and 0.25 g of 50 wt. % MAPTAC (or 0.10 g of CTAB). The mixtures were allowed to equilibrate for 10 minutes before V50 was added to initiate the polymerization. After 15 minutes polymerization of the initial charge, an additional 4.5 g of styrene and 0.25 g of VI dissolved in 4.7 mL water, were added over 5 hours (0.0083 mL/min) from twin 10 mL syringes fitted to a syringe pump (NE-1600, New Era Pump System, Inc., NY). The reaction was stirred at 70°C for an additional 19 hours. The resulting latex was dialyzed for at least one week against deionized water, after which the dialysate conductivity was less than 30μS/cm.

Hydrodynamic diameters of prepared nanoparticles were measured by dynamic light scattering (DLS, Brookhaven Instruments Corporation, BIC) using a detector angle of 90°. Correlation data were analyzed by the BIC DLS software (Windows 9KDLSW Version 3.34) using the cumulant fit method and the scattering intensity was set between 150 and 250 kcounts/s for each measurement. The duration for each measurement was set to 5 min. Electrophoretic mobility measurements were performed by a Zeta PALS instrument (Brookhaven Instruments Corporation) at 25 °C in phase analysis light scattering mode. The reported mobilities were the average of 10 runs, each consisting of 15 scans. Nanoparticle sample mobility was measured either in 5mM NaCl (pH= 6.7±0.4) or 5mM $Na_2CO_3$ (pH= 10.6±0.3). Samples for both dynamic light scattering and electrophoretic mobility measurements were prepared in clean vials by dispersing approximately 0.25 g/L of the nanoparticles in 5mM NaCl.

The colloidal stability of St-VI-1-52 and St-VI-MAPTAC-4-121 in the flotation reagents was probed by relative turbidity [20] and DLS measurements. Nanoparticle dispersions and a series of freshly prepared solutions of flotation reagent (i.e., $Na_2CO_3$, PAX, or Unifroth 250c) were placed into a cuvette. 0.02mL of 37.6 g/L St-VI-MAPTAC-121 was added to 2 mL of solution (prepared by one-component flotation reagent), giving ~0.038 wt % of nanoparticles. A higher concentration of St-VI-1-52 was required for the turbidity measurements. 0.1 mL of 34 g/L St-VI-1-52 was added in a total volume of 2 mL of solution, giving a concentration of 0.17 wt % nanoparticles. The transmittance of nanoparticle dispersion was measured with a UV-vis spectrometer (Beckman Coulter, DU800) at 550 nm. Critical coagulation concentrations (CCC) of the flotation reagents were determined as the reagent concentration at which the transmittance was first outside of the range 0.75 to 1.3 times the value for the stable latex at the same concentration. Measurements of hydrodynamic diameters of the nanoparticle dispersions with DLS were carried out to confirm their colloidal stability at the estimated CCC.

**Flotation:** The flotation procedure used in this study involves both incremental rougher flotation and full circuit simulation (FCS) flotation trials. All of the flotation tests were performed in a 4.2 L Denver flotation cell. 1.0 kg of the crushed -6 mesh sample was ground in a laboratory rod mill in the presence of flotation process water (prepared with soda ash) until 80% (by mass) of the particles were smaller than 106 μm. The ground slurry was then subjected to a desliming process using a Mozley 1 inch hydrocyclone. Following desliming, the cyclone underflow was used as flotation feed and was charged into the flotation cell for the flotation test.

Figure 1 shows the typical flowsheet used in incremental rougher flotation. In the conditioning stage, pH was adjusted with soda ash to the desired range amenable to pentlandite flotation [21], the collector (either nanoparticle collector or PAX, or a combination of both) was added for 5 more minutes of conditioning before each incremental flotation, and the frother (20 ppm Unifroth 250c) was added at 30 seconds before the start of each incremental flotation. The incremental flotation test was performed with the collection of eight incremental forth products for a total of 16 minutes, *i.e.*, 2 minutes for each incremental flotation stage. Table 2 summarizes the experimental conditions for the use of a single collector: PAX, three selected nanoparticle collector (St-VI-1-52, St-VI-MAPTAC-3-92, and St-VI-MAPTAC-4-121), and the control.

FCS flotation tests were performed according to the flowsheet shown in Figure 2. FCS has been extensively used at VBMTD research laboratory for the evaluation of ore flotation performance by generating a grade/recovery relationship. [22] The FCS procedure contains five flotation stages: rougher, scavenger, scavenger cleaner, rougher cleaner, and rougher re-cleaner flotation. Before the rougher flotation and the scavenger cleaner flotation stages, the desliming processes were applied to remove partial Mg/Si slime. Two FCS flotation runs were compared to evaluate whether nanoparticle collector has positive impact on the flotation performance of the ore: one was with PAX alone, and the other was with regular PAX and additional nanoparticle collector (St-VI-MAPTAC-2-68).

Each of flotation products (concentrates, tails and slime) was dried and weighed. The Ni, Fe and MgO content (grade) of the dried solids was measured by a Varian Vista inductively coupled plasma - optical emission spectrophotometer (ICP-OES). Approximately 0.25 g of sample was weighed into a zirconium crucible. 3.4 g of sodium peroxide and 2-3 pellets of sodium hydroxide were added to the sample and mixed. The crucible was then placed into a muffle furnace at 710°C for 35 minutes. The resulting cake was then leached with water and hydrochloric acid. The solution was bulked to a 250 mL volume and read directly on ICP-OES. The flotation results were plotted as curves of cumulative Ni or MgO grade as functions of cumulative Ni recovery, which was determined from mass balance [23] of the flotation products.

The microstructures of recovered solids from flotation runs in the presence of the nanoparticle collector were investigated by using a JEOL JSM-7000F scanning electron microscope (SEM) equipped with energy-dispersive X-ray diffraction (EDX).

## Results

Four functionalized nanoparticle collectors based on poly (styrene-co-1-vinylimidazole) were prepared by emulsion copolymerization - the recipes are summarized in Table 1. The co-monomer 1-vinylimidazole was designed to functionalize the nanoparticle surface leading to an increase pentlandite affinity via ligand-Ni complexation [17]. The co-monomer MAPTAC was employed to modify the nanoparticle surface properties by introducing quaternary ammonium cationic groups to supplement cationic amidine groups from the initiator. Hydrodynamic diameters of the resulting nanoparticles were measured by dynamic light scattering. The average particle diameters of the four synthesized nanoparticles varied from 52 to 121 nm. Table 3 summarizes some of the nanoparticle properties. All of the nanoparticle dispersions (latex) had positive electrophoretic mobilities. At close to neutral pH (pH~6.7, in 5 mM NaCl), St-VI-1-52 was positively charged due to the presence of pH-sensitive amidine groups from the initiator V50 [18]. Cationic charges of St-VI-MAPTAC-2-68, St-VI-MAPTAC-3-92, and St-VI-MAPTAC-4-121 were attributed to both the amidine and the quaternary ammonium on the MAPTAC moieties. The quaternary ammonium displays a pH independent degree of ionization. Therefore, the three MAPTAC modified nanoparticles remained positively charged at relatively high pH (i.e., pH~10.6, in 5mM $Na_2CO_3$), whereas the mobility of St-VI-1-52 was close to zero, $0.53\times10^{-8}$ $m^2s^{-1}V^{-1}$.

The ionic flotation chemicals can induce aggregation of the nanoparticles. Table 4 summarizes the critical coagulation concentrations (CCC) of the flotation reagents for St-VI-1-52 and St-VI-MAPTAC-4-121. 0.75 mM $Na_2CO_3$, or 0.025 mM PAX induced St-VI-1-52 to coagulate, whereas much higher CCC (50 mM $Na_2CO_3$ or 1.0 mM PAX) was measured for St-VI-MAPTAC-4-121. The frother, Unifroth250c, does not destabilize the latex.

Our initial flotation tests using the nanoparticle collector on the Pipe low-grade nickel ore sample were attempted according to a full circuit simulation (FCS) flowsheet (see Figure 2). In addition to PAX, 2400 g/t and 260 g/t St-VI-MAPTAC-2-68 were added into the scavenger and scavenger cleaner flotation respectively. The results (including that with the regular PAX alone) expressed as cumulative Ni and MgO grade as functions of cumulative Ni recovery are shown in Figure 3. The addition of the nanoparticle collector had a significant impact on the flotation results as compared with the test using PAX only. The cumulative Ni recovery (including rougher cleaner and rougher re-cleaner tails) was slightly lower, whereas the Ni grade of the rougher re-cleaner concentrates (first seven points in the figure) were higher - almost doubled (17% to 8.6%, see Figure 3a). The MgO grade of the concentrates shown in Figure 3b was lower upon the addition of the nanoparticle collector (3.5% to 4.5%). Although the resulting Ni and MgO grades were impressive, the cumulative nickel recovery was limited to 67% (72% with PAX). Curves of the Fe recovery and Fe grade as functions of Ni recovery are plotted and shown in Figure 3c. Noticeably, a 15% lower Fe recovery and a10% lower Fe grade were seen from the tests with nanoparticle addition. The higher concentrate Ni grade was probably due to a lower recovery of Fe sulfide minerals that associated with pentlandite. Although we are not sure how nanoparticle collectors reduced the flotation recovery of Fe minerals, clearly the synergetic use of St-VI-MAPTAC-2-68 with PAX gave a much better selectivity towards the nickel-rich pentlandite than PAX alone.

Figure 4 shows SEM micrographs of dried samples collected after the FCS flotation test with additional St-VI-MAPTAC-2-68. Figure 4 A1 and A2 are micrographs of samples collected from the first rougher re-cleaner concentrate (the first point in Figure 3). It is seen that many St-VI-MAPTAC-2-68 nanoparticles were deposited onto the nickel-rich Pn surfaces. Figure 4 B1 and B2 are micrographs of samples collected from the scavenger cleaner tails. Very few nanoparticles were seen on the fibrous tails. Closer examination (Figure 4 A2) revealed that plenty of nanoparticle aggregates were produced and adsorbed on the concentrate surface. Some residual slime fibers escaping from the desliming process were seen on the surface as well.

It should be noted that PAX was used at the same regular dosage in both full circuit simulation tests. A question was raised whether or not the nanoparticles had any collecting power. To answer this question, an incremental rougher flotation (see flowsheet in Figure 1) test was conducted in which no PAX was added while 194 g/t St-VI-MAPTAC-2-68 were added in eight stages in a stage-addition (approximately 25 g/t per stage) and stage-flotation circuit. The results of this test are compared with the results of a 65 g/t PAX (see Table 2) flotation test in Figure 5. Without the addition of any PAX, the St-VI-MAPTAC-2-68 alone floated 49% of the Ni at a cumulative Ni grade of 9.3%. There was a suspicion that the 49% Ni recovery could have been achieved in a collectorless flotation since it is known that sulphide minerals can be floated to some extent without collector if they are oxidized to an appropriate degree. [24-25] In order to elucidate whether the 49% Ni recovery was actually due to the addition of the nanoparticle collector, another control test was performed in which conditions were identical to those of St-VI-MAPTAC-2-68 or PAX test except no collector was added. The results of the control (no collector) test are also shown in Figure 5. The Ni minerals did not float at all without collector. This observation indicates that the 49% Ni recovery in the St-VI-MAPTAC-2-68 flotation test was indeed due to the collecting power of nanoparticles.

Incremental flotation tests with three additional nanoparticle collectors, produced by varying ratios of VI and MAPTAC to styrene (see Table 1), are also shown in Figure 5. The flotation conditions, particularly the nanoparticle dosage and flotation pH, are summarized in Table 2. At a flotation pH of 10.1, the 52 nm St-VI-1-52 gave a similar Ni grade versus recovery curve and selectivity against MgO as that given by PAX, though at lower Ni recovery (66% versus 73.5%). At a natural (without addition of soda ash) slurry pH of 8.6, St-VI-1-52 gave slightly higher Ni grade and a better selectivity against MgO than that given by PAX at a pH of 10.1. The other two nanoparticle collectors (St-VI-MAPTAC-3-92 and St-VI-MAPTAC-4-121) also demonstrated their collecting power though they did not perform as well as did St-VI-1-52. This is probably because the higher ratios of MAPTAC rendered the nanoparticle surface less hydrophobic, thus the nanoparticle-coated Pn was less amenable to flotation. Although the dosages of the nanoparticle collectors were much higher than that of PAX, these tests further confirmed that the functionalized nanoparticles had collecting power towards the Ni sulphide mineral.

The volume-weighted particle size distribution of the first concentrate of the test using 1000 g/t St-VI-1-52 at pH of 8.6 is shown in Figure 6. The distribution was asymmetric with significant lobes at both low ends of the distribution. The surface area mean diameters ($D_{32}$, also known as Sauter mean diameter) for the re-dispersed suspension are given in the figure, *i.e.*17 μm, whereas the volume weighted mean diameter ($D_{43}$) measured as 71 μm is much larger. The corresponding specific surface area (SSA σ, 0.076 $m^2/g$) was estimated from the $D_{32}$ diameter assuming non-porous spherical pentlandite (density ρ, 4.8 $g/cm^3$) particles. This complex distribution indicates that the recovered concentrate may consist of a large quantity of pentlandite particles, aggregated St-VI-1-52, and small amounts of residual fibrous Mg/Si slime.

The ultimate purpose of this study is to enhance the existing flotation efficiency of that attained by the conventional molecular collector (PAX). A series of incremental rougher flotation tests simultaneously using both nanoparticle collector and PAX were performed. Figure 7 shows the flotation results by mixing St-VI-1-52, St-VI-MAPTAC-2-68, or St-VI-MAPTAC-3-92 with regular PAX. The addition of 540 g/t of St-VI-MAPTAC-2-68 or St-VI-MAPTAC-3-92 to the PAX flotation system improved Ni grade versus recovery relationship and reduced the concentrate MgO grade, especially at the early stage of the flotation. The overall Ni recovery increased by 3% to 4% upon addition of these two MAPTAC modified nanoparticles to the PAX control. The non-MAPTAC modified St-VI-1-52 showed better flotation performance. The addition of the St-VI-52 nanoparticle collector at the relatively lower dosage (540 g/t) improved the overall Ni recovery by 6%, though the Ni grade was slightly reduced. By varying the dosage of St-VI-1-52 and PAX, i.e., increasing the St-VI-1-52 up to 1781 g/t and decreasing PAX to 47 g/t, a 7% higher Ni recovery than that given by PAX alone was achieved and the best selectivity (highest Ni grade and lowest MgO grade) of all experiments was attained.

Figure 8 shows SEM micrographs and EDX spectra of dried samples collected after the incremental rougher flotation test using combined collectors (540 g/t St-VI-1-52 and 65 g/t PAX). Figure 8 A1 and A2 are micrographs of samples collected from the first concentrate. Figure 8 B1 and B2 are micrographs of samples collected from the third incremental froth concentrate. With an increase in the incremental flotation stage, a larger quantity of fibrous slime was seen on the mineral surfaces. Similarly to the previous FCS test, plenty of St-VI-1-52 nanoparticles, with some aggregates, were deposited onto the nickel rich surfaces. Very small amounts of nanoparticles were seen to deposit onto the Mg/Si slime. Figure 8C and D are EDX spectra from the selected positions indicated as “X” and “Y” of Figure 8B1 micrograph. The peaks of carbon element further confirmed the extent for St-VI-1-52 selective adsorption onto either the Ni-rich or Mg/Si-rich component of the ore.

## Discussion

The objectives of the current work were to evaluate the feasibility of poly (styrene-co-1-vinyl imidazole) based functionalized nanoparticle collectors in processing a Thompson Pipe low-grade nickel ore, and to enhance the existing flotation efficiency of that attained by the conventional molecular collector (PAX). The results shown in Figure 7 indicated that the addition of nanoparticle collectors coupled with conventional molecular PAX gave both higher recovery and better selectivity (grade).

One of the most important aspects when designing nanoparticle collectors is that the nanoparticles must specifically deposit onto the desired mineral particles, i.e. pentlandite in this study. Pentlandite is negatively charged and Mg/Si slime (predominantly serpentine) is positively charged in the natural ultramafic nickel ore. [3, 17] Thus, cationic polystyrene nanoparticles were used to selectively deposit onto negatively charged pentlandite via electrostatics. In addition, imidazole groups were designed on the nanoparticle surfaces to increase potential chemical affinity of these nanoparticles with pentlandite by ligand (imidazole)-Ni complexation. [17] The micrographs shown in Figure 4 and Figure 8 reflect that the nanoparticle collectors we used had specificity and selectivity - Cationic, imidazole functionalized nanoparticles preferentially bind to Pn other than slime materials.

Optimizing nanoparticle collector properties involves balancing the opposing features. On one hand, less functional groups leave nanoparticles-deposited pentlandite more hydrophobic and thus favor flotation. For example, pristine polystyrene nanoparticles performed better than surface modified counterparts in glass beads flotation. [14] On the other hand, more functional groups promote nanoparticles deposition onto pentlandite and thus favor pentlandite selectivity, but functionalization decreases nanoparticle surface hydrophobicity [17]. For example, the CCC data in Table 4 shows that MAPTAC containing nanoparticles are a more stable colloidal system than MAPTAC-free nanoparticles; however, MAPTAC modification decreases nanoparticle surface hydrophobicity as well [15]. Therefore, the optimization of poly (styrene-co-1-vinyl imidazole) based functionalized nanoparticle collectors should balance the content of VI and MAPTAC when copolymerizing with styrene. The higher ratios of VI/MAPTAC to St in St-VI-MAPTAC-3-92 and St-VI-MAPTAC-4-121 resulted in poorer flotation performances than that with smaller ratios in St-VI-MAPTAC-2-68 and MAPTAC-free St-VI-1-52 (see Table 1 and Figure 5).

St-VI-1-52 was one of the best nanoparticle collectors for final flotation results, but the dosage (also for other nanoparticle collectors) required was much higher than the theoretical minimum dosage for good recoveries. A theoretical calculation based on the assumptions that every nanoparticle would only deposit onto the pentlandite fraction of the ore and a minimum coverage of 10% [14] would be sufficient for a high recovery of pentlandite showed that the required dosage would be only 3.3 g/t for St-VI-1-52. Other parameters used for the calculation included: Pn fraction in the ore was 1.5%; SSA, $\sigma$ of Pn particles was 0.076 $m^2/g$ (see Figure 6); nanoparticle diameter was 52 nm. However, the nanoparticle dosage (540 g/t, 960 g/t, 1781 g/t in Figure 5 and Figure 7) required was approximately two to three orders of magnitudes greater than theoretical dosage in the experiments. The possible reasons for the requirements of very high nanoparticle dosages are listed as follows.

First of all, nanoparticle aggregation was one of major issues under current flotation conditions. Table 4 summarizes CCC data of St-VI-1-52 in one-component flotation reagent solution. St-VI-1-52 aggregates readily when they are exposed to the solution of $Na_2CO_3$ or anionic PAX, whereas the frother has little effect on nanoparticle colloidal stability. As little as 0.75 mM $Na_2CO_3$, or 0.025 mM PAX could induce St-VI-1-52 to coagulate. In flotation tests, approximately 13 mM $Na_2CO_3$ was used to adjust the pH of slurry to 10.1, and 47-65 g/t of PAX in 4.0 L of flotation slurry (0.06~0.08 mM) was used in combination with nanoparticle collectors. Both concentrations of $Na_2CO_3$ and PAX in flotation were higher than the CCC's of St-VI-1-52. It is noted that by mixing $Na_2CO_3$ together with PAX could lead to much lower CCC's of the nanoparticles (results not shown herein). Thus, St-VI-1-52 inevitably aggregated in these flotation tests. A further calculation based on previous analysis will be: if 52 nm particles aggregate to 520 nm particles and all of the aggregates only adsorb to pentlandite, theoretical dosage will require 10 times more (~ 33 g/t). Therefore, the influence of flotation components on nanoparticle colloidal stability should be dealt with in the future application of nanoparticle collectors. Nanoparticle aggregation needs to be avoided, otherwise heavily-aggregated nanoparticles will reduce efficacy.

Secondly, the deposition efficiency for the nanoparticles onto pentlandite surfaces may be relatively low. The functionalized nanoparticle collectors were designed with surface ligand (1-vinyl imidazole) groups. In addition to electrostatics, surface ligand-Ni complexation was proposed to be the additional driving force in directing the nanoparticles to selectively deposit onto Pn. We have demonstrated that the imidazole nanoparticles are capable of binding nickel ions. [17] However, we did not measure the concentration of soluble nickel ions in the ground ore slurry. The imidazole functionalized nanoparticles may react with the free nickel ions when they deposit onto the Pn surfaces. This possible situation may decrease imidazole functionalized nanoparticles deposition efficiency. Clearly, more work will be required to test this analysis. Finally, there may be possible contaminations of the nanoparticle surface. The frother or any other hydrophilic components in the flotation slurry may adsorb onto nanoparticle surfaces and make the nanoparticles too hydrophilic.

Although the nanoparticle aggregation needs to be avoided from the viewpoint of commercial application, the role of nanoparticle aggregates may provide some positive impacts in processing these difficult ultramafic ores. In separate experiments, we have shown that fine pentlandite particles were negatively charged and fine slime/tails were slightly positively charged under the flotation conditions (pH~10). [17] Thus, the small fibers could be readily coated onto the pentlandite surfaces via electrostatic interaction (known as "slime coating"), which is the major reason why these ultramafic ores respond poorly to flotation. The SEM micrographs (*e.g.*, see Figure 4 A2 and Figure 8 B2) showed that the nanoparticle aggregates had larger dimensions than individual nanoparticles (much larger than the size of PAX, which has an extended molecular length of about 1 nm), sticking out of the fibrous Mg/Si slime. These nanoparticle aggregates may facilitate the air bubble/mineral attachment step [26] during flotation, because the nanoparticle aggregates on the Pn surfaces can reach over the masking hydrophilic slime fibers to attach to air bubbles.

An additional promising role of nanoparticle collectors is that the strength of nanoparticle-mineral adhesion is relatively strong. Once the nanoparticles adsorb onto the target mineral surface, these nanoparticles can function over a number of stages during a commercial flotation process. The FCS flowsheet (Figure 2) contains the rougher, scavenger, scavenger cleaner, rougher cleaner, and rougher re-cleaner sequenced flotation units. For the FCS test with the addition of St-VI-MAPTAC-68, the nanoparticles were added into scavenger flotation and scavenger cleaner flotation units. The final froth concentrates were collected from the rougher re-cleaner flotation units. The nanoparticles survived three to four flotation units. The SEM images in Figure 4 show that plenty of nanoparticles remained deposited on the nickel-rich pentlandite surfaces. This observation indicates that a majority of adsorbed nanoparticles will not detach from mineral surfaces, which allows the nanoparticle collectors to be effective over many flotation stages.

All in all then, nanoparticle aggregation is the major unsolved issue for the potential commercial application of this technology to pentlandite flotation. Our ongoing work includes: investigation of effects influencing nanoparticle aggregation, optimization of latex properties by varying comonomer compositions, and investigation of effects influencing latex deposition efficiency.

## Conclusions

In summary, we have reported flotation results for an ultramafic low-grade nickel sulfide ore in the presence of poly (styrene-co-1-vinylimidazole) based functionalized nanoparticle collectors, a new class of flotation collectors. The main conclusions from current work are as follows:

1. Cationic, imidazole functionalized nanoparticles based on poly (styrene-co-1-vinylimidazole) selectively bind to pentlandite and function as ultramafic nickel ore flotation collectors.
2. The required dosages of nanoparticles are orders of magnitude greater than required to give ~10% coverage because our nanoparticles are aggregating in the solution conditions of conventional flotation. Either the nanoparticles must be modified to give increased stability or the ionic strength of the flotation solution must be reduced.
3. There may be advantages in the combined use of PAX and cationic functionalized nanoparticles however care is required to prevent PAX induced nanoparticle aggregation.
4. Most functionalized nanoparticles will not detach from Pn surfaces once deposited.
5. Nanoparticle aggregation may provide some positive impacts. Relatively large scale of nanoparticle aggregates on pentlandite surfaces sticking out of the fibrous Mg/Si slime may facilitate the bubble/mineral attachment step during flotation.

## Acknowledgment

We thank the Centre for Materials and Manufacturing (CMM), a division of the Ontario Centres of Excellence (OCE) in collaboration with Vale Base Metals for funding; Vale, Base Metals Technology Development for funding. The authors are grateful to Vale Canada Limited management for permission to publish this work. We also acknowledge Mr. Miles Montgomery for acquiring some electrophoretic mobility data. Finally, the McMaster team thank Dr. Peter Wells from Vale for patiently teaching us the basics of mineral processing.

# Figures

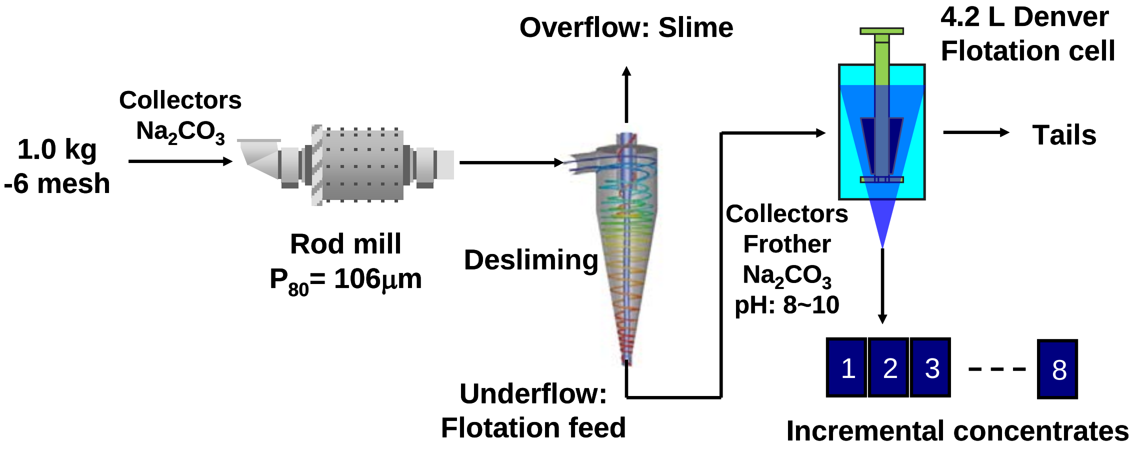

**Figure 1** The flowsheet used in incremental rougher flotation tests (total of ten products: 8 concentrates, tails, and overflow slime).

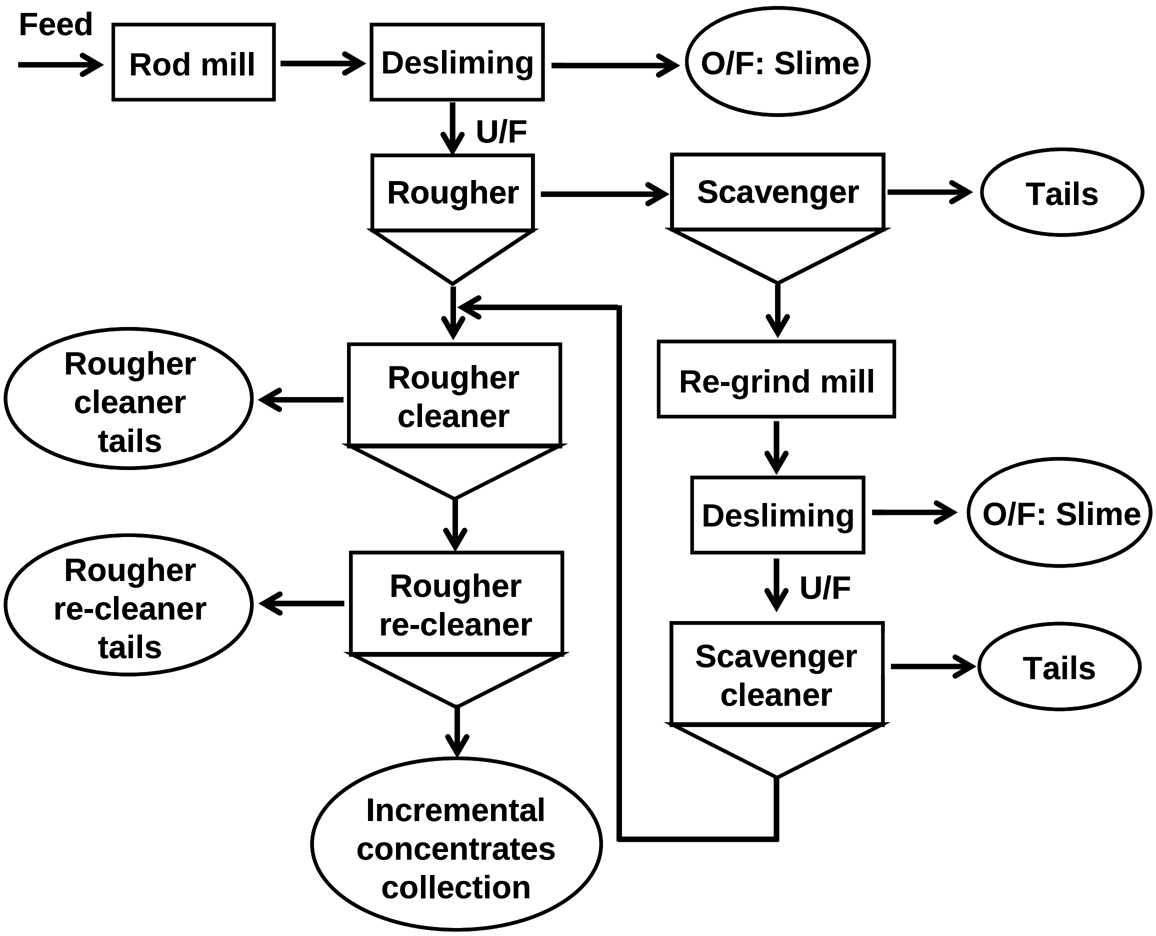

**Figure 2** The flowsheet used in full circuit simulation (FCS) flotation tests, containing five flotation stages: rougher, scavenger, scavenger cleaner, rougher cleaner, and rougher re-cleaner flotation. For the test with additional St-VI-MAPTAC-68, 2400 g/t nanoparticles were added in scavenger flotation, and 260 g/t nanoparticles were added in scavenger cleaner flotation.

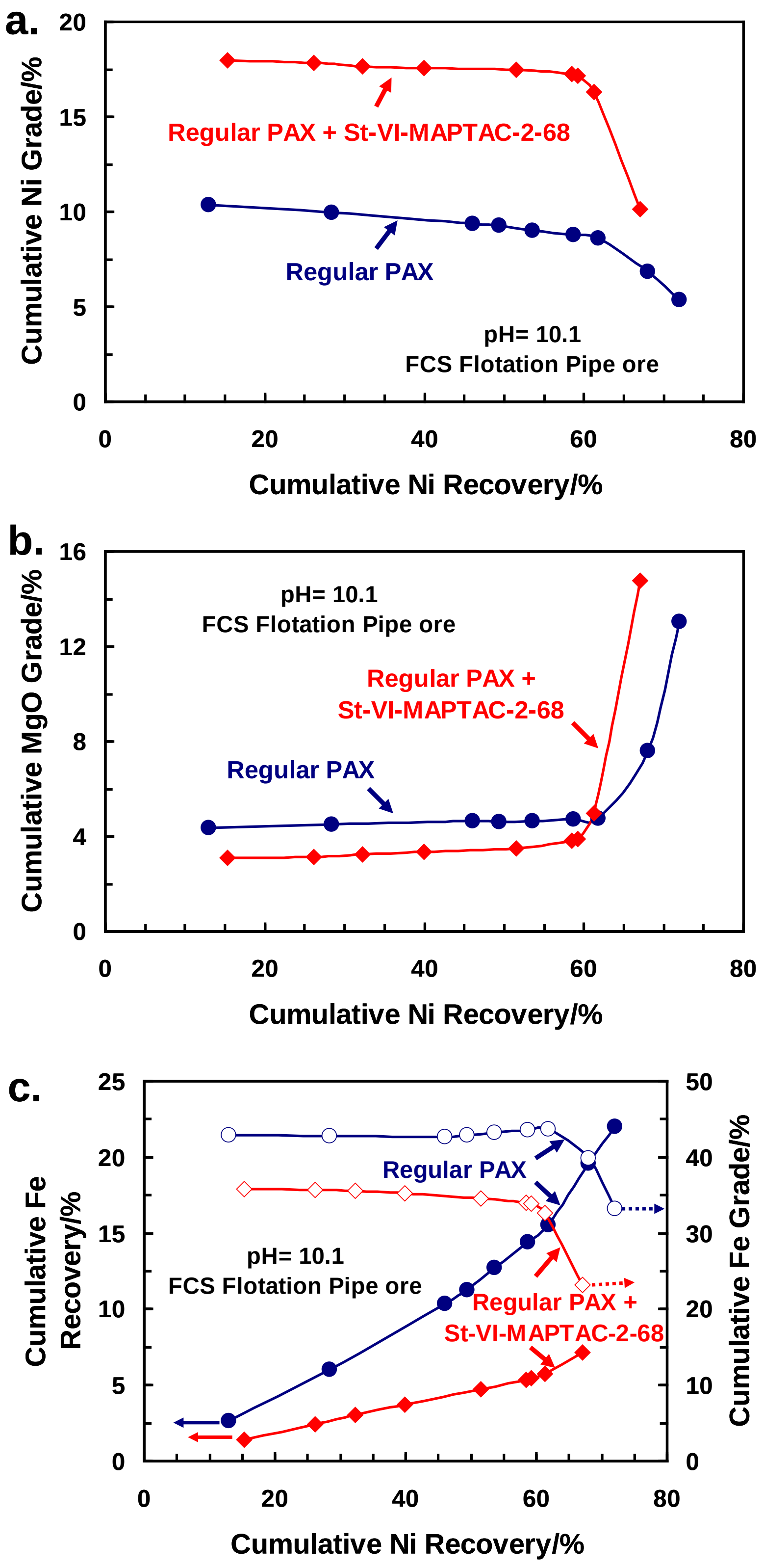
a.
Cumulative Ni Grade/%
0
5
10
15
20
Regular PAX + St-VI-MAPTAC-2-68
Regular PAX
pH= 10.1
FCS Flotation Pipe ore
0
20
40
60
80
Cumulative Ni Recovery/%
b.
Cumulative MgO Grade/%
0
4
8
12
16
pH= 10.1
FCS Flotation Pipe ore
Regular PAX +
St-VI-MAPTAC-2-68
Regular PAX
0
20
40
60
80
Cumulative Ni Recovery/%
c.
Cumulative Fe Recovery/%
0
5
10
15
20
25
Cumulative Fe Grade/%
0
10
20
30
40
50
Regular PAX
pH= 10.1
FCS Flotation Pipe ore
Regular PAX +
St-VI-MAPTAC-2-68
0
20
40
60
80
Cumulative Ni Recovery/%

**Figure 3** Flotation results with FCS procedure for a Thompson Pipe low-grade nickel ore using PAX without and with St-VI-MAPTAC-2-68 (2400 g/t in scavenger, and 260 g/t in scavenger cleaner). **a.** Cumulative Ni grade vs. cumulative Ni recovery; **b.** cumulative MgO grade vs. cumulative Ni recovery; **c.** cumulative Fe recovery and grade vs. cumulative Ni recovery. The nine points of each curve represent seven concentrates collected from rougher re-cleaner flotation, followed by rougher re-cleaner tails and rougher cleaner tails.

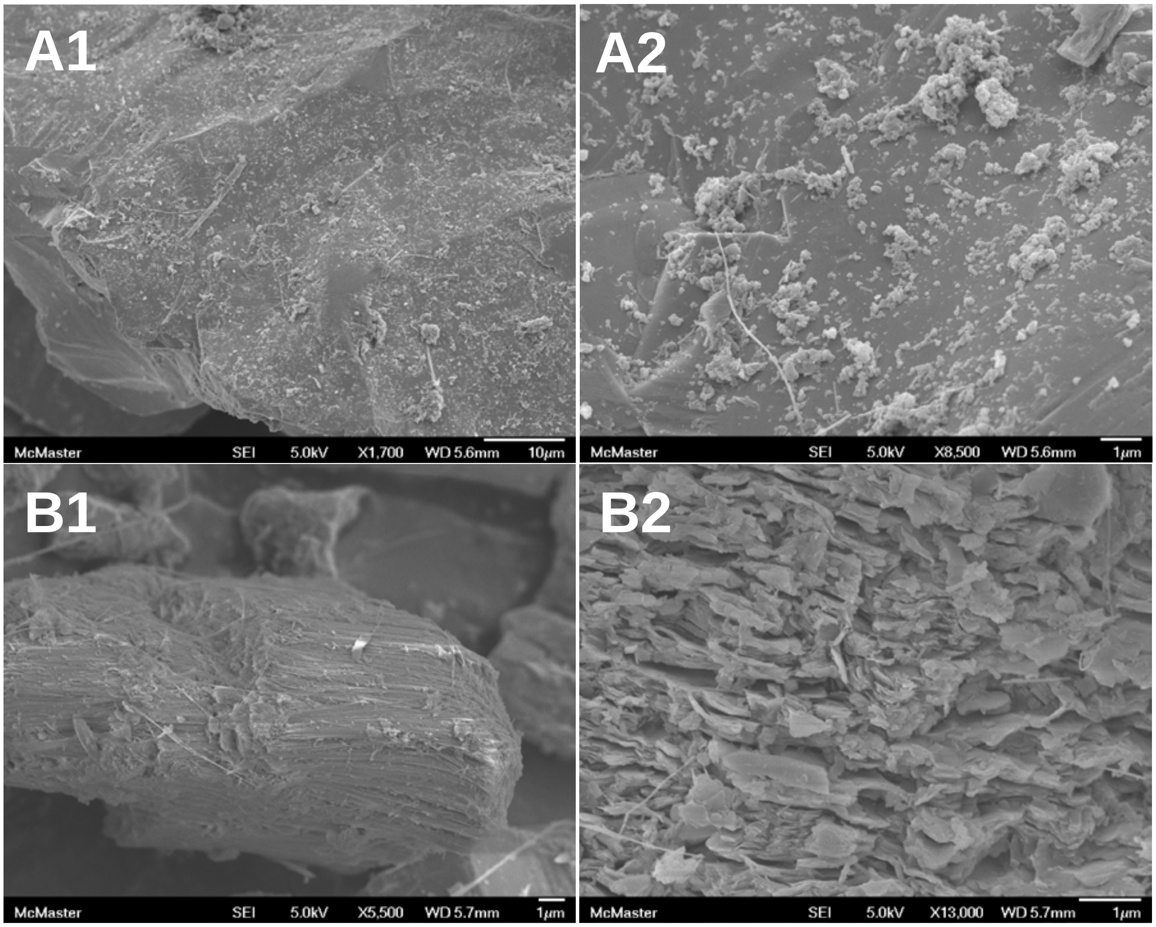

**Figure 4** SEM micrographs of samples collected after the FCS flotation test with St-VI-MAPTAC-2-68. **A1** and **A2** are micrographs of samples collected from the 1st rougher re-cleaner concentrate. **B1** and **B2** are micrographs of samples collected from scavenger cleaner tails. Plenty of St-VI-MAPTAC-2-68 nanoparticles, with some aggregates, were deposited onto the nickel rich surfaces. Very few nanoparticles were seen on the tails.

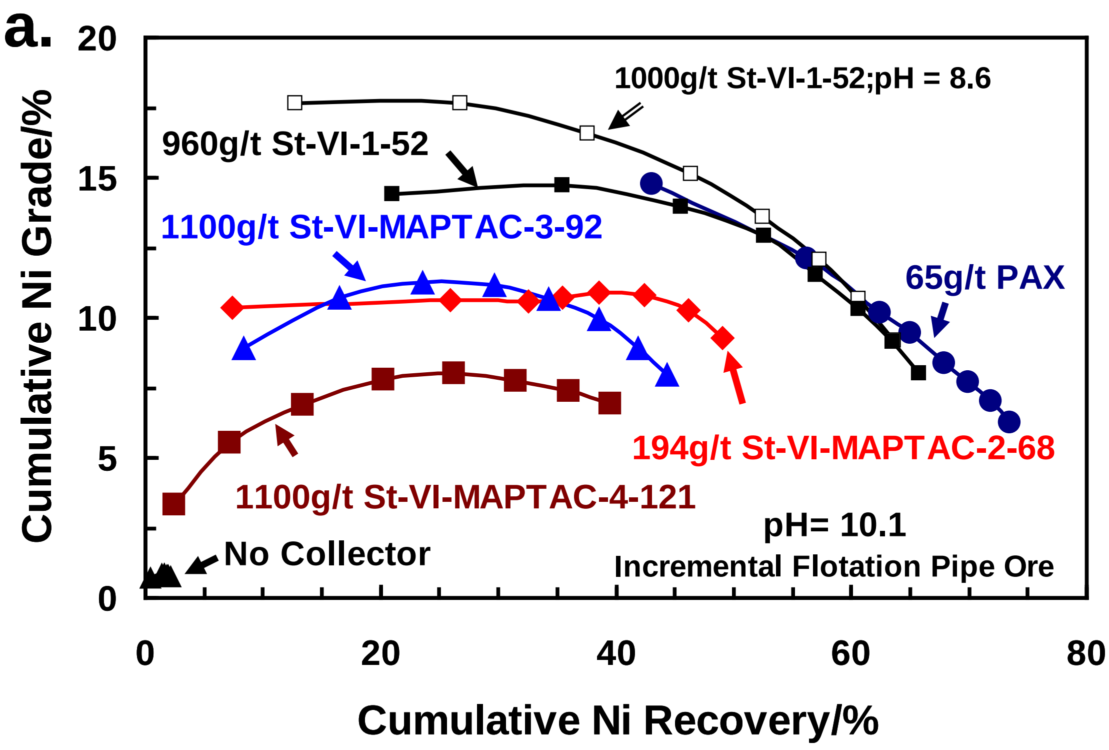
a.
Cumulative Ni Grade/%
Cumulative Ni Recovery/%
0
5
10
15
20
0
20
40
60
80
1000g/t St-VI-1-52;pH = 8.6
960g/t St-VI-1-52
1100g/t St-VI-MAPTAC-3-92
65g/t PAX
194g/t St-VI-MAPTAC-2-68
1100g/t St-VI-MAPTAC-4-121
pH= 10.1
No Collector
Incremental Flotation Pipe Ore

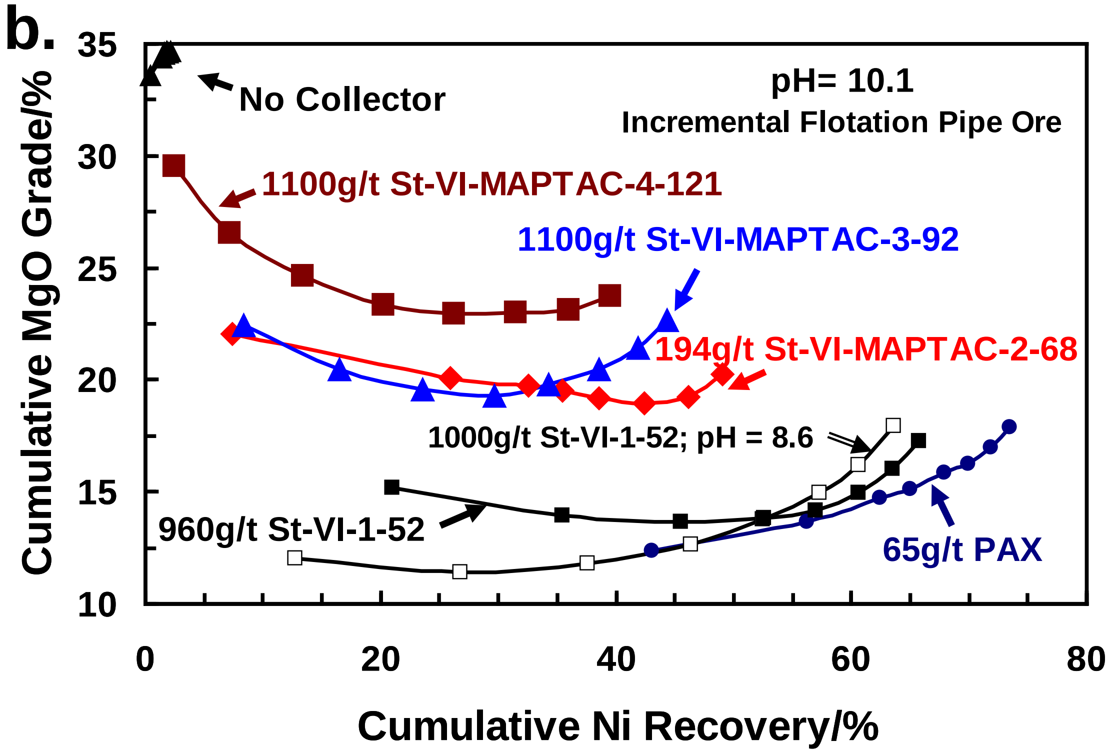
b.
Cumulative MgO Grade/%
Cumulative Ni Recovery/%
10
15
20
25
30
35
0
20
40
60
80
No Collector
pH= 10.1
Incremental Flotation Pipe Ore
1100g/t St-VI-MAPTAC-4-121
1100g/t St-VI-MAPTAC-3-92
194g/t St-VI-MAPTAC-2-68
1000g/t St-VI-1-52; pH = 8.6
960g/t St-VI-1-52
65g/t PAX

**Figure 5** Flotation results with incremental rougher flotation procedure for the Thompson Pipe low-grade nickel ore using a single collector (either each nanoparticle collector or PAX, plus a control: no collector). **a.** Cumulative Ni grade vs. cumulative Ni recovery; **b.** cumulative MgO grade vs. cumulative Ni recovery. The eight points of each curve represent eight collected concentrates.

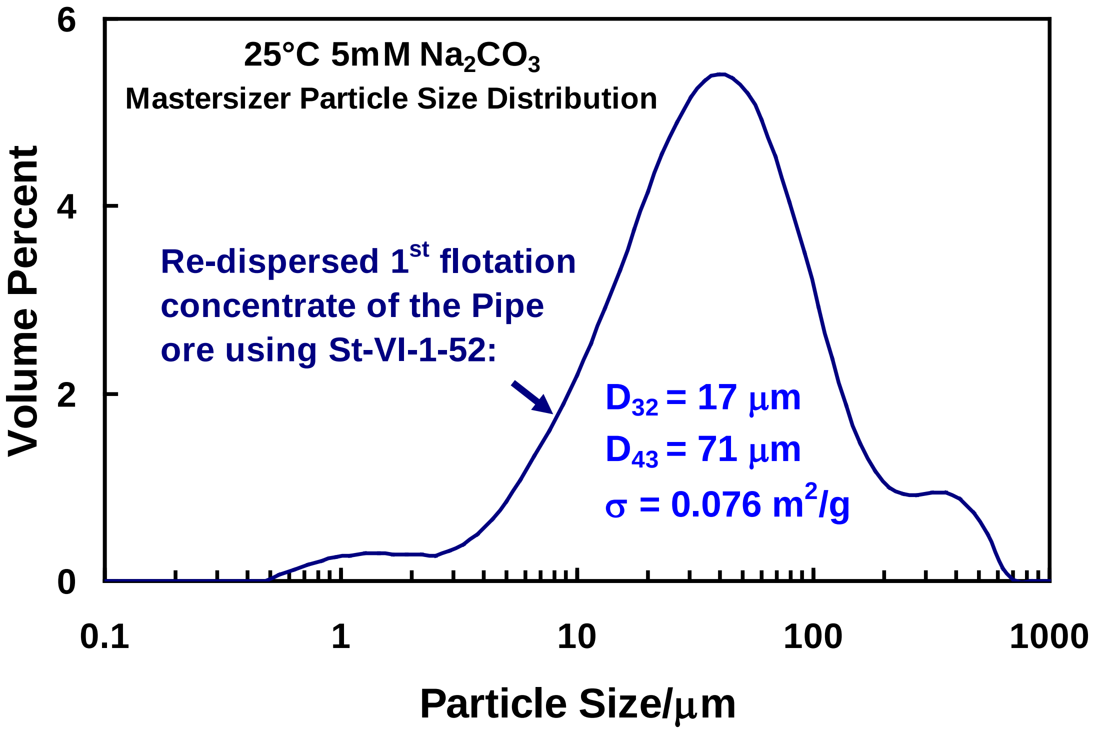

**Figure 6** Particle size distribution of the 1st concentrate of the test using 1000 g/t St-VI-1-52 at pH of 8.6 measured with a Mastersizer laser diffraction instrument. $D_{32}$ is the surface area mean diameter (also known as Sauter mean diameter), $D_{43}$ is the volume weighted mean diameter, and σ is the corresponding specific surface area calculated from $D_{32}$.

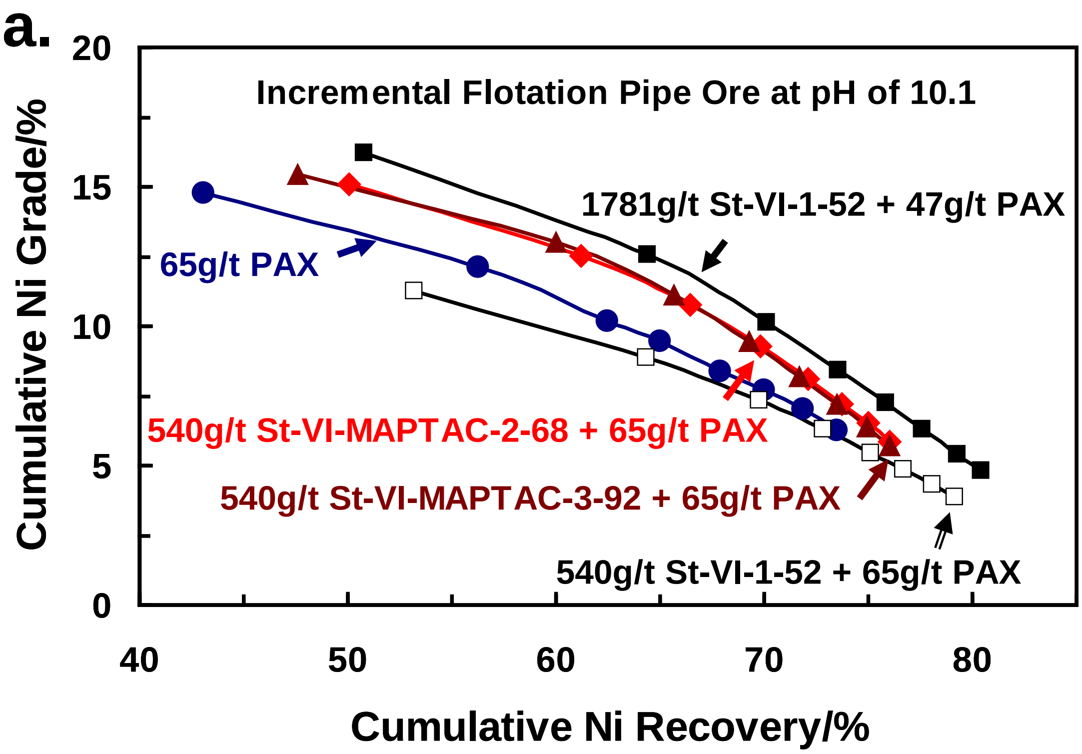
a.
Incremental Flotation Pipe Ore at pH of 10.1
1781g/t St-VI-1-52 + 47g/t PAX
65g/t PAX
540g/t St-VI-MAPTAC-2-68 + 65g/t PAX
540g/t St-VI-MAPTAC-3-92 + 65g/t PAX
540g/t St-VI-1-52 + 65g/t PAX
Cumulative Ni Grade/%
Cumulative Ni Recovery/%
0
5
10
15
20
40
50
60
70
80

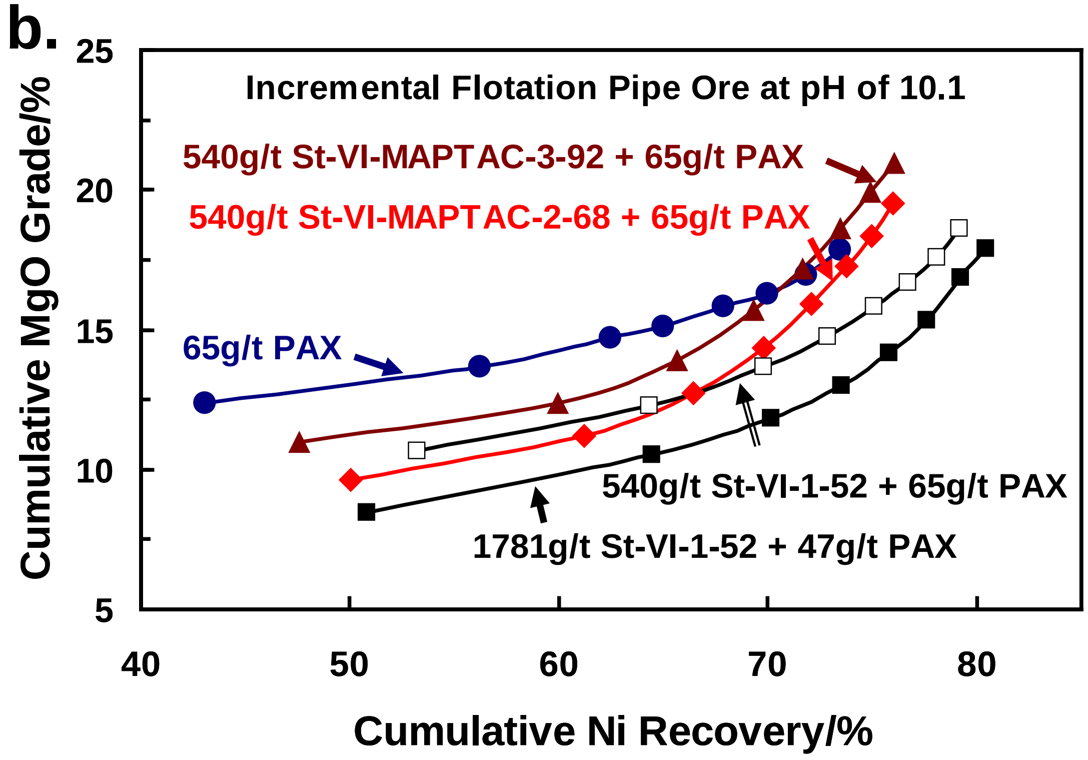
b.
Incremental Flotation Pipe Ore at pH of 10.1
540g/t St-VI-MAPTAC-3-92 + 65g/t PAX
540g/t St-VI-MAPTAC-2-68 + 65g/t PAX
65g/t PAX
540g/t St-VI-1-52 + 65g/t PAX
1781g/t St-VI-1-52 + 47g/t PAX
Cumulative MgO Grade/%
Cumulative Ni Recovery/%
5
10
15
20
25
40
50
60
70
80

**Figure 7** Flotation results with incremental rougher flotation procedure for the Thompson Pipe low-grade nickel ore using combined collectors: both nanoparticle collector and PAX. For comparison, the result using PAX alone is also shown as the blue line of circles. **a.** Cumulative Ni grade vs. cumulative Ni recovery; **b.** cumulative MgO grade vs. cumulative Ni recovery.

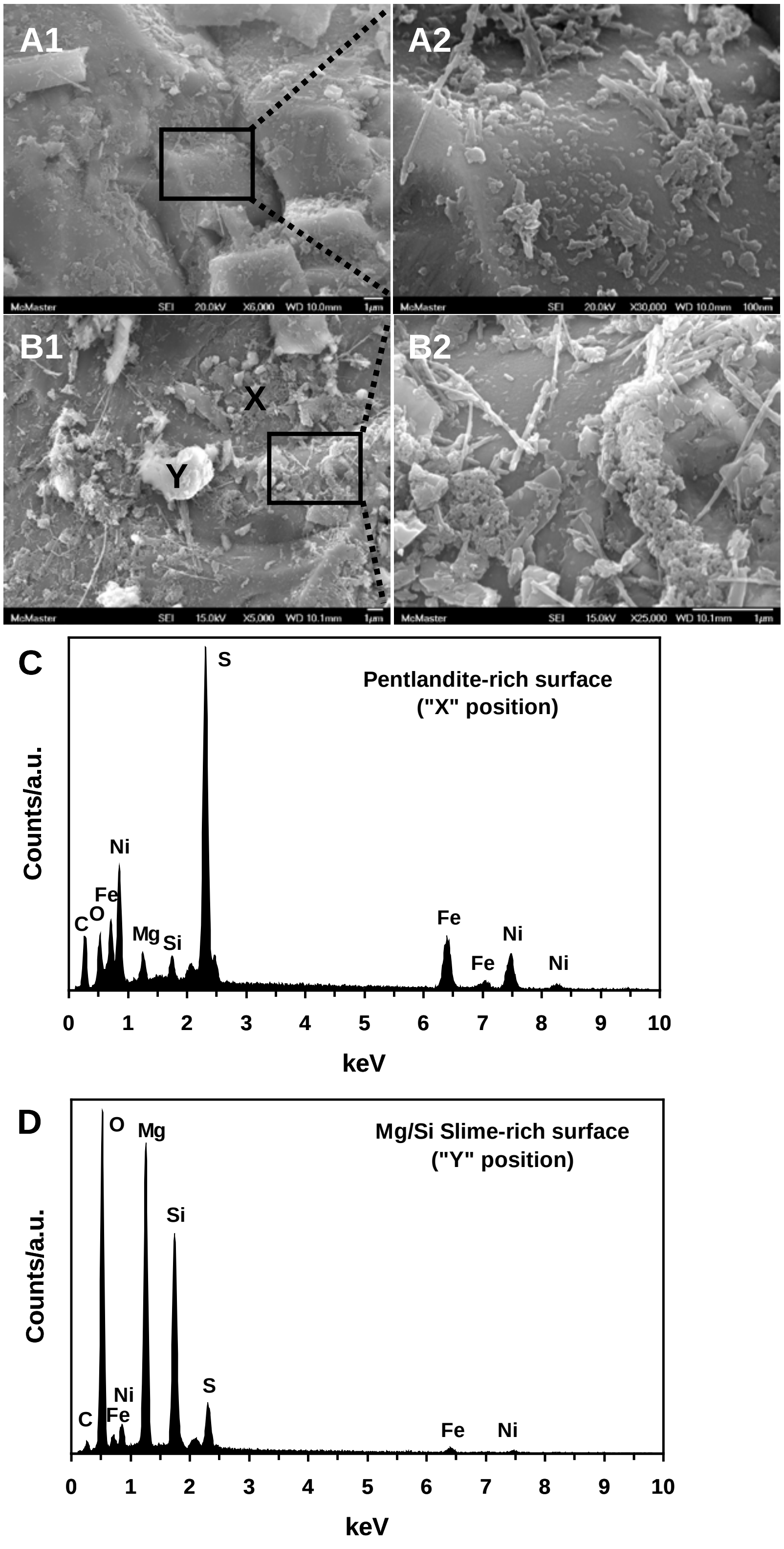
A1
McMaster SEI 20.0kV X6,000 WD 10.0mm 1μm
A2
McMaster SEI 20.0kV X30,000 WD 10.0mm 100nm
B1
X
Y
McMaster SEI 15.0kV X5,000 WD 10.1mm 1μm
B2
McMaster SEI 15.0kV X25,000 WD 10.1mm 1μm
C
Pentlandite-rich surface
("X" position)
Counts/a.u.
S
Ni
Fe
O
C
Mg
Si
Fe
Ni
Fe
Ni
0
1
2
3
4
5
6
7
8
9
10
keV
D
Mg/Si Slime-rich surface
("Y" position)
Counts/a.u.
O
Mg
Si
S
Ni
Fe
C
Fe
Ni
0
1
2
3
4
5
6
7
8
9
10
keV

**Figure 8** **A1**, **A2**, **B1**, and **B2** are SEM micrographs of samples collected after the incremental rougher flotation test using combined collectors: 540 g/t St-VI-1-52 and 65 g/t PAX. **A1** and **A2** are micrographs of the 1st incremental concentrate. **B1** and **B2** are micrographs of the 3rd incremental concentrate. **C** and **D** are EDX spectra from the selected positions indicated as "X" and "Y" of **B1** micrograph. The peaks of carbon element confirmed the extent for St-VI-1-52 selective adsorption onto each metal-rich component of the ore. Plenty of St-VI-1-52 nanoparticles, with some aggregates, were deposited onto the nickel rich surfaces. Very few nanoparticles were seen to deposit onto the Mg/Si slime.

# Tables

**Table 1** Recipes for preparation of functionalized nanoparticle collectors, where the final number in the nanoparticle designation is the average particle diameter.

| Nanoparticle Designation | Initial Reactor Charge (g) | | | | Starved-Feed Charge (g) | | |
|---|---|---|---|---|---|---|---|
| | Water | St | MAPTAC or CTAB | V50 | St | VI | Water |
| **St-VI-1-52** | 100 | 0.5 | 0.10 CTAB | 0.10 | 4.5 | 0.125 | 4.9 |
| **St-VI-MAPTAC-2-68** | 100 | 0.5 | 0.125 MAPTAC | 0.06 | 4.5 | 0.125 | 4.9 |
| **St-VI-MAPTAC-3-92** | 250 | 0.5 | 0.125 MAPTAC | 0.10 | 4.5 | 0.25 | 4.7 |
| **St-VI-MAPTAC-4-121** | 500 | 1.0 | 0.50 MAPTAC | 0.15 | 9.0 | 0.25 | 9.7 |

**Table 2** Experimental conditions used in incremental rougher flotation with a single collector (PAX or nanoparticle collector, plus a control without collector)

| **Collector type** | | **Control: No Collector** | **PAX** | **Nanoparticle collector** | | |
|---|---|---|---|---|---|---|
| | | | | **St-VI-1-52** | **St-VI-MAPTAC-3-92** | **St-VI-MAPTAC-4-121** |
| **Flotation pH** | | **10.1** | **10.1** | **8.6 (Natural)** | **10.1** | **10.1** |
| **pH modifier** | | **$Na_2CO_3$** | **$Na_2CO_3$** | **None, with 5mM NaCl** | **$Na_2CO_3$** | **$Na_2CO_3$** |
| **Collector dosage (g/t)** | Grinding | 0 | 5 | 0 | 100 | 100 |
| | Incremental 1 | 0 | 20 | 100 | 100 | 100 |
| | Incremental 2 | 0 | 5.7 | 100 | 100 | 100 |
| | Incremental 3 | 0 | 5.7 | 100 | 100 | 100 |
| | Incremental 4 | 0 | 5.7 | 120 | 120 | 120 |
| | Incremental 5 | 0 | 5.7 | 120 | 120 | 120 |
| | Incremental 6 | 0 | 5.7 | 120 | 120 | 120 |
| | Incremental 7 | 0 | 5.7 | 170 | 170 | 170 |
| | Incremental 8 | 0 | 5.7 | 170 | 170 | 170 |
| | Total | 0 | 64.9 | 1000 | 1100 | 1100 |

**Other conditions:**

1. Unifroth 250c dosage was 20 g/t for flotation.
2. Conditioning time was 5 minutes before each incremental flotation.
3. Flotation duration was 2 minutes for each incremental flotation stage.

**Table 3** Hydrodynamic diameters and electrophoretic mobilities of functionalized nanoparticle collectors

| **Nanoparticle Designation** | **Hydrodynamic Diameters, nm (Polydispersity)** | **Electrophoretic Mobility, $10^{-8}m^2s^{-1}V^{-1}$** | |
|---|---|---|---|
| | | **5mM NaCl (pH~6.7)** | **5mM $Na_2CO_3$ (pH~10.6)** |
| **St-VI-1-52** | 52 (0.075) | 1.79 ± 0.11 | 0.53 ± 0.08 |
| **St-VI-MAPTAC-2-68** | 68 (0.159) | 1.75 ± 0.19 | 1.55 ± 0.11 |
| **St-VI-MAPTAC-3-92** | 92 (0.112) | 3.65 ± 0.10 | 2.33 ± 0.05 |
| **St-VI-MAPTAC-4-121** | 121 (0.096) | 4.21 ± 0.23 | 2.65 ± 0.10 |

**Table 4** Critical coagulation concentrations (CCC) for St-VI-1-52 and St-VI-MAPTAC-4-12 induced by flotation reagents and the concentrations of flotation reagents used in flotation

| **Flotation Reagent** | **St-VI-1-52** | **St-VI-MAPTAC-4-121** | **Reagent Used in Flotation** |
|---|---|---|---|
| | **CCC, mM** | **CCC, mM** | **mM** |
| **$Na_2CO_3$** | 0.75 | 50 | ~ 13 |
| **PAX** | 0.025 | 1.0 | 0.06 ~ 0.08 |
| **Unifroth250c** | > 0.15 | > 300 | ~ 0.075 |

# References

1. Xu, M.; Scholey, K.; Marcuson, S., Vale-Cytec-University research consortium on processing low grade ultramafic nickel ore. *In COM 2011, Conference of Metallurgists, Montreal* **2011**.

2. Senior, G.; Thomas, S., Development and implementation of a new flowsheet for the flotation of a low grade nickel ore. *Int. J. Miner. Process.* **2005,** 78, (1), 49-61.

3. Edwards, C.; Kipkie, W.; Agar, G., The effect of slime coatings of the serpentine minerals, chrysotile and lizardite, on pentlandite flotation. *Int. J. Miner. Process.* **1980,** 7, (1), 33-42.

4. Pietrobon, M. C.; Grano, S. R.; Sobieraj, S.; Ralston, J., Recovery mechanisms for pentlandite and MgO-bearing gangue minerals in nickel ores from Western Australia. *Miner. Eng.* **1997,** 10, (8), 775-786.

5. Wellham, E.; Elber, L.; Yan, D., The role of carboxy methyl cellulose in the flotation of a nickel sulphide transition ore. *Miner. Eng.* **1992,** 5, (3-5), 381-395.

6. Wang, J.; Somasundaran, P.; Nagaraj, D. R., Adsorption mechanism of guar gum at solid-liquid interfaces. *Miner. Eng.* **2005,** 18, (1), 77-81.

7. Beaussart, A.; Mierczynska-Vasilev, A. M.; Harmer, S. L.; Beattie, D. A., The role of mineral surface chemistry in modified dextrin adsorption. *J. Colloid Interface Sci.* **2011,** 357, (2), 510-520.

8. Beattie, D. A.; Huynh, L.; Kaggwa, G. B. N.; Ralston, J., The effect of polysaccharides and polyacrylamides on the depression of talc and the flotation of sulphide minerals. *Miner. Eng.* **2006,** 19, (6-8), 598-608.

9. Dai, Z.; Garritsen, J.; Wells, P.; Xu, M., Aarsenide depression in flotation of mulitisulfide minerals. *US Patent* **2006,** 7,004,326.

10. Mani, H.; Xu, M.; Quinn, P.; Stratton-Crawley, R., The effect of ultramafic mineralogy on pentlandite flotation. *Processing of Complex Ores* **1997,** 1101, 63-76.

11. Fuerstenau, M.; Jameson, G.; Yoon, R., Froth Flotation: A Century of Innovation, Society for Mining, Metallurgy, and Exploration. *Inc.(SME), Littleton, Colorado, USA* **2007**.

12. Bagci, E.; Ekmekci, Z.; Bradshaw, D., Adsorption behaviour of xanthate and dithiophosphinate from their mixtures on chalcopyrite. *Miner. Eng.* **2007,** 20, (10), 1047-1053.

13. Lotter, N. O.; Bradshaw, D. J., The formulation and use of mixed collectors in sulphide flotation. *Miner. Eng.* **2010,** 23, (11-13), 945-951.

14. Yang, S. T.; Pelton, R.; Raegen, A.; Montgomery, M.; Dalnoki-Veress, K., Nanoparticle Flotation Collectors: Mechanisms Behind a New Technology. *Langmuir* **2011,** 27, (17), 10438-10446.

15. Yang, S. T.; Pelton, R., Nanoparticle Flotation Collectors II: The Role of Nanoparticle Hydrophobicity. *Langmuir* **2011,** 27, (18), 11409-11415.

16. Pelton, R.; Yang, S.; Xu, M.; Dai, Z., Nanoparticle flotation collectors - innovation from collaboration. *In COM 2011, Conference of Metallurgists, Montreal* **2011**.

17. Yang, S.; Pelton, R.; Dai, Z.; Montgomery, M.; Abarca, C.; Xu, M., Functionalized Nanoparticle Flotation Collectors for Pentlandite Isolation. *In Preparation* **2011**.
18. Goodwin, J.; Ottewill, R.; Pelton, R., Studies on the preparation and characterization of monodisperse polystyrene latices V.: The preparation of cationic latices. *Colloid. Polym. Sci.* **1979,** 257, (1), 61-69.
19. Sajjadi, S., Nanoparticle formation by monomer-starved semibatch emulsion polymerization. *Langmuir* **2007,** 23, (3), 1018-1024.
20. Ketelson, H. A.; Pelton, R.; Brook, M. A., Colloidal stability of Stober silica in acetone. *Langmuir* **1996,** 12, (5), 1134-1140.
21. Xu, M.; Wilson, S., Investigation of seasonal metallurgical shift at inco's clarabelle mill* 1. *Miner. Eng.* **2000,** 13, (12), 1207-1218.
22. Dai, Z.; Bos, J.-A.; Quinn, P.; Lee, A.; Xu, M., Flowsheet development for Thompson ultramafic low-grade nickel ores. *In COM 2009, Conference of Metallurgists, Sudbury* **2009**.
23. Dai, Z. F.; Bos, J. A.; Lee, A.; Wells, P., Mass balance and mineralogical analysis of flotation plant survey samples to improve plant metallurgy. *Miner. Eng.* **2008,** 21, (12-14), 826-831.
24. Leroux, M.; Rao, S.; Finch, J., Continuous minicell test of collectorless flotation at Mattabi Mines Ltd. *Can. Min. Metall. Bull.* **1994,** 87, (985), 53-57.
25. Heiskanen, K.; Kirjavainen, V.; Laapas, H., Possibilities of collectorless flotation in the treatment of pentlandite ores. *Int. J. Miner. Process.* **1991,** 33, (1-4), 263-274.
26. Nguyen, A.; Schulze, H.; Ralston, J., Elementary steps in particle--bubble attachment* 1. *Int. J. Miner. Process.* **1997,** 51, (1-4), 183-195.

# Appendix: Supporting Materials for Chapter 6

## Appendix C.6: The goal of this modeling is to calculate the theoretical minimun nanoaprticle dosage required for induce good flotaiton recoveries.

$$\sigma_{sphere}(dia,\rho) \equiv \frac{4\pi \cdot \left(\frac{dia}{2}\right)^2}{\frac{4}{3}\cdot\pi\cdot\left(\frac{dia}{2}\right)^3\cdot\rho}$$

specific surface area of a sphere

$$dia_{sphere}(\rho,\sigma) \equiv \frac{6}{\sigma\cdot\rho}$$

diameter as function of specific surface area

$$\Gamma_{sphere}(dia,\rho) \equiv \frac{\frac{4}{3}\cdot\pi\cdot\left(\frac{dia}{2}\right)^3\cdot\rho}{dia^2}$$

coverage of cubic packed spheres

## Pentlandite Properties

$ore := 1.5\%$ Mass fraction of Pn in ore

$\rho_p := 4.8\frac{gm}{mL}$ density of Pn

$D_p := 16.5\mu m$ area mean radius of Pn particle

$ssa := \sigma_{sphere}(D_p,\rho_p)$ corresponding specific surface area

$$ssa = 0.076\cdot\frac{m^2}{gm}$$

## Nanoparticle Collector Prameters

$D_{np} := 52\text{nm}$ Diameter of nanoparticle

$\rho_{np} := 1.05 \cdot \frac{\text{gm}}{\text{mL}}$ density of nanoparticle

$\Gamma_{max}(D_{np}) := \Gamma_{sphere}(D_{np}, \rho_{np})$

$\Gamma_{max}(D_{np}) = 0.029 \cdot \frac{\text{gm}}{\text{m}^2}$ Coverage corresponding a monolayer of sphere

$\text{Cov} := 10\%$ Assumed fractional coverage required for flotation

## Calculating Latex dose

$m_{ore} := \text{kg}$ Basis 1 kg

$A_{ore} := \text{ssa} \cdot \text{ore} \cdot m_{ore}$

$A_{ore} = 1.136\,\text{m}^2$

$\text{Mp}(D_{np}) := \frac{\Gamma_{max}(D_{np}) \cdot \text{Cov} \cdot A_{ore}}{m_{ore}}$ Mass of latex dose per mass of ore - note the mass of ore cancels out in this equation

$\text{Mp}(D_{np}) = 3.249 \cdot \frac{\text{gm}}{\text{tonne}}$ Assumes 100% deposition only on Pn surface

$\text{dd} := 50\text{nm}, 52\text{nm} .. 500\text{nm}$

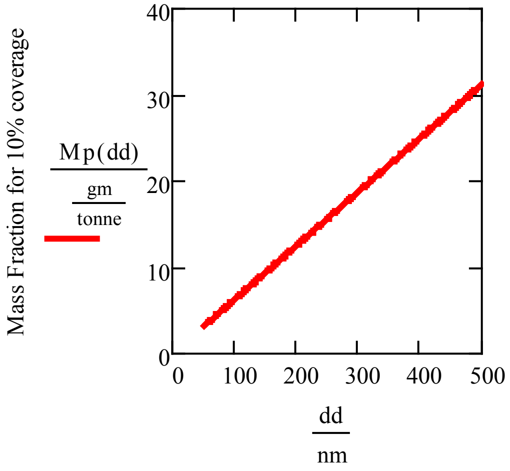

Nanoparticle Diameter

# Chapter 7 Concluding Remarks

## 7.1 Conclusions

To the best of my knowledge, this dissertation work involves a novel application for nanoparticles in the mineral processing industry. The potential of using nanoparticles as flotation collectors has been accessed. The mechanisms behind the application of nanoparticle collectors have been investigated. Key nanoparticle properties and major factors influencing potential industrial application have been identified. Furthermore, the studies on nanoparticle flotation collectors have been extended from original clean model mineral suspensions to more realistic complex natural ores. The research objectives proposed in Chapter 1 have been achieved, and the key findings and major contributions of this work are as follows:

1. For the first time, this work demonstrates that polystyrene nanoparticles, instead of conventional water-soluble molecular surfactants, can function as flotation collectors by floating hydrophilic glass beads, a mineral model. As little as 10% coverage of the bead surfaces with nanoparticles promotes high flotation efficiencies. Smaller and more hydrophobic nanoparticles are the most efficient flotation collectors.

2. We propose that the nanoparticle collectors have the potential to give much more efficient attachment to air bubbles and to be less vulnerable to unwanted detachment than molecular collector. The forces required to pull a nanoparticle-coated sphere from the air/water interface of a bubble into the water was determined via micromechanical measurements. The maximum pull-off force ranged from 0.0086 μN for a clean glass bead, to 1.9 μN for a 55 μm bead bearing adsorbed 46 nm diameter polystyrene spheres.

3. Contact angle measurements were used to correlate nanoparticle surface properties to their ability to promote the flotation of hydrophilic glass beads. The wetting behaviours of nanoparticle-decorated glass depend upon sample history. Starting with dried surfaces, classic sessile drop measurements, $\theta_a$, gave high advancing angles and indeterminable receding angles because of pinning. By contrast, when the glass surfaces were never dried after hydrophobic nanoparticle deposition, the corresponding receding water contact angles formed by attached bubbles, $\theta_r$, were reproducible.

4. Water contact angles on smooth polymer films, formed by spin coating polymer solutions in organic solvent, were used as a measure of nanoparticle hydrophobicity. The minimum nanoparticle water contact angle to give high flotation recovery was in the range $51° < \theta_{npmin} \leq 85°$.

5. Nanoparticle initial dosage, conditioning time, and nanoparticle size are important parameters for the extent of nanoparticle deposition onto bead surfaces. Nanoparticle deposition on to silica surfaces closely obeys Langmuir kinetics model for smaller nanoparticles (e.g., 46 nm and 120 nm ones). The model can be used to predict the extent of nanoparticle covered on mineral surfaces. Nanoparticle coverage on the bead surfaces increases with either higher latex initial dosage or longer conditioning time, leading to superior flotation recoveries.

6. Although nanoparticle size has a large influence on nanoparticle deposition rates onto mineral surfaces, flotation recovery is independent of nanoparticle size when compared at constant high coverage and similar nanoparticle hydrophobicities.

7. Most polystyrene nanoparticles will not detach from glass bead or mineral surfaces once deposited. This observation is important as nanoparticle collectors could function over a number of stages during a commercial flotation process.

8. Nanoparticles can be designed to specifically deposit onto the desired mineral particles. Cationic polystyrene nanoparticles were effective collectors for pentlandite flotation and the imidazole functionalized nanoparticles performed better than the simple cationic nanoparticles. The functionalized nanoparticles with imidazole surface ligands preferentially bind to pentlandite in the presence of oppositely charged tails or even in the presence of same negatively charged glass beads. Aside from electrostatics, we propose that imidazole-Ni complexation accounts for an additional driving force which directs the nanoparticles to selectively deposit onto pentlandite.

9. Cationic, imidazole functionalized nanoparticles based on poly(styrene-co-1-vinylimidazole) can function as ultramafic nickel ore flotation collectors. The required dosages of nanoparticles are orders of magnitude greater than required to give ~10% coverage because our nanoparticles are aggregating in the solution conditions of conventional flotation. There may be advantages in the combined use of PAX and

cationic functionalized nanoparticles however care is required to prevent PAX induced nanoparticle aggregation.

10. The relatively large nanoparticles adsorbed on mineral surfaces may be less susceptible to surface contamination, such as hydrophilic slime coating, compared to small patches of conventional surfactant collectors. Although nanoparticle aggregation should be avoided, the aggregates may provide some positive impacts. Relatively large scale of nanoparticle aggregates on pentlandite surfaces sticking out of the fibrous Mg/Si slime may facilitate the bubble/mineral attachment step during flotation.

## 7.2 Suggestions for Future Research

While this thesis has demonstrated it is possible to develop nanoparticle flotation collectors based on polystyrene nanoparticles, any other organic or inorganic nanoparticles such as polyolefin, fluorochemical, silicone, silica, aluminates, magnetic nanoparticles, would also be interesting to investigate. Experiments shown in Chapters 2, 3, 4 we relied on electrostatic attraction between oppositely charged glass beads and nanoparticles to drive deposition. In Chapters 5 and 6, apart from electrostatic attraction, a possible additional driving force based on imidazole-Ni complexation was applied in directing nanoparticles specifically to deposit onto pentlandite surfaces. However, electrostatic driven deposition and ligand-metal complexation are not prerequisites for the application of nanoparticles as collectors. Any interaction driving hydrophobic nanoparticle deposition such as antibody-antigen, chelation interactions, cis diol-borate, click chemistry, magnetic interactions, could be used to direct nanoparticle deposition on specific types of mineral surfaces.

Conventional collectors have been used and researched for about 100 years, whereas nanoparticle collectors have only been studied in the last 4 years, leaving many scientific and technological questions to be answered. For example, the existing issue of nanoparticles aggregation shown in Chapter 6 is an unsolved issue for the future application. Challenge in future development of nanoparticle collectors involves balancing colloidal stability and nanoparticle hydrophobicity. The effects of dissolved metal ions in flotation slurry on nanoparticle deposition efficiency are required to be identified in future. Loss of fine mineral particles is a long-term issue in mineral industry. Would nanoparticle collectors be able to extend the conventional flotation domain to finer minerals (e.g. < 10 μm) is an important unanswered question. Selective flocculation of mineral fines in the presence of nanoparticle collectors would be a related interesting topic.

From technological perspective, the application of nanoparticle collectors may be extended to any other mineral such as copper, gold-rich minerals, if hydrophobic nanoparticles can specifically deposit onto the desired mineral surfaces.